



Universiteit  
Leiden  
The Netherlands

## **The road to Insurmountability: Novel avenues to better target CC Chemokine Receptors**

Ortiz Zacarías, N.V.

### **Citation**

Ortiz Zacarías, N. V. (2019, December 4). *The road to Insurmountability: Novel avenues to better target CC Chemokine Receptors*. Retrieved from <https://hdl.handle.net/1887/81379>

Version: Publisher's Version

License: [Licence agreement concerning inclusion of doctoral thesis in the Institutional Repository of the University of Leiden](#)

Downloaded from: <https://hdl.handle.net/1887/81379>

**Note:** To cite this publication please use the final published version (if applicable).

Cover Page



Universiteit Leiden



The handle <http://hdl.handle.net/1887/81379> holds various files of this Leiden University dissertation.

**Author:** Ortiz Zacarías, N.V.

**Title:** The road to Insurmountability: Novel avenues to better target CC Chemokine Receptors

**Issue Date:** 2019-12-04

# **The road to Insurmountability**

***Novel avenues to better target  
CC Chemokine Receptors***

***by Natalia V. Ortiz Zacarías***

The research described in this thesis was performed at the Division of Drug Discovery and Safety of the Leiden Academic Centre for Drug Research (LACDR), Leiden University (Leiden, The Netherlands).

*Cover design:* Iñaki Vicuña Contany

*Thesis lay-out:* Natalia V. Ortiz Zacarías

*Printing:* Ridderprint BV

ISBN: 978-94-6375-677-8

© Copyright, Natalia V. Ortiz Zacarías, 2019

All rights reserved. No part of this book may be reproduced in any form or by any means without permission of the author.



# **The road to Insurmountability**

## **Novel avenues to better target CC Chemokine Receptors**

### **PROEFSCHRIFT**

ter verkrijging van

de graad van Doctor aan de Universiteit Leiden,

op gezag van Rector Magnificus prof.mr. C.J.J.M. Stolker,

volgens besluit van het College voor Promoties

te verdedigen op 4 december 2019

klokke 11:15 uur

door

**Natalia Veneranda Ortiz Zacarías**

geboren te Monterrey, Nuevo León, Mexico

in 1987

**Promotors:**

Prof. dr. Ad IJzerman

Dr. Laura Heitman

**Promotiecommissie:**

Prof. dr. Hubertus Irth (voorzitter)

Prof. dr. Joke Bouwstra (secretaris)

Prof. dr. Mette Rosenkilde

Dr. Anna Junker

Dr. Maikel Wijtmans

*Deep roots are not reached by the frost*  
*J.R.R. Tolkien, The Fellowship of the Ring*

*To my family and friends:*  
*the roots in my life*



# TABLE OF CONTENTS

<b>Chapter 1</b>	General Introduction	9
<b>Chapter 2</b>	Intracellular receptor modulation: Novel approach to target GPCRs	23
<b>Chapter 3</b>	Structure of CC Chemokine Receptor 2 with Orthosteric and Allosteric Antagonists	45
<b>Chapter 4</b>	Pyrrolone derivatives as intracellular allosteric modulators for chemokine receptors: Selective and dual-targeting inhibitors of CC Chemokine Receptors 1 and 2	71
<b>Chapter 5</b>	Synthesis and pharmacological evaluation of triazolopyrimidinone derivatives as noncompetitive, intracellular antagonists for CCR2/5 chemokine receptors	109
<b>Chapter 6</b>	Design and characterization of an intracellular covalent ligand for CC Chemokine Receptor 2 (CCR2)	153
<b>Chapter 7</b>	A novel CCR2 antagonist inhibits atherogenesis in apoE deficient mice by achieving high receptor occupancy	183
<b>Chapter 8</b>	Conclusions and Future Perspectives	211
	Summary	227
	Nederlandse Samenvatting	229
	Curriculum Vitae	232
	List of publications	233
	Acknowledgements	235

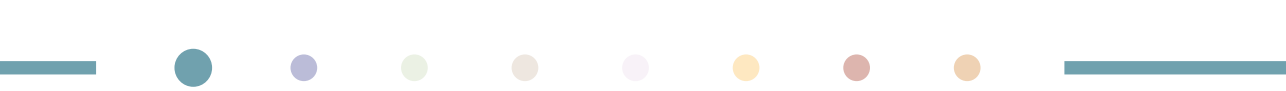


# Chapter 1

---

## General Introduction





The history of drug discovery and medicine can be traced back to the early human civilizations, which used natural products obtained from plants, animal materials and minerals for treating a variety of ailments and diseases.<sup>1</sup> Records of such prescriptions and medicinal recipes have been found in ancient Egyptian papyri, such as the Ebers papyrus written around 3000 BCE,<sup>2</sup> as well as in ancient Chinese texts and Aztec codices among others.<sup>1,3</sup> However, drug research as we know it, only began in the late 19<sup>th</sup> century with the rise of synthetic chemistry and pharmacology.<sup>4</sup> It was until the 1860s that the relationship between chemical structure and pharmacological activity started to be systematically studied,<sup>5</sup> and until the early 20<sup>th</sup> century that the receptor theory started to emerge, including the concepts of drug affinity and efficacy.<sup>6</sup> In the course of the 20<sup>th</sup> century, the advent of new technologies and the development of numerous disciplines led to unprecedented progress in drug discovery and development.<sup>4</sup> Today, more than 1500 drugs have been approved by the U.S. Food and Drug Administration (FDA) and the European Medicines Agency (EMA), and more than 30% of them target one single protein family: the superfamily of G protein-coupled receptors (GPCRs).<sup>7</sup>

## G protein-coupled receptors (GPCRs)

With ~800 members identified, G protein-coupled receptors (GPCRs) comprise the largest family of membrane-bound proteins in the human genome.<sup>8</sup> Based on sequence homology and phylogenetic analysis, human GPCRs can be divided in five families or classes: glutamate family (class C), rhodopsin family (class A), adhesion family, frizzled/taste2 and secretin family (class B).<sup>9,10</sup> Of these, the class A or rhodopsin family is the largest and most studied class of receptors, which includes aminergic receptors, protein receptors and nucleotide receptors, among others. Structurally, class A GPCRs are characterized by a bundle of seven transmembrane  $\alpha$ -helices (TM1-TM7) connected by three extracellular loops (ECL1-3) and three intracellular loops (ICL1-3), an extracellular N-terminus, an intracellular helix 8 (H8) and an intracellular C-terminus (Figure 1).<sup>11,12</sup> GPCRs transduce extracellular signals—such as photons, odorants, small molecules or proteins—into intracellular responses by interacting with different signal transducers, including heterotrimeric G proteins, GPCR kinases (GRKs) and arrestins.<sup>13,14</sup> In general, after binding of an endogenous agonist to its cognate GPCR, the receptor undergoes a series of conformational changes that facilitate the activation of a G protein or recruitment of other signaling effectors, such as  $\beta$ -arrestin.<sup>14</sup> Signaling via GPCRs is linked to many physiological, but also pathological processes, making them potential drug targets for many disease indications. In fact, more than 100 unique non-olfactory GPCRs are currently targets for approved drugs, with many more potential targets in clinical trials.<sup>7,15</sup>



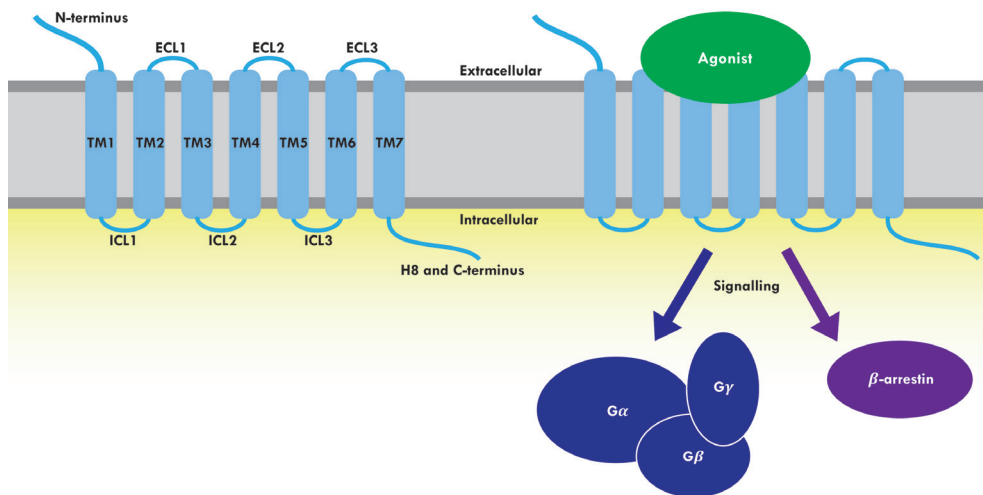


**Figure 1. Schematic representation of a class A G protein-coupled receptor (GPCR) embedded in the cell membrane.** Class A GPCRs share a general architecture of seven transmembrane alpha-helical domains (TM1-TM7) connected by three extracellular loops (ECL1-ECL3) and three intracellular loops (ICL1-ICL3), an N-terminus at the extracellular side, and Helix 8 (H8) and C-terminus at the intracellular side. After binding of an agonist from the extracellular side, the receptor undergoes conformational changes that allow the recruitment of different signaling effectors, such as the heterotrimeric G proteins or  $\beta$ -arrestins.

## Chemokine Receptors

Chemokine receptors encompass a large subfamily of class A GPCRs, which are activated by highly conserved proteins called chemokines (**chemotactic cytokines**). So far, 23 different chemokine receptors and more than 40 different chemokines have been identified, which form a complex and seemingly redundant system: one chemokine receptor can respond to multiple chemokines, and one chemokine can act on multiple receptors (Figure 2).<sup>16, 17</sup> Most chemokine receptors are classified in four different families based on the pattern of N-terminal cysteine residues of their endogenous chemokines: XC, with only one cysteine residue; CC, with two adjacent cysteines; CXC and CX3C, with one or three residues separating the cysteine residues, respectively. In addition, there are five atypical chemokine receptors, which do not (seem to) signal via the heterotrimeric G proteins.<sup>16, 18</sup> Chemokine receptors are widely expressed in leukocytes, and upon activation by chemokine ligands they control a variety of leukocyte functions including migration, differentiation, and survival. According to their main function, chemokine receptors can be divided in inflammatory or homeostatic, depending on whether they regulate functions required during an inflammatory response or under homeostatic conditions.<sup>19</sup>



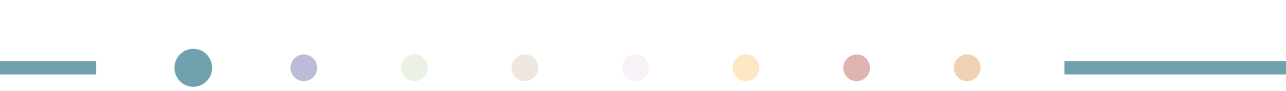
extracellular region—the so-called orthosteric binding site<sup>31</sup> (Figure 3). This orthosteric pocket can be divided into a major and a minor subpocket, formed by TM3-6 or TM1-3 and 7, respectively.<sup>32</sup> Small-molecule antagonists can inhibit chemokine receptor function by binding to only one or both subpockets.<sup>32,33</sup> For example, the CCR2 antagonists BMS-681 and MK-0812 bind exclusively to the minor pocket of the receptor,<sup>20,21</sup> while the CCR5 antagonist Maraviroc appears to extend to both subpockets.<sup>22</sup> Furthermore, the crystal structures of CCR2 (**Chapter 3**) and CCR9 show that small-molecule ligands can also inhibit the receptors by binding to an intracellular binding site<sup>20,26</sup> (Figure 3).

The different structures of chemokine receptors in complex with chemokine ligands<sup>23, 28, 29</sup> have also shed light on several epitopes necessary for chemokine recognition and activation: i) chemokine recognition site 1 (CRS1), where the chemokine first interacts with the N-terminus of the receptor; ii) CRS2, where the N-terminus of the chemokine extends into the TM domain of the receptor; and iii) CRS1.5 between CRS1 and CRS2, where conserved chemokine cysteine motifs and the N-terminus of the receptor are brought in close proximity to allow proper interaction.<sup>31</sup> As such, these structures have extended the so-called “two-site/two-step model” of chemokine-receptor activation, which only considered CRS1 and CRS2.<sup>32</sup> In addition, recent studies on CCR1 have led to the proposal of a three-step model, in which a conformational change of the receptor is also required for receptor activation.<sup>34</sup>

## **Chemokine receptors as drug targets: Focus on CCR1, CCR2 and CCR5.**

CC chemokine receptors 1 (CCR1), 2 (CCR2) and 5 (CCR5) are expressed on many leukocyte cells, including antigen-presenting cells (dendritic cells and macrophages), basophils, neutrophils, natural killer cells and different types of T cells.<sup>19</sup> As inflammatory receptors, they play a key role in the recruitment of leukocytes to sites of inflammation—a process called chemotaxis.<sup>19</sup> Although this inflammatory response is an essential mechanism of defense, an aberrant response can lead to leukocyte accumulation and tissue damage, resulting in many inflammatory or immune diseases.<sup>35</sup>

In this regard, (pre)clinical studies have suggested a critical role of CCR1, CCR2 and CCR5 and their ligands in the pathogenesis of multiple sclerosis (MS)<sup>36,37</sup> and rheumatoid arthritis (RA).<sup>38, 39</sup> Several studies have also shown that CCR1, CCR2 and CCR5 are necessary for monocyte recruitment and accumulation into the atherosclerotic plaques, suggesting a role of these receptors in atherosclerosis.<sup>40-42</sup> These chemokine receptors might also represent potential targets for the treatment of neuropathic pain, diabetes, psoriasis, and transplant



rejection, among others.<sup>35, 43-45</sup> In addition, a recent phase II clinical trial has successfully demonstrated that combined inhibition of CCR2 and CCR5 is beneficial for patients with nonalcoholic steatohepatitis (NASH).<sup>46</sup> Besides its role in inflammatory and immune diseases, CCR5 also acts as a co-receptor for the entry of the CCR5-tropic human immunodeficiency virus-1 (R5-HIV-1) into the host cells.<sup>47</sup> In addition, the chemokine system seems to be involved in tumor growth, tumor progression and metastasis.<sup>48</sup> For example, CCR1 has been implicated in colorectal cancer progression and metastasis to liver and lung,<sup>49-51</sup> while several preclinical studies have suggested a role for CCR2 and CCR5 in breast cancer progression and metastasis,<sup>52-54</sup> pancreatic cancer,<sup>55, 56</sup> and prostate cancer<sup>57, 58</sup> among others.

## Difficulties in targeting Chemokine Receptors

Despite the wealth of evidence regarding the involvement of chemokine receptors in many diseases, only three drugs targeting chemokine receptors have successfully reached market approval: the CCR5 small-molecule antagonist Maraviroc, the CXCR4 small-molecule antagonist Plerixafor, and the CCR4 monoclonal antibody Mogamulizumab. In most cases, preclinical findings have failed to translate into successful chemokine inhibitors, mainly due to lack of efficacy in clinical trials.<sup>59, 60</sup> Overall, difficulties with targeting the chemokine system can be grouped into three main categories: drug-related problems, relevance of the model, and complexity of the system. Drug-related problems include poor drug-like properties, insufficient target occupancy, and off-target effects, among others. For example, it has been predicted that > 90% receptor occupancy is required at all times for a sufficient anti-inflammatory effect, which is not always achieved in clinical trials.<sup>17, 61</sup> Relevance of the model refers to differences between the immune and chemokine systems of humans and animal species such as rodents, which renders these models poorly predictive in immune and inflammatory diseases.<sup>62</sup> For example, some chemokines have different functions in different species, while some others only exist in one species.<sup>62</sup> In addition, the potency of many chemokine receptor inhibitors can differ greatly between species, such as the CCR1 antagonist CP-481,715 that only inhibits the human receptor.<sup>59, 63</sup> Finally, the complexity of the system refers to the “redundancy” of the chemokine system, characterized by multiple cross-interactions between chemokines and chemokine receptors (Figure 2). The latter implies that targeting one single receptor might be insufficient in complex diseases where many chemokines and chemokine receptors are involved.<sup>59, 60, 64</sup> Added to the complexity is the suggested spatiotemporal regulation of the chemokine system, implicating that different biological responses are expected depending on the expression level, site of expression, or interaction with certain chemokine ligands, among others.<sup>17, 65</sup>

## Modulating Chemokine Receptors and GPCRs

Chemokine receptors, and GPCRs in general, are modulated by **orthosteric** or **allosteric** ligands which activate or block the receptor response in different ways. Orthosteric ligands bind to the same site as the endogenous ligand, i.e. at the chemokine binding site. Allosteric ligands, on the other hand, modulate the receptor by binding to a site spatially distinct from the orthosteric site, a so-called allosteric binding site<sup>66</sup> (Figure 3). Such allosteric binding sites have been identified across all GPCR regions, including extracellular, intracellular, and even extrahelical regions.<sup>67</sup> Depending on their functional effect, orthosteric ligands can be classified as **agonists**, **inverse agonists** or **antagonists**. Agonists can fully activate (full agonists) or partially activate (partial agonists) the receptor by inducing or stabilizing an active receptor conformation. Inverse agonists inhibit the constitutive or basal activity of the receptor, while (neutral) antagonists inhibit the agonist response without decreasing the constitutive activity.<sup>68</sup> Similarly, allosteric modulators can be classified as **positive allosteric modulators** (PAMs), which potentiate the affinity and/or efficacy of the orthosteric ligand; **negative allosteric modulators** (NAMs), which decrease the affinity and/or efficacy of the orthosteric ligand; or **neutral allosteric ligand** (NAL), with no effect on the orthosteric ligand.<sup>66</sup>

Ligands are usually designed to bind to their target in a reversible manner: the ligand can freely associate and dissociate from the receptor. Optimization of a ligand's binding kinetics—association ( $k_{on}$ ) and dissociation ( $k_{off}$ ) rate constants—can result in improved *in vivo* efficacy and safety.<sup>69</sup> By calculating the reciprocal of the  $k_{off}$  ( $1/(k_{off})$ ), the **drug-target residence time** (RT) of a ligand can be determined, which measures the lifetime of the drug-target complex. In addition, ligands that bind irreversibly to their target, i.e. **covalent ligands**, have been developed and used in the clinic.<sup>70</sup> These ligands bind in a two-step process, in which the ligand first binds to the receptor in a reversible manner, followed by the formation of the covalent or irreversible bond between the target protein and the reactive group of the ligand.<sup>71</sup> Inhibition via allosteric or covalent binding results in **insurmountable antagonism**, in which the ligand is able to inhibit receptor signalling despite high local concentration of the endogenous agonist, such as the presence of high chemokine levels during inflammatory conditions.<sup>72</sup>

Finally, although ligands have been traditionally designed to selectively act on a single target, recent evidence suggests that targeting one single protein might be insufficient in complex diseases where more than one protein is involved. Thus, inhibition of multiple drug targets (i.e. **polypharmacology**) may be more effective in disrupting complex biological systems than selective inhibition.<sup>73</sup> In this regard, three different approaches to polypharmacology have been proposed: i) drug cocktail, which refers to the administration of two different drugs,

each formulated differently; ii) multicomponent drugs, which refers to a single formulation containing two drugs; and iii) **multitarget ligands**, which refers to the design of one single ligand interacting with multiple targets.<sup>74</sup>

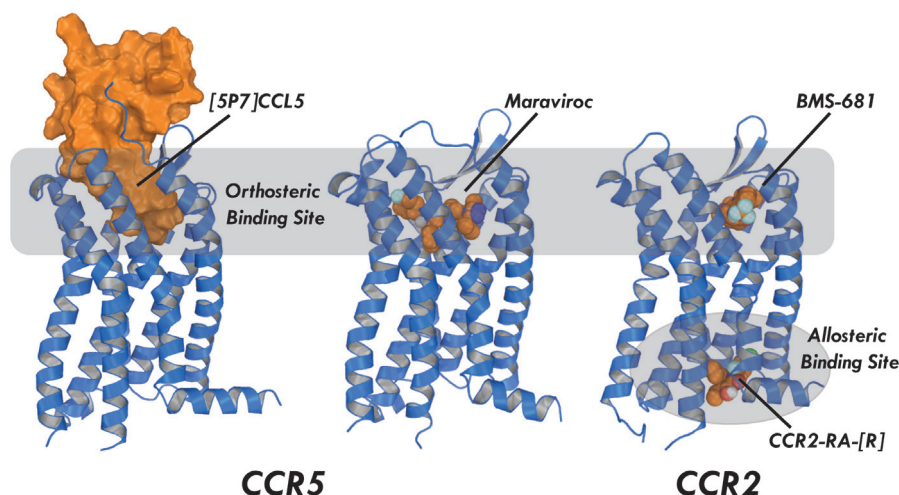


**Figure 3. Representative crystal structures of chemokine receptors.** Figure shows the crystal structure of CCR5 in complex with [5P7]CCL5, an engineered CCL5 variant; the crystal structure of CCR5 in complex with the small-molecule antagonist Maraviroc; and the crystal structure of CCR2 in complex with the small-molecule antagonists BMS-681 and CCR2-RA-[R]. Both Maraviroc and BMS-681 bind to the orthosteric binding site where the chemokines also bind, while CCR2-RA-[R] binds to an allosteric site located in the intracellular region.

## AIM AND OUTLINE OF THIS THESIS

Despite the major advances in drug discovery and development, the attrition rate of drug candidates in clinical trials continues to be high: only ~10% of all drug candidates entering Phase I clinical trials is expected to reach final marketing approval.<sup>75, 76</sup> An analysis of the causes of drug failure has reported lack of efficacy as the main reason of Phase II and Phase III failures<sup>77</sup> and this is no different in the case of chemokine receptors.<sup>59, 60</sup> In this regard, a thorough understanding of the mechanism of action at a molecular level is key for the development of drug candidates with better safety and efficacy profiles. This requires the inclusion of novel concepts and novel tools in early phases of drug discovery, some of which we aimed to explore in this thesis.

**Chapter 2** provides an overview on the available evidence of a common intracellular binding site among chemokine receptors and other class A GPCRs. Furthermore, the different

strategies to target such binding sites are discussed, with special focus on small molecules, as well as the potential advantages of intracellular ligands versus the traditionally designed orthosteric ligands. As crystal structures are paramount in drug discovery programs, **Chapter 3** focuses on the determination of the X-ray structure of human CCR2 in complex with two small-molecule antagonists: BMS-681, binding in the orthosteric binding site, and CCR2-RA-[R], binding in an intracellular binding pocket. The high conservation of this intracellular pocket among chemokine receptors can be exploited for the design of multitarget ligands, such as dual-targeting CCR1/CCR2 (**Chapter 4**) or CCR2/CCR5 (**Chapter 5**) intracellular ligands. Thus, **Chapter 4** explores whether the highly homologous CCR1 can also be targeted with intracellular small molecules. For this purpose, a series of CCR2-RA-[R] derivatives were synthesized and evaluated in both CCR1 and CCR2 using biochemical assays, allowing us to develop structure-affinity relationships for both receptors. A similar medicinal chemistry approach was used in **Chapter 5**, which describes the synthesis and biological evaluation of a series of triazolo-pyrimidinone derivatives in both CCR2 and CCR5, with the aim of gaining insight in the compounds' structural requirements to achieve selectivity and dual activity in the two receptors. With the aim of obtaining the first covalent probe for CCR2, **Chapter 6** describes the design, synthesis, pharmacological characterization and suggested binding mode of a covalent, intracellular NAM for this receptor. As *in vivo* drug efficacy is the ultimate goal of drug discovery efforts, **Chapter 7** investigates whether compound **15a**, an orthosteric antagonist with a long residence time on human CCR2, is efficacious in a mouse model of atherosclerosis. Finally, **Chapter 8** summarizes the results of the work presented in this thesis, as well as the future prospects and challenges in the field. Hopefully, this thesis will contribute to the development of better insurmountable antagonists and improved *in vivo* outcomes.

## REFERENCES

1. Ng, R. Appendix 1: History of drug discovery and development. In *Drugs: From Discovery to Approval*, Second ed.; Ng, R., Ed. 2008.
2. Aboelsoud, N. H. Herbal medicine in ancient Egypt. *J. Med. Plant Res.* **2010**, *4*, 82-86.
3. Peña, J. C. Pre-Columbian medicine and the kidney. *Am. J. Nephrol.* **1999**, *19*, 148-154.
4. Drews, J. Drug discovery: a historical perspective. *Science* **2000**, *287*, 1960-1964.
5. Bynum, W. F. Chemical structure and pharmacological action: a chapter in the history of 19th century molecular pharmacology. *Bull. Hist. Med.* **1970**, *44*, 518-538.
6. Maehle, A.-H.; Prüll, C.-R.; Halliwell, R. F. The emergence of the drug receptor theory. *Nat Rev Drug Discov* **2002**, *1*, 637-641.
7. Sriram, K.; Insel, P. A. G protein-coupled receptors as targets for approved drugs: how many targets and how many drugs? *Mol. Pharmacol.* **2018**, *93*, 251-258.
8. Bjarnadóttir, T. K.; Gloriam, D. E.; Hellstrand, S. H.; Kristiansson, H.; Fredriksson, R.; Schiöth, H. B. Comprehensive repertoire and phylogenetic analysis of the G protein-coupled receptors in human and mouse. *Genomics* **2006**, *88*, 263-273.
9. Fredriksson, R.; Lagerström, M. C.; Lundin, L.-G.; Schiöth, H. B. The G-protein-coupled receptors in the human genome form five main families. Phylogenetic analysis, paralogon groups, and fingerprints. *Mol. Pharmacol.* **2003**, *63*, 1256-1272.
10. G protein-coupled receptors. Accessed on 04/03/2019. IUPHAR/BPS Guide to PHARMACOLOGY, <http://www.guidetopharmacology.org/GRAC/FamilyDisplayForward?familyId=694>.
11. Venkatakrisnan, A. J.; Deupi, X.; Lebon, G.; Tate, C. G.; Schertler, G. F.; Babu, M. M. Molecular signatures of G-protein-coupled receptors. *Nature* **2013**, *494*, 185-194.
12. Katritch, V.; Cherezov, V.; Stevens, R. C. Diversity and modularity of G protein-coupled receptor structures. *Trends Pharmacol. Sci.* **2012**, *33*, 17-27.
13. Lagerstrom, M. C.; Schiöth, H. B. Structural diversity of G protein-coupled receptors and significance for drug discovery. *Nat Rev Drug Discov* **2008**, *7*, 339-357.
14. Rosenbaum, D. M.; Rasmussen, S. G.; Kobilka, B. K. The structure and function of G-protein-coupled receptors. *Nature* **2009**, *459*, 356-363.
15. Hauser, A. S.; Attwood, M. M.; Rask-Andersen, M.; Schiöth, H. B.; Gloriam, D. E. Trends in GPCR drug discovery: new agents, targets and indications. *Nat Rev Drug Discov* **2017**, *16*, 829-842.
16. Bachelier, F.; Ben-Baruch, A.; Charo, I. F.; Combadiere, C.; Farber, J. M.; Förster, R.; Graham, G. J.; Horuk, R.; Locati, M.; Luster, A. D.; Mantovani, A.; Moschovakis, G. L.; Murphy, P. M.; Nibbs, R. J. B.; Nomiya, H.; Oppenheim, J. J.; Power, C. A.; Proudfoot, A. E. I.; Rosenkilde, M. M.; Rot, A.; Sozzani, S.; Thelen, M.; Yoshie, O.; Zlotnik, A. Chemokine Receptors. Accessed on 11/03/2019. In IUPHAR/BPS Guide to PHARMACOLOGY, <http://www.guidetopharmacology.org/GRAC/FamilyDisplayForward?familyId=14>.
17. Schall, T. J.; Proudfoot, A. E. Overcoming hurdles in developing successful drugs targeting chemokine receptors. *Nat Rev Immunol* **2011**, *11*, 355-363.
18. Bachelier, F.; Graham, G. J.; Locati, M.; Mantovani, A.; Murphy, P. M.; Nibbs, R.; Rot, A.; Sozzani, S.; Thelen, M. An atypical addition to the chemokine receptor nomenclature: IUPHAR review 15. *Br J Pharmacol* **2015**, *172*, 3945-3949.
19. Lopez-Cotarelo, P.; Gomez-Moreira, C.; Criado-Garcia, O.; Sanchez, L.; Rodriguez-Fernandez, J. L. Beyond chemoattraction: multifunctionality of chemokine receptors in leukocytes. *Trends Immunol* **2017**, *38*, 927 - 941.
20. Zheng, Y.; Qin, L.; Ortiz Zacarías, N. V.; de Vries, H.; Han, G. W.; Gustavsson, M.; Dabros, M.; Zhao, C.; Cherney, R. J.; Carter, P.; Stamos, D.; Abagyan, R.; Cherezov, V.; Stevens, R. C.; Ilzerman, A. P.; Heitman, L. H.; Tebben, A.; Kufareva, I.; Handel, T. M. Structure of CC chemokine receptor 2 with orthosteric and allosteric antagonists. *Nature* **2016**, *540*, 458-461.



21. Apel, A. K.; Cheng, R. K. Y.; Tautermann, C. S.; Brauchle, M.; Huang, C. Y.; Pautsch, A.; Hennig, M.; Nar, H.; Schnapp, G. Crystal structure of CC chemokine receptor 2A in complex with an orthosteric antagonist provides insights for the design of selective antagonists. *Structure* **2019**, *27*, 427-438.
22. Tan, Q.; Zhu, Y.; Li, J.; Chen, Z.; Han, G. W.; Kufareva, I.; Li, T.; Ma, L.; Fenalti, G.; Li, J. Structure of the CCR5 chemokine receptor–HIV entry inhibitor maraviroc complex. *Science* **2013**, *341*, 1387-1390.
23. Zheng, Y.; Han, G. W.; Abagyan, R.; Wu, B.; Stevens, R. C.; Cherezov, V.; Kufareva, I.; Handel, T. M. Structure of CC chemokine receptor 5 with a potent chemokine antagonist reveals mechanisms of chemokine recognition and molecular mimicry by HIV. *Immunity* **2017**, *46*, 1005-1017.
24. Shaik, M. M.; Peng, H.; Lu, J.; Rits-Volloch, S.; Xu, C.; Liao, M.; Chen, B. Structural basis of coreceptor recognition by HIV-1 envelope spike. *Nature* **2019**, *565*, 318-323.
25. Peng, P.; Chen, H.; Zhu, Y.; Wang, Z.; Li, J.; Luo, R.-H.; Wang, J.; Chen, L.; Yang, L.-M.; Jiang, H.; Xie, X.; Wu, B.; Zheng, Y.-T.; Liu, H. Structure-Based Design of 1-Heteroaryl-1,3-propanediamine Derivatives as a Novel Series of CC-Chemokine Receptor 5 Antagonists. *J. Med. Chem.* **2018**, *61*, 9621-9636.
26. Oswald, C.; Rappas, M.; Kean, J.; Dore, A. S.; Errey, J. C.; Bennett, K.; Deflorian, F.; Christopher, J. A.; Jazayeri, A.; Mason, J. S.; Congreve, M.; Cooke, R. M.; Marshall, F. H. Intracellular allosteric antagonism of the CCR9 receptor. *Nature* **2016**, *540*, 462-465.
27. Wu, B.; Chien, E. Y. T.; Mol, C. D.; Fenalti, G.; Liu, W.; Katritch, V.; Abagyan, R.; Brooun, A.; Wells, P.; Bi, F. C.; Hamel, D. J.; Kuhn, P.; Handel, T. M.; Cherezov, V.; Stevens, R. C. Structures of the CXCR4 chemokine GPCR with small-molecule and cyclic peptide antagonists. *Science* **2010**, *330*, 1066-1071.
28. Qin, L.; Kufareva, I.; Holden, L. G.; Wang, C.; Zheng, Y.; Zhao, C.; Fenalti, G.; Wu, H.; Han, G. W.; Cherezov, V.; Abagyan, R.; Stevens, R. C.; Handel, T. M. Crystal structure of the chemokine receptor CXCR4 in complex with a viral chemokine. *Science* **2015**, *347*, 1117-1122.
29. Burg, J. S.; Ingram, J. R.; Venkatakrisnan, A. J.; Jude, K. M.; Dukkipati, A.; Feinberg, E. N.; Angelini, A.; Waghray, D.; Dror, R. O.; Ploegh, H. L.; Garcia, K. C. Structural basis for chemokine recognition and activation of a viral G protein-coupled receptor. *Science* **2015**, *347*, 1113-1117.
30. Miles, T. F.; Spiess, K.; Jude, K. M.; Tsutsumi, N.; Burg, J. S.; Ingram, J. R.; Waghray, D.; Hjorto, G. M.; Larsen, O.; Ploegh, H. L.; Rosenkilde, M. M.; Garcia, K. C. Viral GPCR US28 can signal in response to chemokine agonists of nearly unlimited structural degeneracy. *eLife* **2018**, *7*, e35850.
31. Kufareva, I. Chemokines and their receptors: insights from molecular modeling and crystallography. *Curr. Opin. Pharmacol.* **2016**, *30*, 27-37.
32. Scholten, D. J.; Canals, M.; Maussang, D.; Roumen, L.; Smit, M. J.; Wijtmans, M.; de Graaf, C.; Vischer, H. F.; Leurs, R. Pharmacological modulation of chemokine receptor function. *Br J Pharmacol* **2012**, *165*, 1617-1643.
33. Arimont, M.; Sun, S. L.; Leurs, R.; Smit, M.; de Esch, I. J.; de Graaf, C. Structural analysis of chemokine receptor–ligand interactions. *J. Med. Chem.* **2017**, *60*, 4735-4779.
34. Sanchez, J.; e Huma, Z.; Lane, J. R.; Liu, X.; Bridgford, J. L.; Payne, R. J.; Canals, M.; Stone, M. J. Evaluation and extension of the two-site, two-step model for binding and activation of the chemokine receptor CCR1. *J. Biol. Chem.* **2019**, *294*, 3464-3475.
35. Viola, A.; Luster, A. D. Chemokines and their receptors: drug targets in immunity and inflammation. *Annu Rev Pharmacol Toxicol.* **2008**, *48*, 171-197.
36. Szczuciński, A.; Losy, J. Chemokines and chemokine receptors in multiple sclerosis. Potential targets for new therapies. *Acta Neurol. Scand.* **2007**, *115*, 137-146.
37. Cheng, W.; Chen, G. Chemokines and chemokine receptors in multiple sclerosis. *Mediators Inflamm.* **2014**, *2014*, 659206.
38. Szekanecz, Z.; Koch, A. E. Successes and failures of chemokine-pathway targeting in rheumatoid arthritis. *Nat. Rev. Rheumatol.* **2016**, *12*, 5-13.
39. Szekanecz, Z.; Vegvari, A.; Szabo, Z.; Koch, A. E. Chemokines and chemokine receptors in arthritis. *Front Biosci (Schol Ed)* **2010**, *2*, 153-167.

40. Tacke, F.; Alvarez, D.; Kaplan, T. J.; Jakubzick, C.; Spanbroek, R.; Llodra, J.; Garin, A.; Liu, J.; Mack, M.; van Rooijen, N.; Lira, S. A.; Habenicht, A. J.; Randolph, G. J. Monocyte subsets differentially employ CCR2, CCR5, and CX3CR1 to accumulate within atherosclerotic plaques. *J. Clin. Invest.* **2007**, *117*, 185-194.
41. Soehnlein, O.; Drechsler, M.; Döring, Y.; Lievens, D.; Hartwig, H.; Kemmerich, K.; Ortega-Gómez, A.; Mandl, M.; Vijayan, S.; Projahn, D.; Garlachs, C. D.; Koenen, R. R.; Hristov, M.; Lutgens, E.; Zernecke, A.; Weber, C. Distinct functions of chemokine receptor axes in the atherogenic mobilization and recruitment of classical monocytes. *EMBO Mol. Med.* **2013**, *5*, 471.
42. van der Vorst, E. P. C.; Döring, Y.; Weber, C. Chemokines and their receptors in atherosclerosis. *J. Mol. Med.* **2015**, *93*, 963-971.
43. White, G. E.; Iqbal, A. J.; Greaves, D. R. CC chemokine receptors and chronic inflammation—therapeutic opportunities and pharmacological challenges. *Pharmacol. Rev.* **2013**, *65*, 47-89.
44. Koelink, P. J.; Overbeek, S. A.; Braber, S.; de Kruijff, P.; Folkerts, G.; Smit, M. J.; Kraneveld, A. D. Targeting chemokine receptors in chronic inflammatory diseases: an extensive review. *Pharmacol Ther* **2012**, *133*, 1-18.
45. Abbadie, C. Chemokines, chemokine receptors and pain. *Trends Immunol* **2005**, *26*, 529-534.
46. Friedman, S. L.; Ratziu, V.; Harrison, S. A.; Abdelmalek, M. F.; Aithal, G. P.; Caballeria, J.; Francque, S.; Farrell, G.; Kowdley, K. V.; Craxi, A. A randomized, placebo-controlled trial of cenicriviroc for treatment of nonalcoholic steatohepatitis with fibrosis. *Hepatology* **2018**, *67*, 1754-1767.
47. Moore, J. P.; Kitchen, S. G.; Pugach, P.; Zack, J. A. The CCR5 and CXCR4 coreceptors—central to understanding the transmission and pathogenesis of human immunodeficiency virus type 1 infection. *AIDS Res. Hum. Retroviruses* **2004**, *20*, 111-126.
48. Lacalle, R. A.; Blanco, R.; Carmona-Rodríguez, L.; Martín-Leal, A.; Mira, E.; Mañes, S. Chapter five - Chemokine receptor signaling and the hallmarks of cancer. In *Int. Rev. Cell Mol. Biol.*, Galluzzi, L., Ed. Academic Press: 2017; Vol. 331, pp 181-244.
49. Kitamura, T.; Fujishita, T.; Loetscher, P.; Revesz, L.; Hashida, H.; Kizaka-Kondoh, S.; Aoki, M.; Taketo, M. M. Inactivation of chemokine (C-C motif) receptor 1 (CCR1) suppresses colon cancer liver metastasis by blocking accumulation of immature myeloid cells in a mouse model. *Proc. Natl. Acad. Sci. U. S. A.* **2010**, *107*, 13063-13068.
50. Inamoto, S.; Itatani, Y.; Yamamoto, T.; Minamiguchi, S.; Hirai, H.; Iwamoto, M.; Hasegawa, S.; Taketo, M. M.; Sakai, Y.; Kawada, K. Loss of SMAD4 promotes colorectal cancer progression by accumulation of myeloid-derived suppressor cells through the CCL15-CCR1 chemokine axis. *Clin. Cancer Res.* **2016**, *22*, 492-501.
51. Yamamoto, T.; Kawada, K.; Itatani, Y.; Inamoto, S.; Okamura, R.; Iwamoto, M.; Miyamoto, E.; Chen-Yoshikawa, T. F.; Hirai, H.; Hasegawa, S.; Date, H.; Taketo, M. M.; Sakai, Y. Loss of SMAD4 promotes lung metastasis of colorectal cancer by accumulation of CCR1+ tumor-associated neutrophils through CCL15-CCR1 axis. *Clin. Cancer Res.* **2017**, *23*, 833-844.
52. Lu, X.; Kang, Y. Chemokine (C-C motif) ligand 2 engages CCR2+ stromal cells of monocytic origin to promote breast cancer metastasis to lung and bone. *J. Biol. Chem.* **2009**, *284*, 29087-29096.
53. Qian, B. Z.; Li, J.; Zhang, H.; Kitamura, T.; Zhang, J.; Campion, L. R.; Kaiser, E. A.; Snyder, L. A.; Pollard, J. W. CCL2 recruits inflammatory monocytes to facilitate breast-tumour metastasis. *Nature* **2011**, *475*, 222-225.
54. Velasco-Velázquez, M.; Jiao, X.; De La Fuente, M.; Pestell, T. G.; Ertel, A.; Lisanti, M. P.; Pestell, R. G. CCR5 antagonist blocks metastasis of basal breast cancer cells. *Cancer Res.* **2012**, *72*, 3839-3850.
55. Singh, S. K.; Mishra, M. K.; Eltoun, I.-E. A.; Bae, S.; Lillard, J. W.; Singh, R. CCR5/CCL5 axis interaction promotes migratory and invasiveness of pancreatic cancer cells. *Sci. Rep.* **2018**, *8*, 1323.
56. Sanford, D. E.; Belt, B. A.; Panni, R. Z.; Mayer, A.; Deshpande, A. D.; Carpenter, D.; Mitchem, J. B.; Plambeck-Suess, S. M.; Worley, L. A.; Goetz, B. D.; Wang-Gillam, A.; Eberlein, T. J.; Denardo, D. G.; Goedegebuure, S. P.; Linehan, D. C. Inflammatory monocyte mobilization decreases patient survival in pancreatic cancer: a role for targeting the CCL2/CCR2 axis. *Clin. Cancer Res.* **2013**, *19*, 3404-3415.
57. Urata, S.; Izumi, K.; Hiratsuka, K.; Maolake, A.; Natsagdorj, A.; Shigehara, K.; Iwamoto, H.; Kadomoto, S.; Makino, T.; Naito, R.; Kadono, Y.; Lin, W.-J.; Wufuer, G.; Narimoto, K.; Mizokami, A. C-C motif ligand 5

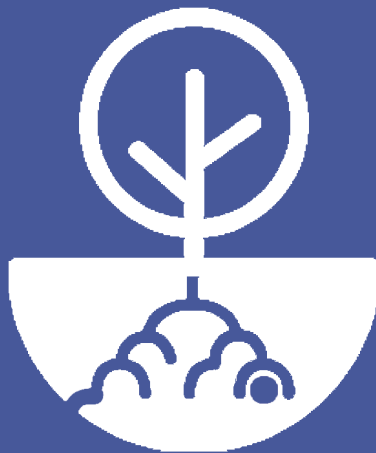
- promotes migration of prostate cancer cells in the prostate cancer bone metastasis microenvironment. *Cancer Sci.* **2018**, 109, 724-731.
58. Lu, Y.; Chen, Q.; Corey, E.; Xie, W.; Fan, J.; Mizokami, A.; Zhang, J. Activation of MCP-1/CCR2 axis promotes prostate cancer growth in bone. *Clin. Exp. Metastasis* **2009**, 26, 161-169.
  59. Horuk, R. Chemokine receptor antagonists: overcoming developmental hurdles. *Nat Rev Drug Discov* **2009**, 8, 23-33.
  60. Pease, J.; Horuk, R. Chemokine receptor antagonists. *J. Med. Chem.* **2012**, 55, 9363-9392.
  61. Dairaghi, D. J.; Zhang, P.; Wang, Y.; Seitz, L. C.; Johnson, D. A.; Miao, S.; Ertl, L. S.; Zeng, Y.; Powers, J. P.; Pennell, A. M.; Bekker, P.; Schall, T. J.; Jaen, J. C. Pharmacokinetic and pharmacodynamic evaluation of the novel CCR1 antagonist CCX354 in healthy human subjects: implications for selection of clinical dose. *Clin. Pharmacol. Ther.* **2011**, 89, 726-734.
  62. Zlotnik, A.; Yoshie, O. The chemokine superfamily revisited. *Immunity* **2012**, 36, 705-716.
  63. Gladue, R. P.; Tylaska, L. A.; Brissette, W. H.; Lira, P. D.; Kath, J. C.; Poss, C. S.; Brown, M. F.; Paradis, T. J.; Conklyn, M. J.; Ogborne, K. T.; McGlynn, M. A.; Lillie, B. M.; DiRico, A. P.; Mairs, E. N.; McElroy, E. B.; Martin, W. H.; Stock, I. A.; Shepard, R. M.; Showell, H. J.; Neote, K. CP-481,715, a potent and selective CCR1 antagonist with potential therapeutic implications for inflammatory diseases. *J. Biol. Chem.* **2003**, 278, 40473-40480.
  64. Horuk, R. Promiscuous drugs as therapeutics for chemokine receptors. *Expert Rev. Mol. Med.* **2009**, 11, e1.
  65. Zweemer, A. J.; Toraskar, J.; Heitman, L. H.; IJzerman, A. P. Bias in chemokine receptor signalling. *Trends Immunol* **2014**, 35, 243-252.
  66. Christopoulos, A.; Changeux, J.-P.; Catterall, W. A.; Fabbro, D.; Burris, T. P.; Cidlowski, J. A.; Olsen, R. W.; Peters, J. A.; Neubig, R. R.; Pin, J.-P.; Sexton, P. M.; Kenakin, T. P.; Ehlert, F. J.; Spedding, M.; Langmead, C. J. International union of basic and clinical pharmacology. XC. Multisite pharmacology: recommendations for the nomenclature of receptor allosterism and allosteric ligands. *Pharmacol. Rev.* **2014**, 66, 918-947.
  67. Congreve, M.; Oswald, C.; Marshall, F. H. Applying structure-based drug design approaches to allosteric modulators of GPCRs. *Trends Pharmacol Sci* **2017**, 38, 837-847.
  68. Wacker, D.; Stevens, R. C.; Roth, B. L. How ligands illuminate GPCR molecular pharmacology. *Cell* **2017**, 170, 414-427.
  69. Copeland, R. A. The dynamics of drug-target interactions: drug-target residence time and its impact on efficacy and safety. *Expert Opin Drug Discov* **2010**, 5, 305-310.
  70. Bauer, R. A. Covalent inhibitors in drug discovery: from accidental discoveries to avoided liabilities and designed therapies. *Drug Discov Today* **2015**, 20, 1061-1073.
  71. Strelow, J. M. A perspective on the kinetics of covalent and irreversible inhibition. *SLAS Discov* **2017**, 22, 3-20.
  72. Vauquelin, G.; Szczuka, A. Kinetic versus allosteric mechanisms to explain insurmountable antagonism and delayed ligand dissociation. *Neurochem. Int.* **2007**, 51, 254-260.
  73. Csermely, P.; Ágoston, V.; Pongor, S. The efficiency of multi-target drugs: the network approach might help drug design. *Trends Pharmacol. Sci.* **2005**, 26, 178-182.
  74. Morphy, R.; Rankovic, Z. Designed multiple ligands. An emerging drug discovery paradigm. *J. Med. Chem.* **2005**, 48, 6523-6543.
  75. Wong, C. H.; Siah, K. W.; Lo, A. W. Estimation of clinical trial success rates and related parameters. *Biostatistics* **2018**, 20, 273-286.
  76. Smietana, K.; Siatkowski, M.; Møller, M. Trends in clinical success rates. *Nat Rev Drug Discov* **2016**, 15, 379-380.
  77. Harrison, R. K. Phase II and phase III failures: 2013-2015. *Nat Rev Drug Discov* **2016**, 15, 817-818.



## Chapter 2

---

# Intracellular receptor modulation: Novel approach to target GPCRs



*Natalia V. Ortiz Zacarías, Eelke B. Lenselink, Adriaan P. IJzerman,  
Tracy M. Handel, and Laura H. Heitman*

*Trends in Pharmacological Sciences 2018, 39 (6): 547-559.*



## ABSTRACT

Recent crystal structures of multiple G protein-coupled receptors (GPCRs) have revealed a highly conserved intracellular pocket that can be used to modulate these receptors from the inside. This novel intracellular site partially overlaps with the G protein and  $\beta$ -arrestin binding site, providing a new manner of pharmacological intervention. Here we provide an update of the architecture and function of the intracellular region of GPCRs, until now portrayed as the signaling domain. We review the available evidence on the presence of intracellular binding sites among chemokine receptors and other class A GPCRs, as well as different strategies to target it, including small molecules, pepducins and nanobodies. Finally, the potential advantages of intracellular (allosteric) ligands over orthosteric ligands are also discussed.

## Highlights

Recent crystal structures have suggested a high diversity of allosteric binding sites, including novel pockets in the intracellular domain of GPCRs. These intracellular sites can potentially be targeted with small molecules, peptidic and nanobodies.

The recent X-ray structures of CCR2, CCR9 and  $\beta_2$ AR have revealed a highly-conserved intracellular pocket for small molecules, suggesting its presence in most chemokine receptors and other class A GPCRs.

Although many allosteric ligands for GPCRs have been described, only few allosteric drugs have reached the market. Yet, the number of allosteric modulators in development stages keeps increasing, including the number of intracellular ligands in (pre)clinical studies.

The discovery of intracellular binding sites, combined with the array of strategies for targeting such sites, opens up new approaches to better study and target GPCRs.

## Multiple binding sites to target a GPCR

G protein-coupled receptors (GPCRs, see Glossary) comprise one of the largest families of drug targets, with approximately 34% of the currently marketed drugs targeting this receptor class.<sup>1</sup> As lack of efficacy continues to be the main reason of failure in Phase II and Phase III clinical trials,<sup>2</sup> novel approaches to successfully target these receptors are still necessary. As it is apparent from most GPCR crystal structures reported so far, small molecules often occupy a binding site exposed to the extracellular solvent—the so-called orthosteric binding site which is used by endogenous ligands<sup>3</sup> (Figure 1a). However, targeting GPCRs has proved to be quite challenging, especially when drugs need to compete with a high (local) concentration of the endogenous ligand, as is the case of targeting chemokine receptors during inflammatory conditions.<sup>4</sup> Hence, the development of allosteric modulators (Box 1) that bind to spatially distinct binding sites<sup>5</sup> has emerged as a promising approach to improve not only drug efficacy, but also selectivity and safety.<sup>6-8</sup> A variety of different allosteric binding sites have already been identified in GPCRs, most of them close to the orthosteric binding site; yet, unexpected ligand binding sites have recently been found in crystal structures of class A and class B GPCRs.<sup>5</sup> In this regard, the recent crystal structures of CC chemokine receptor 2 (CCR2) (**Chapter 3**),<sup>9</sup> CC chemokine receptor 9 (CCR9),<sup>10</sup> and  $\beta_2$ -adrenergic receptor ( $\beta_2$ AR)<sup>11</sup> have for the first time revealed a spatially conserved intracellular binding site for small molecules in class A GPCRs (Figure 1a), providing a new avenue to inhibit or modulate these receptors in different pathologies.

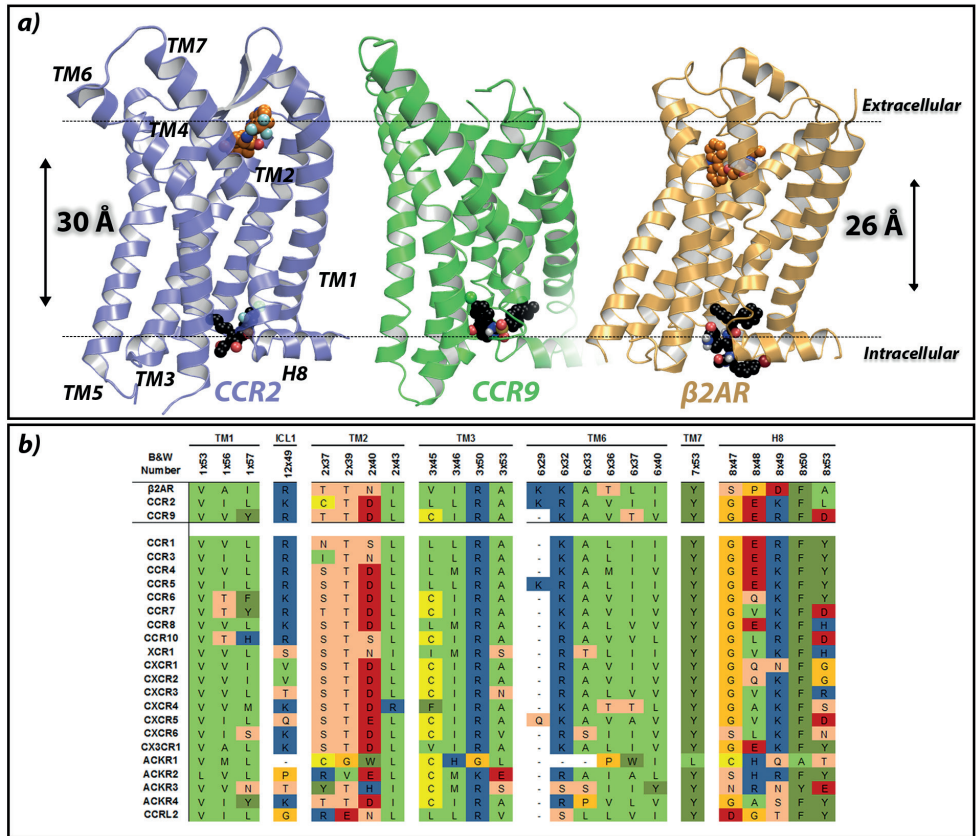


**Figure 1. Novel allosteric binding site in class A GPCRs.** (a) Endogenous ligands bind close to the extracellular region of GPCRs, in the so-called orthosteric binding site. Most of the co-crystallized small molecules also bind in this extracellular region, such as BMS-681 in CCR2 and carazolol in  $\beta_2$ AR. Recently, the crystal structures of CCR2 (purple, PDB 5T1A, **Chapter 3**), CCR9 (green, PDB 5LWE) and  $\beta_2$ AR (yellow, PDB 4XT1) have revealed an allosteric solvent-exposed binding site, located in the intracellular region of GPCRs, around 30 Å away from the orthosteric binding site. This novel binding site challenges the traditional view of the upper 7TM region of GPCRs as ligand binding domain and the intracellular region as signaling domain only. As shown in the structures, this intracellular binding site can also be targeted by small molecules such as CCR2-RA-[R] in CCR2, verciron in CCR9 and 15-PA in  $\beta_2$ AR. Dotted lines represent the plane of the membrane. (b) Sequence conservation among chemokine receptors and  $\beta_2$ AR, based on the GPCR database (GPCRdb, <http://www.gpcrdb.org>). Residues shown are residues involved in the intracellular binding site of CCR2, CCR9 and  $\beta_2$ AR (upper three rows). Some of these residues have also been found to be important for ligand binding to other class A GPCRs, as well as for G protein and  $\beta$ -arrestin binding.



### Box 1. Allosteric modulation in GPCRs

G protein-coupled receptors (GPCRs) are considered natural allosteric proteins, as the site of interaction of the endogenous ligand—the orthosteric binding site—differs from the site of the signaling effectors, such as G proteins and  $\beta$ -arrestins.<sup>74</sup> In addition to the orthosteric site, GPCRs possess a variety of topologically distinct allosteric binding sites where ligands can bind.<sup>5</sup> When allosteric modulators bind, they modulate the activity of orthosteric ligands by inducing conformational changes in the receptor.

Orthosteric ligands are competitive and thus, they replace the endogenous ligand resulting in a single pharmacological state. In contrast, by modulating the activity of another ligand, allosteric ligands have the potential for fine-tuning a receptor response, maximizing the efficacy in some therapeutic contexts,<sup>6,7</sup> and/or minimizing the potential side effects and other liabilities.<sup>6,8</sup> Depending on their effect, allosteric modulators can be divided in:<sup>6,7,75</sup>

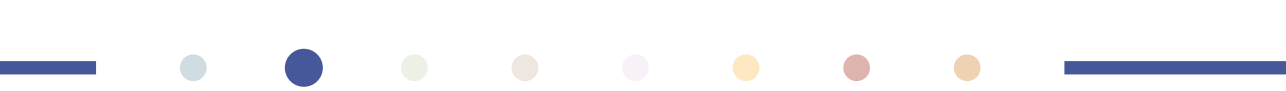
- Positive allosteric modulators (PAMs): Enhance the affinity and/or efficacy of the endogenous or orthosteric ligand.
- Negative allosteric modulators (NAMs): Decrease the affinity and/or efficacy of the endogenous or orthosteric ligand.
- Ago-PAMs: PAMs with some inherent level of agonist activity on their own.
- Silent allosteric modulators (SAMs): Have no effect on the affinity or efficacy of the endogenous or orthosteric ligand. Their presence may lead to for instance enhanced thermostability of the receptor and increased signaling lifetime.

Some key pharmacological properties of allosteric modulators are:

- Insurmountability: The ability of allosteric ligands to cause a decrease in the potency and/or efficacy of the endogenous agonist, even when the endogenous ligand is present at high concentrations.
- Selectivity: Generally, allosteric binding sites show less evolutionary pressure leading to a less-conserved amino acid sequence and thus, higher ligand selectivity than the orthosteric binding site. If an allosteric site is highly conserved, selectivity can be achieved via optimization of cooperativity with the orthosteric ligand or by targeting specific non-conserved amino acids.
- Saturability or ceiling effect: The limit of the pharmacological effect produced by the allosteric ligand due to saturation of the effect after full occupancy of the allosteric site.
- Probe-dependence: Both the magnitude and direction of the allosteric effect achieved by the allosteric modulator are dependent on the orthosteric ligand used as a “probe”.
- Biased signaling: The ability of a ligand to preferentially stabilize a conformation that leads to the selective activation of a signaling pathway.

## Intracellular region of GPCRs: Beyond signaling

In general, GPCRs share a similar structure consisting of three different domains (Figure 1a): the extracellular domain that includes three extracellular loops (ECLs) and the N terminus, which vary in length and structure depending on the GPCR subfamily;<sup>12</sup> the transmembrane (TM) domain that comprises seven TM helices; and the intracellular domain that includes three intracellular loops (ICLs), an amphipathic helix (H8) and the C terminus.<sup>3</sup> Traditionally, the upper TM section and the extracellular domain have been considered to encompass the ligand binding domain. In contrast, the lower TM section and the intracellular domain



have been considered to be the signaling domain.<sup>3, 13</sup> Structurally, the intracellular domain is more highly conserved and flexible than the extracellular region containing the orthosteric binding site,<sup>3, 13</sup> which is probably related to a common mechanism of receptor activation and G protein-coupling.<sup>14</sup> In this regard, analysis of several active- and inactive-state crystal structures has revealed a conserved rearrangement of residue contacts near the G protein-binding site, involving residues 3x46 in TM3, 6x37 in TM6, and 7x53 from the highly conserved NPxxY motif located in TM7 (residues according to structure-based Ballesteros-Weinstein numbering<sup>15</sup>).<sup>14</sup> In addition, this region is also involved in the coupling and selective recognition of different G proteins<sup>16, 17</sup> and other signaling proteins such as  $\beta$ -arrestin,<sup>18</sup> which can lead to a multitude of different signaling pathways upon activation of a GPCR. Recently, the traditional view of a separate ligand binding and signaling domain has been challenged as more evidence suggests that the intracellular domain of GPCRs can also be bound by ligands and thus be used for receptor modulation (Figure 1a) (Chapter 3).<sup>5, 9-11</sup>

## A common intracellular binding site in class A GPCRs

Among GPCRs there is now mutational, pharmacological and structural evidence of ligand binding sites located at their intracellular interface. This evidence is particularly extensive in the case of chemokine receptors (Box 2); thus, before extending to other class A GPCRs, we will first review the evidence available for chemokine receptors.

### Box 2. Chemokine Receptors

Chemokine receptors represent one of the largest subfamilies within class A G protein-coupled receptors (GPCRs). So far, 23 chemokine receptors have been identified that can be activated by more than 45 chemokine ligands (IUPHAR/BPS Guide to Pharmacology, <http://www.guidetopharmacology.org>, accessed on 04-12-2017). Chemokines and chemokine receptors are subdivided in four different families, according to the number and arrangement of conserved cysteine residues in the N-terminus of the chemokine ligands: C, with only one conserved cysteine present; CC, CXC and CX3C, with zero, one and three extra residues between two conserved cysteine residues.<sup>76</sup>

Both chemokines and chemokine receptors comprise the so-called chemokine system, which plays an important role in the migration and positioning of immune cells in homeostatic or pathological conditions.<sup>77</sup> According to their immune function, chemokine receptors can be classified as homeostatic, or dual inflammatory/homeostatic.<sup>78</sup> The chemokine system is a complex, seemingly redundant system in which one chemokine ligand is able to activate multiple chemokine receptors, and one chemokine receptor can be activated by multiple chemokine ligands. Yet, evidence suggests it is a highly fine-tuned system as it is tightly regulated by specific spatial and temporal control of chemokine expression.<sup>79, 80</sup>

Dysregulation of this complex system has been implicated in a variety of inflammatory and immune diseases, including arthritis, diabetes, inflammatory bowel disease and cancer.<sup>81</sup> Three drugs targeting chemokine receptors have already gained market approval: maraviroc, a small-molecule targeting CCR5; plerixafor, a small-molecule targeting CXCR4; and mogamulizumab, an anti-CCR4 antibody.<sup>76</sup>

### ***Intracellular binding site at Chemokine Receptors***

The recent X-ray structure of CCR2 in complex with an orthosteric antagonist and the negative allosteric modulator (NAM, Box 1) CCR2-RA-[R] (PDB 5T1A, **Chapter 3**),<sup>9</sup> and of CCR9 in complex with the NAM vercirnon (PDB 5LWE)<sup>10</sup> (Figure 2) have provided structural confirmation of such intracellular binding site in chemokine receptors. The two structures report an overlapping solvent-exposed binding site in the intracellular domain of these receptors, located more than 30 Å from the orthosteric binding site and enclosed by the intracellular ends of TM1 – TM3, TM6, TM7 and H8 (Figure 1a) (**Chapter 3**).<sup>9,10</sup> The NAMs bind this intracellular pocket where they interact with several conserved amino acid residues (Figure 1b).

Interestingly, before these crystal structures were solved, intracellular ligand binding sites had already been suggested for chemokine receptors. In 2008, a putative intracellular binding site for small-molecule compounds had been identified in CCR4, CCR5, CXCR1 and CXCR2.<sup>19,20</sup> Functional data from these studies suggested that a series of compounds required intracellular access in order to exert their activity. Specifically, for CCR4 it was shown that several compounds similar to compound 1 (Figure 2) exhibited a lack of correlation in their potencies when measured in membrane or cellular assays. However, after permeabilization of the cells with saponin the potencies became comparable in both assays.<sup>19</sup> In CXCR2, the loss of cellular potency seemed to be dependent on the lipophilicity (logD) of the compounds. Lower lipophilicities resulted in a greater loss of potency, indicating that these compounds needed a certain level of lipophilicity to cross the cell membrane and reach the intracellular binding site.<sup>20</sup> A subsequent chimeric approach, with CCR4-CCR5 or CXCR1-CXCR2 chimeras, led to the suggestion that the C terminus was part of the binding site for these molecules.<sup>19,20</sup> In CXCR2, this intracellular binding site was further mapped with help of homology modeling and mutational studies, which resulted in the identification of several C terminal residues as part of this allosteric binding site, including D84<sup>2x40</sup>, T83<sup>2x39</sup>, A249<sup>6x33</sup>, Y314<sup>7x53</sup>, and K320<sup>8x49</sup> (Figure 1b).<sup>20,21</sup> Thus, these studies in CCR4 and CXCR2 provided the first biochemical evidence of the existence of such binding sites.

Using a similar approach, a homologous binding site was discovered in CCR2, where small molecules such as CCR2-RA-[R], JNJ-27141491 and SD-24 can bind (Figure 2).<sup>22,23</sup> Similar key residues were identified, including V244<sup>6x36</sup>, K311<sup>8x49</sup>, Y305<sup>7x53</sup> and F312<sup>8x50</sup> (Figure 1B),<sup>22</sup> which have now been confirmed by the X-ray structure (**Chapter 3**).<sup>9</sup> A similar binding site has also been suggested in CX<sub>3</sub>CR1 after pharmacological characterization of compound AZD8797 (Figure 2), a non-competitive inhibitor of CX<sub>3</sub>CR1 with structural similarity to known CXCR2 intracellular ligands.<sup>24</sup> In addition, several pepducins derived from ICL1 of CXCR4 have been shown to interact selectively with CXCR4 in a non-competitive manner.<sup>25</sup>  
<sup>26</sup> Specifically, CXCR4 pepducin ATI-2341 has been predicted to interact with most of the

residues located in ICL1 – ICL3,<sup>27</sup> indicating that this receptor can also be targeted from the intracellular side. Finally, the structure of the viral chemokine receptor US28 in complex with the chemokine ligand CX3CL1 and the **nanobody** Nb7 shows that Nb7 binds in a similar subpocket composed by the intracellular ends of TM3, TM5, TM6 and H8. Moreover, Nb7 interacts with several residues also involved in the binding of small-molecules or pepducins in human chemokine receptors, or in interactions with signaling proteins.<sup>28,29</sup>

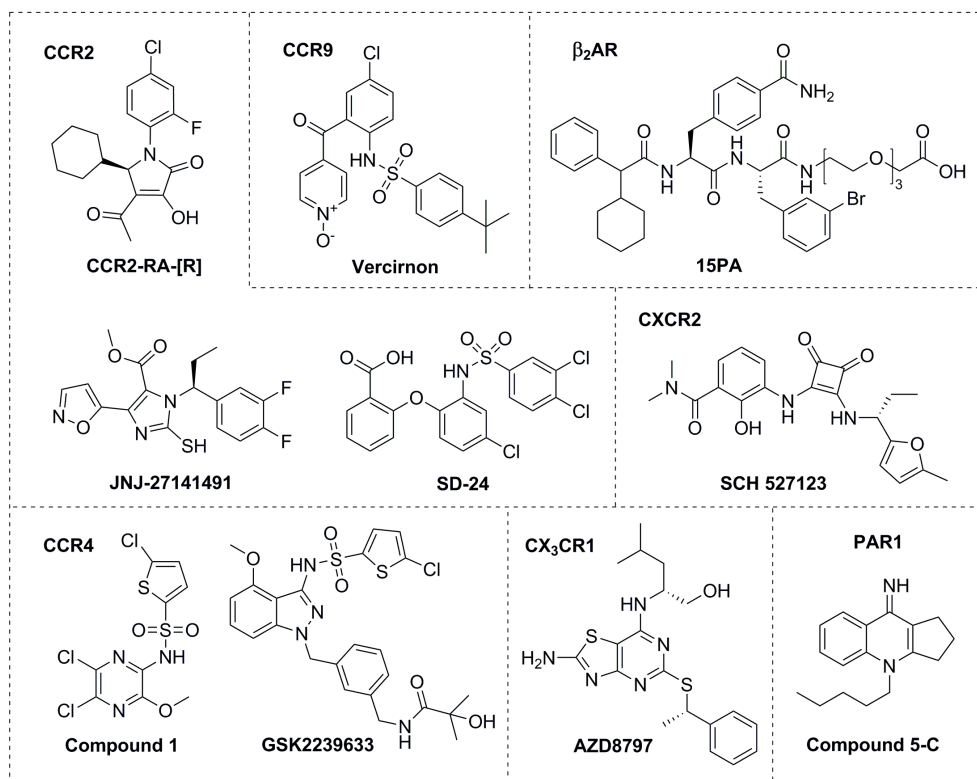


**Figure 2.** Chemical structures of selected intracellular small molecule ligands for different class A GPCRs. Upper row shows the chemical structures of cocrystallized intracellular ligands with their corresponding receptor: CCR2-RA-[R] with CCR2, Vercirnon with CCR9, and 15PA with  $\beta_2$ AR. Vercirnon, SCH 527123 and GSK2239633 are examples of intracellular ligands that have progressed to clinical trials.

### ***Intracellular binding site at other class A GPCRs***

This conserved intracellular binding site is not limited to chemokine receptors, as evidence for this site has been found in other class A GPCRs. In this regard, the crystal structure of  $\beta_2$ AR (PDB 5X7D) has been solved with the small-molecule ligand 15PA (Figure 2), a polyethylene glycol-carboxylic acid derivative of compound 15,<sup>30</sup> co-crystallized at the intracellular interface.<sup>11</sup> Compound 15PA binds in a pocket formed by the intracellular ends

of TM1, TM2, TM6, TM7, H8 and ICL1, where it interacts with key residues also identified in CCR2 and CCR9<sup>11</sup> (Figure 3). Moreover, this binding pocket partially overlaps with the binding site of nanobodies Nb60 and Nb80 in  $\beta_2$ AR,<sup>31, 32</sup> Fab2838 in Adenosine A<sub>2A</sub> receptor (A<sub>2A</sub>AR),<sup>33</sup> Nb9-8 in M2R<sup>34</sup> and Nb39 in the  $\mu$ -opioid receptor ( $\mu$ OR).<sup>35</sup> Previous to these crystal structures, different computational tools predicted intracellular binding pockets in rhodopsin and M2R.<sup>36,37</sup> Molecular docking studies and virtual screening identified several rhodopsin inhibitors that bind at the interface between the GPCR and G protein,<sup>38, 39</sup> in an intracellular pocket resembling that identified in chemokine receptors. More evidence for a generalized intracellular pocket comes from the proteinase activated receptor 1 (PAR1), where a series of small molecules such as compound 5-C (Figure 2) and ICL3-derived pepducins were shown to interact with residues located in TM7 and H8.<sup>40, 41</sup> Similar ICL-derived pepducins have also been developed for PAR2,<sup>42</sup> PAR4,<sup>43</sup> sphingosine-1-phosphate receptor 3 (S1P<sub>3</sub>)<sup>44</sup> and formylpeptide receptors 1 and 2 (FPR1 and FPR2).<sup>45</sup> Taken together, there is mounting evidence for the presence of a spatially conserved intracellular pocket, not only in chemokine receptors but among several class A GPCRs.

## Structural features of the intracellular binding site

The recent X-ray structures of CCR2 (**Chapter 3**),<sup>9</sup> CCR9<sup>10</sup> and  $\beta_2$ AR<sup>11</sup> are providing structural information on the features that determine binding and selectivity in this intracellular binding site (Figure 3, Key Figure). Moreover, these structures provide new opportunities for the application of structure-based drug design (SBDD) methods, such as virtual screening campaigns, which might allow the identification and/or optimization of novel intracellular ligands for these or other homologous receptors.<sup>5, 28</sup> Below, features of this site are discussed in terms of three component parts: a hydrophobic subpocket above H8, a central TM7-H8 binding region, and a region formed by TM3/6 and TM2/ICL1.

### ***Hydrophobic subpocket***

All ligands share a highly conserved hydrophobic subpocket above H8. Three highly conserved residues amongst class A GPCRs form the basis of this pocket: V<sup>1x53</sup> (65% conserved), Y<sup>7x53</sup> (89% conserved) and F<sup>8x50</sup> (65% conserved) (Figure 3, upper panel). While there is only some evidence for the role of V<sup>1x53</sup> in activation,<sup>46</sup> numerous publications have shown the role of the latter two residues in signaling and intracellular ligand binding at different GPCRs.<sup>14, 47, 48</sup> In terms of hydrophobicity, residues 1x56 and 1x57 are also highly conserved (Figure 3, upper panel). However, in CCR9 Y<sup>1x57</sup> adopts an orientation that further opens up the pocket, allowing the large 4-tert-butyl substituent of the ligand to reach deeper into this pocket, indicating a role in conferring ligand selectivity.

### Central TM7-H8 binding region

The central part of the pocket consists of the kink between H8 and TM7, formed by either P<sup>8x48</sup> ( $\beta_2$ AR) or G<sup>8x47</sup> (chemokine receptors). This subpocket includes residues 8x47 to 8x49, which are conserved in terms of polarity, and residue 6x36 (Figure 3, central panel). For chemokine receptors this kink allows ligands to interact with the backbone of residues K/R<sup>8x49</sup> and F<sup>8x50</sup>. In CCR2, the specific conformation of this subpocket allows the ligand to bind closer to H8, where the negatively charged oxygen of the ligand is also able to interact with the backbone of E<sup>8x48</sup>. In  $\beta_2$ AR, P<sup>8x48</sup> forces S<sup>8x47</sup> inwards, allowing it to interact with the oxygen of the amide in the ligand, while a second interaction is formed between the nitrogen of another amide and D<sup>8x49</sup>. Noteworthy is position 6x36 which is not strongly conserved (59% in terms of hydrophobicity) among GPCRs. This residue is key for ligand binding in both  $\beta_2$ AR and CCR2: in  $\beta_2$ AR, T<sup>6x36</sup> forms a hydrogen bond with an amide of 15PA; in CCR2, V<sup>6x36</sup> makes a hydrophobic interaction with the cyclohexyl substituent of the ligand. However, different effects have been reported upon mutation of this residue. While the mutation V<sup>6x36</sup>A abolished ligand binding in CCR2,<sup>22</sup> it increased the stability of CCR9, facilitating its crystallization. In CXCR4, a T<sup>6x36</sup>P mutation abolished signaling,<sup>49</sup> whereas M<sup>6x36</sup>T made the delta opioid receptor a constitutively active mutant (CAM).<sup>50</sup> Finally, in the Adenosine A<sub>2B</sub> receptor (A<sub>2B</sub>AR) this residue acts as a determinant for G protein selectivity,<sup>51</sup> indicating that this position might be crucial for target selectivity of intracellular ligands as well.

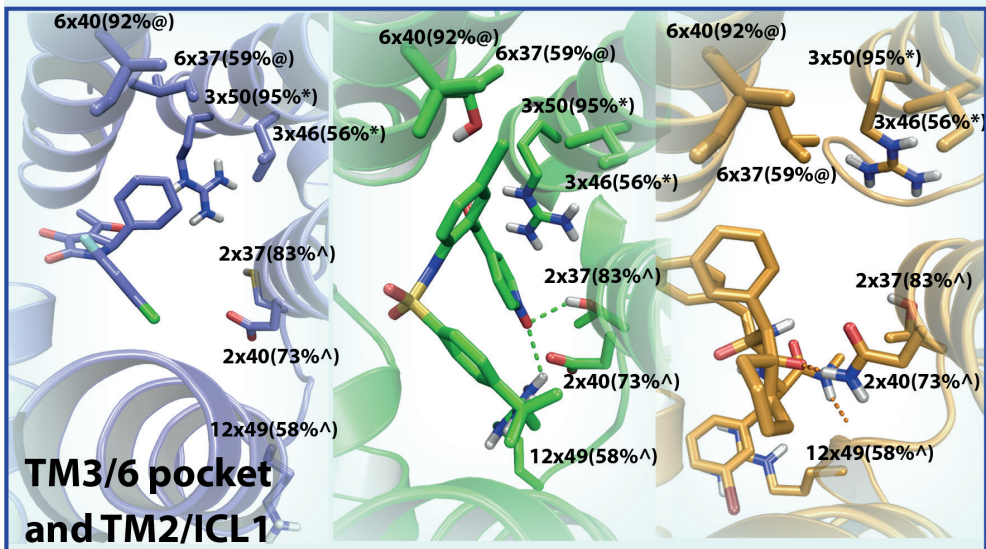
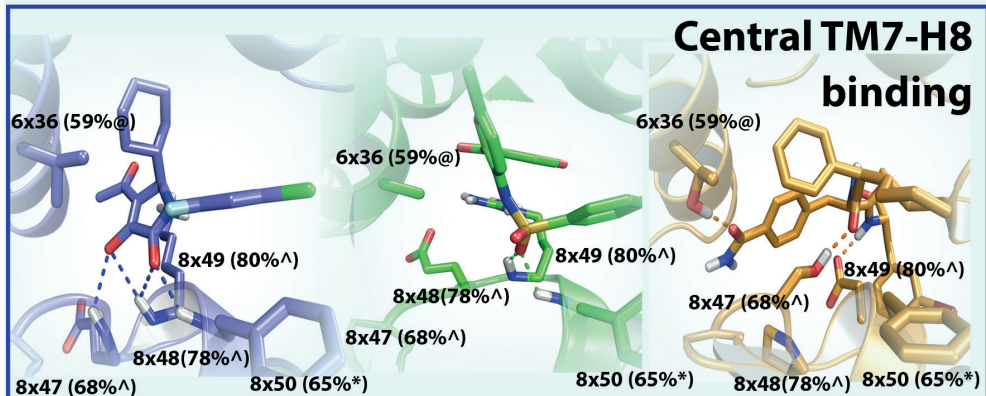
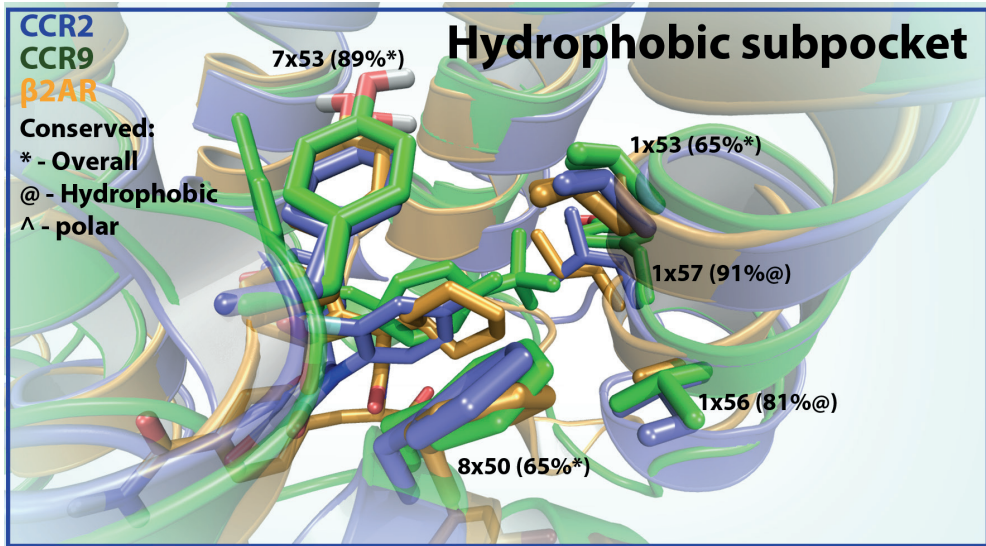
### Region formed by TM3/6 and TM2/ICL1

The largest differences are observed in this region of the binding site; residues found in TM3 include R<sup>3x50</sup> from the highly conserved DRY motif, and residue 6x40 conserved in terms of hydrophobicity (Figure 3, lower panel). Residue 6x37 seems to be important for selectivity, as exemplified by T<sup>6x37</sup> in CCR9 that allows the chloro substituent of vercirnon to go deeper into this pocket. Interestingly, mutation of this residue has been implicated in altered signaling<sup>51</sup> and improved stability of A<sub>2A</sub>AR to facilitate crystallization.<sup>52</sup> Polar residues found at the TM2/ICL1 interface interact with both the CCR9 and  $\beta_2$ AR ligand. For example, R<sup>12x49</sup> (ICL1) forms a cation-pi interaction with the  $\beta_2$ AR ligand while in CCR9 it interacts with both D<sup>2x40</sup> and the nitro group of the ligand. However, these polar residues do not interact with the CCR2 ligand, indicating a different binding mode.

---

**Figure 3. Overview of structural features of the intracellular binding site.** Common features in intracellular ligand binding derived from the crystal structures of CCR2 (PDB 5T1A), CCR9 (PDB 5LWE) and  $\beta_2$ AR (PDB 4XT1). Residues are numbered using structure-based Ballesteros-Weinstein numbers.<sup>15</sup> Residue conservation among all class A GPCRs is shown in the following way; residues that are overall conserved (identical) in class A (>50%) are shown first (\*); for residues that are not conserved we show how conserved they are in terms of polarity (^) or hydrophobicity (@). The three different boxes represent three different sections of the intracellular binding sites, in the upper panel all receptors are superimposed while in the lower two boxes the receptors are shown separately. CCR2 is colored blue, CCR9 is colored green and  $\beta_2$ AR is colored orange.





## Strategies for intracellular modulation

In general, three main strategies have been used to target the intracellular side of GPCRs so far: small molecules, pepducins and nanobodies or “intrabodies”.

### *Small molecules*

Small molecules currently account for the majority of drug types in clinical trials targeting GPCRs.<sup>1</sup> Although most of these small molecules are presumed to be orthosteric, the number of confirmed allosteric modulators targeting GPCRs is increasing in clinical trials.<sup>1</sup> In this regard, several intracellular small molecules have already been identified for a number of GPCRs, but few of these have progressed to clinical trials and none has made it to the market. The largest number of small-molecule intracellular ligands reported so far target chemokine receptors, including CCR2 (**Chapter 3**),<sup>9, 22</sup> CCR4,<sup>19, 53, 54</sup> CCR9,<sup>10</sup> CXCR1 and CXCR2.<sup>20, 21</sup> These intracellular ligands share similar chemical features such as the presence of acidic groups acting as hydrogen-bond acceptors when interacting with the target (Figure 2). A good balance of hydrophobic and polar residues make this binding site highly druggable, as described in a previous section (**Chapter 3**).<sup>9</sup> However, intracellular ligands must cross the cellular membrane in order to exert their effect; therefore attention must be paid to the overall physicochemical properties of these intracellular small molecules, such as lipophilicity and molecular weight to ensure good permeability. Most of these intracellular ligands have been found using a traditional medicinal-chemistry approach. However, in the case of the  $\beta_2$ AR, the co-crystallized compound 15PA (Figure 2) was derived from a novel  $\beta_2$ AR NAM (compound 15) identified in a screening campaign using DNA-encoded small-molecule libraries, suggesting a novel approach to discover intracellular modulators in GPCRs.<sup>30</sup>

One of the suggested intracellular ligands, the CCR2 antagonist CCX140-B from Chemocentryx (structure undisclosed),<sup>55</sup> has recently demonstrated positive results in a Phase II clinical trial in patients with type 2 diabetes and diabetic nephropathy.<sup>56</sup> The CCR9 intracellular antagonist, vercirnon (Figure 2),<sup>10</sup> also showed promising results in Phase II clinical trials in patients with Crohn’s disease;<sup>57</sup> however, it did not demonstrate clinical efficacy in the last Phase III study.<sup>58</sup> In case of CCR4, GlaxoSmithKline (GSK) has identified more than three different chemical scaffolds for intracellular antagonists—termed “site 2” antagonists by GSK.<sup>54</sup> Yet, only one of these ligands, GSK2239633 (Figure 2), progressed to Phase I clinical trials, before failing due to lack of efficacy.<sup>59</sup> Development of CXCR1-CXCR2 intracellular ligands such as SCH 527123 (Figure 2) has also resulted in several clinical trials for the treatment of chronic obstructive pulmonary disease (COPD) and asthma.<sup>60</sup> Although none of these ligands has been approved yet, this strategy has led to several clinical studies that



might ultimately lead to a new marketed therapeutic agent.

### ***Pepducins and Nanobodies***

Another strategy for intracellular targeting of GPCRs is the use of pepducins, peptides derived from the ICLs of the target receptor, or nanobodies. As the use and pharmacology of several pepducins<sup>61, 62</sup> and nanobodies<sup>63, 64</sup> have been recently reviewed elsewhere, we will only briefly discuss them here. The pepducin approach has been explored with several GPCRs, including CXCR1, CXCR2,<sup>65</sup> CXCR4,<sup>26, 66</sup> PAR1<sup>41</sup> and  $\beta_2$ AR.<sup>67</sup> Although in many cases pepducins have been employed as pharmacological tools, several *in vitro* and *in vivo* preclinical studies support the role of pepducins as therapeutic agents.<sup>62</sup> In the case of PAR1, a recent clinical trial involving pepducin PZ-128 demonstrated positive results in patients with coronary artery disease.<sup>68</sup> Finally, the intracellular domain can also be targeted with intracellular nanobodies or “intrabodies”, as exemplified by US28,<sup>29</sup>  $\beta_2$ AR,<sup>16, 31, 32, 69</sup> A<sub>2A</sub>AR,<sup>33</sup> M2R<sup>34</sup> and  $\mu$ OR.<sup>35</sup> Although most of these intrabodies have been used to aid GPCR crystallization and understand receptor function, their therapeutic potential has also been highlighted.<sup>70</sup>

## **Advantages and therapeutic implications of intracellular ligands**

As a consequence of their ability to bind to distinct sites on a GPCR, intracellular allosteric modulators can have unique properties compared to compounds that target the (orthosteric) binding site of endogenous ligands.<sup>8</sup> Some of these key properties include the modulation of affinity and/or efficacy of orthosteric ligands, improved selectivity, polypharmacology, or biased signaling (Box 1, Figure 4).

### ***Modulation of affinity and efficacy of orthosteric ligands***

In  $\beta_2$ AR, two allosteric intrabodies, a NAM and a PAM, were able to modulate the affinity of the orthosteric agonist isoprenaline by more than 15,000-fold, an unexpectedly large dynamic range (Figure 4a).<sup>32</sup> Although both intrabodies insert into the pocket where the G protein binds, they modulate the functional state of the receptor differently by engaging with other residues within the binding pocket. The impact of the PAM and NAM intrabodies on a panel of orthosteric ligands of different efficacies was also shown to be consistent with the presence of multiple receptor states. The concept of more than two functional states—inactive and active—may allow for finer control of functional responses than previously thought. In addition, the demonstrated ability of allosteric ligands to differentially modulate the activity of distinct orthosteric ligands (referred to as probe dependence) has important implications regarding the selectivity of drugs for receptors that are activated by multiple

ligands, as is the case for chemokine receptors. Intracellular NAMs of CCR2 and CCR9 are thought to function by directly inhibiting the interaction with intracellular signaling proteins, while at the same time blocking the outward motion of TM6 and the upward motion of TM3, required for receptor activation (**Chapter 3**).<sup>9,10</sup> By preventing G protein coupling and stabilizing an inactive state, they also presumably reduce the affinity of the endogenous agonists. In addition, intracellular NAMs inhibit the receptor in an insurmountable manner (Figure 4b). As previously demonstrated in CCR2, CCR2-RA-[R] was able to decrease the maximum effect of the endogenous chemokine CCL2, even at the highest CCL2 concentration tested.<sup>23</sup> Another advantage of allosteric over orthosteric inhibitors is their saturability or the so-called “ceiling effect”, which limits the allosteric activity to a certain level, despite further increments in the dose of the modulator.<sup>6-8</sup> Whether compounds targeting this site can be appropriately designed with the right level of saturability will become clear with more intracellular compounds in clinical studies.

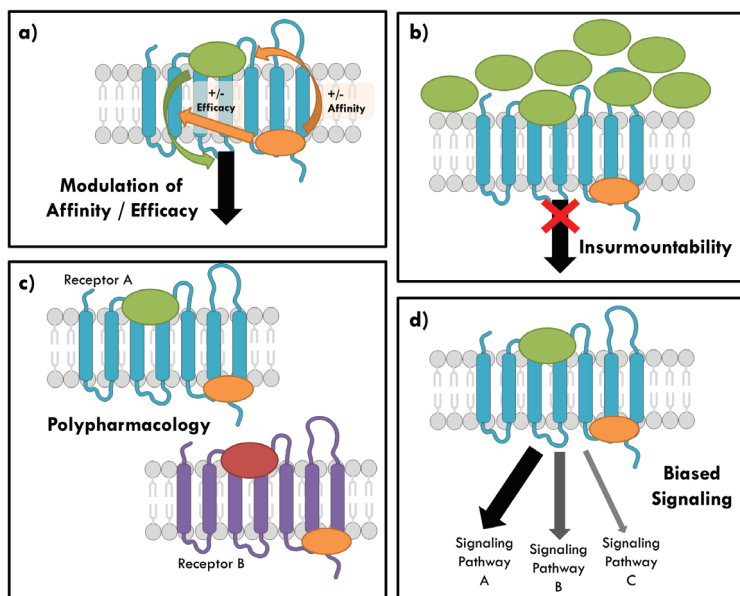


**Figure 4. Potential advantages of intracellular allosteric modulators.** (a) Intracellular allosteric modulators (small molecules, peptidics or intrabodies, shown in orange) have the potential to positively or negatively modulate the affinity and/or the efficacy of the endogenous ligand (shown in green or red) or any orthosteric ligand. The ultimate response depends on the level of positive or negative cooperativity between the two ligands. (b) Intracellular ligands can display insurmountability, as they can inhibit the receptor (shown in blue) even when high concentrations of endogenous ligand are present. (c) A highly-conserved intracellular binding site provides the possibility of designing intracellular ligands that bind and exert their effect in multiple receptors (receptor A in blue and receptor B in purple). These pharmacological ligands, as opposed to selective ligands, might be advantageous in diseases where more than one receptor is involved. (d) Intracellular ligands can also promote biased signaling, by preferentially modulating one signaling pathway over another upon activation by the endogenous ligand. For instance, they can stabilize G protein signaling over  $\beta$ -arrestin signaling. Source of cellular biology illustrations: Servier Medical Art by Servier, available from <https://smart.servier.com/>.

## ***Selectivity vs. Polypharmacology***

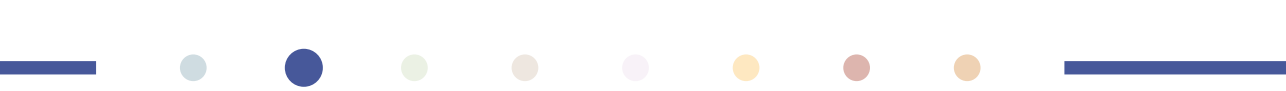
As this intracellular binding site is likely present in most chemokine receptors, it may be a useful site for simultaneously blocking multiple chemokine receptors in disease contexts where polypharmacology has been deemed useful (Figure 4c). This may hold true in multiple sclerosis or rheumatoid arthritis where multiple chemokine receptors have been found to play a role.<sup>71</sup> As allosteric modulators, pepducins may prove useful for polypharmacology because they are derived from the intracellular loops of GPCRs, which often display a high degree of sequence similarity amongst related receptors.<sup>61</sup> For example, the pepducin P4pal-10 was shown to inhibit diverse  $G_q$ -coupled receptors without affecting  $b_2AR$  ( $G_s$ ) or CXCR4 ( $G_i$ ) signaling.<sup>72</sup> Its broad spectrum inhibition profile was exploited to investigate the effect of blocking  $G_q$ -mediated signaling from a number of receptors for the treatment of asthma, which involves multiple GPCRs. On the other hand, intracellular allosteric antagonists exhibiting >100-fold selectivity for CXCR2 over CXCR1 have been discovered indicating that selectivity can also be achieved in this binding site.<sup>20</sup>

## ***Biased signaling***

Pepducins have also been shown to promote biased signaling of GPCRs. Biased signaling tends to involve preferential activation of G protein-dependent over G protein-independent signaling (e.g., via  $\beta$ -arrestin) or vice versa (Figure 4d). AT1-2341 is a pepducin derived from the ICL1 of CXCR4 that promotes specific  $G_i$ -mediated signaling without  $G_{13}$ -coupling or  $\beta$ -arrestin recruitment.<sup>66</sup> Similarly pepducin ICL3-9 derived from ICL3 of  $b_2AR$  showed  $G_s$ -biased signaling,<sup>67</sup> which may be advantageous for the treatment of asthma by limiting  $\beta$ -arrestin-mediated desensitization and potential tachyphylaxis from chronic use of  $\beta$ -agonists.<sup>73</sup>

## **Concluding remarks and Future perspectives**

There is now ample evidence from mutational, computational, and structural studies in class A GPCRs for novel allosteric binding pockets, located in close proximity to the G protein or  $\beta$ -arrestin binding site. This highly-conserved solvent-exposed intracellular pocket can be used to inhibit or modulate the receptor in an allosteric manner. Intracellular receptor modulation is not limited to small molecules, as intracellular pepducins and intrabodies have also been used to modulate GPCRs from the inside. These intracellular agents bring new pharmacological opportunities, but also new challenges including optimization of their selectivity profile, and their permeability properties to allow access to the inside of the cell and ultimately to cross the intestinal wall. These and other key issues have been



summarized in the *Outstanding Questions*. Although none of these intracellular agents is yet on the market, promising (pre)clinical results have been already reported, pointing to their clinical potential. Importantly, the recent crystal structures in complex with these ligands provide a detailed view of the intracellular pockets, allowing for a better understanding and a rational design of novel intracellular ligands to target these and other GPCRs in a wide variety of diseases.

### Outstanding Questions

This intracellular binding site has been suggested in most chemokine receptors and other class A GPCRs. As all GPCRs possess a G protein-binding site, is this site present in all class A GPCRs? And what about other GPCR families?

This intracellular binding site represents one of many uncovered binding pockets in GPCRs. For example, some binding pockets have been found with ligands binding outside the TM bundle within the lipid membrane. In this era of GPCR crystallography, how many other binding sites can we uncover? Are these pockets conserved among GPCR subfamilies or among GPCRs in general?

Intracellular ligands, including small molecules, pepducins and intrabodies, require intracellular access in order to exert their effect. Thus, drug design is key to ensure sufficient and effective cell permeability. How do we design them to achieve this? And if that is not possible, which delivery strategies can we use to increase drug permeability?

Although allosteric binding sites are generally thought as less conserved than orthosteric binding sites, the intracellular binding site present in CCR2 and CCR9 seems to be highly conserved among chemokine receptors. With such high conservation, selectivity remains a challenge. Can we achieve sufficient selectivity among highly-homologous receptors? Can the recent crystal structures help us to better understand drug target selectivity and to rationally design novel selective drugs?

As opposed to selectivity, polypharmacology has been proposed lately as a better approach in diseases in which more than one target is involved. An advantage of the high conservation of this intracellular binding site is that it allows for the development of such multi-target drugs. Is this approach feasible? Does this approach actually improve clinically efficacy? And what are the risks associated with such approach?

## REFERENCES

1. Hauser, A. S.; Attwood, M. M.; Rask-Andersen, M.; Schiöth, H. B.; Gloriam, D. E. Trends in GPCR drug discovery: new agents, targets and indications. *Nat Rev Drug Discov* **2017**, *16*, 829–842.
2. Harrison, R. K. Phase II and phase III failures: 2013–2015. *Nat Rev Drug Discov* **2016**, *15*, 817–818.
3. Venkatakrisnan, A. J.; Deupi, X.; Lebon, G.; Tate, C. G.; Schertler, G. F.; Babu, M. M. Molecular signatures of G-protein-coupled receptors. *Nature* **2013**, *494*, 185–194.
4. Koelink, P. J.; Overbeek, S. A.; Braber, S.; de Kruijf, P.; Folkerts, G.; Smit, M. J.; Kraneveld, A. D. Targeting chemokine receptors in chronic inflammatory diseases: an extensive review. *Pharmacol Ther* **2012**, *133*, 1–18.
5. Congreve, M.; Oswald, C.; Marshall, F. H. Applying structure-based drug design approaches to allosteric modulators of GPCRs. *Trends Pharmacol Sci* **2017**, *38*, 837–847.
6. Foster, D. J.; Conn, P. J. Allosteric Modulation of GPCRs: New Insights and Potential Utility for Treatment of Schizophrenia and Other CNS Disorders. *Neuron* **2017**, *94*, 431–446.
7. Christopoulos, A. Advances in G protein-coupled receptor allostery: from function to structure. *Mol. Pharmacol.* **2014**, *86*, 463–478.
8. Kenakin, T. P. Biased signalling and allosteric machines: new vistas and challenges for drug discovery. *Br J Pharmacol* **2012**, *165*, 1659–1669.
9. Zheng, Y.; Qin, L.; Ortiz Zacarías, N. V.; de Vries, H.; Han, G. W.; Gustavsson, M.; Dabros, M.; Zhao, C.; Cherney, R. J.; Carter, P.; Stamos, D.; Abagyan, R.; Cherezov, V.; Stevens, R. C.; Ilzerman, A. P.; Heitman, L. H.; Tebben, A.; Kufareva, I.; Handel, T. M. Structure of CC chemokine receptor 2 with orthosteric and allosteric antagonists. *Nature* **2016**, *540*, 458–461.
10. Oswald, C.; Rappas, M.; Kean, J.; Dore, A. S.; Errey, J. C.; Bennett, K.; Deflorian, F.; Christopher, J. A.; Jazayeri, A.; Mason, J. S.; Congreve, M.; Cooke, R. M.; Marshall, F. H. Intracellular allosteric antagonism of the CCR9 receptor. *Nature* **2016**, *540*, 462–465.
11. Liu, X.; Ahn, S.; Khsai, A. W.; Meng, K.-C.; Latorraca, N. R.; Pani, B.; Venkatakrisnan, A.; Masoudi, A.; Weis, W. I.; Dror, R. O.; Chen, X.; Lefkowitz, R. J.; Kobilka, B. K. Mechanism of intracellular allosteric  $\beta$ 2AR antagonist revealed by X-ray crystal structure. *Nature* **2017**, *548*, 480–484.
12. Lagerstrom, M. C.; Schiöth, H. B. Structural diversity of G protein-coupled receptors and significance for drug discovery. *Nat Rev Drug Discov* **2008**, *7*, 339–357.
13. Katritch, V.; Cherezov, V.; Stevens, R. C. Diversity and modularity of G protein-coupled receptor structures. *Trends Pharmacol. Sci.* **2012**, *33*, 17–27.
14. Venkatakrisnan, A. J.; Deupi, X.; Lebon, G.; Heydenreich, F. M.; Flock, T.; Miljuz, T.; Balaji, S.; Bouvier, M.; Vepintsev, D. B.; Tate, C. G.; Schertler, G. F. X.; Babu, M. M. Diverse activation pathways in class A GPCRs converge near the G-protein-coupling region. *Nature* **2016**, *536*, 484–487.
15. Isberg, V.; de Graaf, C.; Bortolato, A.; Cherezov, V.; Katritch, V.; Marshall, F. H.; Mordalski, S.; Pin, J.-P.; Stevens, R. C.; Vriend, G.; Gloriam, D. E. Generic GPCR residue numbers – aligning topology maps while minding the gaps. *Trends Pharmacol. Sci.* **2015**, *36*, 22–31.
16. Rasmussen, S. G. F.; DeVree, B. T.; Zou, Y.; Kruse, A. C.; Chung, K. Y.; Kobilka, T. S.; Thian, F. S.; Chae, P. S.; Pardon, E.; Calinski, D.; Mathiesen, J. M.; Shah, S. T. A.; Lyons, J. A.; Caffrey, M.; Gellman, S. H.; Steyaert, J.; Skiniotis, G.; Weis, W. I.; Sunahara, R. K.; Kobilka, B. K. Crystal structure of the  $\beta$ 2 adrenergic receptor-Gs protein complex. *Nature* **2011**, *477*, 549–555.
17. Moreira, I. S. Structural features of the G-protein/GPCR interactions. *Biochimica et Biophysica Acta (BBA) - General Subjects* **2014**, *1840*, 16–33.
18. Kang, Y.; Zhou, X. E.; Gao, X.; He, Y.; Liu, W.; Ishchenko, A.; Barty, A.; White, T. A.; Yefanov, O.; Han, G. W.; Xu, Q.; de Waal, P. W.; Ke, J.; Tan, M. H.; Zhang, C.; Moeller, A.; West, G. M.; Pascal, B. D.; Van Eps, N.; Caro, L. N.; Vishnivetskiy, S. A.; Lee, R. J.; Suino-Powell, K. M.; Gu, X.; Pal, K.; Ma, J.; Zhi, X.; Boutet, S.; Williams, G. J.; Messerschmidt, M.; Gati, C.; Zatsepin, N. A.; Wang, D.; James, D.; Basu, S.; Roy-Chowdhury, S.; Conrad, C. E.; Coe, J.; Liu, H.; Lisova, S.; Kupitz, C.; Grotjohann, I.; Fromme, R.; Jiang, Y.; Tan, M.; Yang, H.; Li, J.; Wang, M.;



- Zheng, Z.; Li, D.; Howe, N.; Zhao, Y.; Standfuss, J.; Diederichs, K.; Dong, Y.; Potter, C. S.; Carragher, B.; Caffrey, M.; Jiang, H.; Chapman, H. N.; Spence, J. C.; Fromme, P.; Weierstall, U.; Ernst, O. P.; Katritch, V.; Gurevich, V. V.; Griffin, P. R.; Hubbell, W. L.; Stevens, R. C.; Cherezov, V.; Melcher, K.; Xu, H. E. Crystal structure of rhodopsin bound to arrestin by femtosecond X-ray laser. *Nature* **2015**, *523*, 561-567.
19. Andrews, G.; Jones, C.; Wreggett, K. A. An intracellular allosteric site for a specific class of antagonists of the CC chemokine G protein-coupled receptors CCR4 and CCR5. *Mol. Pharmacol.* **2008**, *73*, 855-867.
  20. Nicholls, D. J.; Tomkinson, N. P.; Wiley, K. E.; Brammall, A.; Bowers, L.; Grahames, C.; Gaw, A.; Meghani, P.; Shelton, P.; Wright, T. J.; Mallinder, P. R. Identification of a putative intracellular allosteric antagonist binding-site in the CXC chemokine receptors 1 and 2. *Mol. Pharmacol.* **2008**, *74*, 1193-1202.
  21. Salchow, K.; Bond, M. E.; Evans, S. C.; Press, N. J.; Charlton, S. J.; Hunt, P. A.; Bradley, M. E. A common intracellular allosteric binding site for antagonists of the CXCR2 receptor. *Br J Pharmacol* **2010**, *159*, 1429-1439.
  22. Zweemer, A. J.; Bunnik, J.; Veenhuizen, M.; Miraglia, F.; Lenselink, E. B.; Vilums, M.; de Vries, H.; Gibert, A.; Thiele, S.; Rosenkilde, M. M.; IJzerman, A. P.; Heitman, L. H. Discovery and mapping of an intracellular antagonist binding site at the chemokine receptor CCR2. *Mol. Pharmacol.* **2014**, *86*, 358-368.
  23. Zweemer, A. J.; Nederpelt, I.; Vrieling, H.; Hafith, S.; Doornbos, M. L.; de Vries, H.; Abt, J.; Gross, R.; Stamos, D.; Saunders, J.; Smit, M. J.; IJzerman, A. P.; Heitman, L. H. Multiple binding sites for small-molecule antagonists at the CC chemokine receptor 2. *Mol. Pharmacol.* **2013**, *84*, 551-561.
  24. Cederblad, L.; Rosengren, B.; Ryberg, E.; Hermansson, N. O. AZD8797 is an allosteric non-competitive modulator of the human CX3CR1 receptor. *Biochem J.* **2016**, *473*, 641-649.
  25. Janz, J. M.; Ren, Y.; Looby, R.; Kazmi, M. A.; Sachdev, P.; Grunbeck, A.; Haggis, L.; Chinnapen, D.; Lin, A. Y.; Seibert, C.; McMurry, T.; Carlson, K. E.; Muir, T. W.; Hunt, S., 3rd; Sakmar, T. P. Direct interaction between an allosteric agonist pepducin and the chemokine receptor CXCR4. *J Am Chem Soc* **2011**, *133*, 15878-158881.
  26. Tchernychev, B.; Ren, Y.; Sachdev, P.; Janz, J. M.; Haggis, L.; O'Shea, A.; McBride, E.; Looby, R.; Deng, Q.; McMurry, T.; Kazmi, M. A.; Sakmar, T. P.; Hunt, S., 3rd; Carlson, K. E. Discovery of a CXCR4 agonist pepducin that mobilizes bone marrow hematopoietic cells. *Proc. Natl. Acad. Sci. U. S. A.* **2010**, *107*, 22255-22259.
  27. Planesas, J. M.; Perez-Nueno, V. I.; Borrell, J. I.; Teixido, J. Studying the binding interactions of allosteric agonists and antagonists of the CXCR4 receptor. *J Mol Graph Model* **2015**, *60*, 1-14.
  28. Arimont, M.; Sun, S. L.; Leurs, R.; Smit, M.; de Esch, I. J.; de Graaf, C. Structural analysis of chemokine receptor-ligand interactions. *J. Med. Chem.* **2017**, *60*, 4735-4779.
  29. Burg, J. S.; Ingram, J. R.; Venkatakrishnan, A. J.; Jude, K. M.; Dukkupati, A.; Feinberg, E. N.; Angelini, A.; Waghay, D.; Dror, R. O.; Ploegh, H. L.; Garcia, K. C. Structural basis for chemokine recognition and activation of a viral G protein-coupled receptor. *Science* **2015**, *347*, 1113-1117.
  30. Ahn, S.; Kahsai, A. W.; Pani, B.; Wang, Q. T.; Zhao, S.; Wall, A. L.; Strachan, R. T.; Staus, D. P.; Wingler, L. M.; Sun, L. D.; Sinnaeve, J.; Choi, M.; Cho, T.; Xu, T. T.; Hansen, G. M.; Burnett, M. B.; Lamerdin, J. E.; Bassoni, D. L.; Gavino, B. J.; Husemoen, G.; Olsen, E. K.; Franch, T.; Costanzi, S.; Chen, X.; Lefkowitz, R. J. Allosteric "beta-blocker" isolated from a DNA-encoded small molecule library. *Proc. Natl. Acad. Sci. U. S. A.* **2017**, *114*, 1708-1713.
  31. Rasmussen, S. G.; Choi, H. J.; Fung, J. J.; Pardon, E.; Casarosa, P.; Chae, P. S.; Devree, B. T.; Rosenbaum, D. M.; Thian, F. S.; Kobilka, T. S.; Schnapp, A.; Konetzki, I.; Sunahara, R. K.; Gellman, S. H.; Pautsch, A.; Steyaert, J.; Weis, W. I.; Kobilka, B. K. Structure of a nanobody-stabilized active state of the beta(2) adrenoceptor. *Nature* **2011**, *469*, 175-180.
  32. Staus, D. P.; Strachan, R. T.; Manglik, A.; Pani, B.; Kahsai, A. W.; Kim, T. H.; Wingler, L. M.; Ahn, S.; Chatterjee, A.; Masoudi, A.; Kruse, A. C.; Pardon, E.; Steyaert, J.; Weis, W. I.; Prosser, R. S.; Kobilka, B. K.; Costa, T.; Lefkowitz, R. J. Allosteric nanobodies reveal the dynamic range and diverse mechanisms of G-protein-coupled receptor activation. *Nature* **2016**, *535*, 448-452.
  33. Hino, T.; Arakawa, T.; Iwanari, H.; Yurugi-Kobayashi, T.; Ikeda-Suno, C.; Nakada-Nakura, Y.; Kusano-Arai, O.; Weyand, S.; Shimamura, T.; Nomura, N.; Cameron, A. D.; Kobayashi, T.; Hamakubo, T.; Iwata, S.; Murata, T. G-protein-coupled receptor inactivation by an allosteric inverse-agonist antibody. *Nature* **2012**, *482*, 237-240.

34. Kruse, A. C.; Ring, A. M.; Manglik, A.; Hu, J.; Hu, K.; Eitel, K.; Hubner, H.; Pardon, E.; Valant, C.; Sexton, P. M.; Christopoulos, A.; Felder, C. C.; Gmeiner, P.; Steyaert, J.; Weis, W. I.; Garcia, K. C.; Wess, J.; Kobilka, B. K. Activation and allosteric modulation of a muscarinic acetylcholine receptor. *Nature* **2013**, 504, 101-106.
35. Huang, W.; Manglik, A.; Venkatakrisnan, A. J.; Laeremans, T.; Feinberg, E. N.; Sanborn, A. L.; Kato, H. E.; Livingston, K. E.; Thorsen, T. S.; Kling, R. C.; Granier, S.; Gmeiner, P.; Husbands, S. M.; Traynor, J. R.; Weis, W. I.; Steyaert, J.; Dror, R. O.; Kobilka, B. K. Structural insights into  $\mu$ -opioid receptor activation. *Nature* **2015**, 524, 315-321.
36. Miao, Y.; Nichols, S. E.; McCammon, J. A. Mapping of allosteric druggable sites in activation-associated conformers of the M2 muscarinic receptor. *Chem Biol Drug Des* **2014**, 83, 237-246.
37. Yanamala, N.; Klein-Seetharaman, J. Allosteric Modulation of G Protein Coupled Receptors by Cytoplasmic, Transmembrane and Extracellular Ligands. *Pharmaceuticals (Basel)* **2010**, 3, 3324-3342.
38. Taylor, C. M.; Barda, Y.; Kisselev, O. G.; Marshall, G. R. Modulating G-protein coupled receptor/G-protein signal transduction by small molecules suggested by virtual screening. *J. Med. Chem.* **2008**, 51, 5297-5303.
39. Yanamala, N.; Tirupula, K. C.; Balem, F.; Klein-Seetharaman, J. pH-dependent interaction of rhodopsin with cyanidin-3-glucoside. 1. Structural aspects. *Photochem Photobiol* **2009**, 85, 454-462.
40. Dowal, L.; Sim, D. S.; Dilks, J. R.; Blair, P.; Beaudry, S.; Denker, B. M.; Koukos, G.; Kuliopulos, A.; Flaumenhaft, R. Identification of an antithrombotic allosteric modulator that acts through helix 8 of PAR1. *Proc. Natl. Acad. Sci. U. S. A.* **2011**, 108, 2951-2956.
41. Zhang, P.; Leger, A. J.; Baleja, J. D.; Rana, R.; Corlin, T.; Nguyen, N.; Koukos, G.; Bohm, A.; Covic, L.; Kuliopulos, A. Allosteric Activation of a G Protein-coupled Receptor with Cell-penetrating Receptor Mimetics. *J Biol Chem* **2015**, 290, 15785-15798.
42. Sevigny, L. M.; Zhang, P.; Bohm, A.; Lazarides, K.; Perides, G.; Covic, L.; Kuliopulos, A. Interdicting protease-activated receptor-2-driven inflammation with cell-penetrating pepducins. *Proc. Natl. Acad. Sci. U. S. A.* **2011**, 108, 8491-8496.
43. Covic, L.; Misra, M.; Badar, J.; Singh, C.; Kuliopulos, A. Pepducin-based intervention of thrombin-receptor signaling and systemic platelet activation. *Nat. Med.* **2002**, 8, 1161-1165.
44. Severino, B.; Incisivo, G. M.; Fiorino, F.; Bertolino, A.; Frecentese, F.; Barbato, F.; Manganello, S.; Maggioni, G.; Capasso, D.; Caliendo, G.; Santagada, V.; Sorrentino, R.; Roviezzo, F.; Perissutti, E. Identification of a pepducin acting as S1P3 receptor antagonist. *J Pept Sci* **2013**, 19, 717-724.
45. Winther, M.; Gabl, M.; Oprea, T. I.; Jonsson, B.; Boulay, F.; Bylund, J.; Dahlgren, C.; Forsman, H. Antibacterial activity of pepducins, allosterical modulators of formyl peptide receptor signaling. *Antimicrob Agents Chemother* **2014**, 58, 2985-2988.
46. Naville, D.; Barjhoux, L.; Jaillard, C.; Faury, D.; Despert, F.; Esteve, B.; Durand, P.; Saez, J. M.; Begeot, M. Demonstration by transfection studies that mutations in the adrenocorticotropin receptor gene are one cause of the hereditary syndrome of glucocorticoid deficiency. *J Clin Endocrinol Metab.* **1996**, 81, 1442-1448.
47. Chen, A.; Gao, Z.-G.; Barak, D.; Liang, B. T.; Jacobson, K. A. Constitutive Activation of A3 Adenosine Receptors by Site-Directed Mutagenesis. *Biochem Biophys Res Commun.* **2001**, 284, 596-601.
48. Sun, Y.; Hu, W.; Yu, X.; Liu, Z.; Tarran, R.; Ravid, K.; Huang, P. Actinin-1 binds to the C-terminus of A<sub>2B</sub> adenosine receptor (A<sub>2B</sub>AR) and enhances A<sub>2B</sub>AR cell-surface expression. *Biochem J.* **2016**, 473, 2179-2186.
49. Wu, B.; Chien, E. Y. T.; Mol, C. D.; Fenalti, G.; Liu, W.; Katritch, V.; Abagyan, R.; Brooun, A.; Wells, P.; Bi, F. C.; Hamel, D. J.; Kuhn, P.; Handel, T. M.; Cherezov, V.; Stevens, R. C. Structures of the CXCR4 chemokine GPCR with small-molecule and cyclic peptide antagonists. *Science* **2010**, 330, 1066-1071.
50. Tryoen-Tóth, P.; Décaillot, F. M.; Filliol, D.; Befort, K.; Lazarus, L. H.; Schiller, P. W.; Schmidhammer, H.; Kieffer, B. L. Inverse Agonism and Neutral Antagonism at Wild-Type and Constitutively Active Mutant Delta Opioid Receptors. *J. Pharmacol. Exp. Ther.* **2005**, 313, 410-421.
51. Liu, R.; Groenewoud, N. J. A.; Peeters, M. C.; Lenselink, E. B.; Uzman, A. P. A yeast screening method to decipher the interaction between the adenosine A2B receptor and the C-terminus of different G protein  $\alpha$ -subunits. *Purinergic Signal.* **2014**, 10, 441-453.



52. Doré, Andrew S.; Robertson, N.; Errey, James C.; Ng, I.; Hollenstein, K.; Tehan, B.; Hurrell, E.; Bennett, K.; Congreve, M.; Magnani, F.; Tate, Christopher G.; Weir, M.; Marshall, Fiona H. Structure of the Adenosine A2A Receptor in Complex with ZM241385 and the Xanthines XAC and Caffeine. *Structure* **2011**, *19*, 1283-1293.
53. Slack, R. J.; Russell, L. J.; Barton, N. P.; Weston, C.; Nalesso, G.; Thompson, S. A.; Allen, M.; Chen, Y. H.; Barnes, A.; Hodgson, S. T.; Hall, D. A. Antagonism of human CC-chemokine receptor 4 can be achieved through three distinct binding sites on the receptor. *Pharmacol Res Perspect* **2013**, *1*, e00019.
54. Miah, A. H.; Champigny, A. C.; Graves, R. H.; Hodgson, S. T.; Percy, J. M.; Procopiou, P. A. Identification of pyrazolopyrimidine arylsulfonamides as CC-chemokine receptor 4 (CCR4) antagonists. *Bioorg Med Chem* **2017**, *25*, 5327-5340.
55. Carter, P. H. Progress in the discovery of CC chemokine receptor 2 antagonists, 2009 – 2012. *Expert Opin. Ther. Pat.* **2013**, *23*, 549-568.
56. de Zeeuw, D.; Bekker, P.; Henkel, E.; Hasslacher, C.; Gouni-Berthold, I.; Mehling, H.; Potarca, A.; Tesar, V.; Heerspink, H. J.; Schall, T. J. The effect of CCR2 inhibitor CCX140-B on residual albuminuria in patients with type 2 diabetes and nephropathy: a randomised trial. *Lancet Diabetes Endocrinol.* **2015**, *3*, 687-696.
57. Keshav, S.; Vaňásek, T.; Niv, Y.; Petryka, R.; Howaldt, S.; Bafutto, M.; Rác, I.; Hetzel, D.; Nielsen, O. H.; Vermeire, S. A randomized controlled trial of the efficacy and safety of CCX282-B, an orally-administered blocker of chemokine receptor CCR9, for patients with Crohn's disease. *PLoS One* **2013**, *8*, e60094.
58. Feagan, B.; Sandborn, W.; D'Haens, G.; Lee, S.; Allez, M.; Fedorak, R.; Seidler, U.; Vermeire, S.; Lawrance, I.; Maroney, A. Randomised clinical trial: vécirnon, an oral CCR9 antagonist, vs. placebo as induction therapy in active Crohn's disease. *Aliment Pharmacol Ther.* **2015**, *42*, 1170-1181.
59. Cahn, A.; Hodgson, S.; Wilson, R.; Robertson, J.; Watson, J.; Beerah, M.; Hughes, S. C.; Young, G.; Graves, R.; Hall, D. Safety, tolerability, pharmacokinetics and pharmacodynamics of GSK2239633, a CC-chemokine receptor 4 antagonist, in healthy male subjects: results from an open-label and from a randomised study. *BMC Pharmacol Toxicol.* **2013**, *14*, 14.
60. Dwyer, M. P.; Yu, Y. CXCR2 modulators: a patent review (2009–2013). *Expert Opin. Ther. Pat.* **2014**, *24*, 519-534.
61. Carr, R., 3rd; Benovic, J. L. From biased signalling to polypharmacology: unlocking unique intracellular signalling using pepducins. *Biochem Soc Trans* **2016**, *44*, 555-561.
62. Zhang, P.; Covic, L.; Kuliopulos, A. Pepducins and other lipidated peptides as mechanistic probes and therapeutics. In *Cell-Penetrating Peptides: Methods in Molecular Biology*, Langel, Ü., Ed. Human Press: New York, NY, 2015; Vol. 1324, pp 191-203.
63. Mujic-Delic, A.; de Wit, R. H.; Verkaar, F.; Smit, M. J. GPCR-targeting nanobodies: attractive research tools, diagnostics, and therapeutics. *Trends Pharmacol Sci* **2014**, *35*, 247-255.
64. Manglik, A.; Kobilka, B. K.; Steyaert, J. Nanobodies to Study G Protein-Coupled Receptor Structure and Function. *Annu Rev Pharmacol Toxicol.* **2017**, *57*, 19-37.
65. Kaneider, N. C.; Agarwal, A.; Leger, A. J.; Kuliopulos, A. Reversing systemic inflammatory response syndrome with chemokine receptor pepducins. *Nat. Med.* **2005**, *11*, 661-665.
66. Quoyer, J.; Janz, J. M.; Luo, J.; Ren, Y.; Armando, S.; Lukashova, V.; Benovic, J. L.; Carlson, K. E.; Hunt, S. W., 3rd; Bouvier, M. Pepducin targeting the C-X-C chemokine receptor type 4 acts as a biased agonist favoring activation of the inhibitory G protein. *Proc. Natl. Acad. Sci. U. S. A.* **2013**, *110*, E5088-97.
67. Carr, R., 3rd; Du, Y.; Quoyer, J.; Panettieri, R. A., Jr.; Janz, J. M.; Bouvier, M.; Kobilka, B. K.; Benovic, J. L. Development and characterization of pepducins as Gs-biased allosteric agonists. *J Biol Chem* **2014**, *289*, 35668-36684.
68. Gurbel, P. A.; Bliden, K. P.; Turner, S. E.; Tantry, U. S.; Gesheff, M. G.; Barr, T. P.; Covic, L.; Kuliopulos, A. Cell-penetrating pepducin therapy targeting PAR1 in subjects with coronary artery disease. *Arterioscler. Thromb. Vasc. Biol.* **2016**, *36*, 189-197.
69. Staus, D. P.; Wingler, L. M.; Strachan, R. T.; Rasmussen, S. G.; Pardon, E.; Ahn, S.; Steyaert, J.; Kobilka, B. K.; Lefkowitz, R. J. Regulation of beta2-adrenergic receptor function by conformationally selective single-domain intrabodies. *Mol. Pharmacol.* **2014**, *85*, 472-481.



70. Shukla, A. K. Biasing GPCR signaling from inside. *Sci Signal*. **2014**, 7, pe3.
71. Horuk, R. Chemokine receptor antagonists: overcoming developmental hurdles. *Nat Rev Drug Discov* **2009**, 8, 23-33.
72. Carr, R., 3rd; Koziol-White, C.; Zhang, J.; Lam, H.; An, S. S.; Tall, G. G.; Panettieri, R. A., Jr.; Benovic, J. L. Interdicting Gq Activation in Airway Disease by Receptor-Dependent and Receptor-Independent Mechanisms. *Mol. Pharmacol.* **2016**, 89, 94-104.
73. Whalen, E. J.; Rajagopal, S.; Lefkowitz, R. J. Therapeutic potential of beta-arrestin- and G protein-biased agonists. *Trends Mol Med* **2011**, 17, 126-139.
74. Bartuzi, D.; Kaczor, A. A.; Matosiuk, D. Signaling within Allosteric Machines: Signal Transmission Pathways Inside G Protein-Coupled Receptors. *Molecules* **2017**, 22.
75. Müller, C. E.; Schiedel, A. C.; Baqi, Y. Allosteric modulators of rhodopsin-like G protein-coupled receptors: Opportunities in drug development. *Pharmacol Ther.* **2012**, 135, 292-315.
76. Bachelier, F.; Ben-Baruch, A.; Burkhardt, A. M.; Combadiere, C.; Farber, J. M.; Graham, G. J.; Horuk, R.; Sparre-Ulrich, A. H.; Locati, M.; Luster, A. D.; Mantovani, A.; Matsushima, K.; Murphy, P. M.; Nibbs, R.; Nomiyama, H.; Power, C. A.; Proudfoot, A. E.; Rosenkilde, M. M.; Rot, A.; Sozzani, S.; Thelen, M.; Yoshie, O.; Zlotnik, A. International union of basic and clinical pharmacology. LXXXIX. Update on the extended family of chemokine receptors and introducing a new nomenclature for atypical chemokine receptors. *Pharmacol. Rev.* **2014**, 66, 1-79.
77. Griffith, J. W.; Sokol, C. L.; Luster, A. D. Chemokines and chemokine receptors: positioning cells for host defense and immunity. *Annu Rev Immunol* **2014**, 32, 659-702.
78. Lopez-Cotarelo, P.; Gomez-Moreira, C.; Criado-Garcia, O.; Sanchez, L.; Rodriguez-Fernandez, J. L. Beyond chemoattraction: multifunctionality of chemokine receptors in leukocytes. *Trends Immunol* **2017**, 38, 927 - 941.
79. Schall, T. J.; Proudfoot, A. E. Overcoming hurdles in developing successful drugs targeting chemokine receptors. *Nat Rev Immunol* **2011**, 11, 355-363.
80. Zweemer, A. J.; Toraskar, J.; Heitman, L. H.; IJzerman, A. P. Bias in chemokine receptor signalling. *Trends Immunol* **2014**, 35, 243-252.
81. Viola, A.; Luster, A. D. Chemokines and their receptors: drug targets in immunity and inflammation. *Annu Rev Pharmacol Toxicol.* **2008**, 48, 171-197.



## Chapter 3

---

# Structure of CC Chemokine Receptor 2 with Orthosteric and Allosteric Antagonists



*Yi Zheng, Ling Qin, Natalia V. Ortiz Zacarías, Henk de Vries, Gye Won Han, Martin Gustavsson, Marta Dabros, Chunxia Zhao, Robert Cherney, Percy Carter, Dean Stamos, Ruben Abagyan, Vadim Cherezov, Raymond C. Stevens, Adriaan P. IJzerman, Laura H. Heitman, Andrew Tebben, Irina Kufareva, Tracy M. Handel*

*Nature 2016, 540 (7633): 458-461*



## ABSTRACT

CC chemokine receptor 2 (CCR2) is one of 19 members of the chemokine receptor subfamily of human Class A G protein-coupled receptors. CCR2 is expressed on monocytes, immature dendritic cells and T cell subpopulations, and mediates their migration towards endogenous CC chemokine ligands such as CCL2.<sup>1</sup> CCR2 and its ligands are implicated in numerous inflammatory and neurodegenerative diseases<sup>2</sup> including atherosclerosis, multiple sclerosis, asthma, neuropathic pain, and diabetic nephropathy, as well as in cancer.<sup>3</sup> These disease associations have motivated numerous preclinical studies and clinical trials<sup>4</sup> (see ClinicalTrials.gov) in search of therapies that target the CCR2-chemokine axis. To aid drug discovery efforts,<sup>5</sup> here we solve a structure of CCR2 in a ternary complex with an orthosteric (BMS-681<sup>6</sup>) and allosteric (CCR2-RA-[R]<sup>7</sup>) antagonist. BMS-681 inhibits chemokine binding by occupying the orthosteric pocket of the receptor in a previously unseen binding mode. CCR2-RA-[R] binds in a novel, highly druggable pocket that is the most intracellular allosteric site observed in Class A G protein-coupled receptors so far; this site spatially overlaps the G protein-binding site in homologous receptors. CCR2-RA-[R] inhibits CCR2 non-competitively by blocking activation-associated conformational changes and formation of the G protein-binding interface. The conformational signature of the conserved microswitch residues observed in double-antagonist-bound CCR2 resembles the most inactive G protein-coupled receptor structures solved so far. Like other protein-protein interactions, receptor-chemokine complexes are considered challenging therapeutic targets for small molecules, and the present structure suggests diverse pocket epitopes that can be exploited to overcome obstacles in drug design.

## RESULTS AND DISCUSSION

A ternary complex between an engineered construct of human CCR2 isoform b (further referred to as CCR2-T4L or simply CCR2), an orthosteric antagonist BMS-681 (compound 13b in Carter *et al.*<sup>6</sup>), and an allosteric antagonist CCR2-RA-[R]<sup>7</sup> was crystallized using the lipidic cubic phase (LCP) method,<sup>8</sup> and the structure was determined to 2.8 Å resolution (Table S1 and Figure S1). Simultaneous addition of two compounds markedly stabilized detergent-solubilized CCR2-T4L compared with twice the concentration of each compound individually (Figure 1a), suggesting concurrent binding of CCR2-RA-[R] and BMS-681 to the receptor. The presence of both compounds was critical for crystallization.

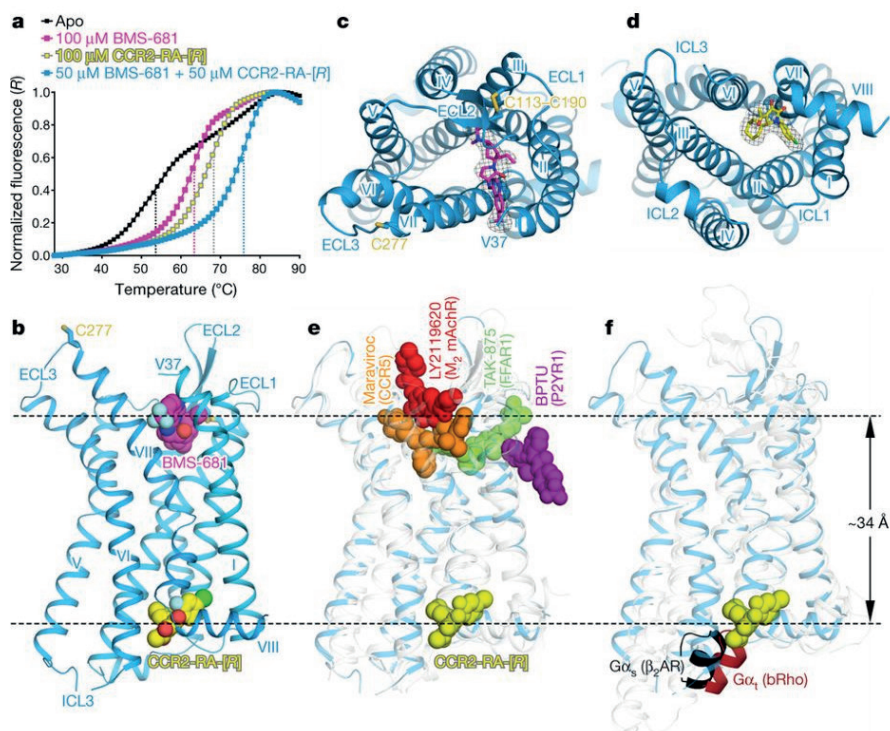
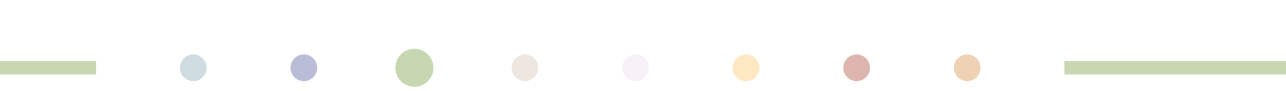


**Figure 1. Structure of a complex between CCR2, BMS-681 and CCR2-RA-[R] and comparison with other allosteric modulators of class A GPCRs.** (a) Thermal denaturation curves demonstrate higher stability of CCR2-T4L in the presence of both BMS-681 and CCR2-RA-[R] compared with each compound individually. Data are representative of three independent experiments conducted on different days. (b) Overall view of double-antagonist-bound CCR2. (c, d) Structure viewed from the extracellular (c) and intracellular (d) side with simulated annealing omit maps of BMS-681 (c) and CCR2-RA-[R] (d) shown at 3 $\sigma$ . (e) CCR2-RA-[R] compared to other allosteric ligands crystallized with Class A GPCRs (PDB accession numbers 4MBS, 4XNV, 4PHU, and 4MQT). (f) CCR2-RA-[R] compared with the carboxy (C)-terminal helix of G $\alpha_s$  bound to the  $\beta_2$ -adrenergic receptor and transducin peptide bound to rhodopsin (PDB accession numbers 3SN6 and 4X1H).



In the structure, CCR2 adopts the canonical fold of class A G protein-coupled receptors (GPCRs) with seven transmembrane (TM) helices connected by three extracellular (EC) and three intracellular (IC) loops (Figure 1b). Both compounds are visible in the electron density (Figures 1b-d); BMS-681 binds in the extracellular orthosteric pocket (Figures 1b,c) while CCR2-RA-[R] is located more than 30Å away (Figures 1b,d), in a site that is the most intracellular allosteric pocket observed in class A GPCRs so far (Figure 1e). The binding site of CCR2-RA-[R] spatially overlaps with the G protein-binding site in homologous receptors (Figure 1f). As for other chemokine receptors,<sup>9-12</sup> CCR2 is expected to have two conserved disulfide bonds in its extracellular domains, with Cys32-Cys277 connecting the amino (N) terminus to ECL3 (NT-ECL3), and Cys113-Cys190 connecting TM3 to ECL2. Electron density is apparent for the ECL2-TM3 disulfide bond but not for the N-terminal residues 1-36 or the NT-ECL3 disulfide bond (Figures 1b,c). Because the NT-ECL3 disulfide bond has been shown to be important for CCR2 signaling,<sup>13</sup> its absence is unlikely to be an inherent feature of the receptor; instead, it might be caused by strain of the bond in the ligand-bound state of the receptor,<sup>14</sup> possibly exacerbated by solvent exposure and radiation damage of the crystals.<sup>15</sup>

As with other chemokine receptors, the extracellular orthosteric pocket of CCR2 can be divided into a major and a minor subpocket, defined by helices III-VII and helices I-III and VII, respectively, and separated by residues Y120<sup>3,32</sup> and E291<sup>7,39</sup> (superscript indicates residue number according to Ballesteros-Weinstein nomenclature). BMS-681 binds predominantly in the minor subpocket (Figures 2a,b) and buries 366.3 Å<sup>2</sup> of surface area. The 6-trifluoromethyl quinazoline moiety protrudes between helices I and VII towards the lipid bilayer, while the tri-substituted cyclohexane packs against W98<sup>2,60</sup>. The  $\gamma$ -lactam secondary exocyclic amine forms a hydrogen bond with the hydroxyl of T292<sup>7,40</sup>, which is critical for binding of chemically related compounds such as BMS-558 (compound 22 in Cherney *et al.*<sup>16</sup>) and the Teijin lead series.<sup>17, 18</sup> This amine is also within hydrogen-bonding distance from the backbone carbonyl of Q288<sup>7,36</sup>. The carbonyl oxygen of the  $\gamma$ -lactam forms a hydrogen bond with Y49<sup>1,39</sup>, which itself is hydrogen-bonded to the side chain of T292<sup>7,40</sup>. The N1 nitrogen of the quinazoline is within 4 Å of the Q288<sup>7,36</sup> side chain. The protonated tertiary amine on the cyclohexane ring is proximal to a structured water molecule in the binding site. Some CCR2 antagonists, particularly those containing a basic amine, are known to depend on the conserved E291<sup>7,39</sup> in the receptor;<sup>19</sup> however, no direct interaction is observed between E291<sup>7,39</sup> and BMS-681. The receptor-bound, bioactive conformation of BMS-681 is strikingly similar to the crystallographic conformation of free BMS-681 (Figure 2c, Table S2), suggesting the absence of internal strain in the bound state.

BMS-681 engages several residues that are critical for CCL2 binding and/or activation of CCR2<sup>17, 18</sup> including Y49<sup>1,39</sup>, W98<sup>2,60</sup>, Y120<sup>3,32</sup>, and T292<sup>7,40</sup>. Thus, it seems to directly compete with chemokine binding to the orthosteric pocket. Additionally, by inserting between

helices I and VII, BMS-681 may put strain onto residues C32-V37 connecting TM1 to ECL3, destabilize the conserved NT-ECL3 disulfide bond (absent in the structure), and prevent the N terminus and TM1 from adopting a productive chemokine binding conformation observed in homologous receptor-chemokine structures<sup>11, 12</sup> (Figure S2).

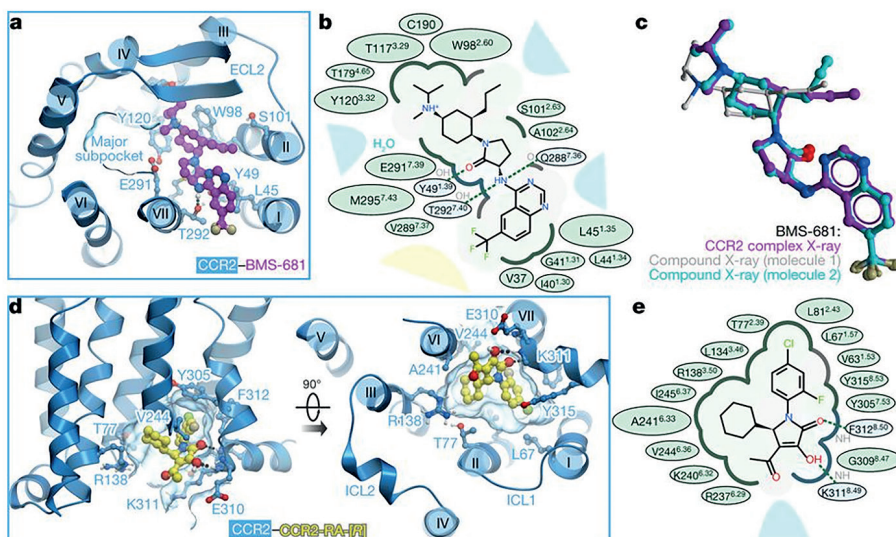
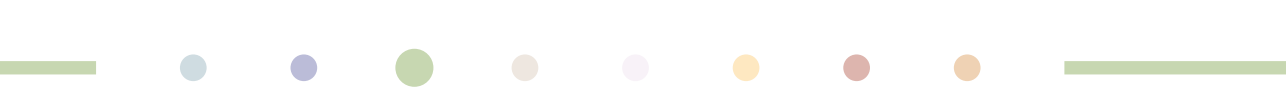


**Figure 2. Ligand binding sites and receptor interactions.** (a, b) BMS-681 interactions with CCR2 viewed in three dimensions from the extracellular side (a) and in a two-dimensional schematic depiction (b). (c) Of the two conformers in the free BMS-681 structure, one is almost identical to the CCR2-complexed conformation. (d, e) CCR2-RA-[R] interactions viewed in three dimensions along the plane of the membrane and from the intracellular side (d), and in a two-dimensional depiction (e). In (b, e) polar and non-polar residue contacts are shown as blue and green, respectively. Bulk solvent and lipid are represented by blue and yellow shading, respectively.

On the opposite side of the receptor, CCR2-RA-[R] is caged by the intracellular ends of helices I-III and VI-VIII and buries 297.8 Å<sup>2</sup> of surface area. The inner hydrophobic part of the cage is made by V63<sup>1.53</sup>, L67<sup>1.57</sup>, L81<sup>2.43</sup>, L134<sup>3.46</sup>, A241<sup>6.33</sup>, V244<sup>6.36</sup>, I245<sup>6.37</sup>, Y305<sup>7.53</sup>, and F312<sup>8.50</sup>, while the outer (cytosol-facing) polar part consists of T77<sup>2.39</sup>, R138<sup>3.50</sup>, G309<sup>8.47</sup>, K311<sup>8.49</sup>, and Y315<sup>8.53</sup> (Figures 2d,e), as well as the backbones of engineered R237<sup>6.29</sup> and K240<sup>6.32</sup>. The binding pocket of CCR2-RA-[R] is highly enclosed and possesses a balanced combination of hydrophobic and polar features, all of which favors pocket ‘druggability’.<sup>5</sup> Owing to the lack of a side-chain on G309<sup>8.47</sup>, the hydroxyl and pyrrolone carbonyl groups of CCR2-RA-[R] can hydrogen-bond to the exposed backbone amides of E310<sup>8.48</sup>, K311<sup>8.49</sup>, and F312<sup>8.50</sup> (Figures 2d,e). The acetyl group of the compound resides near the terminal amine of K311<sup>8.49</sup>. The critical roles of V244<sup>6.36</sup>, Y305<sup>7.53</sup>, K311<sup>8.49</sup>, and F312<sup>8.50</sup> in CCR2-RA-[R] binding were established by an earlier mutagenesis study.<sup>20</sup> Because homologues of several residues in



the CCR2-RA-[R] binding pocket directly couple to the G protein in bovine rhodopsin<sup>21</sup> and the  $\beta_2$  adrenergic receptor ( $\beta_2$ AR)<sup>22</sup> structures (Figure S4), CCR2-RA-[R] appears to sterically interfere with G protein binding to CCR2.

The structure suggests an interesting symmetrical mechanism for the concurrent antagonistic action of the two compounds. BMS-681 interferes with chemokine binding directly and with G protein coupling indirectly, by stabilizing an inactive, presumably G protein-incompatible,<sup>6</sup> conformation of the receptor. Conversely, CCR2-RA-[R] directly prevents G protein coupling and allosterically inhibits binding of the CCL2 chemokine,<sup>23</sup> which, like most GPCR agonists, requires an active, G protein-associated receptor for high affinity binding.<sup>23</sup> Bi-directional allosteric communication between the extra- and intracellular sides of the receptor is reminiscent of that previously observed in adenosine  $A_{2A}$  receptor ( $A_{2A}$ AR)<sup>24</sup> and  $\beta_2$ AR<sup>25</sup> using allosteric inverse agonist antibodies/nanobodies that target the same epitope as CCR2-RA-[R]. Similar to these antibodies, CCR2-RA-[R] was previously shown to allosterically enhance, and to be allosterically enhanced by, binding of orthosteric antagonists,<sup>23</sup> demonstrating positive binding cooperativity.

We further characterized this cooperativity by studying the binding of BMS-681 to wild-type CCR2 and the crystallization construct CCR2-T4L using previously characterized radioactive probes [<sup>3</sup>H]-INCB3344 (orthosteric) and [<sup>3</sup>H]-CCR2-RA (allosteric).<sup>23</sup> In equilibrium competition binding assays on wild-type CCR2, both INCB3344 and CCR2-RA-[R] displaced their homologous radioligand with half-maximum inhibitory concentration ( $IC_{50}$ ) values of 17 and 13 nM, respectively (Figures S4a,b and Table S3), comparable to previously reported values.<sup>23</sup> Compared to wild-type CCR2, the affinity of both antagonists towards CCR2-T4L was improved by approximately twofold, suggesting a slight engineering-related shift towards the inactive state. BMS-681 fully displaced [<sup>3</sup>H]-INCB3344 with nanomolar affinities for both constructs, but did not displace [<sup>3</sup>H]-CCR2-RA. Instead, at 1  $\mu$ M concentration it enhanced the binding of [<sup>3</sup>H]-CCR2-RA by >30% (Figures S4a,b and Table S3).

In kinetic radioligand experiments, the presence of BMS-681 also increased total binding of [<sup>3</sup>H]-CCR2-RA to both wild-type CCR2 and CCR2-T4L, with the increase as high as 62% in the case of CCR2-T4L (Figures S4c,d, and Table S4). BMS-681 (1  $\mu$ M) decreased the dissociation rate constant of [<sup>3</sup>H]-CCR2-RA, while producing a slight increase (wild-type CCR2) or no change (CCR2-T4L) in the observed association rate constants. Moreover, for CCR2-T4L, the presence of BMS-681 changed the biphasic dissociation profile of [<sup>3</sup>H]-CCR2-RA to monophasic, suggesting stabilization of the receptor population in a homogenous conformational state (Table S4). Along with the stability and equilibrium binding data, these results further corroborate the hypothesis that BMS-681 and CCR2-RA-[R] cooperatively stabilize a preferred inactive conformation of CCR2-T4L.



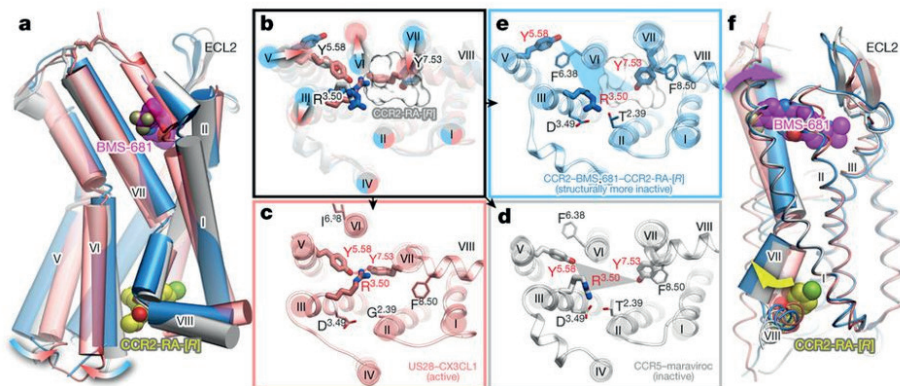


**Figure 3. Crystallographic conformation of double-antagonist-bound CCR2 has pronounced structural signatures of an inactive state.** Structures of active (US28, salmon), inactive (CCR5, grey), and more inactive (CCR2, blue) chemokine receptors viewed along the plane of the membrane (a) and across the membrane from the intracellular side (b-e). (b) Overlay of structures; arrows show the direction of activation-associated conformational changes; sticks show conserved Y<sup>5.58</sup>, R<sup>3.50</sup> and Y<sup>7.53</sup>; the white mesh is CCR2-RA-[R]. (c-e) Detailed, single-receptor depictions of (b). (f) Although located ~30 Å apart, the orthosteric (BMS-681, magenta) and the allosteric (CCR2-RA-[R], yellow) ligands cooperate in stabilizing an inactive conformation of CCR2 through helix VII.

We next analyzed the structure of double-antagonist-bound CCR2-T4L to better understand this conformation. The plethora of existing class A GPCR structures suggests a conserved conformational signature of an active receptor state.<sup>26</sup> This signature involves increased separation between the intracellular end of helix VI and the rest of the TM bundle, an inward repositioning and rotation of helix VII, and concerted repacking of the highly conserved microswitches R<sup>3.50</sup> (of the DR<sup>3.50</sup>Y motif), Y<sup>5.58</sup>, and Y<sup>7.53</sup> (of the NPxxY<sup>7.53</sup> motif) (Figures 3a,b) to form an intracellular binding interface for G protein. Furthermore, rather than adopting either an ‘on’ or ‘off’ state, receptors can occupy an ensemble of intermediate conformations.<sup>27</sup> The active state signature is fully represented in US28, the only agonist-bound chemokine receptor crystallized so far<sup>12</sup> (Figures 3a-c). By contrast, the double-antagonist-bound CCR2 structure appears to occupy the opposite end of the activation spectrum as it shares the conformational microswitch signatures of the most inactive GPCR structures observed thus far (Figures 3a-e).

As in the inactive CCR5-maraviroc complex,<sup>10</sup> the intracellular ends of CCR2 helices III and VI are close together, and the conserved R<sup>3.50</sup> interacts with D<sup>3.49</sup> and T<sup>2.39</sup>, effectively disrupting the G protein-binding pocket (Figures 3b,d,e). Similarly, in both CCR2 and CCR5 structures, the intracellular end of helix VII is in the inactive outward-facing conformation with Y<sup>7.53</sup>

pointing towards helix II rather than the centre of the bundle. However, in CCR5, Y<sup>5.58</sup> is oriented towards the centre of the bundle, whereas in the present CCR2 structure, it faces the lipid and is sterically blocked from approaching R<sup>3.50</sup> and Y<sup>7.53</sup> by F<sup>6.38</sup> (Figures 3d,e). The net result of these interactions is that the crystallographically observed conformation of CCR2 appears to be even more inactive than that of CCR5 and most similar to dark rhodopsin<sup>28</sup> and Fab-bound  $\beta_2$ AR.<sup>29</sup> Although receptor construct engineering appears to contribute to stabilization of this inactive state, the ligand binding and thermal denaturation data suggest that the concerted action of the two antagonists is also important. By directly interacting with the conserved activation microswitch residues, CCR2-RA-[R] is perfectly positioned to stabilize this inactive state: it sterically blocks Y<sup>7.53</sup> from populating the active conformation and is propped against R<sup>3.50</sup>, restricting its orientation away from the G protein interface (Figure 3b). Although located 30 Å away, BMS-681 appears to cooperate with CCR2-RA-[R] through their common interactions with helix VII, which moves outward on the intracellular side (opposite to its movement during activation) and inwards on the extracellular side (relative to CCR5 and US28) (Figure 3f).

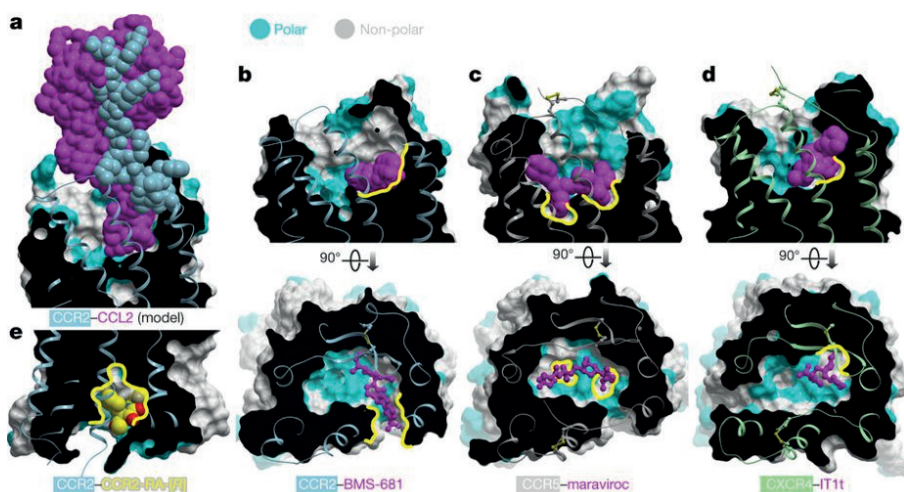


**Figure 4. Structural motifs exploited by small molecule antagonists of chemokine receptors.** Receptor surface meshes are colored by polarity (cyan, polar; grey, nonpolar). (a) Modeled CCR2-CCL2 complex illustrates the extensive receptor-chemokine interface. (b-d) Structures of CCR2-BMS-681 (b), CCR5-maraviroc (PDB 4MBS) (c), and CXCR4-IT1t (PDB 3ODU) (d). Compounds utilize unique non-polar subpockets (yellow contours) within the open polar binding pockets of their target receptors. (e) The allosteric pocket possesses a balanced combination of hydrophobic and polar features, making it a promising target for drug development.

The CCR2 structure has general implications for the design of drugs targeting chemokine receptors as a family. As with most protein-protein interfaces, the orthosteric binding

pockets of chemokine receptors are large, wide open, and highly polar. Chemokines explore numerous hotspots within these pockets and their binding is additionally reinforced by the interaction with the flexible N termini of the receptors<sup>11, 12</sup> (Figure 4a), collectively making for an extensive and versatile interaction that is conceptually difficult to inhibit with small molecules. The structure of CCR2 with BMS-681 and CCR2-RA-[R] extends the repertoire of ideas that can be used to overcome these obstacles. The binding mode of BMS-681 (Figure 4b) contrasts with both the binding mode of maraviroc to CCR5 (Figure 4c) where the ligand spans the major and the minor subpockets of the receptor, and that of IT1t to CXCR4 (Figure 4d) where the ligand is entirely accommodated in the minor subpocket. While occupying the minor subpocket of CCR2, BMS-681 protrudes between helices I and VII towards the lipid bilayer (Figure 4b) in an interaction facilitated by the trifluoromethyl group that is often present in CCR2 antagonists.<sup>30</sup> This interaction enables hydrophobic anchoring of BMS-681 to the otherwise polar and open binding site of CCR2; by doing so, it parallels the role of other unique non-polar subpockets exploited by crystallized small molecule antagonists of CCR5 and CXCR4 (Figures 4b-d). The novel subpocket explored by BMS-681 may have an additional advantage of disrupting the chemokine-compatible conformation of the receptor N terminus (Figure S2).

CCR2-RA-[R] demonstrates a previously unseen binding mode within an allosteric pocket on the intracellular side of CCR2. Although relatively small, this pocket has a desirable balance of polarity and hydrophobicity (Figures 2e, 4e). Homologous pockets may be present in other chemokine receptors, owing to a conserved G<sup>8.47</sup>; in fact, compound binding in homologous regions has been indirectly demonstrated for CCR1 and CCR5, and directly for CCR4,<sup>31</sup> CXCR1, and CXCR2.<sup>32</sup> In most other receptors that have been crystallized thus far, the non-glycine residue at position 8.47 appears to both reduce the pocket volume and block access to the backbone amides of helix 8; consequently, the homologous pockets in these receptors may not be druggable although negative allosteric modulation with antibodies and nanobodies targeting the same region has been reported.<sup>24, 25</sup> By simultaneously competing with G protein and blocking activation-related conformational changes, compound binding in the allosteric pocket seems a powerful way to antagonize the receptor. Therefore, for receptors where in which the allosteric pocket is druggable, targeting it with small molecules may open new avenues for GPCR drug discovery.

## METHODS

### Design and Expression of CCR2-T4L fusion constructs

The sequence of human CCR2 isoform b (Uniprot ID P41597-2) was engineered for crystallization by truncation of C-terminal residues 329-360 and by grafting T4 lysozyme (T4L) into the ICL3. In the process of construct optimization, the native CCR2 residues between L226<sup>5,62</sup> and R240<sup>6,32</sup> (L226<sup>5,62</sup>-KTLRLCRNEKRRH-R240<sup>6,32</sup>) were removed and replaced with corresponding residues from the crystallized structure of M2 muscarinic acetylcholine receptor (PDB accession number 3UON, resulting amino acid sequence S226<sup>5,62</sup>-RASKSRI-T4L-PPPSREK-K240<sup>6,32</sup>). The presence of T4L in ICL3 is expected to prevent receptor activation; however the similar affinities of BMS-681 and CCR2-RA-[R] for both wild-type (WT) CCR2 and CCR2-T4L (Figures S4a,b and Table S3) suggest that the fusion construct is a good surrogate to WT CCR2 for understanding ligand recognition.

The CCR4-T4L coding sequence was cloned into a modified pFastBac1 vector (Invitrogen) with an HA signal sequence followed by a Flag tag at the N terminus and a PreScission protease site followed by a 10× His tag and another Flag tag at the C terminus. The receptor was expressed in *Spodoptera frugiperda* (*Sf9*) cells. High-titre recombinant baculovirus (>10<sup>9</sup> viral particles/ml) was obtained using the Bac-to-Bac Baculovirus Expression System (Invitrogen) as previously described.<sup>11</sup> *Sf9* cells at a cell density of (2–3) × 10<sup>6</sup> cells/ml were infected with P1 virus at a multiplicity of infection of 5. Cells were harvested by centrifugation 48 h after infection and stored at –80 °C until use.

### Purification of CCR2-T4L

Insect cell membranes were prepared by thawing frozen cell pellets in a hypotonic buffer containing 10 mM HEPES (pH 7.5), 10 mM MgCl<sub>2</sub>, 20 mM KCl, and EDTA-free complete protease inhibitor cocktail tablets (Roche). Extensive washing of the raw membranes was performed by repeated douncing and centrifugation in the same hypotonic buffer (two or three times) and then in a high osmotic buffer containing 1.0 M NaCl, 10 mM HEPES (pH 7.5), 10 mM MgCl<sub>2</sub>, 20 mM KCl, and EDTA-free complete protease inhibitor cocktail tablets (three or four times), thereby separating soluble and membrane associated proteins from integral transmembrane proteins. Stock solutions (40 mM) of BMS-681 and CCR2-RA-[R] were made in isopropanol. Washed membranes were resuspended into a buffer containing 50 μM BMS-681, 2 mg/ml iodoacetamide, and EDTA-free complete protease inhibitor cocktail tablets, and incubated at 4 °C for 1 h before solubilization. The membranes were then solubilized in 50 mM HEPES (pH 7.5), 400 mM NaCl, 1% (w/v) *n*-dodecyl-β-D-

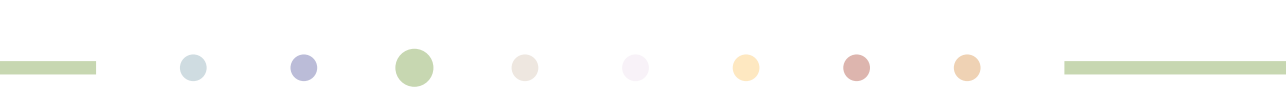
maltopyranoside (DDM, Anatrace), 0.2% (w/v) cholesteryl hemisuccinate (CHS, Sigma) at 4 °C for 3 h. The supernatant was isolated by centrifugation at 50,000g for 30 min, and incubated in 20 mM HEPES (pH 7.5), 400 mM NaCl with TALON IMAC resin (Clontech) overnight at 4 °C. After binding, the resin was washed without addition of ligands with ten column volumes of Wash I Buffer (50 mM HEPES (pH 7.5), 400 mM NaCl, 10% (v/v) glycerol, 0.1% (w/v) DDM, 0.02% (w/v) CHS, 10 mM imidazole), followed by four column volumes of Wash II Buffer (50 mM HEPES (pH 7.5), 400 mM NaCl, 10% (v/v) glycerol, 0.02% (w/v) DDM, 0.01% (w/v) CHS, 50 mM imidazole). The protein was then eluted with three to four column volumes of Elution Buffer (50 mM HEPES (pH 7.5), 1 μM BMS-681, 400 mM NaCl, 10% (v/v) glycerol, 0.02% (w/v) DDM, 0.01% (w/v) CHS, 250 mM imidazole). PD MiniTrap G-25 columns (GE Healthcare) were used to remove imidazole. The protein was then treated overnight with His-tagged PreScission protease to cleave the C-terminal His-tag and Flag-tag. PreScission protease and the cleaved C-terminal fragment were removed by binding to TALON IMAC resin for 2 h at 4 °C. The protein was collected as the TALON IMAC column flow-through. The protein was supplemented with 75 μM each of BMS-681 and CCR2-RA-[R] before being concentrated to 30 mg/ml with a 100 kDa molecular mass cut-off Amicon centrifuge concentrator (Millipore). The estimated final compound concentrations were ~1–2 mM for both compounds.

## Protein stability assays

The thermostability of CCR2-T4L was analyzed by a differential scanning fluorimetry assay adapted from previous publications<sup>33</sup> using a RotorGene Q 6-plex RT-PCR machine (Qiagen). Briefly, 1–5 μg of protein was mixed with 3 μM 7-diethylamino-3-(4'-maleimidylphenyl)-4-methylcoumarin (CPM) dye (2.5 mM stock in DMSO) in 25 mM HEPES pH 7.5, 400 mM NaCl, 0.02% DDM, 0.004% CHS, 10% glycerol, and indicated concentrations of compounds to a final volume of 20 μl; samples were incubated for 5 min at room temperature and then heated gradually from 28 °C to 90 °C at a rate of 0.8 °C/min, with CPM fluorescence (excitation 365 nm, emission 460 nm) recorded every 1 °C. The melting temperature ( $T_m$ ) was determined from the first derivative of the denaturation curve, using the Rotor-Gene Q – Pure Detection software (version 2.0.3).

## Crystallization

Purified CCR2 in complex with BMS-681 and CCR2-RA-[R] was reconstituted into LCP by mixing with molten lipid using a mechanical syringe mixer.<sup>8</sup> The protein–LCP mixture contained 40% (w/w) receptor solution, 54% (w/w) monoolein, and 6% (w/w) cholesterol.



Crystallization trials were performed in 96-well glass sandwich plates (Hampton research) using a Mosquito LCP robot (TTP Labtech) by dispensing 45 nl of protein-laden LCP and 800 nl of precipitant solution per well. Plates were incubated and imaged at 20 °C. Initial crystal hits were found from a precipitant condition containing 100 mM MES, pH 6.5, 30% (v/v) PEG400, 100 mM Li<sub>2</sub>SO<sub>4</sub>. After optimization, diffraction-quality crystals were obtained from 100 mM MES, pH 6.5, 30–32% (v/v) PEG400, 75–85 mM Li<sub>2</sub>SO<sub>4</sub>. Crystals usually grew to a maximum size of 60 μm × 10 μm × 10 μm in 1 week, and were harvested directly from the LCP matrix using MiTeGen micromounts and flash cooled in liquid nitrogen.

## Data collection and structure determination

X-ray diffraction data were collected using a 10 μm collimated minibeam at a wavelength of 1.0332 Å with a Pilatus3 6M direct detector on the 23ID-D beamline (GM/CA CAT) of the Advanced Photon Source at the Argonne National Laboratory. Crystals were located and aligned by the rastering strategy.<sup>34</sup> Among the several hundred crystal samples screened, most crystals diffracted to 2.8–3.5 Å resolution when exposed to 0.3 s of unattenuated beam using 0.3° oscillations. A 93.1% complete data set at 2.80 Å resolution was obtained by merging data from 17 crystals, using XDS<sup>35</sup> and Aimless.<sup>36</sup> As the data showed anisotropy, the UCLA Diffraction Anisotropy Server (<http://services.mbi.ucla.edu/anisoscale/>) was used to truncate the data to 3.0 Å along both *a*\* and *b*\* axes, and to 2.81 Å along the *c*\* axis. Initial phase information was obtained by molecular replacement with the program Phaser<sup>37</sup> using the receptor portion of the CCR5 structure (PDB accession number 4MBS) converted to polyalanines, and the T4L portion of the CXCR4 structure (PDB accession number 3ODU) as search models. The correct molecular replacement solution (translation function Z-score = 14.8) contained one CCR2-T4L molecule in the asymmetric unit. Refinement was performed with Phenix<sup>38</sup> followed by manual examination and rebuilding of the refined coordinates in the program COOT<sup>39</sup> using both  $|2F_o| - |F_c|$  and  $|F_o| - |F_c|$  maps, as well as omit maps. The final model included 295 residues (37–225 and 241–319) of the 360 residues of CCR2 and residues 2–161 of T4L plus 16 residues of two 8-residue linkers. The remaining N- and C-terminal residues were disordered and were not built. Strong electron density for one metal ion was observed. The identity of the ion was determined to be Zn<sup>2+</sup> by X-ray fluorescence scans (Figure S5). The zinc ion is coordinated by a water molecule as well as side chains of H144<sup>3,56</sup>, E238, and E1005. Data collection and refinement statistics are shown in Table S1.

## Crystallization and structure determination of BMS-681

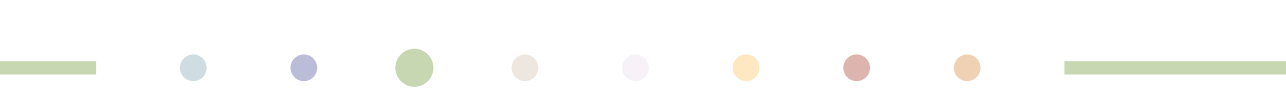
BMS-681 was dissolved in a minimal amount of  $\text{CH}_3\text{CN}$  and then 15% water was added. After standing overnight, the resulting crystals were collected. Data were obtained on a Bruker-AXS X8-Proteum Kappa goniometer and APEXII detector. Intensities were measured using Cu  $\text{K}\alpha$  radiation ( $\lambda = 1.5418 \text{ \AA}$ ) with the crystal kept at a constant temperature using an Oxford cryo system during data collection. Indexing and processing of the measured intensity data were performed with the SAINT-APEX2 (Bruker-AXS) program suite, structure solution with SHELXS-97, and structure refinement with SHELXL-97.

The derived atomic parameters (coordinates and temperature factors) were refined through full matrix least-squares. The function minimized in the refinements was  $\sum_w (|F_o| - |F_c|)^2$ .  $R$  is defined as  $\sum |F_o| - |F_c| / \sum |F_o|$  while  $R_w = [\sum_w (|F_o| - |F_c|)^2 / \sum_w |F_o|^2]^{1/2}$  where  $w$  is an appropriate weighting function based on errors in the observed intensities. Hydrogens were introduced in idealized positions with isotropic temperature factors, but no hydrogen parameters were varied. It should be noted that the refinement model illustrates disorder and partial occupancy factors of 'guest' solvent/water molecules within the crystalline lattice. The atomic positions of these disordered molecules were taken from the difference map analysis, which showed peaks of electron density of varying intensities at the refined positions representing the disordered solvent/water molecules. Data collection and refinement statistics are shown in Table S2.

## Cell culture and transfections

Chinese hamster ovary (CHO) cells (provided by H. den Dulk, Leiden University, The Netherlands; originally obtained from and certified by American Type Culture Collection) were cultured in Dulbecco's Modified Eagle Medium/F-12 Nutrient Mixture (DMEM/F-12) supplemented with 10% (v/v) newborn calf serum, 50 IU/ml penicillin, and 50  $\mu\text{g}/\text{ml}$  streptomycin; they were maintained at 37 °C and in 5%  $\text{CO}_2$ . Cells were subcultured twice a week at a ratio of 1:30 to 1:50 by trypsinization. Transient transfection of CHO cells with WT CCR2 and CCR2-T4L constructs was performed using a polyethylenimine method, as described previously.<sup>23</sup> Briefly, CHO cells were grown on plates (diameter 15 cm) to around 50% confluence and then transfected with a DNA/polyethylenimine mixture containing 10  $\mu\text{g}$  plasmid DNA—previously diluted in 150 mM NaCl solution—mixed with polyethylenimine solution (1 mg/ml) at a 1:6 DNA:polyethylenimine mass ratio. Before adding 1 ml of the transfection mixture to each plate, the culture medium of the cells was refreshed and the mixture incubated for 20 min at room temperature. Following transfection, cells were incubated for 48 h at 37 °C and 5%  $\text{CO}_2$  before membrane preparation. Twenty-four hours





after transfection, sodium butyrate was added to each plate at a final concentration of 3 mM to increase receptor expression. CHO cells were tested for mycoplasma contamination before use, the outcome of which was negative.

## Membrane preparation

Membranes from CHO cells transiently expressing the WT CCR2 or CCR2-T4L were prepared as described previously.<sup>23</sup> Briefly, cells were detached from plates (diameter 15 cm) using 5 ml of phosphate-buffered saline and centrifuged for 5 min at 3000g. The membranes were separated from the cytosolic fractions by several centrifugation and homogenization steps. First, the pellets were resuspended and homogenized in ice-cold membrane buffer (50 mM Tris-HCl buffer, supplemented with 5 mM MgCl<sub>2</sub>, pH 7.4) using an Ultra Thurrax Homogenizer (IKA-Werke, Staufen, Germany). Homogenized membranes were then centrifuged in an Optima LE-80 K ultracentrifuge (Beckman Coulter, Fullerton, California, USA) at 31,000g for 20 min at 4 °C. The final membrane pellet was resuspended also in ice-cold membrane buffer and aliquoted before storage. Membrane aliquots were stored at -80 °C and protein concentrations were measured using a standard BCA protein determination assay (Pierce Chemical Company, Rockford, Illinois, USA).

## Radioligand binding assays

[<sup>3</sup>H]-INCB3344 (specific activity 32 Ci mmol<sup>-1</sup>) and [<sup>3</sup>H]-CCR2-RA (specific activity 63 Ci mmol<sup>-1</sup>) were custom-labeled by Vitrax (Placentia, California, USA). JNJ-27141491 was synthesized as described previously.<sup>40</sup> INCB3344 and CCR2-RA-[R] were synthesized in-house as described previously.<sup>7,41</sup>

All radioligand binding assays were performed at 25 °C in a 100 µl reaction volume containing assay buffer (50 mM Tris-HCl buffer (pH 7.4), 5 mM MgCl<sub>2</sub>, 0.1% CHAPS) and 30 µg of membrane protein from CHO cells transiently expressing WT CCR2 or CCR2-T4L. For competition binding assays with [<sup>3</sup>H]-INCB3344, a concentration of 5 nM [<sup>3</sup>H]-INCB3344 was used, and non-specific binding was determined with 10 µM of unlabelled INCB3344. In the case of [<sup>3</sup>H]-CCR2-RA competition binding assays, a radioligand concentration of 3 nM was used and non-specific binding was determined with 10 µM of JNJ-27141491. In all cases, homologous or competition displacement assays were performed using six increasing concentrations of competing ligands. Kinetic experiments were also performed at 25 °C using 7 nM [<sup>3</sup>H]-CCR2-RA and 30 µg of membrane protein in a 100 µl reaction volume. For association experiments, CHO-CCR2 or CHO-CCR2-T4L membranes were added to the reaction at eight different time points, in the absence or presence of 1 µM BMS-681. For



dissociation experiments, membranes were first incubated with radioligand for 90 min; dissociation was then initiated by addition of 10  $\mu\text{M}$  of CCR2-RA-[R] at 12 different time points, in the presence or absence of 1  $\mu\text{M}$  BMS-681. More time points were used in the dissociation assays, to characterize the biphasic profile of [ $^3\text{H}$ ]-CCR2-RA dissociation. In all cases, total radioligand binding did not exceed 10% of the total radioligand added to avoid ligand depletion. For all experiments, incubation was terminated by dilution with ice-cold wash buffer (50 mM Tris-HCl buffer (pH 7.4), 5 mM  $\text{MgCl}_2$ , 0.05% CHAPS). Separation of bound from free radioligand was achieved by rapid filtration over a 96-well GF/B filter plate using a Perkin Elmer Filtermate-harvester (Perkin Elmer, Groningen, The Netherlands) and filter-bound radioactivity was determined in a Perkin Elmer 2450 Microbeta2 plate counter after addition of 25  $\mu\text{l}$  Microscint scintillation cocktail per well (Perkin-Elmer, Groningen, The Netherlands).

## Statistical Methods

No statistical methods were used to predetermine sample size. The experiments were not randomized. The investigators were not blinded to allocation during experiments and outcome assessment.

All radioligand binding data were analyzed using Prism 6.0 and 7.0 (GraphPad Software, San Diego, California, USA). The  $\text{pIC}_{50}$  values were obtained by nonlinear regression analysis of competition displacement assays. Apparent association rate constants ( $k_{\text{obs}}$ ) and maximum binding ( $B_{\text{max}}$ , used to calculate  $\%B/B_{\text{control}}$ ) were determined by fitting the association data to a one-phase exponential association function. Dissociation rate constants were determined by fitting the dissociation data to a monophasic ( $k_{\text{off}}$ ) or biphasic ( $k_{\text{off, fast}}$  and  $k_{\text{off, slow}}$ ) exponential decay model. All data shown represent means  $\pm$  s.e.m. of at least three independent experiments performed in duplicate. An unpaired, two-tailed Student's *t*-test was used to compare differences in  $\text{pIC}_{50}$  as well as differences in kinetic parameters. Differences in binding enhancement (%Binding) in the absence (set at 100%) or presence of BMS-681 were analyzed using a one-way analysis of variance with Dunnett's post-hoc test. Significant differences are denoted as follows: \* $P < 0.05$ , \*\* $P < 0.01$ , \*\*\* $P < 0.001$ , \*\*\*\* $P < 0.0001$ .

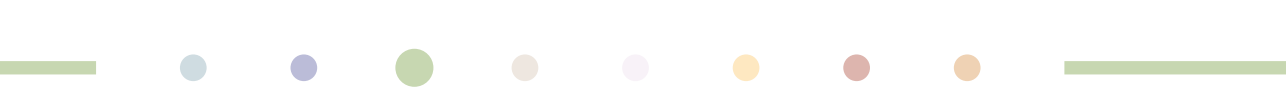


## Data availability

The atomic coordinates and structure factors for the CCR2–BMS-681–CCR2-RA-[*R*] complex have been deposited in the Protein Data Bank under accession number 5T1A. The structure of free BMS-681 is deposited in the Cambridge Crystallographic Data Centre (<http://www.ccdc.cam.ac.uk/>) under accession number 1479580. All other data are available from the corresponding authors upon reasonable request.

## REFERENCES

1. Scholten, D. J.; Canals, M.; Maussang, D.; Roumen, L.; Smit, M. J.; Wijtmans, M.; de Graaf, C.; Vischer, H. F.; Leurs, R. Pharmacological modulation of chemokine receptor function. *Br J Pharmacol* **2012**, *165*, 1617-1643.
2. O'Connor, T.; Borsig, L.; Heikenwalder, M. CCL2-CCR2 Signaling in Disease Pathogenesis. *Endocr Metab Immune Disord Drug Targets* **2015**, *15*, 105-118.
3. Lim, S. Y.; Yuzhalin, A. E.; Gordon-Weeks, A. N.; Muschel, R. J. Targeting the CCL2-CCR2 signaling axis in cancer metastasis. *Oncotarget* **2016**, *7*, 28697-28710.
4. Solari, R.; Pease, J. E.; Begg, M. "Chemokine receptors as therapeutic targets: Why aren't there more drugs?". *Eur. J. Pharmacol.* **2015**, *746*, 363-367.
5. Cooke, R. M.; Brown, A. J.; Marshall, F. H.; Mason, J. S. Structures of G protein-coupled receptors reveal new opportunities for drug discovery. *Drug Discov Today* **2015**, *20*, 1355-1364.
6. Carter, P. H.; Brown, G. D.; Cherney, R. J.; Batt, D. G.; Chen, J.; Clark, C. M.; Cvijic, M. E.; Duncia, J. V.; Ko, S. S.; Mandlekar, S.; Mo, R.; Nelson, D. J.; Pang, J.; Rose, A. V.; Santella, J. B., 3rd; Tebben, A. J.; Traeger, S. C.; Xu, S.; Zhao, Q.; Barrish, J. C. Discovery of a Potent and Orally Bioavailable Dual Antagonist of CC Chemokine Receptors 2 and 5. *ACS Med Chem Lett* **2015**, *6*, 439-444.
7. Dasse, O.; Evans, J.; Zhai, H.-X.; Zou, D.; Kintigh, J.; Chan, F.; Hamilton, K.; Hill, E.; Eckman, J.; Higgins, P. Novel, acidic CCR2 receptor antagonists: lead optimization. *Letts. Drug. Des. Discov.* **2007**, *4*, 263-271.
8. Caffrey, M.; Cherezov, V. Crystallizing membrane proteins using lipidic mesophases. *Nat Protoc* **2009**, *4*, 706-731.
9. Wu, B.; Chien, E. Y. T.; Mol, C. D.; Fenalti, G.; Liu, W.; Katritch, V.; Abagyan, R.; Brooun, A.; Wells, P.; Bi, F. C.; Hamel, D. J.; Kuhn, P.; Handel, T. M.; Cherezov, V.; Stevens, R. C. Structures of the CXCR4 chemokine GPCR with small-molecule and cyclic peptide antagonists. *Science* **2010**, *330*, 1066-1071.
10. Tan, Q.; Zhu, Y.; Li, J.; Chen, Z.; Han, G. W.; Kufareva, I.; Li, T.; Ma, L.; Fenalti, G.; Li, J. Structure of the CCR5 chemokine receptor-HIV entry inhibitor maraviroc complex. *Science* **2013**, *341*, 1387-1390.
11. Qin, L.; Kufareva, I.; Holden, L. G.; Wang, C.; Zheng, Y.; Zhao, C.; Fenalti, G.; Wu, H.; Han, G. W.; Cherezov, V.; Abagyan, R.; Stevens, R. C.; Handel, T. M. Crystal structure of the chemokine receptor CXCR4 in complex with a viral chemokine. *Science* **2015**, *347*, 1117-1122.
12. Burg, J. S.; Ingram, J. R.; Venkatakrishnan, A. J.; Jude, K. M.; Dukkipati, A.; Feinberg, E. N.; Angelini, A.; Waghray, D.; Dror, R. O.; Ploegh, H. L.; Garcia, K. C. Structural basis for chemokine recognition and activation of a viral G protein-coupled receptor. *Science* **2015**, *347*, 1113-1117.
13. Monteclaro, F. S.; Charo, I. F. The amino-terminal domain of CCR2 is both necessary and sufficient for high affinity binding of monocyte chemoattractant protein 1. Receptor activation by a pseudo-tethered ligand. *J Biol Chem* **1997**, *272*, 23186-23190.
14. Zhang, K.; Zhang, J.; Gao, Z. G.; Zhang, D.; Zhu, L.; Han, G. W.; Moss, S. M.; Paoletta, S.; Kiselev, E.; Lu, W.; Fenalti, G.; Zhang, W.; Müller, C. E.; Yang, H.; Jiang, H.; Cherezov, V.; Katritch, V.; Jacobson, K. A.; Stevens, R. C.; Wu, B.; Zhao, Q. Structure of the human P2Y12 receptor in complex with an antithrombotic drug. *Nature* **2014**, *509*, 115-118.
15. Weik, M.; Ravelli, R. B.; Kryger, G.; McSweeney, S.; Raves, M. L.; Harel, M.; Gros, P.; Silman, I.; Kroon, J.; Sussman, J. L. Specific chemical and structural damage to proteins produced by synchrotron radiation. *Proc Natl Acad Sci U S A* **2000**, *97*, 623-628.
16. Cherney, R. J.; Mo, R.; Meyer, D. T.; Nelson, D. J.; Lo, Y. C.; Yang, G.; Scherle, P. A.; Mandlekar, S.; Wasserman, Z. R.; Jezak, H.; Solomon, K. A.; Tebben, A. J.; Carter, P. H.; Decicco, C. P. Discovery of disubstituted cyclohexanes as a new class of CC chemokine receptor 2 antagonists. *J Med Chem* **2008**, *51*, 721-724.
17. Berkhout, T. A.; Blaney, F. E.; Bridges, A. M.; Cooper, D. G.; Forbes, I. T.; Gribble, A. D.; Groot, P. H.; Hardy, A.; Ife, R. J.; Kaur, R.; Moores, K. E.; Shillito, H.; Willetts, J.; Witherington, J. CCR2: characterization of the antagonist binding site from a combined receptor modeling/mutagenesis approach. *J Med Chem* **2003**, *46*, 4070-4086.

- 
18. Hall, S. E.; Mao, A.; Nicolaidou, V.; Finelli, M.; Wise, E. L.; Nedjai, B.; Kanjanapangka, J.; Harirchian, P.; Chen, D.; Selchau, V.; Ribeiro, S.; Schyler, S.; Pease, J. E.; Horuk, R.; Vaidehi, N. Elucidation of binding sites of dual antagonists in the human chemokine receptors CCR2 and CCR5. *Mol Pharmacol* **2009**, *75*, 1325-1336.
  19. Cherney, R. J.; Nelson, D. J.; Lo, Y. C.; Yang, G.; Scherle, P. A.; Jezak, H.; Solomon, K. A.; Carter, P. H.; Decicco, C. P. Synthesis and evaluation of cis-3,4-disubstituted piperidines as potent CC chemokine receptor 2 (CCR2) antagonists. *Bioorg Med Chem Lett* **2008**, *18*, 5063-5065.
  20. Zweemer, A. J.; Bunnik, J.; Veenhuizen, M.; Miraglia, F.; Lenselink, E. B.; Vilums, M.; de Vries, H.; Gibert, A.; Thiele, S.; Rosenkilde, M. M.; Iljerman, A. P.; Heitman, L. H. Discovery and mapping of an intracellular antagonist binding site at the chemokine receptor CCR2. *Mol. Pharmacol.* **2014**, *86*, 358-368.
  21. Blankenship, E.; Vahedi-Faridi, A.; Lodowski, D. T. The high-resolution structure of activated opsin reveals a conserved solvent network in the transmembrane region essential for activation. *Structure* **2015**, *23*, 2358-2364.
  22. Rasmussen, S. G.; DeVree, B. T.; Zou, Y.; Kruse, A. C.; Chung, K. Y.; Kobilka, T. S.; Thian, F. S.; Chae, P. S.; Pardon, E.; Calinski, D.; Mathiesen, J. M.; Shah, S. T.; Lyons, J. A.; Caffrey, M.; Gellman, S. H.; Steyaert, J.; Skiniotis, G.; Weis, W. I.; Sunahara, R. K.; Kobilka, B. K. Crystal structure of the  $\beta_2$  adrenergic receptor-Gs protein complex. *Nature* **2011**, *477*, 549-555.
  23. Zweemer, A. J.; Nederpelt, I.; Vrieling, H.; Hafith, S.; Doornbos, M. L.; de Vries, H.; Abt, J.; Gross, R.; Stamos, D.; Saunders, J.; Smit, M. J.; Iljerman, A. P.; Heitman, L. H. Multiple binding sites for small-molecule antagonists at the CC chemokine receptor 2. *Mol. Pharmacol.* **2013**, *84*, 551-561.
  24. Hino, T.; Arakawa, T.; Iwanari, H.; Yurugi-Kobayashi, T.; Ikeda-Suno, C.; Nakada-Nakura, Y.; Kusano-Arai, O.; Weyand, S.; Shimamura, T.; Nomura, N.; Cameron, A. D.; Kobayashi, T.; Hamakubo, T.; Iwata, S.; Murata, T. G-protein-coupled receptor inactivation by an allosteric inverse-agonist antibody. *Nature* **2012**, *482*, 237-240.
  25. Staus, D. P.; Strachan, R. T.; Manglik, A.; Pani, B.; Kahsai, A. W.; Kim, T. H.; Wingler, L. M.; Ahn, S.; Chatterjee, A.; Masoudi, A.; Kruse, A. C.; Pardon, E.; Steyaert, J.; Weis, W. I.; Prosser, R. S.; Kobilka, B. K.; Costa, T.; Lefkowitz, R. J. Allosteric nanobodies reveal the dynamic range and diverse mechanisms of G-protein-coupled receptor activation. *Nature* **2016**, *535*, 448-452.
  26. Katritch, V.; Cherezov, V.; Stevens, R. C. Structure-function of the G protein-coupled receptor superfamily. *Annu Rev Pharmacol Toxicol.* **2013**, *53*, 531-556.
  27. Manglik, A.; Kim, T. H.; Masureel, M.; Altenbach, C.; Yang, Z.; Hilger, D.; Lerch, M. T.; Kobilka, T. S.; Thian, F. S.; Hubbell, W. L.; Prosser, R. S.; Kobilka, B. K. Structural insights into the dynamic process of  $\beta_2$ -adrenergic receptor signaling. *Cell* **2015**, *161*, 1101-1111.
  28. Palczewski, K.; Kumasaka, T.; Hori, T.; Behnke, C. A.; Motoshima, H.; Fox, B. A.; Le Trong, I.; Teller, D. C.; Okada, T.; Stenkamp, R. E.; Yamamoto, M.; Miyano, M. Crystal structure of rhodopsin: a G protein-coupled receptor. *Science* **2000**, *289*, 739-745.
  29. Rasmussen, S. G.; Choi, H. J.; Rosenbaum, D. M.; Kobilka, T. S.; Thian, F. S.; Edwards, P. C.; Burghammer, M.; Ratnala, V. R.; Sanishvili, R.; Fischetti, R. F.; Schertler, G. F.; Weis, W. I.; Kobilka, B. K. Crystal structure of the human  $\beta_2$  adrenergic G-protein-coupled receptor. *Nature* **2007**, *450*, 383-387.
  30. Pease, J.; Horuk, R. Chemokine receptor antagonists. *J. Med. Chem.* **2012**, *55*, 9363-9392.
  31. Andrews, G.; Jones, C.; Wreggett, K. A. An intracellular allosteric site for a specific class of antagonists of the CC chemokine G protein-coupled receptors CCR4 and CCR5. *Mol. Pharmacol.* **2008**, *73*, 855-867.
  32. Nicholls, D. J.; Tomkinson, N. P.; Wiley, K. E.; Brammall, A.; Bowers, L.; Grahames, C.; Gaw, A.; Meghani, P.; Shelton, P.; Wright, T. J.; Mallinder, P. R. Identification of a putative intracellular allosteric antagonist binding-site in the CXC chemokine receptors 1 and 2. *Mol. Pharmacol.* **2008**, *74*, 1193-1202.
  33. Alexandrov, A. I.; Mileni, M.; Chien, E. Y. T.; Hanson, M. A.; Stevens, R. C. Microscale fluorescent thermal stability assay for membrane proteins. *Structure* **2008**, *16*, 351-359.
  34. Cherezov, V.; Hanson, M. A.; Griffith, M. T.; Hilgart, M. C.; Sanishvili, R.; Nagarajan, V.; Stepanov, S.; Fischetti, R. F.; Kuhn, P.; Stevens, R. C. Rastering strategy for screening and centering of microcrystal samples of human membrane proteins with a sub-10  $\mu\text{m}$  size X-ray synchrotron beam. *J R Soc Interface* **2009**, *6 Suppl 5*, S587-S597.

35. Kabsch, W. Xds. *Acta Crystallogr D Biol Crystallogr* **2010**, *66*, 125-132.
36. Winn, M. D.; Ballard, C. C.; Cowtan, K. D.; Dodson, E. J.; Emsley, P.; Evans, P. R.; Keegan, R. M.; Krissinel, E. B.; Leslie, A. G.; McCoy, A.; McNicholas, S. J.; Murshudov, G. N.; Pannu, N. S.; Pottterton, E. A.; Powell, H. R.; Read, R. J.; Vagin, A.; Wilson, K. S. Overview of the CCP4 suite and current developments. *Acta Crystallogr D Biol Crystallogr* **2011**, *67*, 235-242.
37. McCoy, A. J.; Grosse-Kunstleve, R. W.; Adams, P. D.; Winn, M. D.; Storoni, L. C.; Read, R. J. Phaser crystallographic software. *J Appl Crystallogr* **2007**, *40*, 658-674.
38. Adams, P. D.; Afonine, P. V.; Bunkoczi, G.; Chen, V. B.; Davis, I. W.; Echols, N.; Headd, J. J.; Hung, L. W.; Kapral, G. J.; Grosse-Kunstleve, R. W.; McCoy, A. J.; Moriarty, N. W.; Oeffner, R.; Read, R. J.; Richardson, D. C.; Richardson, J. S.; Terwilliger, T. C.; Zwart, P. H. PHENIX: a comprehensive Python-based system for macromolecular structure solution. *Acta Crystallogr D Biol Crystallogr* **2010**, *66*, 213-221.
39. Emsley, P.; Lohkamp, B.; Scott, W. G.; Cowtan, K. Features and development of Coot. *Acta Crystallogr D Biol Crystallogr* **2010**, *66*, 486-501.
40. Doyon, J.; Coesemans, E.; Boeckx, S.; Buntinx, M.; Hermans, B.; Van Wauwe, J. P.; Gilissen, R. A.; De Groot, A. H.; Corens, D.; Van Lommen, G. Discovery of potent, orally bioavailable small-molecule inhibitors of the human CCR2 receptor. *ChemMedChem* **2008**, *3*, 660-669.
41. Brodmerkel, C. M.; Huber, R.; Covington, M.; Diamond, S.; Hall, L.; Collins, R.; Leffet, L.; Gallagher, K.; Feldman, P.; Collier, P.; Stow, M.; Gu, X.; Baribaud, F.; Shin, N.; Thomas, B.; Burn, T.; Hollis, G.; Yeleswaram, S.; Solomon, K.; Friedman, S.; Wang, A.; Xue, C. B.; Newton, R. C.; Scherle, P.; Vaddi, K. Discovery and pharmacological characterization of a novel rodent-active CCR2 antagonist, INCB3344. *J Immunol* **2005**, *175*, 5370-5378.
42. Chen, V. B.; Arendall, W. B., 3rd; Headd, J. J.; Keedy, D. A.; Immormino, R. M.; Kapral, G. J.; Murray, L. W.; Richardson, J. S.; Richardson, D. C. MolProbity: all-atom structure validation for macromolecular crystallography. *Acta Crystallogr D Biol Crystallogr* **2010**, *66*, 12-21.

## SUPPORTING INFORMATION

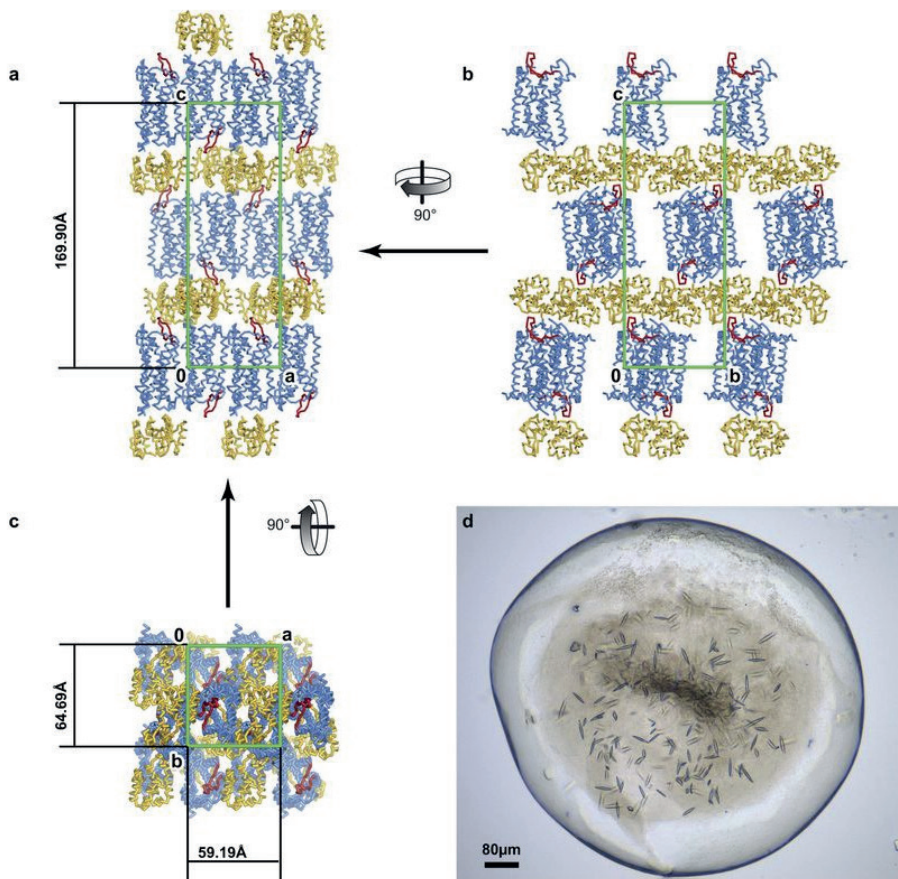


**Figure S1. CCR2-T4L crystals and crystal packing.** (a-c) Crystal packing of CCR2-T4L. CCR2 is a blue ribbon with ECL2 colored red and T4L yellow. The unit cell is shown as a green box. CCR2-T4L molecules are arranged in a type I packing with hydrophilic stacking mediated by T4L and T4L-ECL2 interactions along axis c. (a) Crystal packing in the ac plane. CCR2 makes abundant hydrophobic contacts with its neighbor via an interface mediated by antiparallel helix IV–helix VI interactions related by a screw axis along axis a. (b) Crystal packing in the bc plane. Contacts between receptors and T4L involve ECL2 and the intracellular surface of CCR2 including helix VIII. Direct contacts between T4L are along axis b. One layer of CCR2-T4L molecules at the very top of the stacking column is omitted for clarity. (c) Crystal packing in the ab plane. There are no direct interactions between T4L along axis a. (d) Crystals of CCR2-T4L in the LCP bolus. Average crystals grew to  $60 \mu\text{m} \times 10 \mu\text{m} \times 10 \mu\text{m}$  before harvesting.

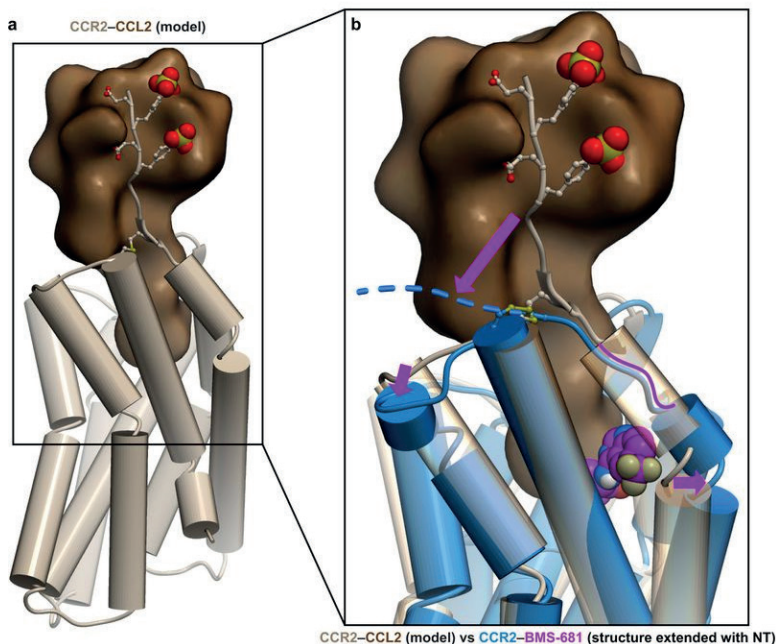


**Figure S2. BMS-681 binding may disrupt a chemokine-recognizing conformation of the CCR2 N terminus and helix I.** (a) Model of CCR2-CCL2 built by homology from the structure of CXCR4-vMIP-II<sup>11</sup> suggests that a productive chemokine-compatible conformation of the receptor requires re-orientation of the N terminus from almost parallel to almost perpendicular to the membrane plane, and formation of an extra helical turn in helix I to bring it closer to helix VII and ECL3. (b) Binding of BMS-681 may disrupt this chemokine-compatible conformation by inserting between helices I and VII.

	TM1-ICL1-TM2						TM3-ICL2						TM5-ICL3-TM6						TM7-H8																
CCR2 residue	63	66	67	71	72	75	77	78	81	134	138	141	142	144	145	148	149	150	225	228	229	236	237	240	241	244	245	248	305	308	309	310	311	312	315
CCR2-RA-[R] contacts	•	•	•	•	•	•	•	•	•	•	•	•	•	•	•	•	•	•	•	•	•	•	•	•	•	•	•	•	•	•	•	•	•	•	•
CCR2	V	I	L	K	C	T	D	I		L	R	A	I	H	A	A	L	K	I	T	L	K	R	A	V	I	I	Y	V	G	E	K	F	Y	
bRho	T	V	T	.	.	T	L	N	.	.	.	V	V	K	P	N	F	R	L	.	V	.	A	E	V	M	V	M	.	M	N	K	Q	.	C
$\beta_2$ AR	A	I	E	R	.	N	I	.	I	.	.	.	S	P	Y	Q	S	V	E	A	L	.	K	.	T	L	.	R	S	P	D	.	A		
Gat-CT contacts (bRho)									•	•	•	•	•	•	•	•	•	•	•	•	•	•	•	•	•	•	•	•	•	•	•	•	•		
Gas-CT contacts ( $\beta_2$ AR)									•	•	•	•	•	•	•	•	•	•	•	•	•	•	•	•	•	•	•	•	•	•	•	•	•		

**Figure S3. CCR2-RA-[R] directly binds to CCR2 residues that are homologous to those involved in G protein coupling in other GPCRs.** Partial alignment of intracellular regions of CCR2 and homologous regions in bovine Rho (bRho) and  $\beta_2$  adrenergic receptor ( $\beta_2$ AR), alongside profile of contacts that CCR2-RA-[R], the  $G_{\alpha_i}$  C-terminal peptide,<sup>21</sup> and  $G_{\alpha_s}$  C terminus<sup>22</sup> make with the three respective receptors. Contacts are shown by circles above and below the alignment, with circle area indicative of contact strength. Backbone and side-chain contacts are gray and black, respectively. Assuming structural homology between the CCR2-G protein interface and at least one of the bRho- $G_{\alpha_i}$  and  $\beta_2$ AR- $G_{\alpha_s}$  interfaces, several residue positions seem to be involved in binding both CCR2-RA-[R] and the C terminus of the G protein.



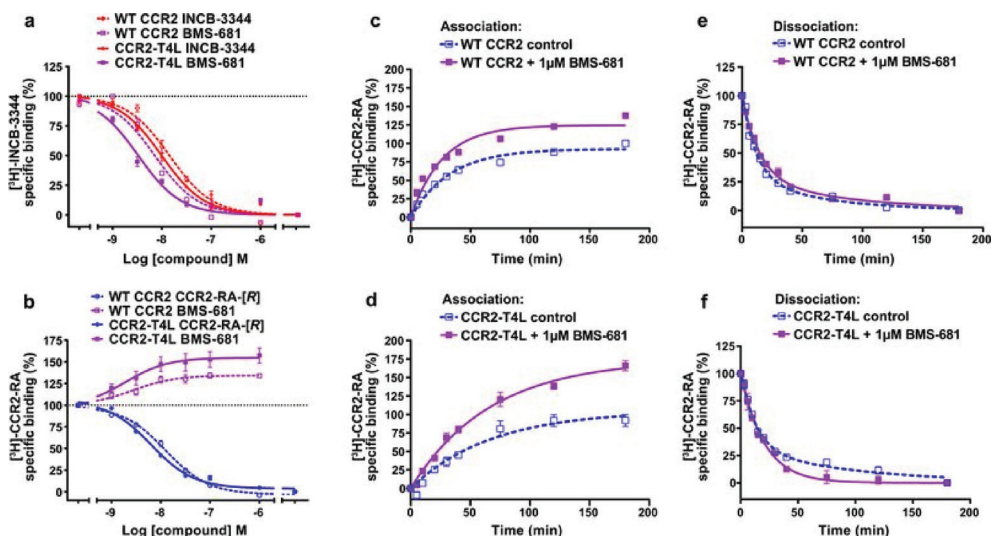


**Figure S4. Equilibrium binding and binding kinetics of BMS-681 and CCR2-RA-[R] with WT CCR2 and CCR2-T4L.** (a, b) Displacement of [<sup>3</sup>H]-INCB3344 (5nM, a) and [<sup>3</sup>H]-CCR2-RA (3 nM, b) from WT CCR2 and CCR2-T4L in CHO cells by increasing concentrations of unlabelled INCB3344, CCR2-RA-[R] and BMS-681. (c, d) Association and (e, f) dissociation of 7 nM [<sup>3</sup>H]-CCR2-RA from CHO cell membranes transiently expressing WT CCR2 (c, e) or CCR2-T4L (d, f) at 25°C, in the absence or presence of 1 μM BMS-681. Figures represent normalized and combined data from three independent experiments performed in duplicate, with results presented as mean ± S.E.M percentage of specific [<sup>3</sup>H]-CCR2-RA binding.

**Figure S5. A Zn<sup>2+</sup> binding site was identified by X-ray fluorescence emission analysis of the CCR2-T4L-BMS-681-CCR2-RA-[R] crystals.** (a) View of the Zn<sup>2+</sup> ion at an interface formed by CCR2 helices III and VI and the N terminus of T4L. The Zn<sup>2+</sup> ion is coordinated by side chains of H144, E238, and E1005 (from T4L) as well as a structured water. (b) Background fluorescence signal of an empty MiTeGen micromount is low, indicating the absence of metal ion. Excitation at 12 keV results in a peak at 11.7 keV (owing to the incidence beam). (c) X-ray fluorescence emission signal from a wide fluorescence scan of the CCR2-T4L crystal. The fluorescence peaks at 8.60 keV and 9.53 keV correspond to X-ray emission lines K $\alpha$  (8.64 keV) and K $\beta$  (9.57 keV) and indicate the presence of Zn<sup>2+</sup> bound to CCR2-T4L. (d) A zoomed-in view of the X-ray fluorescence emission signal from (c).

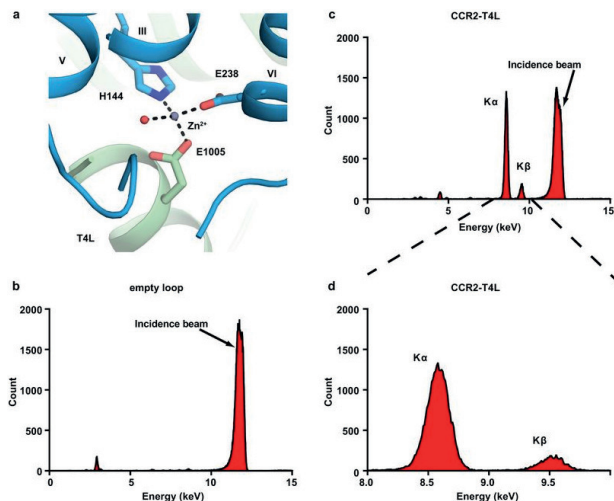




**Table S1. Data collection and refinement statistics (molecular replacement)**

	CCR2-T4L-BMS-681-CCR2-RA-[R] <sup>a</sup>
Data collection <sup>b</sup> Wavelength (Å)	1.03319
Space group	P2 <sub>1</sub> 2 <sub>1</sub> 2 <sub>1</sub>
Unit cell parameters a,b,c (Å)	59.19 64.69 169.90
Number of reflections measured	82,111
Number of unique reflections	15,550
Resolution (Å)	48-2.8 (2.95-2.8)
R <sub>merge</sub> (%)	22.5(101)
R <sub>pim</sub> (%)	12.8(88.4)
Mean I/s(I)	6.9(0.8)
Completeness (%)	93.1(66.6)
Redundancy	5.3(1.8)
<b>Refinement</b>	
Resolution (Å)	25-2.81 (3.0, 3.0, 2.81)
Number of reflections (test set)	14515 (746)
R <sub>work</sub> /R <sub>free</sub>	0.233/0.274 (0.319/0.392)
Number of atoms	3,580
CCR2	2,215
T4L	1,243
BMS-681	35
CCR2-RA-[R]	24
Monoolein	25
Sulfate	20
Water	17
Zn	1
Mean overall B value (Å <sup>2</sup> )	41.4
Wilson B	40.4
Protein	41.5
Ligands	41.3
Water	22.9
<b>Root mean square deviation</b>	
Bond lengths (Å)	0.003
Bond angles (°)	0.85
<b>Ramachandran plot statistics<sup>c</sup> (%)</b>	
Favored regions	97.1
Allowed regions	2.9
Disallowed regions	0

<sup>a</sup>Diffraction data from 17 crystals were merged into a complete data set

<sup>b</sup>Highest resolution shell statistics are shown in parentheses

<sup>c</sup>As defined in MolProbity.<sup>42</sup>

**Table S2. Small Molecule (BMS-681) X-ray data collection and refinement.**

Empirical formula	C26 H36 F3 N5 O3.58
Formula weight	532.80
Temperature	173(2) K
Wavelength	1.54178 Å
Crystal system	Tetragonal
Space group	P4 <sub>3</sub> 2 <sub>1</sub> 2
Unit cell dimensions	a = 20.4436(4) Å $\alpha = 90^\circ$ . b = 20.4436(4) Å $\beta = 90^\circ$ . c = 28.9325(7) Å $\gamma = 90^\circ$ .
Volume	12092.1(4) Å <sup>3</sup>
Z	16
Density (calculated)	1.171 Mg/m <sup>3</sup>
Absorption coefficient	0.768 mm <sup>-1</sup>
F(000)	4522
Crystal size	0.46 x 0.18 x 0.16 mm <sup>3</sup>
Theta range for data collection	2.65 to 58.78°.
Resolution range	16.7 to 0.9 Å
Index ranges	-22 ≤ h ≤ 22, -21 ≤ k ≤ 22, -31 ≤ l ≤ 14
Reflections collected	108743
Independent reflections	8518 [R(int) = 0.1259]
Completeness to theta = 58.78°	98.6 %
Absorption correction	None
Refinement method	Full-matrix least-squares on F <sup>2</sup>
Data / restraints / parameters	8518 / 22 / 713
Goodness-of-fit on F <sup>2</sup>	1.058
Final R indices [I > 2σ(I)]	R1 = 0.0770, wR2 = 0.2087
R indices (all data)	R1 = 0.0860, wR2 = 0.2178
Absolute structure parameter; Flack(x)	0.1(2)
Absolute structure parameter; Hooft(y), P3true	0.03(5), 1.000
Largest diff. peak and hole	0.543 and -0.405 e.Å <sup>-3</sup>

**Table S3. Displacement of specific [<sup>3</sup>H]-INCB3344 (5 nM) and [<sup>3</sup>H]-CCR2-RA (3 nM) binding from CCR2 constructs transiently expressed on CHO cells.**

Construct	[ <sup>3</sup> H]-INCB3344 displacement by INCB-3344	[ <sup>3</sup> H]-INCB3344 displacement by BMS-681	[ <sup>3</sup> H]-CCR2-RA displacement by CCR2-RA-[R]	[ <sup>3</sup> H]-CCR2-RA enhancement by BMS-681
	pIC <sub>50</sub> ± S.E.M (IC <sub>50</sub> <sup>a</sup> nM)			%Binding
WT CCR2	7.8 ± 0.0 (17)	8.1 ± 0.0 (8)	7.9 ± 0.0 (13)	134 ± 3% <sup>a</sup> ***
CCR2-T4L	8.1 ± 0.1* (8)	8.6 ± 0.1** (3)	8.2 ± 0.0** (6)	157 ± 13% <sup>a</sup> ****

Values represent mean ± S.E.M of at least three independent experiments performed in duplicate. <sup>a</sup>Percentage of [<sup>3</sup>H]-CCR2-RA (3 nM) binding in presence of BMS-681 (1 μM). Values higher than 100% represent binding enhancement compared with the 100% control without BMS-681. Differences in pIC<sub>50</sub> values between constructs were analyzed using a Student's t-test, with significant differences noted as follows: \**P* < 0.05, \*\**P* < 0.01. Differences in percentage Binding in the absence (100%) and presence of BMS-681 were analyzed using a one-way analysis of variance with Dunnett's post-hoc test, with significant differences noted as follows: \*\**P* < 0.01, \*\*\*\**P* < 0.0001.

**Table S4. Observed association and dissociation rate constants of [<sup>3</sup>H]-CCR2-RA (7 nM) on membranes from CHO cells transiently expressing WT CCR2 and CCR2-T4L, in the absence or presence of 1 μM BMS-681.**

	CHO-CCR2		CHO-CCR2-T4L	
	Control	+ 1 μM BMS-681	Control	+ 1 μM BMS-681
k <sub>obs</sub> (min <sup>-1</sup> )	0.031 ± 0.002	0.038 ± 0.003*	0.015 ± 0.003	0.015 ± 0.001
% B/B <sub>control</sub> <sup>a</sup>	100 ± 0.0	135 ± 2.0****	100 ± 0.0	162 ± 8.4**
k <sub>off,fast</sub> (min <sup>-1</sup> )	0.089 ± 0.015	0.069 ± 0.012*	0.077 ± 0.013	0.049 ± 0.003 <sup>b</sup>
k <sub>off,slow</sub> (min <sup>-1</sup> )	0.016 ± 0.005	0.012 ± 0.004	0.010 ± 0.003	
%fast	70 ± 10	71 ± 11	69 ± 8	N/A <sup>b</sup>

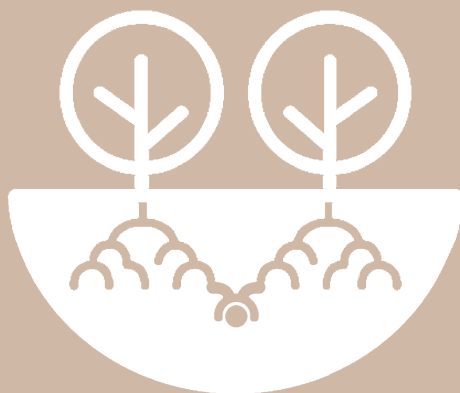
Values represent mean ± S.E.M of three independent experiments performed in duplicate. <sup>a</sup>The percentage of maximum binding in the absence (B<sub>control</sub>) or presence (B) of BMS-681 (1 μM). <sup>b</sup>For CHO-CCR2-T4L only, dissociation kinetics of [<sup>3</sup>H]-CCR2-RA (7 nM) in the presence of BMS-681 (1 μM) fitted best with a monophasic exponential decay model, resulting in a single k<sub>off</sub> value, as shown in the table. Thus for CHO-CCR2-T4L, the statistical significance between k<sub>off</sub> measurements with and without BMS-681 could not be calculated. Statistical significance was analyzed using a Student's t-test, with significant differences versus control noted as follows: \**P* < 0.05, \*\**P* < 0.01, \*\*\*\**P* < 0.0001



## Chapter 4

---

# Pyrrolone derivatives as intracellular allosteric modulators for chemokine receptors: Selective and dual-targeting inhibitors of CC Chemokine Receptors 1 and 2



*Natalia V. Ortiz Zacarías, Jacobus P.D. van Veldhoven, Laura Portner, Eric van Spronsen, Salviana Ullo, Margo Veenhuizen, Wijnand J.C. van der Velden, Annelien J.M. Zweemer, Roy M. Kreekel, Kenny Oenema, Eelke B. Lenselink, Laura H. Heitman, and Adriaan P. IJzerman*

*Journal of Medicinal Chemistry* 2018, 61 (20): 9146-9161



## ABSTRACT

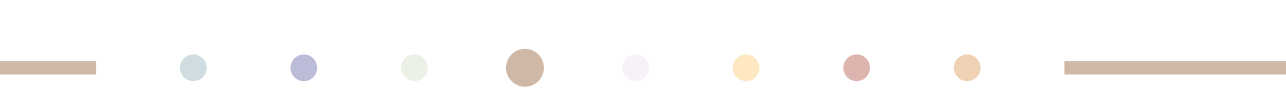
The recent crystal structures of CC chemokine receptors 2 and 9 (CCR2 and CCR9) have provided structural evidence for an allosteric, intracellular binding site. The high conservation of residues involved in this site suggests its presence in most chemokine receptors, including the close homolog CCR1. By using [<sup>3</sup>H]CCR2-RA-[R], a high-affinity, CCR2 intracellular ligand, we report an intracellular binding site in CCR1, where this radioligand also binds with high affinity. In addition, we report the synthesis and biological characterization of a series of pyrrolone derivatives for CCR1 and CCR2, which allowed us to identify several high-affinity intracellular ligands, including selective and potential multi-target antagonists. Evaluation of selected compounds in a functional [<sup>35</sup>S]GTPγS assay revealed that they act as inverse agonists in CCR1, providing a new manner of pharmacological modulation. Thus, this intracellular binding site enables the design of selective and multi-target inhibitors as a novel therapeutic approach.

## INTRODUCTION

Chemokines are chemotactic cytokines that control the migration and positioning of immune cells during physiological and pathological conditions by interacting with more than 20 different chemokine receptors.<sup>1</sup> Chemokine receptors mainly belong to the class A of G protein-coupled receptors (GPCRs), and can be divided into four different subtypes—namely C, CC, CXC and CX3C—according to the pattern of specific cysteine residues in their major endogenous chemokines.<sup>2</sup> To exert their function, chemokines bind at the extracellular side of their receptors in a binding mechanism involving the N-terminal domain, extracellular loops and the upper half of the transmembrane bundle.<sup>3,4</sup> After activation, most chemokine receptors signal through heterotrimeric G proteins, mainly  $G_{i/o}$  class, and  $\beta$ -arrestins.<sup>2</sup> CC Chemokine receptors 1 (CCR1) and 2 (CCR2) are two of the ten members of the CC subtype of chemokine receptors. CCR1 and CCR2 are expressed in a variety of immune cells, such as monocytes, dendritic cells and T helper type-1 ( $T_H1$ ) cells, from where they regulate diverse inflammatory and homeostatic functions.<sup>5</sup> Multiple chemokines activate these two receptors, including CCL3, CCL5 and CCL8 in the case of CCR1; and CCL2, CCL7 and CCL8 in the case of CCR2.<sup>2</sup>

Dysregulation of CCR1, CCR2 and their ligands has been linked to several inflammatory and immune diseases,<sup>6,7</sup> which has resulted in many drug discovery efforts to develop small molecules that target these receptors.<sup>8,9</sup> Several lines of evidence support a role for both CCR1 and CCR2 in the pathogenesis of diseases such as rheumatoid arthritis (RA) and multiple sclerosis (MS): increased expression of both receptors and their ligands in disease models and patients;<sup>10,11</sup> protective effect of genetic knockout of CCR1 or CCR2 in disease models;<sup>12,13</sup> and positive preclinical studies with chemokine-neutralizing monoclonal antibodies or small-molecule inhibitors of CCR1 or CCR2.<sup>14-16</sup> Yet, only few clinical studies have shown promising results,<sup>17,18</sup> while most of the drugs developed so far have failed in clinical trials due to lack of efficacy.<sup>8,9</sup> In this regard, the development of multi-target drugs has been proposed as a strategy to overcome the lack of efficacy. Multi-target drugs are designed to specifically act on more than one drug target, which might be necessary in highly heterogeneous diseases, such as RA and MS, where more than one chemokine receptor is involved.<sup>19</sup> The design of dual-antagonists has been previously undertaken for CCR1/CCR3,<sup>20</sup> CCR2/CCR5,<sup>21</sup> CCR5/CXCR4,<sup>22</sup> and CXCR1/CXCR2;<sup>23</sup> however no CCR1/CCR2 dual-antagonists have so far been reported.

Recently, the crystal structures of CCR2 (**Chapter 3**)<sup>24</sup> and CCR9<sup>25</sup> have revealed a novel allosteric binding site for small molecules in chemokine receptors. Both CCR2-RA-[R] in CCR2 and vercirnon in CCR9 bind in a pocket located in the intracellular surface of the receptors, partially overlapping with the binding site for G proteins and  $\beta$ -arrestins (**Chapter**



3).<sup>24, 25</sup> These intracellular ligands can inhibit the receptors in a non-competitive and insurmountable manner with regard to chemokine binding, as demonstrated previously in CCR2.<sup>26</sup> This might result in higher efficacy even in the presence of a high local concentration of chemokines during a disease state. Together with the potential advantages of allosteric modulators of chemokine receptors, this intracellular binding site seems to be quite conserved among chemokine receptors, which suggests the presence of homologous pockets in other receptors such as CCR1 (**Chapter 2**).<sup>27</sup> This conservation might provide an opportunity for the design of both selective and dual-targeting inhibitors of CCR1 and CCR2, as a novel approach to treat inflammatory and immune diseases.

For CCR2, several compounds belonging to different scaffolds have already been reported to bind to this intracellular binding site, including pyrrolone derivatives such as CCR2-RA-[R], sulfonamide derivatives and 2-mercapto imidazoles.<sup>26, 28</sup> When tested for selectivity, some of these compounds also displayed a moderate activity on CCR1,<sup>29-31</sup> suggesting that they might also bind to CCR1. Thus, we selected the pyrrolone scaffold to explore a potential intracellular binding site in CCR1. In our current study, we report the synthesis and the biological evaluation of novel and previously patented pyrrolone derivatives<sup>32, 33</sup> at both CCR1 and CCR2, in order to determine their selectivity and structure-affinity relationships (SAR) for both receptors. Finally, compounds were tested in a [<sup>35</sup>S]GTPγS binding assay, in order to determine their functional effects in CCR1 and CCR2. Overall, our results provide evidence that CCR1 can also be targeted with intracellular allosteric modulators, and that this binding site can be used for the design of multi-target compounds.

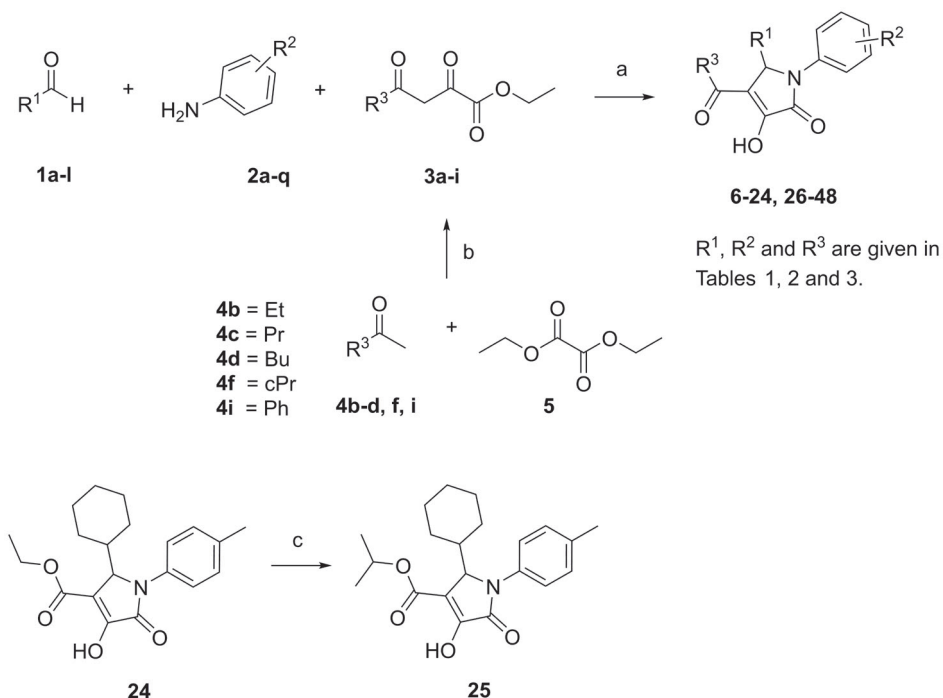


## RESULTS AND DISCUSSION

### Synthesis of pyrrolone derivatives

The racemic pyrrolones (**6-24**, **26-46**) depicted in Scheme 1 were synthesized via a one pot three component condensation reaction, starting from the commercially available substituted aldehydes **1a-l**, anilines **2a-q** and ethyl 2,4-dioxo-butanoates **3a-i** in acetic acid<sup>33</sup> (**6-23**, **26-46**) or THF<sup>29</sup> (**24**). The ethyl 2,4-dioxo-butanoates (**3b-d**, **f**, **i**), which were not commercially available, were prepared by a Claisen condensation starting from the methyl ketones (**4b-d**, **f**, **i**) and diethyl oxalate **5**.<sup>34</sup> Pyrrolone **25** was prepared via a transesterification of **24** by the use of *p*-toluenesulfonic acid in 2-propanol.

**Scheme 1. Synthesis route of pyrrolones 6 – 48, with different R<sup>1</sup>, R<sup>2</sup> and R<sup>3</sup> substituents<sup>a</sup>**



<sup>a</sup>Reagents and conditions: (a) acetic acid, reflux for 2-4 h or THF, rt, overnight; (b) Na, EtOH, 0-20 °C, overnight; (c) *p*-toluenesulfonic acid, 2-propanol, reflux, 48 h.

## Characterization of [<sup>3</sup>H]-CCR2-RA-[R] binding on CCR1 and CCR2

[<sup>3</sup>H]-CCR2-RA-[R] is the (*R*)-isomer of [<sup>3</sup>H]-CCR2-RA, a high-affinity radioligand previously characterized in our group for CCR2.<sup>26</sup> To avoid a possible effect of the lower-affinity isomer, we used the tritium-labeled (*R*)-isomer in the present study. As expected, [<sup>3</sup>H]-CCR2-RA-[R] binds with high-affinity to osteosarcoma (U2OS) cells stably expressing CCR2b (U2OS-CCR2) as shown by saturation experiments ( $K_D$  of 6.3 nM and  $B_{max}$  of 2.6 pmol/mg, Figure S1 and Table S1). Kinetic characterization showed that [<sup>3</sup>H]-CCR2-RA-[R] associates and dissociates in a biphasic manner (Table S1), consistent with the previously reported [<sup>3</sup>H]-CCR2-RA kinetics.<sup>26</sup> We had reported that [<sup>3</sup>H]-CCR2-RA binds with low affinity to CCR5 ( $K_D$  of 100 nM),<sup>28</sup> suggesting that CCR2-RA-[R] is a non-selective antagonist that can bind several chemokine receptors. In this regard, CCR1 is a close homolog of CCR2, with 61% amino acid similarity and 47% identity; furthermore, this amino acid similarity is > 90% when only considering the amino acid residues involved in the intracellular binding site of CCR2-RA-[R] in CCR2 (**Chapters 2 and 3**)<sup>24, 27</sup> (Figure S2). This prompted us to investigate the binding of [<sup>3</sup>H]-CCR2-RA-[R] in membrane preparations from U2OS cells stably expressing CCR1 (U2OS-CCR1). [<sup>3</sup>H]-CCR2-RA-[R] homologous displacement assays on U2OS-CCR1 yielded a  $K_D$  of 13.5 nM and a  $B_{max}$  of 6.1 pmol/mg (Figure 1a, Table S1), suggesting the presence of an intracellular site in CCR1 and making it a suitable tool to study such binding pocket. Binding of [<sup>3</sup>H]-CCR2-RA-[R] to U2OS-CCR1 was also assessed in kinetic experiments at 25 °C. These experiments showed that [<sup>3</sup>H]-CCR2-RA-[R] associates and dissociates in a biphasic manner, similar to our findings in CCR2, but the association and dissociation rates were significantly higher in CCR1 than in CCR2 (Figure S1 and Table S1).

Overall, these findings allowed us to set up a [<sup>3</sup>H]-CCR2-RA-[R] competitive displacement assay on both U2OS-CCR1 and U2OS-CCR2, to determine the binding affinity ( $K_i$ ) of unlabeled compounds. Using this assay, we first determined the ability of known ligands to displace this radioligand from CCR1, i.e. the CCR2 intracellular ligands SD-24 and JNJ-27141491,<sup>26, 28</sup> and the CCR1 orthosteric antagonist BX471<sup>35</sup> (Figure 1b). SD-24 and JNJ-27141491 fully displaced [<sup>3</sup>H]-CCR2-RA-[R] from CCR1 in a concentration-dependent manner, indicating that these compounds bind at the same binding site as CCR2-RA-[R]. SD-24 displaced the radioligand with a  $pK_i$  of  $7.45 \pm 0.05$  ( $K_i = 36$  nM), while JNJ-27141491 displaced [<sup>3</sup>H]-CCR2-RA-[R] with a  $pK_i$  of  $6.9 \pm 0.06$  ( $K_i = 138$  nM), consistent with previously reported activities in CCR1.<sup>30, 31</sup> To rule out that these compounds bind at the orthosteric binding site of CCR1, we also investigated the effect of BX471 in [<sup>3</sup>H]-CCR2-RA-[R] binding. As expected, BX471 was not able to displace the radioligand (Figure 1b); on the contrary, BX471 significantly enhanced the binding of [<sup>3</sup>H]-CCR2-RA-[R] by approximately 20% ( $116 \pm 2\%$  in the presence of 10  $\mu$ M BX471), in a similar manner as previously reported with CCR2 orthosteric antagonists (**Chapter 3**).<sup>24, 26</sup> This allosteric enhancement is consistent with two different binding sites in

CCR1: the orthosteric binding site where BX471 binds and an intracellular pocket for CCR2-RA-[R], SD-24 and JNJ-27141491.

This [ $^3\text{H}$ ]-CCR2-RA-[R] assay was also used to determine the affinity of the synthesized pyrrolone derivatives. All pyrrolone derivatives **6** – **46** were first tested at a single concentration of 1  $\mu\text{M}$  in both U2OS-CCR1 and U2OS-CCR2 (Tables 1 – 3). Compounds which displaced more than 50% of [ $^3\text{H}$ ]-CCR2-RA-[R] binding were further evaluated in this assay using at least six different concentrations of unlabeled compound in order to determine their binding affinity for the corresponding receptor subtypes (Figures 1c,d and Tables 1 – 3). Finally, we selected four compounds (**39**, **41**, **43** and **45**) to be tested in a functional [ $^{35}\text{S}$ ] GTP $\gamma\text{S}$  binding assay (Figure 3). The potency ( $\text{pIC}_{50}$ ) of these compounds was determined in the presence of an  $\text{EC}_{80}$  concentration of CCL3 (8 nM) or CCL2 (20 nM) in U2OS-CCR1 or U2OS-CCR2 membranes, respectively.

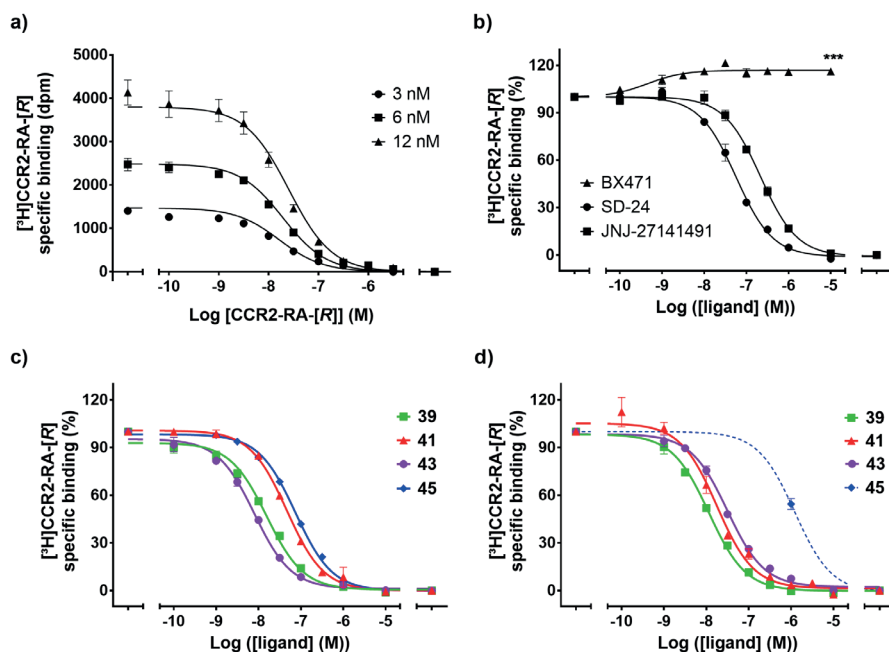


**Figure 1.** (a) Homologous displacement curves of 3, 6 and 12 nM [ $^3\text{H}$ ]-CCR2-RA-[R] specific binding by increasing concentrations of CCR2-RA-[R] in U2OS-CCR1, at 25°C. (b) Displacement curves of 6 nM [ $^3\text{H}$ ]-CCR2-RA-[R] specific binding by increasing concentrations of SD-24, JNJ-27141491 and BX471 in U2OS-CCR1 at 25°C. BX471 significantly enhanced the binding of [ $^3\text{H}$ ]-CCR2-RA-[R] up to 120%. Statistical significance between binding in absence (100%) and presence of 10  $\mu\text{M}$  BX471 ( $116 \pm 2\%$ ) was determined using an unpaired, two-tailed Student's *t*-test with Welch's correction. (c, d) Displacement curves of 6 nM [ $^3\text{H}$ ]-CCR2-RA-[R] specific binding by compounds **39**, **41**, **43** and **45** (c) in U2OS-CCR1 or (d) in U2OS-CCR2, at 25°C. In the case of U2OS-CCR2, compound **45** did not displace more than 50% of [ $^3\text{H}$ ]-CCR2-RA-[R], thus, only single-point data at 1  $\mu\text{M}$  is shown. The dashed blue line corresponds to the non-linear regression fit for compound **45** by GraphPad Prism 7.0. Data shown are mean  $\pm$  SEM of at least three experiments performed in duplicate.

## Docking of CCR2-RA-[R] in CCR1 and CCR2

In order to better understand the binding mode of CCR2-RA-[R] in both human CCR1 and CCR2b, we docked this compound into models of both receptors (Figure 2). In the case of CCR2, homology modeling was used to model the CCR2 residues between Ser226<sup>5x62</sup> and Lys240<sup>6x32</sup> (residues according to structure-based Ballesteros-Weinstein numbering<sup>36</sup>), which correspond to the M2 muscarinic acetylcholine receptor sequence in the CCR2b crystal structure (PDB ID:5T1A, **Chapter 3**).<sup>24</sup> These residues were modelled because this region is in close proximity to the CCR2-RA-[R] binding site. As expected from the sequence alignment (Figure S2), CCR2-RA-[R] was predicted to bind to CCR1 in an overlapping binding site as the one reported in the crystal structure of CCR2 (**Chapter 3**),<sup>24</sup> in a solvent-exposed intracellular pocket found between the intracellular ends of transmembrane segments 1 – 3, 6, 7 and helix 8 (Figure 2). The vinylogous carboxylic acid functionality makes similar interactions in CCR1 as in CCR2: the hydroxyl and the two carbonyl groups are involved in hydrogen-bond interactions with the side chain of Arg131<sup>3x50</sup>, and the backbone of Arg307<sup>8x49</sup> and Phe308<sup>8x50</sup> (Figure 2). A similar hydrophobic subpocket is also observed around the cyclohexyl moiety, which interacts with Ala<sup>6x33</sup>, Val/Leu<sup>6x36</sup>, Ile<sup>6x37</sup> and Ile<sup>6x40</sup>. Interestingly, Val244<sup>6x36</sup> in CCR2 is replaced by the bigger Leu240<sup>6x36</sup> in CCR1, which pushes the ligand down against Arg131<sup>3x50</sup>, resulting in a slightly different binding orientation of CCR2-RA-[R] in this receptor (Figure 2). In addition, the exchange of Lys311<sup>8x49</sup> in CCR2 by Arg307<sup>8x49</sup> in CCR1 might also contribute to the stabilization of this slightly altered binding pose. This difference in orientation could result in CCR1 selectivity, as this orientation seems to open up the subpockets in the proximity of the cyclohexyl and the acetyl group of CCR2-RA-[R] in CCR1, allowing the introduction of bigger and more lipophilic substituents at these positions.

## Structure-Affinity Relationships (SAR)

### *Modifications replacing the cyclohexyl group (R<sup>1</sup>, Table 1)*

Several pyrrolone derivatives have been previously evaluated at CCR2,<sup>29, 32, 33, 37</sup> resulting in the identification of CCR2-RA-[R] as a hit compound for further development,<sup>29</sup> but characterization of these compounds in CCR1 is mostly missing. Compound **6**, previously reported and characterized in CCR2 by Zou *et al.* (2007),<sup>37</sup> was selected as our starting point for the analysis of SAR in both CCR1 and CCR2. In our assay, compound **6** showed an affinity of 81 nM for CCR2, and a slightly higher affinity of 56 nM for CCR1 (Table 1). To note, the binding affinities reported previously for these pyrrolone derivatives were obtained with a <sup>125</sup>I-CCL2 binding assay,<sup>29, 37</sup> resulting in lower affinities compared with our [<sup>3</sup>H]-CCR2-RA-[R] binding assay, as previously observed in our group.<sup>26</sup> For our SAR study, we first examined

different C5 substituents of the pyrrolone core ( $R^1$ ), as shown in Table 1. In line with previous studies,<sup>29</sup> we found that increasing the size of the cycloalkyl group from cyclohexyl (**6**) to cycloheptyl (**7**) or cyclooctyl (**8**) resulted in a decrease in binding affinity for CCR2; however, the affinity for CCR1 was retained, indicating that bulkier groups are better tolerated in CCR1 than in CCR2, and providing an avenue for selectivity on CCR1 over CCR2. Previous studies showed that decreasing the size of the cycloalkyl group was also detrimental for CCR2,<sup>29</sup> so we decided not to explore smaller ring sizes.

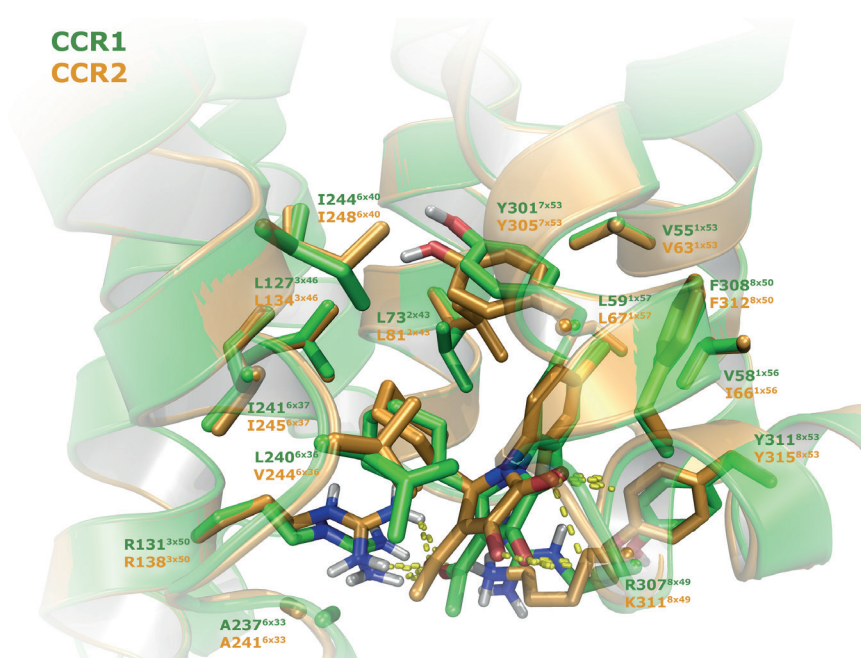


**Figure 2.** Proposed binding mode of compound CCR2-RA-[R] in the homology models of CCR1 and CCR2, based on the crystal structure of CCR2 (PDB ID: 5T1A, **Chapter 3**).<sup>24</sup> For CCR1 representative residues are shown as green ‘sticks’, and for CCR2 as orange ‘sticks’. In all cases, oxygen and nitrogen atoms are represented in red and blue, respectively; and hydrogen bonds with dashed yellow lines. Residues are numbered based on the corresponding residue numbers and with structure-based Ballesteros-Weinstein numbers in superscript.<sup>36</sup>

Substitution of the cycloalkyl group by a phenyl group (**9**) led to a great loss of CCR2 affinity (39% displacement at 1  $\mu$ M), consistent with previously reported values showing a decreased affinity for an almost similar pair of compounds.<sup>37</sup> Yet this substitution only led to a 3-fold decrease in CCR1 affinity ( $K_i$  of 162 nM), thus showing much higher selectivity for CCR1. Next, we explored the effect of *N*-aryl modifications in both affinity and selectivity (compounds **10** – **17**), specifically the effect of para and meta substituents. In general, *N*-aryl groups on the  $R^1$  position resulted in increased selectivity towards CCR1, as most compounds did not displace more than 36% [ $^3$ H]-CCR2-RA-[R] binding in CCR2 at a concentration of 1  $\mu$ M. Only

compounds **12** and **13**, with halogen substitutions in para position (Cl and Br, respectively) regained CCR2 affinity (**12**, 207 nM; **13**, 214 nM). Furthermore, para-substituted derivatives displayed significantly higher affinities compared with their meta-substituted analogues.

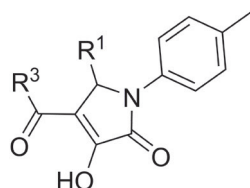
In the case of CCR1, introduction of a para-methyl moiety (**10**) resulted in a slight decrease in affinity compared with the unsubstituted **9**; in contrast, the meta-substituted analogue (**14**) showed less than 50% displacement at 1  $\mu$ M. Introduction of an electron-donating substituent (methoxy, **11** and **15**) was not well tolerated in any position, as it led to an approximately 3-fold decrease in affinity when placed in para position (**11**, 541 nM) and a near complete loss of affinity when placed in meta position (**15**, 28% displacement at 1  $\mu$ M). Halogen substituents in para position were also more favored in the case of CCR1, yielding higher affinities compared with the unsubstituted **9** and regardless of the halogen used (67 nM for R<sup>1</sup> = 4-Cl phenyl (**12**),  $p < 0.0001$  to **9**; 87 nM for R<sup>1</sup> = 4-Br phenyl (**13**);  $p = 0.0002$  to **9**). However, selectivity for CCR1 was notably reduced considering that these compounds displayed binding affinities of around 200 nM in CCR2. Although moving the halogens to the meta position (**16** and **17**) decreased the affinities more than 2-fold compared with their para analogues, selectivity for CCR1 was restored as these compounds showed less than 20% displacement of [<sup>3</sup>H]-CCR2-RA-[R] binding in CCR2. Together, the results for compounds **6** to **17** indicate that in CCR1 aliphatic groups yield higher affinities, while aromatic groups yield lower affinities but improved selectivity over CCR2.

### ***Modifications to the acetyl group (R<sup>3</sup>, Table 1)***

Previous modifications to the vinylogous carboxylic acid functionality in CCR2 showed detrimental effects in binding affinity.<sup>29, 37</sup> Indeed, mutagenesis and structural studies have shown crucial interactions of the hydroxyl and the two carbonyl groups with Glu310<sup>8x48</sup>, Lys311<sup>8x49</sup> and Phe312<sup>8x50</sup> in CCR2 (**Chapter 3**).<sup>24, 28</sup> Sequence alignment of CCR1 and CCR2 (Figure S2) and our docking study (Figure 2) suggest similar interactions in CCR1, as only position 8.49 differs (arginine in CCR1 and lysine in CCR2). Therefore, we decided to keep the vinylogous carboxylic acid moiety and explore different modifications to the acetyl group at the R<sup>3</sup> position (Table 1). A gradual increase in the length of the alkyl chain from a methyl group (**6**) to a butyl group (**18** – **20**) resulted in a ~2-fold increase in CCR1 affinity (30 nM for R<sup>3</sup> = ethyl (**18**),  $p = 0.0004$  against **6**; 29 nM for R<sup>3</sup> = propyl (**19**),  $p = 0.0002$  against **6**; and 31 nM for R<sup>3</sup> = butyl (**20**),  $p = 0.0010$  against **6**). In contrast, for CCR2 we observed a similar or a slight decrease in affinity. Introduction of a bulkier isopropyl group led to a decrease in affinity in both receptors, with a more drastic effect in CCR2 affinity. Replacing the isopropyl group with cyclopropyl (**22**) or *tert*-butyl (**23**) restored the affinity in CCR2 to values similar to compound **20** (**22**, 160 nM; **23**, 158 nM); in CCR1, these modifications further improved the binding affinity to approximately 20 nM, yielding compounds with the highest affinity

and selectivity observed in these series of R<sup>1</sup> and R<sup>3</sup> modifications (**22**, 19 nM; **23**, 22 nM). These results suggest a larger hydrophobic subpocket in CCR1, able to accommodate larger and branched alkyl chains.

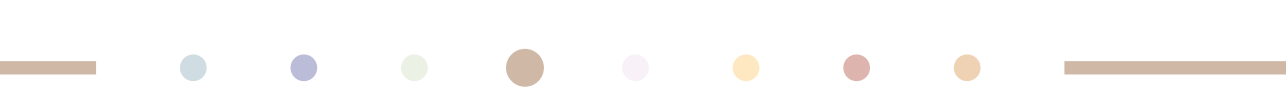
**Table 1. Binding affinities of compounds 6 – 26 on human CCR1 and human CCR2.**



Compound	R <sup>1</sup>	R <sup>3</sup>	pK <sub>i</sub> ± SEM (K <sub>i</sub> , nM) <sup>a</sup> or displacement at 1 μM (%) <sup>b</sup>	
			CCR1	CCR2
<b>6</b>	c-hexyl	Me	7.26 ± 0.04 (56)	7.10 ± 0.03 (81)
<b>7</b>	c-heptyl	Me	7.26 ± 0.03 (56)	7.02 ± 0.06 (96)
<b>8</b>	c-octyl	Me	7.24 ± 0.01 (57)	6.79 ± 0.09 (170)
<b>9</b>	Ph	Me	6.79 ± 0.04 (162)	39% (38, 40)
<b>10</b>	4-Me Ph	Me	6.71 ± 0.06 (198)	36% (42, 31)
<b>11</b>	4-OMe Ph	Me	6.27 ± 0.01 (541)	5% (5, 5)
<b>12</b>	4-Cl Ph	Me	7.17 ± 0.01 (67)	6.70 ± 0.08 (207)
<b>13</b>	4-Br Ph	Me	7.07 ± 0.07 (87)	6.67 ± 0.04 (214)
<b>14</b>	3-Me Ph	Me	47% (51, 44)	11% (14, 8)
<b>15</b>	3-OMe Ph	Me	28% (34, 22)	0% (3, -3)
<b>16</b>	3-Cl Ph	Me	6.70 ± 0.01 (198)	19% (25, 14)
<b>17</b>	3-Br Ph	Me	6.74 ± 0.02 (181)	19% (20, 18)
<b>18</b>	c-hexyl	Et	7.52 ± 0.01 (30)	6.99 ± 0.06 (104)
<b>19</b>	c-hexyl	Pr	7.54 ± 0.04 (29)	6.86 ± 0.10 (144)
<b>20</b>	c-hexyl	Bu	7.50 ± 0.004 (31)	6.81 ± 0.05 (158)
<b>21</b>	c-hexyl	<i>i</i> -Pr	7.39 ± 0.06 (42)	6.50 ± 0.05 (316)
<b>22</b>	c-hexyl	<i>c</i> -Pr	7.74 ± 0.08 (19)	6.80 ± 0.05 (160)
<b>23</b>	c-hexyl	<i>t</i> -Bu	7.66 ± 0.05 (22)	6.81 ± 0.07 (158)
<b>24</b>	c-hexyl	OEt	6.70 ± 0.01 (200)	31% (36, 26)
<b>25</b>	c-hexyl	<i>O</i> /Pr	36% (45, 26)	6% (10, 1)
<b>26</b>	c-hexyl	-Ph	7.11 ± 0.01 (77)	37% (45, 30)

<sup>a</sup>pK<sub>i</sub> and K<sub>i</sub> (nM) values obtained from [<sup>3</sup>H]-CCR2-RA-[R] binding assays on U2OS membranes stably expressing human CCR1 or human CCR2. Values are means ± standard error of the mean (SEM) of at least three independent experiments performed in duplicate. <sup>b</sup>% of [<sup>3</sup>H]-CCR2-RA-[R] displacement by 1 μM compound. Values represent the mean of two independent experiments performed in duplicate.





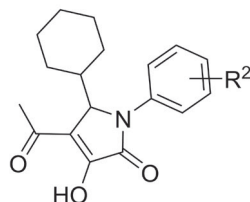
We also explored the effect of adding heteroatoms—oxygen in this case—between the carbonyl and an ethyl or isopropyl group (**24** and **25**, respectively). Overall, this led to a drastic drop in affinity for both receptors. This detrimental effect was most pronounced in compound **25**, which displaced less than 40% of [<sup>3</sup>H]-CCR2-RA-[R] binding in CCR1 and less than 10% in CCR2. The transformation of the ketone into an ester might decrease the electron density on the carbonyl oxygen, as well as the acidity of the adjacent protons, thus weakening or disrupting key hydrogen bonding interactions with Lys<sup>8x49</sup> in CCR2 (**Chapter 3**)<sup>24, 28</sup> or Arg<sup>8x49</sup> in CCR1. The need of an acidic function for intracellular antagonists has also been reported in a study with *N*-benzylindole-2-carboxylic acids, where the authors found a correlation between higher acidity and higher CCR2 affinity.<sup>38</sup> Finally, replacing the methyl group in R<sup>3</sup> with a phenyl group (**26**) had no effect on CCR1 affinity, while it only displaced 37% of [<sup>3</sup>H]-CCR2-RA-[R] binding in CCR2. Altogether these findings indicate that bigger, more lipophilic groups in R<sup>3</sup> are better tolerated in CCR1, while in CCR2 methyl is preferred.

### **Modifications to the phenyl ring (R<sup>2</sup>, Table 2)**

In addition, we explored different *N*-aryl modifications in the phenyl ring (R<sup>2</sup>, Table 2), starting with modifications in para position. Removing the methyl group in **6** yielded compound **27**, with an unsubstituted phenyl group, which displaced less than 50% of the radioligand in both receptors. Increasing the size of the alkyl group from methyl (**6**) to ethyl (**28**) caused a 3-fold decrease in CCR1 affinity, while the affinity in CCR2 was maintained (**28**, 168 nM in CCR1 versus 66 nM in CCR2). Adding an electron-donating methoxy group was unfavorable for both receptors, as affinities dropped to 260 nM in CCR1 and 217 nM in CCR2. In contrast, an electron-withdrawing substituent (trifluoromethyl, **32**) restored the affinity to 92 nM in CCR2, similar to our starting compound **6**, and to 144 nM in CCR1. The substitution of the para-methyl group with halogens yielded derivatives with improved binding affinities in both receptors (**30** and **31**), but no gain in selectivity. Substitution with a chlorine (**30**) or bromine atom (**31**) led to a 4.5-fold increase in CCR2 affinity compared with **6**, with K<sub>i</sub> values around 20 nM regardless of the halogen. In the case of CCR1, the bromine atom (**31**) led to a 2-fold increase compared with **6** (**31**, 24 nM), while the smaller chlorine atom did not affect the affinity much (**30**, 39 nM). Although not synthesized in our study, Dasse *et al.* (2007),<sup>29</sup> showed that the para-fluoro analogue performed worse in CCR2 than other para-halogen derivatives. In this regard, from fluoro to chloro there is an important increase in polarity ( $\sigma$ ), lipophilicity ( $\pi$ ) and size, whereas from chloro to bromo only lipophilicity and size increase.<sup>39, 40</sup> Taken together, these results suggest that lipophilicity and size of the halogen might be more important in CCR1 than in CCR2, while electronegativity or polarity could play a bigger role in CCR2.



**Table 2. Binding affinities of compounds 6, 27 – 42 on human CCR1 and human CCR2.**



Compound	R <sup>2</sup>	pK <sub>i</sub> ± SEM (K <sub>i</sub> , nM) <sup>a</sup> or displacement at 1 μM (%) <sup>b</sup>	
		CCR1	CCR2
<b>27</b>	H	42% (41, 42)	45% (44, 45)
<b>6</b>	4-Me	7.26 ± 0.04 (56)	7.10 ± 0.03 (81)
<b>28</b>	4-Et	6.78 ± 0.02 (168)	7.19 ± 0.05 (66)
<b>29</b>	4-OMe	6.60 ± 0.07 (260)	6.67 ± 0.05 (217)
<b>30</b>	4-Cl	7.41 ± 0.05 (40)	7.73 ± 0.08 (19)
<b>31</b>	4-Br	7.62 ± 0.05 (24)	7.80 ± 0.12 (17)
<b>32</b>	4-CF <sub>3</sub>	6.86 ± 0.08 (144)	7.04 ± 0.02 (92)
<b>33</b>	3-Me	6.31 ± 0.07 (500)	6.58 ± 0.06 (265)
<b>34</b>	3-F	44% (45, 42)	47% (48, 47)
<b>35</b>	3-Cl	6.28 ± 0.08 (541)	6.62 ± 0.02 (239)
<b>36</b>	3-CF <sub>3</sub>	25% (23, 27)	6.54 ± 0.11 (305)
<b>37</b>	2-F, 4-Me	7.56 ± 0.10 (29)	7.44 ± 0.05 (37)
<b>38 (CCR2-RA)</b>	2-F, 4-Cl	7.82 ± 0.06 (15)	8.00 ± 0.09 (11)
<b>39</b>	2-F, 4-Br	7.98 ± 0.04 (11)	8.25 ± 0.02 (6)
<b>40</b>	3,4-diMe	7.37 ± 0.03 (43)	7.75 ± 0.02 (18)
<b>41</b>	3-Me, 4-Cl	7.51 ± 0.01 (31)	8.09 ± 0.08 (9)
<b>42</b>	3-F, 4-Me	7.32 ± 0.07 (49)	7.24 ± 0.02 (57)

<sup>a</sup>pK<sub>i</sub> and K<sub>i</sub> (nM) values obtained from [<sup>3</sup>H]-CCR2-RA-[R] binding assays on U2OS membranes stably expressing human CCR1 or human CCR2. Values are means ± standard error of the mean (SEM) of at least three independent experiments performed in duplicate. <sup>b</sup>% of [<sup>3</sup>H]-CCR2-RA-[R] displacement by 1 μM compound. Values represent the mean of two independent experiments performed in duplicate.

Moving the substituents from the para to the meta position resulted in poor affinities for both receptors, compared with their para-substituted analogues. In CCR1, the *meta*-methyl (**33**) and *meta*-chlorine (**35**) groups led to a 9-fold and 13-fold decrease in affinity, respectively; in CCR2, the affinities decreased 3-fold and 13-fold after the same substitutions. The addition of a trifluoromethyl group in meta position (**36**) also led to a 3-fold decrease in CCR2 affinity compared with its para-substituted analogue **32**. In CCR1 **36** only displaced 25% of [<sup>3</sup>H]-CCR2-RA-[R] binding at a concentration of 1 μM, displaying the highest selectivity towards

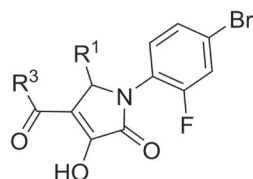
CCR2 in these series of modifications. Also detrimental was the addition of a fluorine group in meta position (**34**), which led to less than 50% displacement of [<sup>3</sup>H]-CCR2-RA-[R] binding in both receptors. Overall, substituents in para position were more favored in both receptors, especially halogen substituents, yet none of the compounds displayed selectivity towards CCR1. Similarly as reported by Dasse *et al.* (2007),<sup>29</sup> attempts to introduce different substituents in the ortho position were unsuccessful, thus we continued to explore different combinations of phenyl substituents.

As part of our SAR analysis we synthesized compound **38** (also referred as CCR2-RA), which corresponds to the racemic mixture of the radioligand [<sup>3</sup>H]-CCR2-RA-[R] used in this study. This compound displayed an affinity of 15 nM in CCR1 and 10 nM in CCR2, similar to the  $K_d$  values obtained in homologous displacement or saturation assays (Table S1). Replacing the para-chloro group in **38** with a methyl moiety (**37**), while keeping the ortho-fluorine group, led to an expected decrease in affinity for both receptors, as compound **6** with a methyl group in para position performed worse than **30** with a chlorine atom in the same position. When the para substituent was replaced with a bromine atom (**39**), the affinity was restored to 11 nM in CCR1 and 6 nM in CCR2. Subsequent combinations of meta and para substituents (**40 – 42**) generated compounds with decreased CCR1 affinities compared with **38**, as expected from the data on the mono-substituted meta analogues. Compound **41** displayed a slightly higher selectivity for CCR2 (8 nM in CCR2 *versus* 31 nM in CCR1). Overall, disubstituted derivatives performed better than the mono-substituted compounds in both receptors; however, no clear trend in selectivity was observed in these series.

In an attempt to improve both affinity and selectivity for CCR1, we decided to combine some of the best features observed at R<sup>1</sup>, R<sup>2</sup> and R<sup>3</sup> positions: a disubstituted phenyl ring with an ortho-fluoro and para-bromo moieties for R<sup>2</sup>, in order to retain the high affinity of **39**; a cyclopropyl group or an unsubstituted phenyl ring at R<sup>3</sup> (**22** and **26**) to gain selectivity; and a meta-bromo phenyl ring at R<sup>1</sup> (**17**) to further improve selectivity for CCR1. These combinations resulted in four final compounds shown in Table 3 (**43 – 46**). To maintain a high affinity for CCR1, we kept the 2-fluoro-4-bromophenyl group at R<sup>2</sup> constant and we combined it with different R<sup>1</sup> and R<sup>3</sup> substituents. The combination with a cyclopropyl group at R<sup>3</sup> position (**43**) led to the highest CCR1 affinity in our study ( $K_i$  of 5 nM), but selectivity over CCR2 was reduced compared with **22** (3-fold *versus* 8-fold). Replacing the cyclopropyl group at R<sup>3</sup> by a phenyl group (**44**) decreased the affinity for CCR1 by more than 5-fold compared with **43**. Compound **43**, somewhat unexpectedly, bound to CCR2 with an affinity of 66 nM, more than 15-fold better than **26**. Replacing the cyclohexyl group at R<sup>1</sup> (**43**) by a 3-bromo-phenyl group (**45**) resulted in an improved selectivity over CCR2, as this compound did not displace more than 50% of [<sup>3</sup>H]-CCR2-RA-[R] binding at 1 μM, whereas it showed an affinity of 50 nM in CCR1. Finally, replacing the cyclopropyl with a methyl group at R<sup>3</sup> (**46**)

maintained the affinity for CCR1 and restored the affinity for CCR2 (65 nM in CCR1 and 216 nM in CCR2), with a concomitant loss of selectivity.

**Table 3. Binding affinities of compounds 43 – 46 on human CCR1 and human CCR2.**



Compound	R <sup>1</sup>	R <sup>3</sup>	pK <sub>i</sub> ± SEM (K <sub>i</sub> , nM) <sup>a</sup> or displacement at 1 μM (%) <sup>b</sup>	
			CCR1	CCR2
<b>43</b>	c-hexyl	c-propyl	8.27 ± 0.02 (5)	7.82 ± 0.04 (15)
<b>44</b>	c-hexyl	Ph	7.56 ± 0.04 (28)	7.18 ± 0.03 (66)
<b>45</b>	3-Br Ph	c-propyl	7.30 ± 0.01 (50)	45% (49, 42)
<b>46</b>	3-Br Ph	Me	7.19 ± 0.02 (65)	6.67 ± 0.01 (216)

<sup>a</sup>pK<sub>i</sub> and K<sub>i</sub> (nM) values obtained from [<sup>3</sup>H]-CCR2-RA-[R] binding assays on U2OS membranes stably expressing human CCR1 or human CCR2. Values are means ± standard error of the mean (SEM) of at least three independent experiments performed in duplicate. <sup>b</sup>% of [<sup>3</sup>H]-CCR2-RA-[R] displacement by 1 μM compound. Values represent the mean of two independent experiments performed in duplicate.

## Functional characterization of selected compounds

Following the SAR analysis, four compounds (**39**, **41**, **43** and **45**) were selected for further characterization in a G protein-dependent functional assay, in order to assess their inhibitory potencies (pIC<sub>50</sub>) in both CCR1 and CCR2. The four compounds were selected based on their affinity and selectivity profile: compounds **43** and **39**, with the highest affinity for either CCR1 or CCR2 respectively; compound **41**, with higher selectivity towards CCR2; and compound **45**, with higher selectivity towards CCR1. As functional assay we used a previously reported [<sup>35</sup>S]GTPγS binding assay on U2OS-CCR2 membranes, which had been applied in the functional characterization of several allosteric and orthosteric CCR2 ligands.<sup>26</sup> Similarly as reported by Zweemer *et al.* (2013),<sup>26</sup> CCL2 stimulated [<sup>35</sup>S]GTPγS binding in a concentration-dependent manner, displaying a potency of 5 nM in CCR2 (pEC<sub>50</sub> = 8.3 ± 0.09, Figure 3a). Using the same assay conditions, we characterized the G protein activation of CCL3 in U2OS-CCR1 membranes. In this assay, CCL3 induced [<sup>35</sup>S]GTPγS binding in CCR1 with a higher potency than CCL2 in CCR2 (1.3 nM, pEC<sub>50</sub> = 8.9 ± 0.06), and with a higher maximum effect (E<sub>max</sub>) (Figure 3a). It should be noted that the potency of CCL3 in our study is lower than previously reported,<sup>41</sup> which might be related to the differences in cell line and/or assay conditions.

For the antagonist assays, we used a submaximal EC<sub>80</sub> concentration of CCL3 (8 nM) and CCL2 (20 nM) in CCR1 or CCR2, respectively, in order to evoke 80% stimulation of [<sup>35</sup>S]GTPγS binding. Although all compounds were able to inhibit CCL3- or CCL2-induced G protein activation, their potencies (IC<sub>50</sub>) ranged between 30 nM to 8 μM (Table 4 and Figure 3b,c). In CCR2, the potency of the compounds increased in the same order observed for affinity (Figure 3c, **45** < **43** < **41** < **39**). In CCR1 **39** displayed the highest potency (590 nM), followed by **43** (950 nM), contrary to their binding affinity (Figure 3b, **43** > **39**). In addition, the moderate selectivity observed in the binding assays was lost in this functional assay: except for **45**, all compounds were more potent inhibitors of CCR2 than CCR1, as their potencies were 3-fold (**43**), 19-fold (**39**) or 48-fold (**41**) lower in CCR1. Upon comparison of potencies in the [<sup>35</sup>S]GTPγS assay and the affinities in the [<sup>3</sup>H]-CCR2-RA-[R] binding assay, we observed that all compounds displayed between 5 to 10-fold difference between assays in CCR2 (Tables 2 – 4), in agreement with previous characterization of CCR2-RA-[R] on this receptor.<sup>26</sup> In contrast, all compounds displayed at least a 50-fold difference between assays when tested on CCR1. Such lack of correlation between apparent potencies and binding affinities in CCR1 might be dependent on the assay conditions used, G protein concentrations, or the chemokine used in this study; thus, further studies are warranted to fully characterize these ligands for their selectivity.

**Table 4. Functional characterization of compounds 37, 39, 41 and 43 in U2OS-CCR1 and U2OS-CCR2 using a [<sup>35</sup>S]GTPγS binding assay.**

Compound	Inhibition of [ <sup>35</sup> S]GTPγS binding <sup>a</sup>					
	CCR1 <sup>b</sup>			CCR2 <sup>c</sup>		
	pIC <sub>50</sub> ± SEM	(IC <sub>50</sub> , μM)	Hill slope	pIC <sub>50</sub> ± SEM	(IC <sub>50</sub> , μM)	Hill slope
<b>39</b>	6.26 ± 0.10	(0.59)***	-0.62 ± 0.05**	7.57 ± 0.08	(0.03)	-0.94 ± 0.18
<b>41</b>	5.73 ± 0.09	(1.94)***	-0.72 ± 0.08*	7.47 ± 0.10	(0.04)	-0.88 ± 0.13
<b>43</b>	6.03 ± 0.04	(0.95)	-0.73 ± 0.02*	6.54 ± 0.16	(0.33)	-0.80 ± 0.13
<b>45</b>	5.07 ± 0.05	(8.64)	-0.93 ± 0.01	5.06 ± 0.05	(8.77)	-1.20 ± 0.08

<sup>a</sup>All values are means ± SEM. of at least three independent experiments performed in duplicate. Unpaired *t*-test analysis with Welch's correction was performed to analyze differences in pIC<sub>50</sub> values between receptors, with differences noted as \*\*\*, *p* < 0.001. One-way ANOVA with Dunnett's post-hoc test was performed to compare pseudo-Hill slopes against compound **45**, which showed a pseudo-Hill slope of approx. unity in both receptors, with significant differences displayed as \*, *p* < 0.05; \*\*, *p* < 0.01. <sup>b</sup>Inhibition of CCL3-induced [<sup>35</sup>S]GTPγS binding in U2OS membranes stably expressing human CCR1. A concentration of 8 nM CCL3 was used in the assays to evoke an 80% response. <sup>c</sup>Inhibition of CCL2-induced [<sup>35</sup>S]GTPγS binding in U2OS membranes stably expressing human CCR2. A concentration of 20 nM CCL2 was used in the assays to evoke an 80% response.

In CCR1, all compounds behaved as inverse agonists, as they all significantly decreased the basal activity of CCR1 at the highest concentration tested (Figure S3a). In this regard, it was previously demonstrated that CCR1 exhibits constitutive activity leading to ligand-independent G protein-activation,  $\beta$ -arrestin recruitment and receptor internalization,<sup>42</sup> which points to the development of inverse agonists as a potential therapeutic option for inflammatory diseases. Yet, only BX471<sup>35</sup> has been reported to act as inverse agonist in CCR1.<sup>42</sup> This prompted us to further characterize these compounds as inverse agonists in CCR1, by measuring their inhibitory potency in absence of the agonist CCL3 (Figure S3b and Table S2). Compounds **39** and **41** were more potent inverse agonists than antagonists, displaying a 3-fold and almost 10-fold higher potency, respectively, as inverse agonists. As such, their potencies as inverse agonists were more comparable to their binding affinities (Table 2 and Table S2). In contrast, **43** and **45** showed similar potencies when measured in the absence or presence of CCL3, and thus, displayed more than 130-fold difference between functional and binding assays (Table 2 and Table S2). Interestingly, both compounds **43** and **45** have a cyclopropyl in the R<sup>3</sup> position while **39** and **41** have a methyl group (Tables 2 and 3), which suggests that this larger group might be responsible for the difference in their efficacy and functional profile. Moreover, most compounds displayed pseudo-Hill slopes of less than unity in CCR1, when tested in the presence or absence of CCL3 (Table 4 and Table S2), indicative of a more complex mechanism of inhibition, combining negative allosteric modulation and inverse agonism.<sup>43</sup> Of note, the basal levels of constitutive activity in the [<sup>35</sup>S]GTP $\gamma$ S assay are very dependent on the assay conditions used, such as GDP concentrations. Yet, at a single-concentration (100  $\mu$ M) tested, all compounds consistently decreased the basal activity in CCR1 after varying GDP concentrations. For instance, compound **41** decreased basal activity by 22% (1  $\mu$ M GDP), 26% (10  $\mu$ M GDP) and 25% (20  $\mu$ M GDP) (data not shown). To the best of our knowledge, these compounds represent the first intracellular ligands with demonstrated inverse agonism in CCR1. Both **45** and **43** decreased the basal activity of CCR2 to a similar or smaller level than in CCR1 (**45**, maximal decrease of 58%; **43**, maximal decrease of 27%), indicative of inverse agonism (Figure S3a). However, no constitutive activity has been reported for CCR2, with only one constitutively active mutant (CAM) described so far.<sup>44</sup> In fact, Gilliland *et al.* (2013) showed that CCR2 was not able to induce ligand-independent cell migration or to constitutively associate with  $\beta$ -arrestin, pointing to a lack of constitutive activity.<sup>42</sup> Moreover, several classes of orthosteric and allosteric CCR2 ligands did not show evidence of inverse agonism when previously tested in a similar [<sup>35</sup>S]GTP $\gamma$ S binding assay.<sup>26</sup> Thus, the inverse agonism observed in this study might be the consequence of the expression level, ligand concentration and/or assay conditions employed, so further research is warranted to investigate ligand-independent signaling in CCR2.

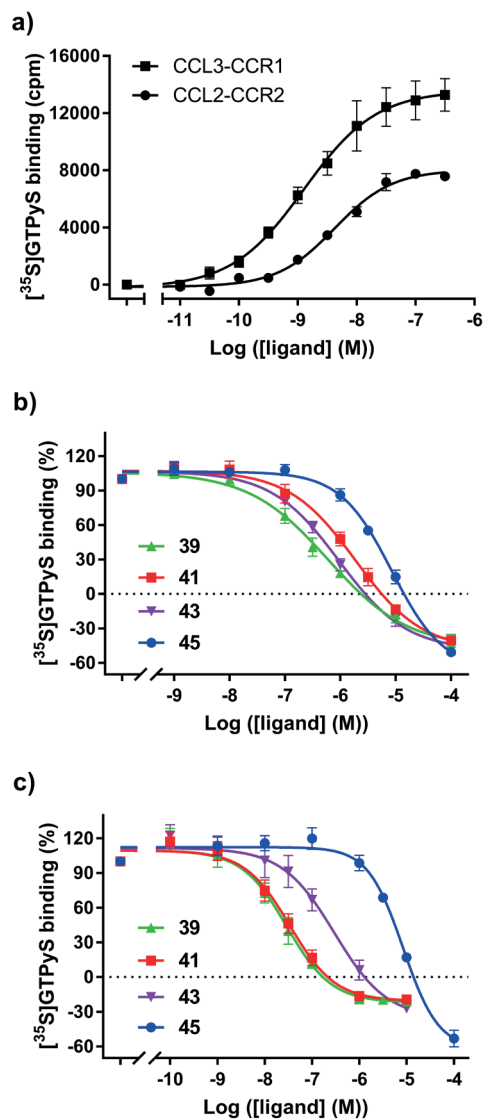


**Figure 3.** (a) [<sup>35</sup>S]GTPγS binding upon stimulation of U2OS-CCR1 and U2OS-CCR2 by increasing concentrations of CCL3 and CCL2, respectively. In both cases, the response was corrected by subtracting the basal activity (approx. 8000 dpm for both CCR1 and CCR2). (b) Inhibition of CCL3-induced [<sup>35</sup>S]GTPγS binding by compounds **39**, **41**, **43** and **45** in U2OS-CCR1. (c) Inhibition of CCL2-induced [<sup>35</sup>S]GTPγS binding by compounds **39**, **41**, **43** and **45** in U2OS-CCR2. The level of basal activity in U2OS-CCR1 and U2OS-CCR2 is indicated by a dashed line. In all cases data shown are mean ± SEM of at least three experiments performed in duplicate.

## CONCLUSIONS

In this study we have characterized [<sup>3</sup>H]-CCR2-RA-[R], a high-affinity intracellular antagonist previously described for CCR2,<sup>26</sup> in both CCR1 and CCR2, which allowed us to conclude that this radioligand binds to CCR1 with a similar high-affinity. By characterizing this radioligand in CCR1, we have provided evidence that CCR1 possesses an intracellular binding site that can be used for the design of non-competitive compounds. In addition, this intracellular radioligand allowed us to explore the SAR of a series of pyrrolone derivatives in both CCR1 and CCR2. Although some of these derivatives had been previously described for CCR2, their characterization in CCR1 had not been reported. With the SAR analysis we learned that introduction of bulkier and more lipophilic groups at R<sup>1</sup> and R<sup>3</sup> positions was better tolerated in CCR1, allowing us to obtain better selectivity for this receptor. The high conservation between the intracellular pockets of CCR1 and CCR2 prevented us from finding high selectivity in these series of compounds, but allowed us to find several potential dual-target antagonists. Finally, characterization of four selected compounds in a functional assay allowed us to determine their functional effects as antagonists in CCR2 and inverse agonists in the constitutively-active CCR1, which opens up a novel avenue to modulate these receptors in inflammatory diseases. In addition, this highly-conserved binding site might allow the design of both selective and multi-target inhibitors for chemokine receptors, beyond CCR1 and CCR2.

## EXPERIMENTAL SECTION

### Chemistry

#### General methods.

All solvents and reagents were purchased from commercial sources and were of analytical grade. Demineralized water is simply referred to as H<sub>2</sub>O, as was used in all cases unless stated otherwise (i.e. brine). <sup>1</sup>H NMR spectra were recorded on a Bruker AV 400 liquid spectrometer (<sup>1</sup>H NMR, 400 MHz) at ambient temperature. Chemical shifts are reported in parts per million (ppm), are designated by  $\delta$  and are downfield to the internal standard tetramethylsilane (TMS) in CDCl<sub>3</sub>. Coupling-constants are reported in Hz and are designated as *J*. As a representative example of the obtained <sup>1</sup>H NMR spectra, Figure S4 shows the <sup>1</sup>H NMR spectrum of compound **43**. Analytical purity of the final compounds was determined by high pressure liquid chromatography (HPLC) with a Phenomenex Gemini 3 × C18 110A column (50 × 4.6 mm, 3  $\mu$ m), measuring UV absorbance at 254 nm. Sample preparation and HPLC method was—unless stated otherwise—as follows: 0.3–0.8 mg of compound was dissolved in 1 mL of a 1:1:1 mixture of CH<sub>3</sub>CN/H<sub>2</sub>O/tBuOH and eluted from the column within 15 min, with a three component system of H<sub>2</sub>O/CH<sub>3</sub>CN/1% TFA in H<sub>2</sub>O, decreasing polarity of the solvent mixture in time from 80/10/10 to 0/90/10. All compounds showed a single peak at the designated retention time and are at least 95% pure. Liquid chromatography–mass spectrometry (LC–MS) analyses were performed using Thermo Finnigan Surveyor – LCQ Advantage Max LC–MS system and a Gemini C18 Phenomenex column (50 × 4.6 mm, 3  $\mu$ m). The elution method was set up as follows: 1–4 min isocratic system of H<sub>2</sub>O/CH<sub>3</sub>CN/1% TFA in H<sub>2</sub>O, 80:10:10, from the 4th min, a gradient was applied from 80:10:10 to 0:90:10 within 9 min, followed by 1 min of equilibration at 0:90:10 and 1 min at 80:10:10. Thin-layer chromatography (TLC) was routinely performed to monitor the progress of reactions, using aluminum coated Merck silica gel F254 plates. Purification by column chromatography was achieved by use of Grace Davison DAVISIL silica column material (LC60A 30–200 micron). Yields and reaction conditions were not optimized. Additionally, all compounds were screened using FAF-Drugs<sup>45, 46</sup> in order to detect potential Pan-Assay Interference Compounds (PAINS). None of the compounds was identified as PAINS after application of three different filters based on Baell *et al.*<sup>47</sup>



## General procedure for the synthesis of compounds 6 – 23, 26 – 46.<sup>33</sup>

The respective aldehyde **1a-l** (1.0 eq.), aniline **2a-q** (1.0 eq.) and ethyl 2,4-dioxo-butanoate analogue **3a-i** (1.0 eq.) were dissolved in acetic acid (2.5 mL/mmol) and heated at 95°C for 2-4 h under a nitrogen atmosphere. Upon completion of the reaction (TLC 1/7 EtOAc/Pet ether) acetic acid was removed under reduced pressure, the residue was triturated with Et<sub>2</sub>O and stirred for 30 minutes after which the pure product was collected by filtration.

### **4-Acetyl-5-cyclohexyl-3-hydroxy-1-(4-methylphenyl)-1,5-dihydro-2H-pyrrol-2-one (6).**<sup>33</sup>

Started from cyclohexane carboxaldehyde **1a** (243  $\mu$ L, 2.00 mmol, 1.00 eq.), 4-methylaniline (214 mg, 2.00 mmol, 1.00 eq.) and ethyl 2,4-dioxopentanoate **3a** (251  $\mu$ L, 2.00 mmol, 1.00 eq.) in 5 mL of acetic acid. Yield: 287 mg, 46%, white solid. <sup>1</sup>H NMR (400 MHz, DMSO):  $\delta$  7.38 (d,  $J$  = 8.4 Hz, 2H), 7.24 (d,  $J$  = 8.4 Hz, 2H), 4.99 (d,  $J$  = 1.2 Hz, 1H), 2.43 (s, 3H), 2.32 (s, 3H), 1.83 (t,  $J$  = 11.2 Hz, 1H), 1.65-1.56 (m, 1H), 1.52-1.27 (m, 4H), 0.53 (qd,  $J$  = 12.4, 2.8 Hz, 1H) ppm. MS [ESI+H]<sup>+</sup>: 313.93.

### **4-Acetyl-5-cycloheptyl-3-hydroxy-1-(4-methylphenyl)-1,5-dihydro-2H-pyrrol-2-one (7).**<sup>32</sup>

Started from cycloheptylcarboxaldehyde **1b**<sup>48</sup> (375 mg, 3.00 mmol, 1.00 eq.), 4-methylaniline **2b** (321 mg, 3.00 mmol, 1.00 eq.) and ethyl 2,4-dioxopentanoate **3a** (377  $\mu$ L, 3.00 mmol, 1.00 eq.) in 7.5 mL of acetic acid. Purified by recrystallization from a mixture of EtOAc and Pet. Ether. Yield: 102 mg, 13%, off-white solid. <sup>1</sup>H NMR (400 MHz, CDCl<sub>3</sub>):  $\delta$  7.26-7.22 (m, 4H), 4.95 (d,  $J$  = 1.6 Hz, 1H), 2.54 (s, 3H), 2.38 (s, 3H) ppm, 2.09-2.03 (m, 1H), 1.61-1.47 (m, 4H), 1.46-1.32 (m, 4H), 1.31-1.12 (m, 4H), 0.80 (qd,  $J$  = 10.8, 3.2 Hz, 1H) ppm. MS: [ESI+H]<sup>+</sup>: 328.13.

### **4-Acetyl-5-cyclooctyl-3-hydroxy-1-(4-methylphenyl)-1,5-dihydro-2H-pyrrol-2-one (8).**<sup>32</sup>

Started from cyclooctylcarboxaldehyde **1c** (648 mL, 4.42 mmol, 1.00 eq.), 4-methylaniline **2b** (474 mg, 4.42 mmol, 1.00 eq.) and ethyl 2,4-dioxopentanoate **3a** (554  $\mu$ L, 4.42 mmol, 1.00 eq.) in 10 mL of acetic acid. Purified by column chromatography using as eluent 1/6 EtOAc/Pet ether. Yield: 118 mg, 8%, white solid. <sup>1</sup>H NMR (400 MHz, CDCl<sub>3</sub>):  $\delta$  7.26-7.21 (m, 4H), 4.90 (d,  $J$  = 1.6 Hz, 1H), 2.53 (s, 3H), 2.37 (s, 3H), 2.22-2.14 (m, 1H), 1.62-1.52 (m, 1H), 1.50-1.15 (m, 13H) 0.89-0.78 (m, 1H) ppm. MS: [ESI+H]<sup>+</sup>: 342.20.

### **4-Acetyl-3-hydroxy-1-(4-methylphenyl)-5-phenyl-1,5-dihydro-2H-pyrrol-2-one (9).**<sup>32</sup>

Started from benzaldehyde **1d** (449 mL, 4.42 mmol, 1.00 eq.), 4-methylaniline **2b** (474 mg, 4.42 mmol, 1.00 eq.) and ethyl 2,4-dioxopentanoate **3a** (554  $\mu$ L, 4.42 mmol, 1.00 eq.) in 10 mL of acetic acid. Yield: 867 mg, 64%, off-white solid. <sup>1</sup>H NMR (400 MHz, CDCl<sub>3</sub>):  $\delta$  7.28-7.24 (m, 5H), 7.22 (d,  $J$  = 6.0 Hz, 2H), 7.07 (d,  $J$  = 8.0 Hz, 2H), 5.75 (s, 1H), 2.49 (s, 3H), 2.16 (s, 3H) ppm. MS [ESI+H]<sup>+</sup>: 308.00.

**4-Acetyl-3-hydroxy-5-(4-methylphenyl)-1-(4-methylphenyl)-1,5-dihydro-2H-pyrrol-2-one (10).** Started from 4-methylbenzaldehyde **1e** (521 mL, 4.42 mmol, 1.00 eq.), 4-methylaniline **2b** (474 mg, 4.42 mmol, 1.00 eq.) and ethyl 2,4-dioxopentanoate **3a** (554  $\mu$ L, 4.42 mmol, 1.00 eq.) in 10 mL of acetic acid. Purified by recrystallization from acetone/hexanes. Yield: 257 mg, 18% yellowish solid. <sup>1</sup>H NMR (400 MHz, DMSO-*d*<sub>6</sub>):  $\delta$  7.42 (d,  $J$  = 8.4 Hz, 2H), 7.12-7.04 (m, 4H), 6.98 (d,  $J$  = 8.0 Hz, 2H), 5.94 (s, 1H), 2.30 (s, 3H), 2.19 (s, 3H), 2.16 (s, 3H) ppm. MS [ESI+H]<sup>+</sup>: 322.00.

**4-Acetyl-3-hydroxy-5-(4-methoxyphenyl)-1-(4-methylphenyl)-1,5-dihydro-2H-pyrrol-2-one (11).**<sup>49</sup> Started from 4-methoxybenzaldehyde **1f** (527 mL, 4.42 mmol, 1.00 eq.), 4-methylaniline **2b** (474 mg, 4.42 mmol, 1.00 eq.) and ethyl 2,4-dioxopentanoate **3a** (554  $\mu$ L, 4.42 mmol, 1.00 eq.) in 10 mL of acetic acid. The desired product was obtained by column chromatography using a gradient of 1/6 EtOAc/Pet Ether to 1/3 EtOAc/Pet Ether, yielding 34 mg, 2% as an off-white solid. <sup>1</sup>H NMR (400 MHz, DMSO-*d*<sub>6</sub>):  $\delta$  7.42 (d,  $J$  = 8.4 Hz, 2H), 7.12 (d,  $J$  = 8.4 Hz, 2H), 7.08 (d,  $J$  = 8.8 Hz, 2H), 6.73 (d,  $J$  = 8.8 Hz, 2H) 5.93 (s, 1H), 3.64 (s, 3H), 2.30 (s, 3H), 2.20 (s, 3H) ppm. MS [ESI+H]<sup>+</sup>: 337.80.

**4-Acetyl-5-(4-chlorophenyl)-3-hydroxy-1-(4-methylphenyl)-1,5-dihydro-2H-pyrrol-2-one (12).**<sup>32</sup> Started from 4-chlorobenzaldehyde **1g** (621 mg, 4.42 mmol, 1.00 eq.), 4-methylaniline **2b** (474 mg, 4.42 mmol, 1.00 eq.) and ethyl 2,4-dioxopentanoate **3a** (554  $\mu$ L, 4.42 mmol, 1.00 eq.) in 10 mL of acetic acid. The desired product was obtained by column chromatography using 1/6 EtOAc/Pet ether as eluent, yielding 96 mg, 6% as a white solid. <sup>1</sup>H NMR (400 MHz, DMSO-*d*<sub>6</sub>):  $\delta$  7.43 (d, *J* = 8.4 Hz, 2H), 7.30-7.18 (m, 4H), 7.08 (d, *J* = 8.4 Hz, 2H), 5.98 (s, 1H), 2.30 (s, 3H), 2.20 (s, 3H) ppm. MS [ESI+H]<sup>+</sup>: 342.00.

**4-Acetyl-5-(4-bromophenyl)-3-hydroxy-1-(4-methylphenyl)-1,5-dihydro-2H-pyrrol-2-one (13).**<sup>32</sup> Started from 4-bromobenzaldehyde **1h** (818 mg, 4.42 mmol, 1.00 eq.), 4-methylaniline **2b** (474 mg, 4.42 mmol, 1.00 eq.) and ethyl 2,4-dioxopentanoate **3a** (554  $\mu$ L, 4.42 mmol, 1.00 eq.) in 10 mL of acetic acid. Yield: 1.23 g, 72%, yellowish solid. <sup>1</sup>H NMR (400 MHz, CDCl<sub>3</sub>):  $\delta$  7.39 (d, *J* = 8.8 Hz, 2H), 7.25 (d, *J* = 8.8 Hz, 2H), 7.11-7.08 (m, 4H), 5.73 (s, 1H), 2.27 (s, 3H), 2.23 (s, 3H) ppm. MS [ESI+H]<sup>+</sup>: 387.93.

**4-Acetyl-3-hydroxy-5-(3-methylphenyl)-1-(4-methylphenyl)-1,5-dihydro-2H-pyrrol-2-one (14).** Started from 3-methylbenzaldehyde **1i** (600 mg, 5.00 mmol, 1.00 eq.), 4-methylaniline **2b** (536 mg, 5.00 mmol, 1.00 eq.) and ethyl 2,4-dioxopentanoate **3a** (627  $\mu$ L, 5.00 mmol, 1.00 eq.) in 12 mL of acetic acid. Yield: 560 mg, 35%, white solid. <sup>1</sup>H NMR (400 MHz, DMSO-*d*<sub>6</sub>):  $\delta$  7.43 (d, *J* = 8.4 Hz, 2H), 7.11-7.05 (m, 3H), 7.02 (d, *J* = 8.4 Hz, 2H), 6.93 (d, *J* = 7.2 Hz, 1H), 5.94 (s, 1H), 2.31 (s, 3H), 2.19 (s, 3H), 2.18 (s, 3H) ppm. MS [ESI+H]<sup>+</sup>: 321.93

**4-Acetyl-3-hydroxy-5-(3-methoxyphenyl)-1-(4-methylphenyl)-1,5-dihydro-2H-pyrrol-2-one (15).** Started from 3-methoxybenzaldehyde **1j** (681 mg, 5.00 mmol, 1.00 eq.), 4-methylaniline **2b** (536 mg, 5.00 mmol, 1.00 eq.) and ethyl 2,4-dioxopentanoate **3a** (627  $\mu$ L, 5.00 mmol, 1.00 eq.) in 12 mL of acetic acid. Yield: 1.27 g, 75%, white solid. <sup>1</sup>H NMR (400 MHz, DMSO-*d*<sub>6</sub>):  $\delta$  7.44 (d, *J* = 8.4 Hz, 2H), 7.12 - 7.07 (m, 3H), 6.79 (s, 1H), 6.75 (d, *J* = 0.8 Hz, 1H), 6.69 (dd, *J* = 8.0, 2.2 Hz, 1H), 5.97 (s, 1H), 3.65 (s, 3H), 2.32 (s, 3H), 2.20 (s, 3H) ppm. MS [ESI+H]<sup>+</sup>: 337.39.

**4-Acetyl-5-(3-chlorophenyl)-3-hydroxy-1-(4-methylphenyl)-1,5-dihydro-2H-pyrrol-2-one (16).** Started from 3-chlorobenzaldehyde **1k** (703 mg, 5.00 mmol, 1.00 eq.), 4-methylaniline **2b** (536 mg, 5.00 mmol, 1.00 eq.) and ethyl 2,4-dioxopentanoate **3a** (627  $\mu$ L, 5.00 mmol, 1.00 eq.) in 12 mL of acetic acid. Yield: 619 mg, 36%, light yellow solid. <sup>1</sup>H NMR (400 MHz, CDCl<sub>3</sub>):  $\delta$  7.28 (d, *J* = 8.4 Hz, 2H), 7.21-7.18 (m, 3H), 7.17-7.13 (m, 1H), 7.10 (d, *J* = 8.4 Hz, 2H), 5.75 (s, 1H), 2.29 (s, 3H), 2.27 (s, 3H) ppm. MS [ESI+H]<sup>+</sup>: 341.80

**4-Acetyl-5-(3-bromophenyl)-3-hydroxy-1-(4-methylphenyl)-1,5-dihydro-2H-pyrrol-2-one (17).** Started from 3-bromobenzaldehyde **1l** (925 mg, 5.00 mmol, 1.00 eq.), 4-methylaniline **2b** (536 mg, 5.00 mmol, 1.00 eq.) and ethyl 2,4-dioxopentanoate **3a** (627  $\mu$ L, 5.00 mmol, 1.00 eq.) in 12 mL of acetic acid. Yield: 993 mg, 51%, brown solid. <sup>1</sup>H NMR (400 MHz, DMSO-*d*<sub>6</sub>):  $\delta$  7.48 (t, *J* = 1.6 Hz, 1H), 7.44 (d, *J* = 8.4 Hz, 2H), 7.34-7.30 (m, 1H), 7.20 (dt, *J* = 8.0, 1.6 Hz, 1H), 7.14 (t, *J* = 7.6 Hz, 1H), 7.10 (d, *J* = 8.4 Hz, 2H), 6.02 (s, 1H), 2.33 (s, 3H), 2.20 (s, 3H) ppm. MS [ESI+H]<sup>+</sup>: 386.67

**5-Cyclohexyl-3-hydroxy-4-propionyl-1-(4-methylphenyl)-1,5-dihydro-2H-pyrrol-2-one (18).** Started from cyclohexane carboxaldehyde **1a** (129 mg, 1.15 mmol, 1.00 eq.), 4-methylaniline **2b** (123 mg, 1.15 mmol, 1.00 eq.) and ethyl 2,4-dioxohexanoate<sup>50</sup> **3b** (198 mg, 1.15 mmol, 1.00 eq.) in 3 mL of acetic acid. Yield: 65 mg, 19%, white solid. <sup>1</sup>H NMR (400 MHz, CDCl<sub>3</sub>):  $\delta$  7.31-7.23 (m, 4H), 4.96 (s, 1H), 2.95-2.82 (m, 2H), 2.38 (s, 3H), 1.90 (t, *J* = 10.8 Hz, 1H), 1.66-1.54 (m, 4H), 1.43-1.41 (m, 1H), 1.17 (t, *J* = 7.2 Hz, 3H), 1.09-1.03 (m, 3H), 0.98-0.86 (m, 1H), 0.71-0.61 (m, 1H) ppm. MS [ESI+H]<sup>+</sup>: 328.13.

**4-Butyryl-5-cyclohexyl-3-hydroxy-1-(4-methylphenyl)-1,5-dihydro-2H-pyrrol-2-one (19).**<sup>32</sup> Started from cyclohexane carboxaldehyde **1a** (605  $\mu$ L, 5.00 mmol, 1.00 eq.), 4-methylaniline **2b** (536 mg, 5.00 mmol, 1.00 eq.) and ethyl 2,4-dioxoheptanoate<sup>34</sup> **3c** (198 mg, 1.15 mmol, 1.00 eq.) in 12 mL of acetic acid. Yield: 669 mg (39%) as a white solid. <sup>1</sup>H NMR (400 MHz, DMSO):  $\delta$  7.39 (d, *J* = 8.4 Hz, 2H), 7.24 (d, *J* = 8.0 Hz, 2H), 5.02 (s, 1H), 2.89-2.70 (m, 2H), 2.32 (s, 3H), 1.84-1.78 (m, 1H), 1.61-1.32 (m, 7H), 0.97-0.80 (m, 6H), 0.80-0.73 (m, 1H), 0.57-0.48 (m, 1H) ppm. MS [ESI+H]<sup>+</sup>: 341.87.

**4-Pentanoyl-5-cyclohexyl-3-hydroxy-1-(4-methylphenyl)-1,5-dihydro-2H-pyrrol-2-one (20).**

Started from cyclohexane carboxaldehyde **1a** (266 mg, 2.37 mmol, 1.00 eq.), 4-methylaniline **2b** (253 mg, 2.37 mmol, 1.00 eq.) and ethyl 2,4-dioxooctanoate<sup>34</sup> **3d** (475 mg, 2.37 mmol, 1.00 eq.) in 5 mL of acetic acid. Yield: 237 mg, 28%, white solid. <sup>1</sup>H NMR (400 MHz, DMSO): δ 12.02 (br s, 1H), 7.39 (d, *J* = 8.0 Hz, 2H), 7.24 (d, *J* = 7.6 Hz, 2H), 5.02 (s, 1H), 2.92-2.73 (m, 2H), 2.32 (s, 3H), 1.85-1.75 (m, 1H), 1.58-1.28 (m, 9H), 0.91-0.65 (m, 7H) 0.57-0.50 (m, 1H) ppm. MS [ESI+H]<sup>+</sup>: 356.00.

**5-Cyclohexyl-3-hydroxy-4-isobutyryl-1-(4-methylphenyl)-1,5-dihydro-2H-pyrrol-2-one (21).**

Started from cyclohexane carboxaldehyde **1a** (535 μL, 4.42 mmol, 1.00 eq.), 4-methylaniline **2b** (474 mg, 4.42 mmol, 1.00 eq.) and ethyl 2,4-dioxo-5-methylhexanoate **3e** (823 mg, 4.42 mmol, 1.00 eq.) in 10 mL of acetic acid. Yield: 255 mg, 17%, white solid. <sup>1</sup>H NMR (400 MHz, DMSO-*d*<sub>6</sub>): δ 12.07 (br s, 1H), 7.40 (d, *J* = 7.6 Hz, 2H), 7.24 (d, *J* = 7.6 Hz, 2H), 5.03 (d, *J* = 1.6 Hz, 1H), 3.44-3.41 (m, 1H), 2.32 (s, 3H), 1.80-1.70 (m, 1H), 1.62-1.59 (m, 1H), 1.46-1.37 (m, 4H), 1.09 (d, *J* = 6.8 Hz, 3H), 1.02 (d, *J* = 6.8 Hz, 3H), 0.97-0.77 (m, 4H), 0.59-0.53 (m, 1H) ppm. MS [ESI+H]<sup>+</sup>: 342.13.

**5-Cyclohexyl-4-(cyclopropanecarbonyl)-3-hydroxy-1-(4-methylphenyl)-1,5-dihydro-2H-pyrrol-2-one (22).** Started from cyclohexane carboxaldehyde **1a** (605 μL, 5.00 mmol, 1.00 eq.), 4-methylaniline **2b** (550 μL, 5.00 mmol, 1.00 eq.) and ethyl 4-cyclopropyl-2,4-dioxobutanoate<sup>51</sup> **3f** (920 mg, 5.00 mmol, 1.00 eq.) in 10 mL of AcOH. Yield: 60 mg, 4%, white solid. <sup>1</sup>H NMR (400 MHz, MeOD): δ 7.34 (d, *J* = 8.4 Hz, 2H), 7.27 (d, *J* = 7.6 Hz, 2H), 5.01 (d, *J* = 2.0 Hz, 1H), 3.01-2.95 (m, 1H), 2.38 (s, 3H), 1.88 (t, *J* = 10.4 Hz, 1H), 1.72-1.64 (m, 1H), 1.60-1.48 (m, 3H), 1.41 (d, *J* = 11.2 Hz, 1H), 1.04-0.86 (m, 8H), 0.72-0.62 (m, 1H) ppm. MS [ESI+Na]<sup>+</sup>: 363.10.

**5-Cyclohexyl-3-hydroxy-1-(4-methylphenyl)-4-pivaloyl-1,5-dihydro-2H-pyrrol-2-one (23).<sup>32</sup>**

Started from cyclohexane carboxaldehyde **1a** (121 μL, 1.00 mmol, 1.00 eq.), 4-methylaniline **2b** (107 mg, 1.00 mmol, 1.00 eq.) and ethyl 5,5-dimethyl-2,4-dioxohexanoate **3g** (175 μL, 1.00 mmol, 1.00 eq.) in 3 mL of acetic acid. Yield: 20 mg, 6%, white solid. <sup>1</sup>H NMR (400 MHz, DMSO-*d*<sub>6</sub>): δ 7.41 (d, *J* = 8.4 Hz, 2H), 7.25 (d, *J* = 8.4 Hz, 2H), 5.11 (d, *J* = 2.2 Hz, 1H), 2.32 (s, 3H), 1.63-1.58 (m, 2H), 1.52-1.46 (m, 3H), 1.31-1.28 (m, 1H) 1.25 (s, 9H) 1.01-0.69 (m, 4H), 0.69-0.59 (m, 1H) ppm. MS [ESI+H]<sup>+</sup>: 356.13.

**Ethyl 2-cyclohexyl-4-hydroxy-5-oxo-1-(4-methylphenyl)-2,5-dihydro-1H-pyrrole-3-carboxylate (24).**<sup>29</sup> Sodium 1,4-diethoxy-1,4-dioxobut-2-en-2-olate (1.25 g, 6.00 mmol) was dissolved in 25 mL H<sub>2</sub>O and 25 mL Et<sub>2</sub>O was added. Acidified to pH 2 with 6M HCl (aq.) and was extracted with Et<sub>2</sub>O from the aqueous phase, dried over MgSO<sub>4</sub> and concentrated *in vacuo* yielding 1.05 g, 4.97 mmol, 83% diethyl 2-oxosuccinate as a yellow oil.<sup>52</sup> Diethyl 2-oxosuccinate **3h** (1.05 g, 4.97 mmol, 1.12 eq.) was added to a mixture of cyclohexane carboxaldehyde **1a** (534 μL, 4.42 mmol, 1.00 eq.) and 4-methylaniline **2b** (474 mg, 4.42 mmol, 1.00 eq.) in 10 mL of dry THF and stirred at room temperature overnight. The reaction mixture was concentrated *in vacuo*, Et<sub>2</sub>O was added and the white precipitate was collected by filtration. Yield: 400 mg, 26%, white solid. <sup>1</sup>H NMR (400 MHz, CDCl<sub>3</sub>): δ 11.24 (s, 1H), 7.40 (d, *J* = 8.4 Hz, 2H), 7.24 (d, *J* = 8.4 Hz, 2H), 5.00 (d, *J* = 1.8 Hz, 1H), 4.32-4.13 (m, 2H), 2.32 (s, 3H), 1.85-1.76 (m, 1H), 1.66-1.59 (m, 1H), 1.56-1.44 (m, 3H), 1.32 (d, *J* = 12.0 Hz, 1H), 1.26 (t, *J* = 7.2 Hz, 3H), 1.06-0.75 (m, 4H), 0.63-0.53 (m, 1H) ppm. MS [ESI+H]<sup>+</sup>: 344.07.

**Isopropyl 2-cyclohexyl-4-hydroxy-5-oxo-1-(4-methylphenyl)-2,5-dihydro-1H-pyrrole-3-carboxylate (25).** Ester **22** (343 mg, 1.00 mmol, 1.00 eq.) and *p*-toluenesulfonic acid (172 mg, 1.00 mmol, 1.00 eq.) were dissolved in 10 mL of 2-propanol and the reaction mixture was refluxed for 48 hours. The solvent was removed under reduced pressure, the crude product was dissolved in 50 mL EtOAc and washed 3x with H<sub>2</sub>O, dried over MgSO<sub>4</sub>, filtered and concentrated under reduced pressure. The crude product was purified by column chromatography (4/1 EtOAc/Pet ether) and yielded 150 mg, 9.5%, brownish solid. <sup>1</sup>H NMR (400 MHz, CDCl<sub>3</sub>): δ 9.33 (s, 1H), 7.30 (d, *J* = 8.4 Hz, 2H), 7.22 (d, *J* = 8.4 Hz, 2H), 5.31-5.23 (m, 1H), 4.79 (d, *J* = 2.0 Hz, 1H), 2.37 (s, 3H), 1.88 (td, *J* = 9.6, 2.8 Hz, 1H), 1.73-1.66 (m, 1H), 1.63-1.50 (m, 3H), 1.38 (d, *J* = 6.8 Hz, 6H), 1.29-1.19 (m, 1H), 1.13-0.90 (m, 4H), 0.74-0.64 (m, 1H) ppm. MS [ESI+H]<sup>+</sup>: 357.93.

**4-Benzoyl-5-cyclohexyl-3-hydroxy-1-(4-methylphenyl)-1,5-dihydro-2H-pyrrol-2-one (26).** Started from cyclohexane carboxaldehyde **1a** (484  $\mu\text{L}$ , 4.00 mmol, 1.00 eq.), 4-methylaniline **2b** (428 mg, 4.00 mmol, 1.00 eq.) and ethyl 2,4-dioxo-4-phenylbutanoate<sup>53</sup> **3i** (880 mg, 4.00 mmol, 1.00 eq.) in 10 mL of AcOH. Yield: 53 mg, 4%, white solid. <sup>1</sup>H NMR (400 MHz, DMSO-*d*<sub>6</sub>):  $\delta$  7.85 (d, *J* = 7.6 Hz, 2H), 7.69-7.62 (m, 1H), 7.58-7.52 (m, 2H), 7.49 (d, *J* = 8.0 Hz, 2H), 7.29 (d, *J* = 8.4 Hz, 2H), 5.32 (s, 1H), 2.35 (s, 3H), 1.73-1.62 (m, 2H), 1.58-1.51 (m, 2H), 1.49-1.37 (m, 2H), 1.05-0.94 (m, 1H), 0.88-0.74 (m, 4H) ppm. MS [ESI+H]<sup>+</sup>: 375.93.

**4-Acetyl-5-cyclohexyl-3-hydroxy-1-phenyl-1,5-dihydro-2H-pyrrol-2-one (27).**<sup>32</sup> Started from cyclohexane carboxaldehyde **1a** (534  $\mu\text{L}$ , 4.42 mmol, 1.00 eq.), aniline **2a** (400  $\mu\text{L}$ , 4.42 mmol, 1.00 eq.) and ethyl 2,4-dioxopentanoate **3a** (554  $\mu\text{L}$ , 4.42 mmol, 1.00 eq.) in 10 mL of AcOH. Yield: 1.00 g, 76%, yellow solid. <sup>1</sup>H NMR (400 MHz, CDCl<sub>3</sub>):  $\delta$  7.47-7.44 (m, 4H), 7.32-7.28 (m, 1H), 4.99 (d, *J* = 2.0 Hz, 1H), 2.54 (s, 3H), 1.97-1.90 (m, 1H), 1.69-1.66 (m, 1H), 1.59-1.48 (m, 3H), 1.45-1.41 (m, 1H), 1.10-0.99 (m, 3H), 0.92-0.86 (m, 1H), 0.63 (qd, *J* = 9.2, 3.6 Hz, 1H) ppm. MS [ESI+H]<sup>+</sup>: 300.07

**4-Acetyl-5-cyclohexyl-1-(4-ethylphenyl)-3-hydroxy-1,5-dihydro-2H-pyrrol-2-one (28).**<sup>32</sup> Started from cyclohexane carboxaldehyde **1a** (534  $\mu\text{L}$ , 4.42 mmol, 1.00 eq.), 4-ethylaniline **2c** (553  $\mu\text{L}$ , 4.42 mmol, 1.00 eq.) and ethyl 2,4-dioxopentanoate **3a** (554  $\mu\text{L}$ , 4.42 mmol, 1.00 eq.) in 10 mL of AcOH. Yield: 134 mg, 9%, light-yellow solid. <sup>1</sup>H NMR (400 MHz, CDCl<sub>3</sub>):  $\delta$  7.32 (d, *J* = 8.4 Hz, 2H), 7.25 (d, *J* = 6.4 Hz, 2H), 4.94 (s, 1H), 2.68 (q, *J* = 7.6 Hz, 2H), 2.54 (s, 3H), 1.95-1.90 (m, 1H), 1.68-1.66 (m, 1H), 1.67-1.51 (m, 3H), 1.43-1.41 (m, 1H), 1.26 (t, *J* = 7.6 Hz, 3H), 1.10-0.98 (m, 4H), 0.90-0.87 (m, 1H), 0.69-0.60 (m, 1H) ppm. MS [ESI+H]<sup>+</sup>: 328.13

**4-Acetyl-5-cyclohexyl-3-hydroxy-1-(4-methoxyphenyl)-1,5-dihydro-2H-pyrrol-2-one (29).**<sup>32</sup> Started from cyclohexane carboxaldehyde **1a** (534  $\mu\text{L}$ , 4.42 mmol, 1.00 eq.), 4-methoxyaniline **2d** (560 mg, 4.42 mmol, 1.00 eq.) and ethyl 2,4-dioxopentanoate **3a** (554  $\mu\text{L}$ , 4.42 mmol, 1.00 eq.) in 10 mL of AcOH. Yield: 805 mg, 56%, light-yellow solid. <sup>1</sup>H NMR (400 MHz, DMSO-*d*<sub>6</sub>):  $\delta$  7.41 (d, *J* = 8.8 Hz, 2H), 7.00 (d, *J* = 9.2 Hz, 2H), 4.96 (d, *J* = 1.2 Hz, 1H), 3.77 (s, 3H), 2.43 (s, 3H), 1.86-1.80 (m, 1H), 1.60-1.58 (m, 1H), 1.40-1.37 (m, 2H), 1.35-1.32 (m, 2H), 0.99-0.91 (m, 3H), 0.87-0.75 (m, 1H), 0.58-0.55 (m, 1H) ppm. MS [ESI+H]<sup>+</sup>: 330.07

**4-Acetyl-1-(4-chlorophenyl)-5-cyclohexyl-3-hydroxy-1,5-dihydro-2H-pyrrol-2-one (30).**<sup>32</sup> Started from cyclohexane carboxaldehyde **1a** (534  $\mu\text{L}$ , 4.42 mmol, 1.00 eq.), 4-chloroaniline **2e** (544 mg, 4.42 mmol, 1.00 eq.) and ethyl 2,4-dioxopentanoate **3a** (554  $\mu\text{L}$ , 4.42 mmol, 1.00 eq.) in 10 mL of AcOH. Yield: 713 mg, 48%, light-yellow solid. <sup>1</sup>H NMR (400 MHz, CDCl<sub>3</sub>):  $\delta$  8.75 (s br, 1H), 7.42 (d, *J* = 8.8 Hz, 2H), 7.39 (d, *J* = 9.2 Hz, 2H), 4.95 (d, *J* = 2.0 Hz, 1H), 2.53 (s, 3H), 1.96-1.84 (m, 1H), 1.75-1.65 (m, 1H), 1.63-1.51 (m, 3H), 1.45-1.40 (m, 1H), 1.11-0.97 (m, 3H), 0.95-0.86 (m, 1H), 0.66 (qd, *J* = 12.4, 3.2 Hz, 1H) ppm. MS [ESI+H]<sup>+</sup>: 334.1

**4-Acetyl-1-(4-bromophenyl)-5-cyclohexyl-3-hydroxy-1,5-dihydro-2H-pyrrol-2-one (31).**<sup>32</sup> Started from cyclohexane carboxaldehyde **1a** (534  $\mu\text{L}$ , 4.42 mmol, 1.00 eq.), 4-bromoaniline **2f** (760 mg, 4.42 mmol, 1.00 eq.) and ethyl 2,4-dioxopentanoate **3a** (554  $\mu\text{L}$ , 4.42 mmol, 1.00 eq.) in 10 mL of AcOH. Yield: 910 mg, 53%, white solid. <sup>1</sup>H NMR (400 MHz, CDCl<sub>3</sub>):  $\delta$  7.57 (d, *J* = 8.4 Hz, 2H), 7.33 (d, *J* = 8.4 Hz, 2H), 4.96 (s, 1H), 2.53 (s, 3H), 1.97-1.87 (m, 1H), 1.73-1.65 (m, 1H), 1.62-1.49 (m, 3H), 1.45-1.37 (m, 1H), 1.15-0.97 (m, 1H), 0.95-0.86 (m, 1H), 0.66 (qd, *J* = 12.4, 3.2 Hz, 1H) ppm. MS [ESI+H]<sup>+</sup>: 378.1

**4-Acetyl-5-cyclohexyl-3-hydroxy-1-(4-(trifluoromethyl)phenyl)-1,5-dihydro-2H-pyrrol-2-one (32).**<sup>32</sup> Started from cyclohexane carboxaldehyde **1a** (534  $\mu\text{L}$ , 4.42 mmol, 1.00 eq.), 4-trifluoromethylaniline **2g** (556  $\mu\text{L}$ , 4.42 mmol, 1.00 eq.) and ethyl 2,4-dioxopentanoate **3a** (554  $\mu\text{L}$ , 4.42 mmol, 1.00 eq.) in 10 mL of AcOH. Yield: 80 mg, 5%, white solid. <sup>1</sup>H NMR (400 MHz, DMSO-*d*<sub>6</sub>):  $\delta$  12.25 (s, 1H), 7.82 (s, 4H), 5.19 (s, 1H), 2.46 (s, 3H), 1.85 (t, *J* = 11.2 Hz, 1H), 1.60 (d, *J* = 10.8 Hz, 1H), 1.54-1.43 (m, 3H), 1.38 (d, *J* = 12.4 Hz, 1H), 1.05-0.74 (m, 4H), 0.52 (d, *J* = 12.4 Hz, 1H) ppm. MS [ESI+H]<sup>+</sup>: 369.07

**4-Acetyl-5-cyclohexyl-3-hydroxy-1-(3-methylphenyl)-1,5-dihydro-2H-pyrrol-2-one (33).**<sup>29</sup> Started from cyclohexane carboxaldehyde **1a** (534  $\mu\text{L}$ , 4.42 mmol, 1.00 eq.), 3-methylaniline **2h** (474

$\mu\text{L}$ , 4.42 mmol, 1.00 eq.) and ethyl 2,4-dioxopentanoate **3a** (554  $\mu\text{L}$ , 4.42 mmol, 1.00 eq.) in 10 mL of AcOH. Yield: 511 mg, 37%, white solid.  $^1\text{H}$  NMR (400 MHz,  $\text{CDCl}_3$ ):  $\delta$  7.32 (t,  $J = 8.0$  Hz, 1H), 7.26 (s, 1H), 7.19 (d,  $J = 8.0$  Hz, 1H), 7.11 (d,  $J = 7.6$  Hz, 1H), 4.96 (d,  $J = 2.0$  Hz, 1H), 2.53 (s, 3H), 2.40 (s, 3H), 1.95-1.88 (m, 1H), 1.69-1.65 (m, 1H), 1.59-1.50 (m, 3H), 1.45-1.39 (m, 1H), 1.15-0.84 (m, 4H), 0.64 (qd,  $J = 12.4$ , 3.6 Hz, 1H) ppm. MS [ESI+H] $^+$ : 314.07

**4-Acetyl-5-cyclohexyl-1-(3-fluorophenyl)-3-hydroxy-1,5-dihydro-2H-pyrrol-2-one (34).**<sup>32</sup>

Started from cyclohexane carboxaldehyde **1a** (534  $\mu\text{L}$ , 4.42 mmol, 1.00 eq.), 3-fluoroaniline **2i** (425  $\mu\text{L}$ , 4.42 mmol, 1.00 eq.) and ethyl 2,4-dioxopentanoate **3a** (554  $\mu\text{L}$ , 4.42 mmol, 1.00 eq.) in 10 mL of AcOH. Yield: 226 mg, 16%, white solid.  $^1\text{H}$  NMR (400 MHz,  $\text{CDCl}_3$ ):  $\delta$  8.99 (s br, 1H), 7.45-7.34 (m, 1H), 7.29-7.25 (m, 1H), 7.21 (d,  $J = 8.0$  Hz, 1H), 7.01 (td,  $J = 8.0$ , 2.0 Hz, 1H), 4.97 (d,  $J = 2.0$  Hz, 1H), 2.55 (s, 3H), 1.94 (td,  $J = 12.0$ , 2.0 Hz, 1H), 1.70-1.67 (m, 1H), 1.62-1.53 (m, 3H), 1.47-1.40 (m, 1H), 1.15-0.97 (m, 3H), 0.96-0.84 (m, 1H), 0.66 (qd,  $J = 12.4$ , 3.6 Hz, 1H) ppm. MS [ESI+H] $^+$ : 318.27

**4-Acetyl-1-(3-chlorophenyl)-5-cyclohexyl-3-hydroxy-1,5-dihydro-2H-pyrrol-2-one (35).**<sup>29</sup>

Started from cyclohexane carboxaldehyde **1a** (534  $\mu\text{L}$ , 4.42 mmol, 1.00 eq.), 3-chloroaniline **2j** (468  $\mu\text{L}$ , 4.42 mmol, 1.00 eq.) and ethyl 2,4-dioxopentanoate **3a** (554  $\mu\text{L}$ , 4.42 mmol, 1.00 eq.) in 10 mL of AcOH. Yield: 805 mg, 55%, yellow solid.  $^1\text{H}$  NMR (400 MHz,  $\text{CDCl}_3$ ):  $\delta$  8.92 (s br, 1H), 7.51 (t,  $J = 1.6$  Hz, 1H), 7.38 (t,  $J = 8.0$  Hz, 1H), 7.32 (d,  $J = 8.0$  Hz, 1H), 7.29-7.25 (m, 1H), 4.96 (d,  $J = 2.0$  Hz, 1H), 2.55 (s, 3H), 1.93 (td,  $J = 12.4$ , 2.0 Hz, 1H), 1.71-1.68 (m, 1H), 1.60-1.54 (m, 3H), 1.46-1.43 (m, 1H), 1.15-0.99 (m, 3H), 0.98-0.86 (m, 1H), 0.65 (qd,  $J = 12.4$ , 2.8 Hz, 1H) ppm. MS [ESI+H] $^+$ : 334.13

**4-Acetyl-5-cyclohexyl-3-hydroxy-1-(3-(trifluoromethyl)phenyl)-1,5-dihydro-2H-pyrrol-2-one (36).**

Started from cyclohexane carboxaldehyde **1a** (534  $\mu\text{L}$ , 4.42 mmol, 1.00 eq.), 3-trifluoromethylaniline **2k** (552  $\mu\text{L}$ , 4.42 mmol, 1.00 eq.) and ethyl 2,4-dioxopentanoate **3a** (554  $\mu\text{L}$ , 4.42 mmol, 1.00 eq.) in 10 mL of AcOH. Yield: 560 mg, 34%, brown solid.  $^1\text{H}$  NMR (400 MHz,  $\text{DMSO}-d_6$ ):  $\delta$  12.26 (br s, 1H), 7.98 (s, 1H), 7.86 (d,  $J = 7.6$  Hz, 1H), 7.69 (t,  $J = 8.0$  Hz, 1H), 7.64 (d,  $J = 7.6$  Hz, 1H), 5.23 (d,  $J = 1.2$  Hz, 1H), 2.45 (s, 3H), 1.86 (t,  $J = 11.2$  Hz, 1H), 1.62-1.58 (m, 1H), 1.47-1.35 (m, 4H), 1.00-0.85 (m, 3H), 0.80-0.71 (m, 1H), 0.47 (qd,  $J = 12.8$  Hz, 3.2 Hz, 1H) ppm. MS [ESI+H] $^+$ : 368.13

**4-Acetyl-5-cyclohexyl-1-(2-fluoro-4-methylphenyl)-3-hydroxy-1,5-dihydro-2H-pyrrol-2-one (37).**<sup>29</sup>

Started from cyclohexane carboxaldehyde **1a** (534  $\mu\text{L}$ , 4.42 mmol, 1.00 eq.), 2-fluoro-4-methylaniline **2l** (499  $\mu\text{L}$ , 4.42 mmol, 1.00 eq.) and ethyl 2,4-dioxopentanoate **3a** (554  $\mu\text{L}$ , 4.42 mmol, 1.00 eq.) in 10 mL of AcOH. Yield: 508 mg, 35%, white solid.  $^1\text{H}$  NMR (400 MHz,  $\text{CDCl}_3$ ):  $\delta$  9.35 (br s, 1H), 7.28-7.22 (m, 1H), 7.04-6.98 (m, 2H), 4.93 (d,  $J = 1.6$  Hz, 1H), 2.52 (s, 3H), 2.39 (s, 3H), 1.98-1.91 (m, 1H), 1.69-1.63 (m, 1H), 1.57-1.41 (m, 4H), 1.13-1.02 (m, 3H), 0.92-0.82 (m, 1H), 0.62 (qd,  $J = 12.8$  Hz, 3.2 Hz, 1H) ppm. MS [ESI+H] $^+$ : 332.1

**4-Acetyl-1-(4-chloro-2-fluorophenyl)-5-cyclohexyl-3-hydroxy-1,5-dihydro-2H-pyrrol-2-one (38).**<sup>29</sup>

Started from cyclohexane carboxaldehyde **1a** (534  $\mu\text{L}$ , 4.42 mmol, 1.00 eq.), 4-chloro-2-fluoroaniline **2m** (490  $\mu\text{L}$ , 4.42 mmol, 1.00 eq.) and ethyl 2,4-dioxopentanoate **3a** (554  $\mu\text{L}$ , 4.42 mmol, 1.00 eq.) in 10 mL of AcOH. Yield: 190 mg, 12%, light yellow solid.  $^1\text{H}$  NMR (400 MHz,  $\text{CDCl}_3$ ):  $\delta$  9.07 (br s, 1H), 7.37 (t,  $J = 8.4$  Hz, 1H), 7.28-7.22 (m, 2H), 4.96 (d,  $J = 2.0$  Hz, 1H), 2.52 (s, 3H), 2.00-1.91 (m, 1H), 1.72-1.65 (m, 1H), 1.63-1.44 (m, 4H), 1.14-1.00 (m, 2H), 0.99-0.82 (m, 2H), 0.61 (qd,  $J = 12.8$  Hz, 3.6 Hz, 1H) ppm. MS [ESI+H] $^+$ : 352.1

**4-Acetyl-1-(4-bromo-2-fluorophenyl)-5-cyclohexyl-3-hydroxy-1,5-dihydro-2H-pyrrol-2-one (39).**<sup>32</sup>

Started from cyclohexane carboxaldehyde **1a** (303  $\mu\text{L}$ , 2.50 mmol, 1.00 eq.), 4-bromo-2-fluoroaniline **2n** (475  $\mu\text{L}$ , 2.50 mmol, 1.00 eq.) and ethyl 2,4-dioxopentanoate **3a** (395  $\mu\text{L}$ , 2.50 mmol, 1.00 eq.) in 5 mL of AcOH. Purified by silica column chromatography using EtOAc/Pet Ether (1/6). The resulting impure product was stirred in diisopropylether and the pure product was obtained by filtration. Yield: 36 mg, 4%, white solid.  $^1\text{H}$  NMR (400 MHz,  $\text{CDCl}_3$ ):  $\delta$  8.97 (s br, 1H, OH), 7.43-7.36 (m, 2H), 7.31 (t,  $J = 8.0$  Hz, 1H), 4.96 (d,  $J = 1.2$  Hz, 1H), 2.52 (s, 3H), 1.94 (t,  $J = 11.6$  Hz, 1H), 1.68 (d,  $J = 13.2$  Hz, 1H), 1.57-1.42 (m, 4H), 1.15-0.84 (m, 4H), 0.62 (qd,  $J = 12.4$ , 3.2 Hz, 1H) ppm. MS [ESI+H] $^+$ : 395.67

**4-Acetyl-5-cyclohexyl-1-(3,4-dimethylphenyl)-3-hydroxy-1,5-dihydro-2H-pyrrol-2-one (40).**<sup>32</sup> Started from cyclohexane carboxaldehyde **1a** (303  $\mu$ L, 2.50 mmol, 1.00 eq.), 3,4-dimethylaniline **2o** (303  $\mu$ L, 2.50 mmol, 1.00 eq.) and ethyl 2,4-dioxopentanoate **3a** (395  $\mu$ L, 2.50 mmol, 1.00 eq.) in 5 mL of AcOH. Yield: 167 mg, 20%, white solid. <sup>1</sup>H NMR (400 MHz, CDCl<sub>3</sub>):  $\delta$  9.06 (s br, 1H, OH), 7.21-7.16 (m, 2H), 7.10 (dd,  $J$  = 8.0, 1.6 Hz, 1H), 4.92 (d,  $J$  = 2.0 Hz, 1H), 2.53 (s, 3H), 2.29 (s, 3H), 2.28 (s, 3H), 1.92 (t,  $J$  = 11.6 Hz, 1H), 1.73-1.65 (m, 1H), 1.60-1.49 (m, 3H), 1.42 (d,  $J$  = 12.4 Hz, 1H), 1.13-0.98 (m, 3H), 0.94-0.84 (m, 1H), 0.65 (qd,  $J$  = 12.0, 3.2 Hz, 1H) ppm. MS [ESI+H]<sup>+</sup>: 327.87

**4-Acetyl-1-(4-chloro-3-methylphenyl)-5-cyclohexyl-3-hydroxy-1,5-dihydro-2H-pyrrol-2-one (41).**<sup>29</sup> Started from cyclohexane carboxaldehyde **1a** (534  $\mu$ L, 4.42 mmol, 1.00 eq.), 4-chloro-3-methylaniline **2p** (626 mg, 4.42 mmol, 1.00 eq.) and ethyl 2,4-dioxopentanoate **3a** (554  $\mu$ L, 4.42 mmol, 1.00 eq.) in 10 mL of AcOH. Yield: 505 mg, 33%, white solid. <sup>1</sup>H NMR (400 MHz, CDCl<sub>3</sub>):  $\delta$  9.39 (s br, 1H, OH), 7.40 (d,  $J$  = 8.4 Hz, 1H), 7.32 (d,  $J$  = 2.0 Hz, 1H), 7.17 (dd,  $J$  = 8.4, 2.4 Hz, 1H), 4.94 (d,  $J$  = 2.0 Hz, 1H), 2.55 (s, 3H), 2.42 (s, 3H), 1.93 (td,  $J$  = 12.0, 2.4 Hz, 1H), 1.72-1.64 (m, 1H), 1.60-1.49 (m, 3H), 1.46-1.34 (m, 1H), 1.15-0.96 (m, 3H), 0.94-0.84 (m, 1H), 0.65 (qd,  $J$  = 12.8, 3.6 Hz, 1H) ppm. MS [ESI+H]<sup>+</sup>: 348.0

**4-Acetyl-5-cyclohexyl-1-(3-fluoro-4-methylphenyl)-3-hydroxy-1,5-dihydro-2H-pyrrol-2-one (42).**<sup>32</sup> Started from cyclohexane carboxaldehyde **1a** (534  $\mu$ L, 4.42 mmol, 1.00 eq.), 3-fluoro-4-methylaniline **2q** (506  $\mu$ L, 4.42 mmol, 1.00 eq.) and ethyl 2,4-dioxopentanoate **3a** (554  $\mu$ L, 4.42 mmol, 1.00 eq.) in 10 mL of AcOH. Yield: 160 mg, 10%, white solid. <sup>1</sup>H NMR (400 MHz, CDCl<sub>3</sub>):  $\delta$  7.24 (t,  $J$  = 8.0 Hz, 1H), 7.18 (dd,  $J$  = 6.8, 2.0 Hz, 1H), 7.09 (dd,  $J$  = 8.4, 2.0 Hz, 1H), 4.92 (d,  $J$  = 2.0 Hz, 1H), 2.54 (s, 3H), 2.30 (d,  $J$  = 1.6 Hz, 3H), 1.94 (td,  $J$  = 12.0, 2.0 Hz, 1H), 1.74-1.64 (m, 1H), 1.64-1.48 (m, 3H), 1.48-1.39 (m, 1H), 1.14-0.98 (m, 3H), 0.98-0.84 (m, 1H), 0.67 (qd,  $J$  = 12.8, 3.2 Hz, 1H). MS [ESI+H]<sup>+</sup>: 332.00

**1-(4-Bromo-2-fluorophenyl)-5-cyclohexyl-4-(cyclopropanecarbonyl)-3-hydroxy-1,5-dihydro-2H-pyrrol-2-one (43).** Started from cyclohexane carboxaldehyde **1a** (242  $\mu$ L, 2.00 mmol, 1.00 eq.), 4-bromo-2-fluoroaniline **2n** (380 mg, 2.00 mmol, 1.00 eq.) and ethyl 4-cyclopropyl-2,4-dioxobutanoate<sup>51</sup> **3f** (368 mg, 2.00 mmol, 1.00 eq.) in 5 mL of AcOH. Yield: 240 mg, 28%, white solid. <sup>1</sup>H NMR (400 MHz, CDCl<sub>3</sub>):  $\delta$  7.43-7.34 (m, 3H), 5.06 (d,  $J$  = 1.6 Hz, 1H), 2.39-2.33 (m, 1H), 1.92 (t,  $J$  = 12.0 Hz, 1H), 1.72 (d,  $J$  = 12.4 Hz, 1H), 1.64-1.48 (m, 4H), 1.35-1.31 (m, 1H), 1.25-1.22 (m, 1H), 1.13-1.01 (m, 5H), 0.99-0.90 (m, 1H), 0.68 (qd,  $J$  = 12.4, 3.2 Hz, 1H) ppm. MS [ESI+H]<sup>+</sup>: 421.67

**4-Benzoyl-1-(4-bromo-2-fluorophenyl)-5-cyclohexyl-3-hydroxy-1,5-dihydro-2H-pyrrol-2-one (44).** Started from cyclohexane carboxaldehyde **1a** (242  $\mu$ L, 2.00 mmol, 1.00 eq.), 4-bromo-2-fluoroaniline **2n** (380 mg, 2.00 mmol, 1.00 eq.) and ethyl 2,4-dioxo-4-phenylbutanoate<sup>53</sup> **3i** (440 mg, 2.00 mmol, 1.00 eq.) in 5 mL of AcOH. Yield: 210 mg, 23%, white solid. <sup>1</sup>H NMR (400 MHz, DMSO):  $\delta$  7.84 (d,  $J$  = 6.8 Hz, 2H), 7.78 (dd,  $J$  = 10.4, 2.0 Hz, 1H), 7.67-7.60 (m, 2H), 7.58-7.51 (m, 3H), 5.21 (d,  $J$  = 2.0 Hz, 1H), 1.64-1.44 (m, 6H), 1.00-0.70 (m, 5H) ppm. MS [ESI+H]<sup>+</sup>: 459.87

**1-(4-Bromo-2-fluorophenyl)-5-(3-bromophenyl)-4-(cyclopropanecarbonyl)-3-hydroxy-1,5-dihydro-2H-pyrrol-2-one (45).** Started from 3-bromobenzaldehyde **1l** (233  $\mu$ L, 2.00 mmol, 1.00 eq.), 4-bromo-2-fluoroaniline **2n** (380 mg, 2.00 mmol, 1.00 eq.) and ethyl 4-cyclopropyl-2,4-dioxobutanoate<sup>51</sup> **3f** (440 mg, 2.00 mmol, 1.00 eq.) in 5 mL of AcOH. Yield: 205 mg, 21%, off-white solid. <sup>1</sup>H NMR (400 MHz, CDCl<sub>3</sub>):  $\delta$  7.40 (d,  $J$  = 6.8 Hz, 1H), 7.35-7.27 (m, 2H), 7.22 (d,  $J$  = 8.4 Hz, 1H), 7.19-7.11 (m, 2H), 7.07 (t,  $J$  = 8.0 Hz, 1H), 5.84 (s, 1H), 1.93-1.85 (m, 1H), 1.22-1.19 (m, 1H), 1.07-0.97 (m, 2H), 0.82-0.74 (m, 1H) ppm. MS [ESI+H]<sup>+</sup>: 495.67

**4-Acetyl-1-(4-bromo-2-fluorophenyl)-5-(3-bromophenyl)-3-hydroxy-1,5-dihydro-2H-pyrrol-2-one (46).** Started from 3-bromobenzaldehyde **1l** (291  $\mu$ L, 2.50 mmol, 1.00 eq.), 4-bromo-2-fluoroaniline **2n** (475 mg, 2.50 mmol, 1.00 eq.) and ethyl 2,4-dioxopentanoate **3a** (395 mg, 2.50 mmol, 1.00 eq.) in 5 mL of AcOH. Purified by silica column chromatography using EtOAc/Pet Ether (1/19). Yield: 82 mg, 5%, yellow solid. <sup>1</sup>H NMR (400 MHz, CDCl<sub>3</sub>):  $\delta$  7.41 (dt,  $J$  = 7.6, 1.6 Hz, 1H), 7.33-7.24 (m, 2H), 7.22 (d,  $J$  = 8.4 Hz, 1H), 7.19-7.11 (m, 2H), 7.08 (t,  $J$  = 8.0 Hz, 1H), 5.74 (s, 1H), 2.17 (s, 3H) ppm. MS [ESI+H]<sup>+</sup>: 469.60



## In vitro characterization of compound's activity

### Chemicals and reagents

[<sup>3</sup>H]-CCR2-RA-[R] (specific activity 59.6 Ci mmol<sup>-1</sup>), corresponding to the (*R*)-isomer of compound **38** ([<sup>3</sup>H]-(*R*)-4-acetyl-1-(4-chloro-2-fluorophenyl)-5-cyclohexyl-3-hydroxy-1,5-dihydro-2H-pyrrol-2-one)), was custom-labeled by Vitrax (Placentia, CA). [<sup>35</sup>S]GTPγS (guanosine 5'-*O*-(3-[<sup>35</sup>S]thio)triphosphate), with a specific activity of 1250 Ci mmol<sup>-1</sup>, was purchased from PerkinElmer (Waltham, MA). CCR2-RA-[R], SD-24 and JNJ-27141491 were synthesized as described previously.<sup>30, 37, 54</sup> BX471 was purchased from Cayman Chemical (Ann Arbor, MI, USA). Chemokine ligands CCL2 and CCL3 were purchased from PeproTech (Rocky Hill, NJ). Bovine serum albumin (BSA, fraction V) was purchased from Sigma (St. Louis, MO, USA). Bicinchoninic acid (BCA) and BCA protein assay reagent were purchased from Pierce Chemical Company (Rockford, IL, USA). Tango™ CCR1-*bla* and Tango™ CCR2-*bla* osteosarcoma (U2OS) cells stably expressing the human CCR1 or human CCR2b (U2OS-CCR1 or U2OS-CCR2, respectively) were obtained from Invitrogen (Carlsbad, CA). All other chemicals were obtained from standard commercial sources.

### Cell culture and membrane preparation

U2OS-CCR1 and U2OS-CCR2 were grown in a humidified atmosphere at 37 °C and 5% CO<sub>2</sub> in McCoy's 5A medium supplemented with 10% fetal calf serum, 2 mM glutamine, 0.1 mM nonessential amino acids (NEAAs), 25 mM HEPES, 1 mM sodium pyruvate, 100 IU/ml penicillin, 100 µg/ml streptomycin, 100 µg/ml G418, 50 µg/ml hygromycin, and 125 µg/ml zeocin (200 µg/ml zeocin for U2OS-CCR1). Cells were subcultured twice a week at a ratio of 1:3 to 1:8 on 10-cm Ø plates by trypsinization. For membrane preparation cells were subcultured on 15-cm Ø plates using dialyzed fetal calf serum. Membranes from U2OS-CCR1 and U2OS-CCR2 cells were prepared as described previously.<sup>26</sup> Briefly, cells were detached from confluent 15-cm Ø plates by scraping them into 5 ml of phosphate-buffered saline (PBS), collected and centrifuged for 5 minutes at 3000 rpm (700g). The pellets were resuspended in ice-cold 50 mM Tris-HCl buffer, pH 7.4, supplemented with 5 mM MgCl<sub>2</sub>, and homogenized with an Ultra Turrax homogenizer (IKA-Werke GmbH & Co. KG, Staufen, Germany). Membranes were separated from the cytosolic fraction by several centrifugation steps in an Optima LE-80 K ultracentrifuge (Beckman Coulter, Inc., Fullerton, CA) at 31,000 rpm for 20 minutes at 4°C. Finally, the membrane pellets were resuspended in 50 mM Tris-HCl buffer supplemented with 5 mM MgCl<sub>2</sub>, pH 7.4, divided into aliquots of 100 µl and 250 µl and stored at -80°C. Membrane protein concentrations were measured using a BCA protein determination with BSA as a standard.<sup>55</sup>

## **[<sup>3</sup>H]-CCR2-RA-[R] binding assays**

[<sup>3</sup>H]-CCR2-RA-[R] (homologous) displacement assays in U2OS-CCR1 and U2OS-CCR2 were performed in a 100  $\mu$ L reaction volume containing assay buffer (50 mM Tris-HCl, 5 mM MgCl<sub>2</sub> and 0.1% CHAPS, pH 7.4), 6 nM [<sup>3</sup>H]-CCR2-RA-[R], 8 to 15  $\mu$ g of membrane protein and the competing ligand. Homologous displacement assays were carried out with 3 different concentrations of [<sup>3</sup>H]-CCR2-RA-[R], namely 3, 6 and 12 nM. In all cases, at least 6 concentrations of competing ligand were used and the reaction mixture was incubated for 120 min at 25 °C. Non-specific binding was determined in the presence of 10  $\mu$ M CCR2-RA-[R]. Total radioligand binding did not exceed 10% of the amount added to prevent ligand depletion. [<sup>3</sup>H]-CCR2-RA-[R] saturation binding assays in U2OS-CCR2 were also performed in a 100  $\mu$ L reaction volume containing assay buffer, [<sup>3</sup>H]-CCR2-RA-[R] in 12 different concentrations ranging from 0.05 nM to 70 nM, and 15  $\mu$ g of membrane protein. Non-specific binding was determined in the presence of 10  $\mu$ M JNJ-27141491 at 4 different concentrations of radioligand, namely 0.1, 0.4, 2.5 and 20 nM. In association assays, U2OS-CCR1 and U2OS-CCR2 membrane preparations were added to the reaction mix at different time points of incubation, ranging from 1 min to 180 min incubation; in dissociation assays, membranes were first incubated with 6 nM [<sup>3</sup>H]-CCR2-RA-[R] for 90 min, and dissociation was initiated by the addition of 10  $\mu$ M CCR2-RA-[R] at different time points, up to 150 min for CCR1 and 180 min for CCR2. For all experiments, incubations were terminated by dilution with ice-cold wash-buffer (50 mM Tris-HCl buffer supplemented with 5mM MgCl<sub>2</sub> and 0.05% CHAPS, pH 7.4). Separation of bound from free radioligand was performed by rapid filtration through a 96-well GF/B filter plate using a Perkin Elmer Filtermate harvester (Perkin Elmer, Groningen, the Netherlands). Filters were washed 10 times with ice-cold wash buffer. 25  $\mu$ L of Microscint scintillation cocktail (Perkin-Elmer, Groningen, the Netherlands) was added to each well and the filter-bound radioactivity was determined by scintillation spectrometry using the P-E 2450 Microbeta<sup>2</sup> scintillation plate-counter (Perkin Elmer, Groningen, The Netherlands).

## **[<sup>35</sup>S]GTP $\gamma$ S Binding assays**

[<sup>35</sup>S]GTP $\gamma$ S binding assays were performed as described previously.<sup>26</sup> Briefly, binding assays were performed in a 100  $\mu$ L reaction volume containing assay buffer (50mM Tris-HCl, 5mM MgCl<sub>2</sub>, 100mM NaCl, 1mM EDTA, and 0.05% BSA, pH 7.4), 10  $\mu$ M GDP, 10  $\mu$ g of saponin and 10  $\mu$ g of membrane, either U2OS-CCR1 or U2OS-CCR2. To determine the EC<sub>50</sub> value of CCL2 and CCL3, the membrane mixture was preincubated with increasing concentrations of chemokine for 30 min at 25 °C. To determine the IC<sub>50</sub> values of the ligands, the membrane mixture was preincubated with increasing concentrations of the ligand of interest in absence



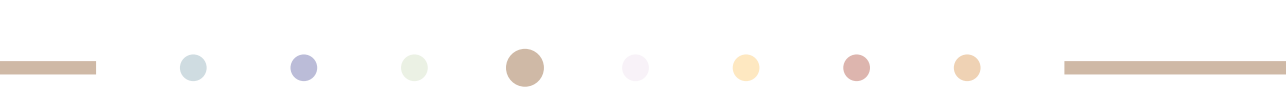
or presence of a fixed concentration of CCL2 (20 nM) or CCL3 (8 nM). Basal activity was determined in the absence of any ligand or chemokine. Finally, the mixture was incubated for another 90 min at 25 °C after the addition of 0.3 nM [<sup>35</sup>S]GTPγS in all cases. For all experiments, incubations were terminated by dilution with ice-cold 50mM Tris-HCl, 5mM MgCl<sub>2</sub> buffer. Separation of bound from free [<sup>35</sup>S]GTPγS was performed as described under “[<sup>3</sup>H]-CCR2-RA-[R] binding assays”.

## Data analysis

All experiments were analyzed using GraphPad Prism 7.0 (GraphPad Software Inc., San Diego, CA, U.S.A.). The  $K_D$  and  $B_{max}$  values of [<sup>3</sup>H]-CCR2-RA-[R] in U2OS-CCR2 were calculated from saturation experiments, by fitting the data to the equation  $Bound = (B_{max} * [L]) / ([L] + K_D)$ , where  $B_{max}$  is the maximum number of binding sites and  $K_D$  is the concentration required to reach half-maximum binding at equilibrium conditions. In the case of U2OS-CCR1 membranes, the  $K_D$  and  $B_{max}$  values were calculated from homologous binding experiments by non-linear regression analysis, using the “One site – Homologous” model that assumes that unlabeled and labeled CCR2-RA-[R] have identical affinities. The (p)IC<sub>50</sub> values of unlabeled ligands from [<sup>3</sup>H]-CCR2-RA-[R] binding assays were obtained by non-linear regression analysis of the displacement curves, and further converted into (p)K<sub>i</sub> values using the Cheng-Prusoff equation.<sup>56</sup> The (p)IC<sub>50</sub> or (p)EC<sub>50</sub> values from [<sup>35</sup>S]GTPγS curves were also obtained by non-linear regression. The observed association rate constants ( $k_{obs,fast}$ ;  $k_{obs,slow}$ ) were calculated by fitting the data to a two-phase exponential association function; similarly, dissociation rate constants ( $k_{off,fast}$ ;  $k_{off,slow}$ ) were calculated using a two-phase exponential decay function. All values obtained are means ± standard error of the mean (SEM) of at least three independent experiments performed in duplicate, unless stated otherwise. Differences in kinetic rates and pIC<sub>50</sub> values between receptors or between assay formats (in absence or presence of chemokine) were analyzed using an unpaired, two-tailed Student’s *t*-test with Welch’s correction; differences in pK<sub>i</sub> values between compounds, in maximal [<sup>35</sup>S]GTPγS inhibition against basal activity or in pseudo-Hill slopes from [<sup>35</sup>S]GTPγS inhibition curves against compound **45**, which showed a pseudo-Hill slope of approx. unity, were analyzed using a one-way ANOVA with Dunnett’s post-hoc test. Significant differences are displayed as \*,  $p < 0.05$ ; \*\*,  $p < 0.01$ ; \*\*\*,  $p < 0.001$ ; and \*\*\*\*,  $p < 0.0001$ .

## Computational Receptor Modeling and Docking

All modeling was performed in the Schrodinger suite,<sup>57</sup> Figures 3b and 3c were made in a later version<sup>58</sup> that includes the interaction and orientation of residues (e.g. backbone,



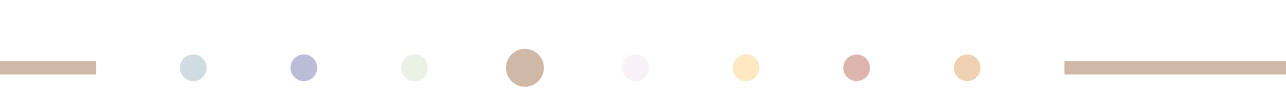
sidechain). As a starting point for the structure-based studies we used the recently published crystal structure of CCR2b in complex with both BMS-681 and CCR2-RA-[R] (PDB ID: 5T1A, **Chapter 3**).<sup>24</sup> We replaced the sequence (CCR2b: sequence between L226<sup>5x62</sup> and R240<sup>6x32</sup>) of the M2 muscarinic acetylcholine receptor, close to the intracellular binding site, by the CCR2b sequence using homology modelling<sup>59-61</sup> and CCR5 as template (PDB ID: 4MBS).<sup>62</sup> A homology model of CCR1 was constructed on the basis of this CCR2b model. For both models the knowledge-based scoring function was used. For the ligand docked, the  $pK_a$  of the hydroxyl hydrogen was calculated to be 4.5 using Jaguar;<sup>63, 64</sup> therefore, the negatively charged protonation state was used. Compound CCR2-RA-[R] was docked in both models using Induced fit docking.<sup>65, 66</sup> Visualizations were created using PyMOL;<sup>67</sup> residues within 5Å of the ligand and facing the binding site are shown.

## REFERENCES

1. Griffith, J. W.; Sokol, C. L.; Luster, A. D. Chemokines and chemokine receptors: positioning cells for host defense and immunity. *Annu. Rev. Immunol.* **2014**, *32*, 659-702.
2. Bachelier, F.; Ben-Baruch, A.; Burkhardt, A. M.; Combadiere, C.; Farber, J. M.; Graham, G. J.; Horuk, R.; Sparre-Ulrich, A. H.; Locati, M.; Luster, A. D.; Mantovani, A.; Matsushima, K.; Murphy, P. M.; Nibbs, R.; Nomiyama, H.; Power, C. A.; Proudfoot, A. E.; Rosenkilde, M. M.; Rot, A.; Sozzani, S.; Thelen, M.; Yoshie, O.; Zlotnik, A. International union of basic and clinical pharmacology. LXXXIX. Update on the extended family of chemokine receptors and introducing a new nomenclature for atypical chemokine receptors. *Pharmacol. Rev.* **2014**, *66*, 1-79.
3. Kleist, A. B.; Getschman, A. E.; Ziarek, J. J.; Nevins, A. M.; Gauthier, P. A.; Chevigne, A.; Szpakowska, M.; Volkman, B. F. New paradigms in chemokine receptor signal transduction: moving beyond the two-site model. *Biochem. Pharmacol.* **2016**, *114*, 53-68.
4. Kufareva, I. Chemokines and their receptors: insights from molecular modeling and crystallography. *Curr. Opin. Pharmacol.* **2016**, *30*, 27-37.
5. Lopez-Cotarelo, P.; Gomez-Moreira, C.; Criado-Garcia, O.; Sanchez, L.; Rodriguez-Fernandez, J. L. Beyond chemoattraction: multifunctionality of chemokine receptors in leukocytes. *Trends Immunol* **2017**, *38*, 927 - 941.
6. Viola, A.; Luster, A. D. Chemokines and their receptors: drug targets in immunity and inflammation. *Annu Rev Pharmacol Toxicol.* **2008**, *48*, 171-197.
7. White, G. E.; Iqbal, A. J.; Greaves, D. R. CC chemokine receptors and chronic inflammation—therapeutic opportunities and pharmacological challenges. *Pharmacol. Rev.* **2013**, *65*, 47-89.
8. Pease, J.; Horuk, R. Chemokine receptor antagonists. *J. Med. Chem.* **2012**, *55*, 9363-9392.
9. Szekanecz, Z.; Koch, A. E. Successes and failures of chemokine-pathway targeting in rheumatoid arthritis. *Nat. Rev. Rheumatol.* **2016**, *12*, 5-13.
10. Haringman, J. J.; Smeets, T. J.; Reinders-Blankert, P.; Tak, P. P. Chemokine and chemokine receptor expression in paired peripheral blood mononuclear cells and synovial tissue of patients with rheumatoid arthritis, osteoarthritis, and reactive arthritis. *Ann. Rheum. Dis.* **2006**, *65*, 294-300.
11. Eltayeb, S.; Berg, A.-L.; Lassmann, H.; Wallström, E.; Nilsson, M.; Olsson, T.; Ericsson-Dahlstrand, A.; Sunnemark, D. Temporal expression and cellular origin of CC chemokine receptors CCR1, CCR2 and CCR5 in the central nervous system: insight into mechanisms of MOG-induced EAE. *J. Neuroinflammation* **2007**, *4*, 14.
12. Fife, B. T.; Huffnagle, G. B.; Kuziel, W. A.; Karpus, W. J. CC chemokine receptor 2 is critical for induction of experimental autoimmune encephalomyelitis. *J Exp Med* **2000**, 192.
13. Rottman, J. B.; Slavin, A. J.; Silva, R.; Weiner, H. L.; Gerard, C. G.; Hancock, W. W. Leukocyte recruitment during onset of experimental allergic encephalomyelitis is CCR1 dependent. *Eur. J. Immunol.* **2000**, *30*, 2372-2377.
14. Brühl, H.; Cihak, J.; Schneider, M. A.; Plachý, J.; Rupp, T.; Wenzel, I.; Shakarami, M.; Milz, S.; Ellwart, J. W.; Stangassinger, M.; Schlöndorff, D.; Mack, M. Dual role of CCR2 during initiation and progression of collagen-induced arthritis: evidence for regulatory activity of CCR2<sup>+</sup> T cells. *J. Immunol.* **2004**, *172*, 890-898.
15. Amat, M.; Benjamim, C. F.; Williams, L. M.; Prats, N.; Terricabras, E.; Beleta, J.; Kunkel, S. L.; Godessart, N. Pharmacological blockade of CCR1 ameliorates murine arthritis and alters cytokine networks in vivo. *Br. J. Pharmacol.* **2006**, *149*, 666-675.
16. Wang, Y.; Cui, L.; Gonsiorek, W.; Min, S.-H.; Anilkumar, G.; Rosenblum, S.; Kozlowski, J.; Lundell, D.; Fine, J. S.; Grant, E. P. CCR2 and CXCR4 regulate peripheral blood monocyte pharmacodynamics and link to efficacy in experimental autoimmune encephalomyelitis. *J. Inflamm.* **2009**, *6*, 32.

17. Dairaghi, D. J.; Zhang, P.; Wang, Y.; Seitz, L. C.; Johnson, D. A.; Miao, S.; Ertl, L. S.; Zeng, Y.; Powers, J. P.; Pennell, A. M.; Bekker, P.; Schall, T. J.; Jaen, J. C. Pharmacokinetic and pharmacodynamic evaluation of the novel CCR1 antagonist CCX354 in healthy human subjects: implications for selection of clinical dose. *Clin. Pharmacol. Ther.* **2011**, *89*, 726-734.
18. Tak, P. P.; Balanescu, A.; Tseluyko, V.; Bojin, S.; Drescher, E.; Dairaghi, D.; Miao, S.; Marchesin, V.; Jaen, J.; Schall, T. J. Chemokine receptor CCR1 antagonist CCX354-C treatment for rheumatoid arthritis: CARAT-2, a randomised, placebo controlled clinical trial. *Ann. Rheum. Dis.* **2013**, *72*, 337-344.
19. Horuk, R. Promiscuous drugs as therapeutics for chemokine receptors. *Expert Rev. Mol. Med.* **2009**, *11*, e1.
20. Sabroe, I.; Peck, M. J.; Van Keulen, B. J.; Jorritsma, A.; Simmons, G.; Clapham, P. R.; Williams, T. J.; Pease, J. E. A small molecule antagonist of chemokine receptors CCR1 and CCR3. Potent inhibition of eosinophil function and CCR3-mediated HIV-1 entry. *J. Biol. Chem.* **2000**, *275*, 25985-25992.
21. Junker, A.; Kokornaczyk, A. K.; Zweemer, A. J.; Frehland, B.; Schepmann, D.; Yamaguchi, J.; Itami, K.; Faust, A.; Hermann, S.; Wagner, S.; Schafers, M.; Koch, M.; Weiss, C.; Heitman, L. H.; Kopka, K.; Wunsch, B. Synthesis, binding affinity and structure-activity relationships of novel, selective and dual targeting CCR2 and CCR5 receptor antagonists. *Org. Biomol. Chem.* **2015**, *13*, 2407-2422.
22. Cox, B. D.; Prosser, A. R.; Sun, Y.; Li, Z.; Lee, S.; Huang, M. B.; Bond, V. C.; Snyder, J. P.; Krystal, M.; Wilson, L. J.; Liotta, D. C. Pyrazolo-piperidines exhibit dual inhibition of CCR5/CXCR4 HIV entry and reverse transcriptase. *ACS Med. Chem. Lett.* **2015**, *6*, 753-757.
23. Moriconi, A.; Cesta, M. C.; Cervellera, M. N.; Aramini, A.; Coniglio, S.; Colagioia, S.; Beccari, A. R.; Bizzarri, C.; Cavicchia, M. R.; Locati, M. Design of noncompetitive interleukin-8 inhibitors acting on CXCR1 and CXCR2. *J. Med. Chem.* **2007**, *50*, 3984-4002.
24. Zheng, Y.; Qin, L.; Ortiz Zacarias, N. V.; de Vries, H.; Han, G. W.; Gustavsson, M.; Dabros, M.; Zhao, C.; Cherney, R. J.; Carter, P.; Stamos, D.; Abagyan, R.; Cherezov, V.; Stevens, R. C.; Ilzerman, A. P.; Heitman, L. H.; Tebben, A.; Kufareva, I.; Handel, T. M. Structure of CC chemokine receptor 2 with orthosteric and allosteric antagonists. *Nature* **2016**, *540*, 458-461.
25. Oswald, C.; Rappas, M.; Kean, J.; Dore, A. S.; Errey, J. C.; Bennett, K.; Deflorian, F.; Christopher, J. A.; Jazayeri, A.; Mason, J. S.; Congreve, M.; Cooke, R. M.; Marshall, F. H. Intracellular allosteric antagonism of the CCR9 receptor. *Nature* **2016**, *540*, 462-465.
26. Zweemer, A. J.; Nederpelt, I.; Vrieling, H.; Hafith, S.; Doornbos, M. L.; de Vries, H.; Abt, J.; Gross, R.; Stamos, D.; Saunders, J.; Smit, M. J.; Ilzerman, A. P.; Heitman, L. H. Multiple binding sites for small-molecule antagonists at the CC chemokine receptor 2. *Mol. Pharmacol.* **2013**, *84*, 551-561.
27. Ortiz Zacarias, N. V.; Lenselink, E. B.; Ilzerman, A. P.; Handel, T. M.; Heitman, L. H. Intracellular receptor modulation: novel approach to target GPCRs. *Trends Pharmacol Sci* **2018**, *39*, 547-559.
28. Zweemer, A. J.; Bunnik, J.; Veenhuizen, M.; Miraglia, F.; Lenselink, E. B.; Vilums, M.; de Vries, H.; Gibert, A.; Thiele, S.; Rosenkilde, M. M.; Ilzerman, A. P.; Heitman, L. H. Discovery and mapping of an intracellular antagonist binding site at the chemokine receptor CCR2. *Mol. Pharmacol.* **2014**, *86*, 358-368.
29. Dasse, O.; Evans, J.; Zhai, H.-X.; Zou, D.; Kintigh, J.; Chan, F.; Hamilton, K.; Hill, E.; Eckman, J.; Higgins, P. Novel, acidic CCR2 receptor antagonists: lead optimization. *Letts. Drug. Des. Discov.* **2007**, *4*, 263-271.
30. Peace, S.; Philp, J.; Brooks, C.; Piercy, V.; Moores, K.; Smethurst, C.; Watson, S.; Gaines, S.; Zippoli, M.; Mookherjee, C.; Ife, R. Identification of a sulfonamide series of CCR2 antagonists. *Bioorg. Med. Chem. Lett.* **2010**, *20*, 3961-3964.
31. Buntinx, M.; Hermans, B.; Goossens, J.; Moechars, D.; Gilissen, R. A.; Doyon, J.; Boeckx, S.; Coesemans, E.; Van Lommen, G.; Van Wauwe, J. P. Pharmacological profile of JNJ-27141491 [(S)-3-[3, 4-difluorophenyl]-propyl]-5-isoxazol-5-yl-2-thioxo-2, 3-dihydro-1H-imidazole-4-carboxyl acid methyl ester], as a noncompetitive and orally active antagonist of the human chemokine receptor CCR2. *J. Pharmacol. Exp. Ther.* **2008**, *327*, 1-9.
32. Zou, D.; Dasse, O.; Evans, J.; Higgins, P.; Kintigh, J.; Kondru, R.; Schwartz, E.; Knerr, L.; Zhai, H. X. Pyrrolidinone Derivatives. U.S. Patent 6,727,275 B2. **2004**.
33. Zou, D.; Dasse, O.; Evans, J.; Higgins, P.; Kintigh, J.; Kondru, R.; Schwartz, E.; Knerr, L.; Zhai, H. X. Pyrrolidinone Derivatives. U.S. Patent Application 2003/0149081 A1. **2003**.

34. Kopp, M.; Lancelot, J. C.; Dallemagne, P.; Rault, S. Synthesis of novel pyrazolopyrrolopyrazines, potential analogs of sildenafil. *J. Heterocycl. Chem.* **2001**, *38*, 1045-1050.
35. Liang, M.; Mallari, C.; Rosser, M.; Ng, H. P.; May, K.; Monahan, S.; Bauman, J. G.; Islam, I.; Ghannam, A.; Buckman, B.; Shaw, K.; Wei, G. P.; Xu, W.; Zhao, Z.; Ho, E.; Shen, J.; Oanh, H.; Subramanyam, B.; Vergona, R.; Taub, D.; Dunning, L.; Harvey, S.; Snider, R. M.; Hesselgesser, J.; Morrissey, M. M.; Perez, H. D. Identification and characterization of a potent, selective, and orally active antagonist of the CC chemokine receptor-1. *J. Biol. Chem.* **2000**, *275*, 19000-19008.
36. Isberg, V.; de Graaf, C.; Bortolato, A.; Cherezov, V.; Katritch, V.; Marshall, F. H.; Mordalski, S.; Pin, J.-P.; Stevens, R. C.; Vriend, G.; Gloriam, D. E. Generic GPCR residue numbers – aligning topology maps while minding the gaps. *Trends Pharmacol. Sci.* **2015**, *36*, 22-31.
37. Zou, D.; Zhai, H.-X.; Eckman, J.; Higgins, P.; Gillard, M.; Knerr, L.; Carre, S.; Pasau, P.; Collart, P.; Grassi, J. Novel, acidic CCR2 receptor antagonists: from hit to lead. *Letts. Drug. Des. Discov.* **2007**, *4*, 185-191.
38. Kettle, J. G.; Faull, A. W.; Barker, A. J.; Davies, D. H.; Stone, M. A. N-benzylindole-2-carboxylic acids: potent functional antagonists of the CCR2b chemokine receptor. *Bioorg. Med. Chem. Lett.* **2004**, *14*, 405-408.
39. Cavallo, G.; Metrangolo, P.; Milani, R.; Pilati, T.; Priimagi, A.; Resnati, G.; Terraneo, G. The halogen bond. *Chem. Rev.* **2016**, *116*, 2478-2601.
40. Hansch, C.; Leo, A.; Taft, R. A survey of Hammett substituent constants and resonance and field parameters. *Chem. Rev.* **1991**, *91*, 165-195.
41. Chou, C. C.; Fine, J. S.; Pugliese-Sivo, C.; Gonsiorek, W.; Davies, L.; Deno, G.; Petro, M.; Schwarz, M.; Zavodny, P. J.; Hipkin, R. W. Pharmacological characterization of the chemokine receptor, hCCR1 in a stable transfectant and differentiated HL-60 cells: antagonism of hCCR1 activation by MIP-1 $\beta$ . *Br. J. Pharmacol.* **2002**, *137*, 663-675.
42. Gilliland, C. T.; Salanga, C. L.; Kawamura, T.; Trejo, J.; Handel, T. M. The chemokine receptor CCR1 is constitutively active, which leads to G protein-independent,  $\beta$ -arrestin-mediated internalization. *J. Biol. Chem.* **2013**, *288*, 32194-32210.
43. Prinz, H. Hill coefficients, dose-response curves and allosteric mechanisms. *J. Chem. Biol.* **2010**, *3*, 37-44.
44. Alvarez Arias, D.; Navenot, J.-M.; Zhang, W.-b.; Broach, J.; Peiper, S. C. Constitutive activation of CCR5 and CCR2 induced by conformational changes in the conserved TXP motif in transmembrane helix 2. *J. Biol. Chem.* **2003**, *278*, 36513-36521.
45. Lagorce, D.; Sperandio, O.; Baell, J. B.; Miteva, M. A.; Villoutreix, B. O. FAF-Drugs3: a web server for compound property calculation and chemical library design. *Nucleic Acids Res.* **2015**, *43*, W200-W207.
46. Lagorce, D.; Douguet, D.; Miteva, M. A.; Villoutreix, B. O. Computational analysis of calculated physicochemical and ADMET properties of protein-protein interaction inhibitors. *Sci. Rep.* **2017**, *7*, 46277.
47. Baell, J. B.; Holloway, G. A. New substructure filters for removal of pan assay interference compounds (PAINS) from screening libraries and for their exclusion in bioassays. *J. Med. Chem.* **2010**, *53*, 2719-2740.
48. Cormier, M.; Chardon, A.; Blanchet, J.; Rouden, J.; Maddaluno, J.; De Paolis, M. An organocatalytic access to spiro[4.5]decanes and spiro[4.6]undecanes containing aminolactones and 3-aminopyrrolidines. *Synthesis* **2015**, *47*, 2549-2553.
49. Koz'minykh, V.; Igidov, N.; Zykova, S.; Kolla, V.; Shuklina, N.; Odegova, T. Synthesis and pharmacological activity of 3-hydroxy-1,5-diaryl-4-pivaloyl-2,5-dihydro-2-pyrrolones. *Pharm. Chem. J.* **2002**, *36*, 188-191.
50. Kraïem, J. B.; Amri, H. Concise synthesis of  $\alpha$ -(hydroxymethyl) alkyl and aryl vinyl ketones. *Synth. Commun.* **2013**, *43*, 110-117.
51. Frank, R.; Bahrenberg, G.; Christoph, T.; Schiene, K.; De, V. J.; Damann, N.; Frommann, S.; Lesch, B.; Lee, J.; Kim, Y. S. Substituted Aromatic Carboxamide and Urea Derivatives as Vanilloid Receptor Ligands. Patent WO 2010/127855 A1. **2010**.
52. Carpino, P. A.; Sanner, M. A. Cannabinoid Receptor Ligands and Uses Thereof. Patent WO 2007/020502 A2. **2007**.

- 
53. Chonan, T.; Tanaka, H.; Yamamoto, D.; Yashiro, M.; Oi, T.; Wakasugi, D.; Ohoka-Sugita, A.; Ito, F.; Koretsune, H.; Hiratate, A. Design and synthesis of disubstituted (4-piperidinyl)-piperazine derivatives as potent acetyl-CoA carboxylase inhibitors. *Bioorg. Med. Chem. Lett.* **2010**, *20*, 3965-3968.
  54. Doyon, J.; Coesemans, E.; Boeckx, S.; Buntinx, M.; Hermans, B.; Van Wauwe, J. P.; Gilissen, R. A.; De Groot, A. H.; Corens, D.; Van Lommen, G. Discovery of potent, orally bioavailable small-molecule inhibitors of the human CCR2 receptor. *ChemMedChem* **2008**, *3*, 660-669.
  55. Smith, P. K.; Krohn, R. I.; Hermanson, G. T.; Mallia, A. K.; Gartner, F. H.; Provenzano, M. D.; Fujimoto, E. K.; Goeke, N. M.; Olson, B. J.; Klenk, D. C. Measurement of protein using bicinchoninic acid. *Anal. Biochem.* **1985**, *150*, 76-85.
  56. Cheng, Y.; Prusoff, W. H. Relationship between the inhibition constant (K<sub>1</sub>) and the concentration of inhibitor which causes 50 per cent inhibition (I<sub>50</sub>) of an enzymatic reaction. *Biochem. Pharmacol.* **1973**, *22*, 3099-3108.
  57. *Maestro Release 2017-1*; Schrödinger, LLC, New York, 2017.
  58. *Maestro Release 2017-2*; Schrödinger, LLC, New York, 2017.
  59. *Prime Release 2017-1*; Schrödinger, LLC, New York, 2017.
  60. Jacobson, M. P.; Friesner, R. A.; Xiang, Z.; Honig, B. On the role of the crystal environment in determining protein side-chain conformations. *J. Mol. Biol.* **2002**, *320*, 597-608.
  61. Jacobson, M. P.; Pincus, D. L.; Rapp, C. S.; Day, T. J.; Honig, B.; Shaw, D. E.; Friesner, R. A. A hierarchical approach to all-atom protein loop prediction. *Proteins* **2004**, *55*, 351-367.
  62. Tan, Q.; Zhu, Y.; Li, J.; Chen, Z.; Han, G. W.; Kufareva, I.; Li, T.; Ma, L.; Fenalti, G.; Li, J. Structure of the CCR5 chemokine receptor–HIV entry inhibitor maraviroc complex. *Science* **2013**, *341*, 1387-1390.
  63. *Jaguar Release 2017-1*; Schrödinger, LLC, New York, 2017.
  64. Bochevarov, A. D.; Harder, E.; Hughes, T. F.; Greenwood, J. R.; Braden, D. A.; Philipp, D. M.; Rinaldo, D.; Halls, M. D.; Zhang, J.; Friesner, R. A. Jaguar: a high-performance quantum chemistry software program with strengths in life and materials sciences. *Int. J. Quantum Chem.* **2013**, *113*, 2110-2142.
  65. *Glide Release 2017-1*; *Schrödinger Suite Prime 2017-1 Induced Fit Docking protocol*; Schrödinger, LLC, New York, 2017.
  66. Sherman, W.; Day, T.; Jacobson, M. P.; Friesner, R. A.; Farid, R. Novel procedure for modeling ligand/receptor induced fit effects. *J. Med. Chem.* **2006**, *49*, 534-553.
  67. *The PyMOL Molecular Graphics System*, version 1.8; Schrödinger, LLC, New York, 2015.

## SUPPORTING INFORMATION

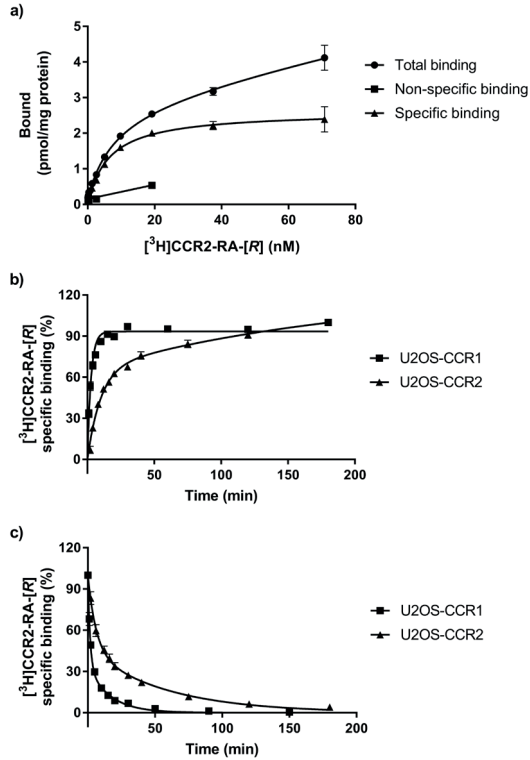


**Figure S1.** (a) Saturation binding of 0.05 – 70 nM  $[^3\text{H}]\text{-CCR2-RA-[R]}$  to U2OS-CCR2 at 25°C, in absence (total binding) or presence (non-specific binding) of 10  $\mu\text{M}$  JNJ-27141491. (b) Association kinetics of 6 nM  $[^3\text{H}]\text{-CCR2-RA-[R]}$  to U2OS-CCR1 (squares) and U2OS-CCR2 (triangles) at 25°C. In both CCR1 and CCR2, data were best fitted using a two-phase association function. (c) Dissociation kinetics of 6 nM  $[^3\text{H}]\text{-CCR2-RA-[R]}$  from U2OS-CCR1 (squares) and U2OS-CCR2 (triangles) at 25°C. In both CCR1 and CCR2, data were best fitted using a two-phase exponential decay function. For all experiments data shown are mean  $\pm$  SEM of at least three experiments performed in duplicate. See Supplementary Table 1 for  $pK_{D1}$ ,  $B_{max}$  and rate constants.

	TM1			TM2			TM3			TM6				TM7		H8						
B&W Number	1x53	1x56	1x57	2x39	2x40	2x43	3x46	3x50	3x53	6x30	6x32	6x33	6x34	6x36	6x37	6x40	7x53	7x56	8x47	8x48	8x49	8x50
hCCR2b	V	I	L	T	D	L	L	R	A	R	R	A	V	V	I	I	Y	V	G	E	K	F
hCCR1	V	V	L	T	S	L	L	R	A	K	K	A	V	L	I	I	Y	V	G	E	R	F

**Figure S2.** Sequence conservation of the key residues involved in the intracellular binding of CCR2-RA-[R] in CCR2,<sup>24</sup> as obtained by sequence alignment of human CCR1 and human CCR2b using the “Structure-based alignment” tool and the “Similarity search” tool of the GPCR database (GPCRdb, <http://www.gpcrdb.org>).<sup>36</sup> The residues are numbered according to the structure-based Ballesteros-Weinstein system,<sup>36</sup> which corresponds to the system used by the GPCRdb. Different amino acids in both CCR1 and CCR2 are highlighted.

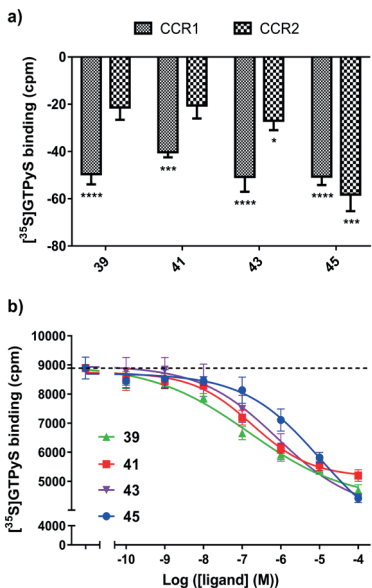


**Figure S3.** Compounds behave as inverse agonists in CCR1. (a) Maximal inhibition of CCL2 or CCL3-induced  $[^{35}\text{S}]$ GTPyS binding achieved by the highest concentration tested of compounds **39**, **41**, **43** and **45** in U2OS-CCR1 (100  $\mu\text{M}$ ) and U2OS-CCR2 (**45** at 100  $\mu\text{M}$ , **39**, **41**, **43** at 10  $\mu\text{M}$ ). One-way ANOVA with Dunnett's post-hoc test was performed to compare the maximal inhibition against basal  $[^{35}\text{S}]$ GTPyS binding in CCR1 or CCR2. Significant differences are displayed as \*,  $p < 0.05$ ; \*\*\*,  $p < 0.001$ ; and \*\*\*\*,  $p < 0.0001$ . (b) Inhibition of basal  $[^{35}\text{S}]$ GTPyS binding in absence of agonist CCL3 by compounds **39**, **41**, **43** and **45** in U2OS-CCR1. The level of basal activity in U2OS-CCR1 is indicated by a dashed line. Data shown are mean  $\pm$  SEM of at least three experiments performed in duplicate.

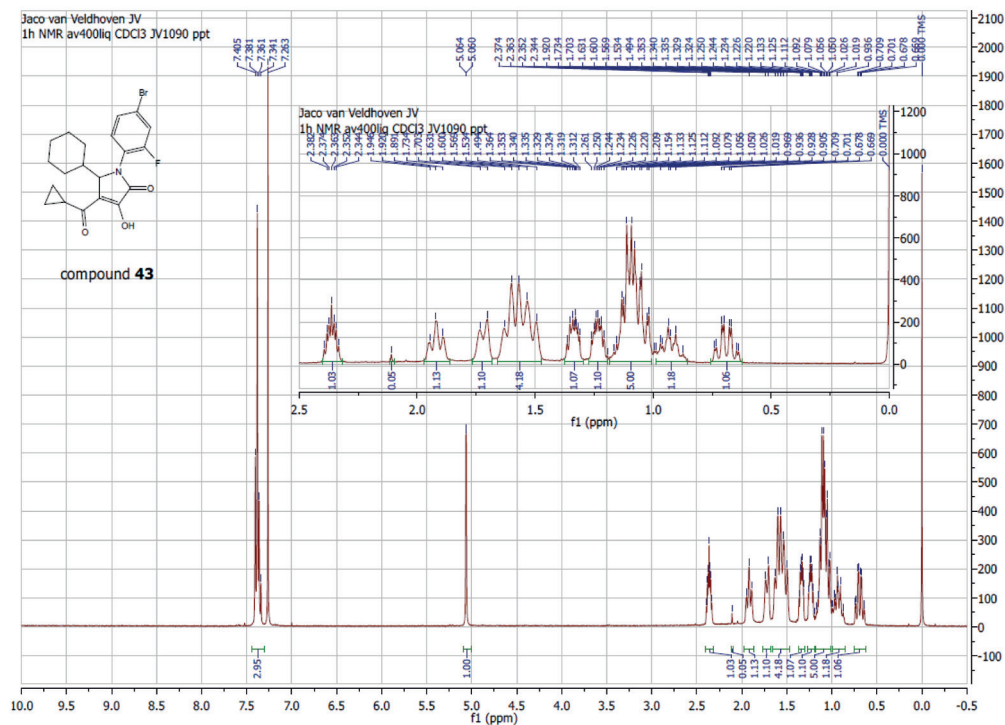




**Table S1. Characterization of [<sup>3</sup>H]CCR2-RA-[R] in U2OS-CCR1 and U2OS-CCR2.<sup>a</sup>**

	U2OS-CCR1	U2OS-CCR2
$pK_D$ ( $K_D$ , nM)	7.87 ± 0.03 (13.5) <sup>b</sup>	8.20 ± 0.05 (6.3) <sup>c</sup>
$B_{max}$ (pmol/mg)	6.13 ± 0.24 <sup>b</sup>	2.63 ± 0.28 <sup>c</sup>
$k_{obs,fast}$ (min <sup>-1</sup> ) <sup>d</sup>	0.69 ± 0.08	0.12 ± 0.01*
$k_{obs,slow}$ (min <sup>-1</sup> ) <sup>d</sup>	0.11 ± 0.007	0.01 ± 0.001**
%fast	62 ± 2	55 ± 3
$k_{off,fast}$ (min <sup>-1</sup> ) <sup>e</sup>	0.62 ± 0.08	0.18 ± 0.02*
$k_{off,slow}$ (min <sup>-1</sup> ) <sup>e</sup>	0.06 ± 0.002	0.02 ± 0.002***
%fast	66 ± 2	54 ± 4

<sup>a</sup>Values are means ± SEM of at least three independent experiments performed in duplicate. Unpaired *t*-test analysis with Welch's correction was performed to analyze differences in kinetic rates between receptors, with differences noted as \*, *p* < 0.05; \*\*, *p* < 0.01; \*\*\*, *p* < 0.001. <sup>b</sup>Values obtained from homologous displacement of 3, 6 and 12 nM [<sup>3</sup>H]-CCR2-RA-[R] from U2OS-CCR1 at 25°C. <sup>c</sup>Values obtained from saturation binding of 0.05 – 70 nM [<sup>3</sup>H]-CCR2-RA-[R] to U2OS-CCR2 at 25°C. <sup>d</sup>Observed association and <sup>e</sup>dissociation rate constants of [<sup>3</sup>H]-CCR2-RA-[R] in U2OS-CCR1 or -CCR2 at 25°C.

**Table S2. Inhibition of basal [<sup>35</sup>S]GTPγS binding, i.e. in the absence of agonist CCL3, by compounds 37, 39, 41 and 43 in U2OS-CCR1.**

Compound	$pIC_{50} \pm SEM$ ( $IC_{50}$ , μM) <sup>a</sup>	Hill slope <sup>a</sup>
39	6.78 ± 0.04 (0.17)**	-0.4 ± 0.06*
41	6.70 ± 0.08 (0.21)**	-0.6 ± 0.05
43	6.13 ± 0.15 (0.85)	-0.4 ± 0.07*
45	5.17 ± 0.01 (6.73)	-0.5 ± 0.07*

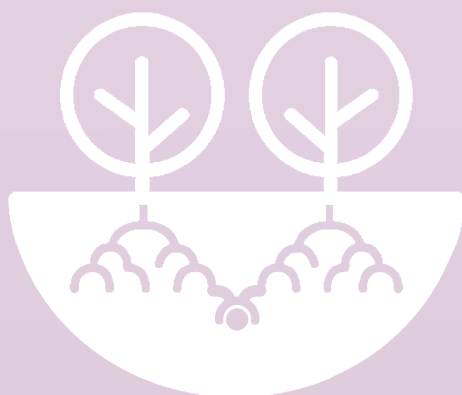
<sup>a</sup>All values are means ± SEM of at least three independent experiments performed in duplicate. Unpaired *t*-test analysis with Welch's correction was performed to analyze differences in their inhibitory potencies and pseudo-Hill slopes as antagonists and inverse agonists in CCR1, with differences noted as \*, *p* < 0.05; and \*\*, *p* < 0.01.



## Chapter 5

---

# Synthesis and pharmacological evaluation of triazolo-pyrimidinone derivatives as noncompetitive, intracellular antagonists for CCR2/5 chemokine receptors



*Natalia V. Ortiz Zacarías, Jacobus P. D. van Veldhoven, Lisa S. den Hollander, Burak Dogan, Joseph Openy, Ya-Yun Hsiao, Eelke B. Lensenlink, Laura H. Heitman and Adriaan P. IJzerman*

*Manuscript submitted*




## ABSTRACT

Both CC Chemokines receptors 2 (CCR2) and 5 (CCR5) are involved in a variety of inflammatory and immunological diseases; however, with the exception of maraviroc, clinical trials with selective CCR2 and CCR5 antagonists have been unsuccessful. Preclinical and clinical evidence suggests that dual CCR2/CCR5 inhibition might represent a more effective strategy for the treatment of multifactorial diseases. In this regard, the high conservation of a recently discovered intracellular binding site in chemokine receptors provides a potential new avenue for the design of multitarget allosteric modulators. In this study, we synthesized and evaluated the biological activity of a series of triazolo-pyrimidinone derivatives, previously reported as CCR2 antagonists. By performing radioligand binding assays, we first confirmed that these compounds bind to the intracellular site of CCR2 with high affinity. In addition, functional assays were used to evaluate their activity on CCR5, allowing us to explore structure-affinity/activity relationships in both receptors, and thus to gain understanding of the structural requirements to modulate selectivity. Overall, triazolo-pyrimidinone derivatives were mostly selective towards CCR2; however compounds **39** and **43** were able to inhibit CCL3-induced  $\beta$ -arrestin recruitment in CCR5 with approximately 100 nM potency. Finally, these compounds displayed an insurmountable mechanism of inhibition in both receptors, which holds promise for improved efficacy in inflammatory diseases characterized by elevated levels of endogenous chemokines.

## INTRODUCTION

CC Chemokine receptors 2 (CCR2) and 5 (CCR5) are two membrane-bound G protein-coupled receptors (GPCRs), which belong to the subfamily of chemokine receptors. Chemokine receptors are widely expressed in leukocytes, and thus, they regulate different homeostatic and inflammatory leukocyte functions upon interaction with their endogenous chemokines.<sup>1</sup> <sup>2</sup> In general, chemokine receptors interact with multiple endogenous chemokines, such as CCL2, CCL7 and CCL8 in the case of CCR2, and CCL3, CCL4 and CCL5 in the case of CCR5.<sup>1</sup> Furthermore, most chemokines can interact with multiple chemokine receptors, allowing for a very complex and fine-tuned system.<sup>3,4</sup> Dysregulation of this system has been linked to the development of several pathophysiological conditions. For example, both CCR2 and CCR5 have been implicated in many inflammatory and immune diseases such as rheumatoid arthritis, multiple sclerosis, atherosclerosis, diabetes mellitus and psoriasis,<sup>5,6</sup> rendering these proteins attractive targets for the pharmaceutical industry. As a result, many efforts have been made to bring CCR2 and CCR5 small-molecule antagonists into the clinic, although with limited success. Only maraviroc, an HIV-1 entry inhibitor selectively targeting CCR5, has been approved by the FDA and EMA,<sup>7</sup> while all other drug candidates have failed in clinical trials.

Recently, it has been suggested that the development of multitarget drugs—designed to interact with multiple receptors—represents a more effective approach in the treatment of complex multifactorial diseases.<sup>8,9</sup> Thus, dual targeting of CCR2 and CCR5 emerges as a potentially more efficacious strategy in diseases where both receptors are involved. Indeed, combined CCR2/CCR5 inhibition has resulted in beneficial effects in several preclinical disease models and clinical studies, further supporting the use of dual antagonists.<sup>10,11</sup> In this regard, several antagonists with dual CCR2/CCR5 activity have been reported in the last years, including the first dual antagonist TAK-779 and the clinical candidate cenicriviroc.<sup>12</sup> All of these antagonists bind to the extracellular region of CCR2 and CCR5, in a site overlapping with the chemokine's binding pocket.<sup>13</sup> Yet, the crystal structures of CCR2 (**Chapter 3**) and CCR9 have demonstrated that chemokine receptors can also be targeted with intracellular allosteric modulators.<sup>14,15</sup> These intracellular ligands offer a number of advantages, such as noncompetitive binding and, as a consequence, insurmountable inhibition; which is particularly important due to the high local concentration of chemokines during pathological conditions (**Chapter 2**).<sup>16,17</sup> In addition, the high conservation of this intracellular site allows for the design of multitarget antagonists (**Chapters 2 and 4**).<sup>17,18</sup> Several high-affinity intracellular ligands have been already identified for CCR2,<sup>19,20</sup> but not for CCR5; although intracellular compounds developed for CCR2 or CCR4 have been reported to bind CCR5 with much lower potency.<sup>20,21</sup>



In the current study we first report that previously patented CCR2 antagonists with a triazolo-pyrimidinone scaffold, such as compound **8** (Figure 1),<sup>22</sup> bind to the intracellular site of the receptor with high affinity. In addition, we show that this compound is able to inhibit CCR5 with moderate activity, suggesting a potential dual CCR2/CCR5 activity for this class of compounds. Thus, a series of novel and previously reported triazolo-pyrimidinone derivatives were synthesized according to published methods<sup>22</sup> in order to obtain structure-affinity/activity relationships (SAR) in both CCR2 and CCR5. Radioligand binding assays and functional assays were used to evaluate their affinity towards CCR2 and activity towards CCR5. In addition, characterization of two selected compounds (**39** and **43**) in a [<sup>35</sup>S]GTPγS binding assay demonstrated that these compounds inhibit both receptors in a noncompetitive, insurmountable manner. Finally, compound **43** was docked into the CCR2 crystal structure in order to shed light on the binding mode of these derivatives, in comparison to that of the crystalized CCR2-RA-[R] (**Chapter 3**).<sup>14</sup> In summary, our findings provide some insight on the CCR2/CCR5 selectivity profile of triazolo-pyrimidinone derivatives, as well as on the structural requirements for the design of multitarget or selective intracellular ligands for these receptors.

## RESULTS AND DISCUSSION

### Chemistry

Triazolo-pyrimidinone derivatives **6** - **43** were synthesized using a three-step synthesis approach as described by Bengtsson *et al.*<sup>22</sup> (Scheme 1). First, if not commercially available, the  $\beta$ -keto esters **1a-n** were synthesized from ethyl acetoacetate **1a** and the respective bromo or iodo alkanes **2f-h,j,k** or benzylbromide **2n**. Benzylation of the  $\beta$ -keto esters **1a-n** with the corresponding R<sup>1</sup>-substituted benzylbromides (**3a-v**), at reflux, resulted in a series of benzylated  $\beta$ -keto esters **4aa-na**, **4bb-bq**, **4eq-ev** in yields between 8% and 97% (Scheme 1, Table S1). Finally a cyclisation reaction of the benzylated  $\beta$ -keto esters **4aa-na**, **4bb-bq**, **4eq-ev** with the commercially available 3,5-diamino triazole **5c** in ionic liquid BMIM-PF<sub>6</sub> (1-butyl-3-methylimidazolium hexafluorophosphate) at 200°C under microwave irradiation resulted in final compounds **6**, **9-43** in yields ranging from 4% to 83%. However final compound **7** (R<sup>2</sup> = H) was synthesized using H<sub>3</sub>PO<sub>4</sub> in ethanol conditions and **8** (R<sup>2</sup> = Me) in *p*-toluenesulfonic acid monohydrate conditions.

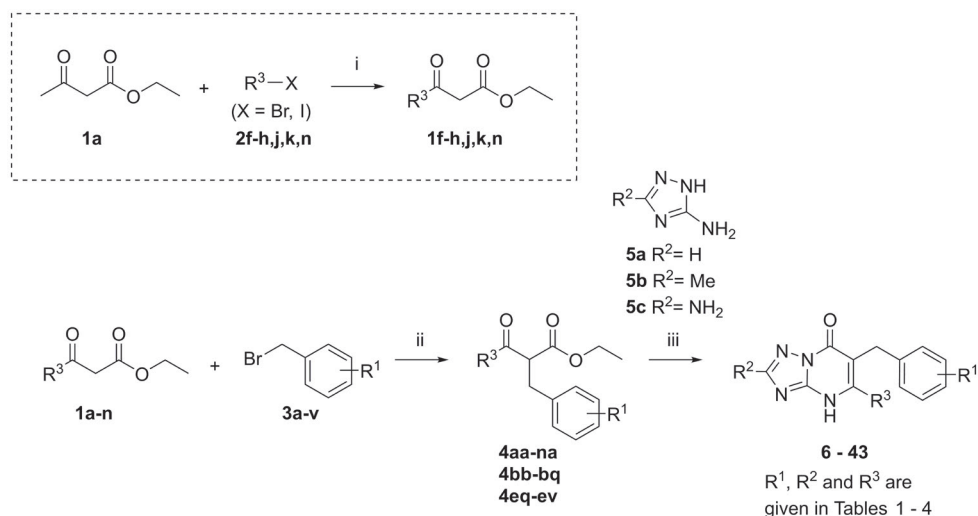
### Biology

We have previously identified several CCR2 intracellular ligands belonging to different chemical scaffolds, such as CCR2-RA-[R], SD-24 and JNJ-27141491 (Figure 1).<sup>19,20</sup> In contrast to CCR2 orthosteric ligands, these intracellular ligands lack a basic nitrogen, have lower molecular weights, unsaturated systems with haloarenes and acidic groups capable of forming hydrogen bonds.<sup>17,19</sup> Other CCR2 antagonists with similar features have been described in literature, including the triazolo- or pyrazolo-pyrimidinone derivatives described in two different patents.<sup>22,23</sup> To test whether they also bind to the intracellular site of the receptor, we synthesized “example 1” from the patent by Bengtsson *et al.*,<sup>22</sup> corresponding to the triazolo-pyrimidinone derivative **8** in our study (Figure 1). Using a [<sup>3</sup>H]-CCR2-RA-[R] binding assay as previously described,<sup>18</sup> we found that compound **8** fully displaced [<sup>3</sup>H]-CCR2-RA-[R] binding from U2OS cells stably expressing hCCR2b (U2OS-CCR2) with high affinity and a pseudo-Hill slope ( $n_H$ ) close to unity, indicating a competitive interaction with [<sup>3</sup>H]-CCR2-RA-[R] for the intracellular binding site. **8** displaced [<sup>3</sup>H]-CCR2-RA-[R] with a pK<sub>i</sub> of 8.90 ± 0.04 (K<sub>i</sub> = 1.3 nM, Figure 2a and Table 1), consistent with its previously reported activity in a CCR2 calcium flux assay (IC<sub>50</sub> = 16 nM).<sup>22</sup>

Previous studies have shown that some of these intracellular ligands are able to bind and inhibit multiple chemokine receptors, enabling the design of selective and multitarget

inhibitors.<sup>18, 20, 21</sup> In this regard, CCR5 is the closest homolog to CCR2, with > 90% sequence similarity of their intracellular binding pockets. From the main interactions of CCR2-RA-[R] to CCR2, only Val244<sup>6x36</sup> is exchanged to Leu236<sup>6x36</sup> in CCR5<sup>14</sup> (residues named according to structure-based Ballesteros—Weinstein nomenclature<sup>24</sup>). Thus, we investigated whether compound **8** is also able to inhibit the highly homologous CCR5. However, the much lower affinity of [<sup>3</sup>H]-CCR2-RA-[R] for CCR5 compared to CCR2 hindered us from performing radioligand binding assays;<sup>20</sup> thus, we assessed the CCR5 activity of **8** with a functional  $\beta$ -arrestin recruitment assay after stimulation with CCL3, one of the endogenous agonists of CCR5. For this assay, we also included the intracellular ligands CCR2-RA-[R], SD-24 and JNJ-27141491, as well as the CCR2/CCR5 orthosteric antagonist TAK-779 as a positive control (Figure 1), since it is a potent CCR5 antagonist in a variety of functional assays.<sup>25, 26</sup>

### Scheme 1. Synthesis scheme of the triazolo-pyrimidinone derivatives **6 – 43**<sup>a</sup>



<b>1a</b> $R^3 = Me$	<b>1h</b> $R^3 = Pent$	<b>3a</b> $R^1 = 3-Cl$	<b>3l</b> $R^1 = 4-Me$	<b>4aa</b> $R^3 = Me, R^1 = 3-Cl$
<b>1b</b> $R^3 = cPr$	<b>1i</b> $R^3 = cPent$	<b>3b</b> $R^1 = H$	<b>3m</b> $R^1 = 4-F$	<b>4ba</b> $R^3 = cPr, R^1 = 3-Cl$
<b>1c</b> $R^3 = Et$	<b>1j</b> $R^3 = Hex$	<b>3c</b> $R^1 = 2-Me$	<b>3n</b> $R^1 = 4-Cl$	...
<b>1d</b> $R^3 = Pr$	<b>1k</b> $R^3 = Hept$	<b>3d</b> $R^1 = 2-Cl$	<b>3o</b> $R^1 = 4-Br$	Full list in Table S1
<b>1e</b> $R^3 = iPr$	<b>1l</b> $R^3 = Ph$	<b>3e</b> $R^1 = 2-OMe$	<b>3p</b> $R^1 = 4-OMe$	
<b>1f</b> $R^3 = Bu$	<b>1m</b> $R^3 = 4-MePh$	<b>3f</b> $R^1 = 3-Me$	<b>3q</b> $R^1 = 3,4-diCl$	
<b>1g</b> $R^3 = 2-EtBu$	<b>1n</b> $R^3 = CH_2CH_2Ph$	<b>3g</b> $R^1 = 3-F$	<b>3r</b> $R^1 = 2,3-diCl$	
		<b>3h</b> $R^1 = 3-Br$	<b>3s</b> $R^1 = 2,5-diCl$	
		<b>3i</b> $R^1 = 3-I$	<b>3t</b> $R^1 = 3,5-diCl$	
		<b>3j</b> $R^1 = 3-OMe$	<b>3u</b> $R^1 = 3,5-diBr$	
		<b>3k</b> $R^1 = 3-CF_3$	<b>3v</b> $R^1 = 3-Br, 4-Cl$	

<sup>a</sup>Reagents and conditions: (i) NaH, n-BuLi, THF, overnight, 0°C to rt (**1a-e,i,l,m** were commercially available); (ii) DIPEA, LiCl, THF, reflux, overnight; (iii) (**8-43**,  $R^2 = NH_2$ ) BMIM-PF<sub>6</sub>, 200°C, 1h or (**6**,  $R^2 = H$ ) H<sub>3</sub>PO<sub>4</sub>, EtOH, 170°C, 10h or (**7**,  $R^2 = Me$ ) p-toluenesulfonic acid monohydrate, 180°C, 30 min.



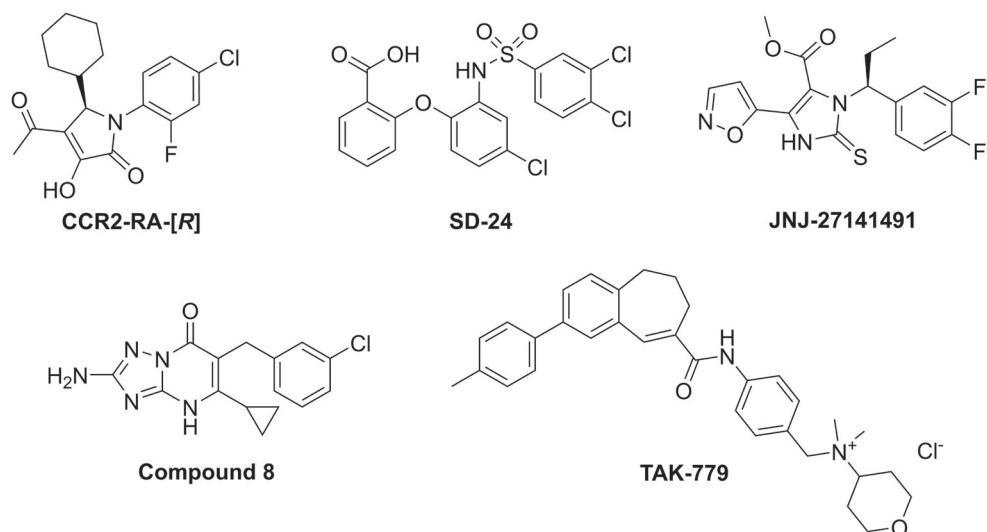


**Figure 1.** Chemical structures of the orthosteric CCR2/CCR5 antagonist TAK-779 and the CCR2 intracellular ligands CCR2-RA-[R], SD-24, JNJ-27141491 and the triazolo-pyrimidinone derivative **8**. [ $^3\text{H}$ ]-CCR2-RA-[R] was used in radioligand binding assays for CCR2.

In this assay, CCL3 induced  $\beta$ -arrestin recruitment to U2OS cells stably expressing hCCR5 (U2OS-CCR5) with a  $p\text{EC}_{50}$  of  $8.3 \pm 0.08$  (6 nM) (Figure S1a), similar to values reported in literature.<sup>27</sup> As expected, TAK-779 was able to completely inhibit  $\beta$ -arrestin recruitment induced by an  $\text{EC}_{80}$  concentration of CCL3 ( $p\text{EC}_{80} = 7.9 \pm 0.08$ ), when tested at a single concentration of  $1 \mu\text{M}$  (Figure S1b). In contrast, none of the intracellular ligands was able to fully inhibit CCL3-induced  $\beta$ -arrestin recruitment to the same level as TAK-779; in fact, only compound **8** displayed more than 70% inhibition when tested at  $1 \mu\text{M}$  (Figure S1b), while CCR2-RA-[R], SD-24 and JNJ-27141491 led to approximately 50% inhibition or less at the same concentration of  $1 \mu\text{M}$  (Figure S1b). Consistent with this low inhibition in CCR5, it was previously shown that CCR2-RA-[R], JNJ-27141491 and SD-24 inhibited inositol phosphate (IP) formation in CCR5 with 7 to 22-fold lower potency compared to CCR2 inhibition, respectively.<sup>20</sup> Preincubation of U2OS-CCR5 cells with increasing concentrations of TAK-779, before exposure to CCL3, resulted in an inhibitory potency ( $\text{IC}_{50}$ ) of 6 nM, consistent with previously reported values (Table S2).<sup>26</sup> Also in agreement with a previous study,<sup>20</sup> the reference intracellular ligand CCR2-RA-[R] inhibited CCL3-induced  $\beta$ -arrestin recruitment with an  $\text{IC}_{50}$  value of 703 nM (Table S2). Moreover, while TAK-779 inhibited CCL3-induced  $\beta$ -arrestin recruitment with a pseudo-Hill slope close to unity ( $n_{\text{H}} = -1.1$ ), while CCR2-RA-[R] inhibition showed a significantly higher Hill slope ( $n_{\text{H}} = -2.4$ ), indicative of two different binding sites for CCL3 and CCR2-RA-[R] (Table S2).<sup>28</sup>

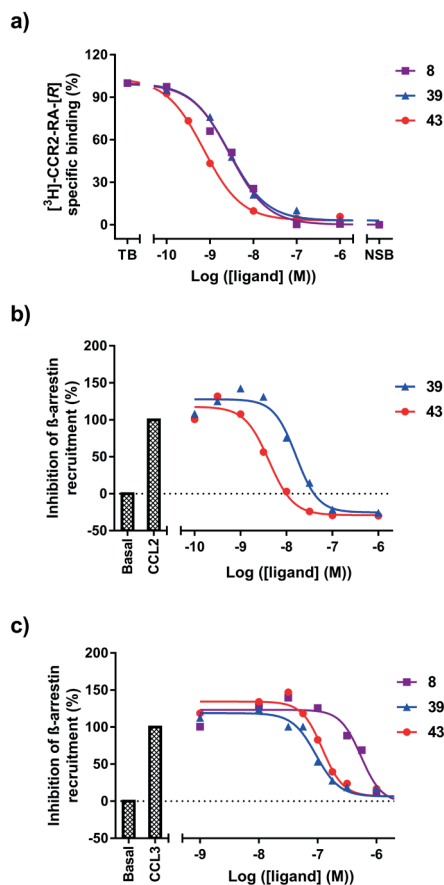


**Figure 2. Characterization of ligands in U2OS-CCR2 and U2OS-CCR5.** (a)  $[^3\text{H}]\text{-CCR2-RA-[R]}$  displacement by increasing concentrations of triazolo-pyrimidinone derivatives **8**, **39** and **43** in U2OS-CCR2 at 25°C. Data are normalized to specific binding in the absence of compound (set as 100%). (b) Inhibition of CCL2-stimulated  $\beta$ -arrestin recruitment in U2OS-CCR2 by increasing concentrations of compounds **39** and **43**, after stimulation with an  $\text{EC}_{80}$  concentration of CCL2 (set as 100%). (c) Inhibition of CCL3-stimulated  $\beta$ -arrestin recruitment in U2OS-CCR5 by increasing concentrations of compounds **8**, **39** and **43**, after stimulation with an  $\text{EC}_{80}$  concentration of CCL3 (set as 100%). All data are from single, representative experiments performed in duplicate.

As compound **8** was the best CCR5 inhibitor in this assay, displaying an  $\text{IC}_{50}$  value of 571 nM and a Hill slope of  $-2.2 \pm 0.3$  (Figure 2c and Table 1), we then synthesized several triazolo-pyrimidinone derivatives to explore their structure-affinity/activity relationships (SAR) in CCR2 and CCR5. All synthesized triazolo-pyrimidinone derivatives were evaluated in  $[^3\text{H}]\text{-CCR2-RA-[R]}$  binding assays to determine their binding affinity for CCR2, and in  $\beta$ -arrestin recruitment assays to determine their activity towards CCR5 (Figure 2 and Tables 1 – 3).

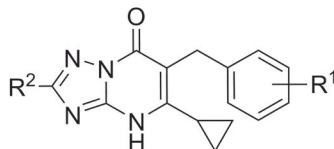
In CCR5, compounds were first screened at a concentration of 1  $\mu$ M, and only those that displayed > 70% inhibition at this concentration were further evaluated in a concentration-inhibition curve to determine their potency. For better comparison, two compounds (**39** and **43**) were also tested in a CCR2  $\beta$ -arrestin recruitment assay as previously described (Figure 2b).<sup>19</sup> Finally, we determined the mechanism of inhibition of **39** and **43** in both CCR2 and CCR5 using a [<sup>35</sup>S]GTP $\gamma$ S binding assay (Figure 3, Table 4).

## Structure-affinity/activity relationships (SAR) in CCR2 and CCR5

Analysis of the triazolo-pyrimidinone derivatives started by modifying the amino group ( $R^2$ ) of the triazolo moiety ( $R^2$ , Table 1). Compared to **8**, removing the amino group (**6**) resulted in a similar affinity towards CCR2, in agreement with the similar reported  $IC_{50}$  values of approximately 20 nM for both compounds, when tested in a calcium flux assay.<sup>22</sup> However, in CCR5 **6** displayed a lower potency, as the inhibition of CCL3-stimulated recruitment of  $\beta$ -arrestin decreased to 60%, compared to 76% inhibition by **8**. The introduction of a methyl group in  $R^2$  (**7**) was less favourable for both receptors, as both affinity for CCR2 and activity to CCR5 were reduced compared to **8**. As compound **8** displayed the highest affinity/activity for both receptors, we decided to keep the amino group in  $R^2$  and explore different phenyl substituents ( $R^1$ , Table 1), taking **8** as the starting point.

Compared to **8**, the unsubstituted **9** showed a 5-fold decrease in affinity towards CCR2, while in CCR5 it was only able to inhibit 35% of the receptor response at 1  $\mu$ M. Next, we investigated the effect of several benzyl modifications, including the influence of different substituent positions (Table 1). In the case of CCR2, meta-substituted derivatives also yielded the highest affinities in this series of compounds (**13** – **18**), whereas ortho-substituted derivatives yielded the lowest (**10** – **12**). None of the ortho-substitutions led to an improvement in affinity over **8** or the unsubstituted **9**. Introduction of a methyl (**10**) or a chloro (**11**) group in this position resulted in affinities lower than 10 nM, while the introduction of an electron-donating methoxy group further reduced the affinity to 105 nM (**12**), displaying the lowest CCR2 affinity in this series (Table 1). Moving the methyl group to meta (**13**) or para (**19**) position slightly improved the CCR2 binding affinity compared to **9**, achieving the highest affinity in meta position (**19**, 3 nM). Similarly, moving the methoxy group to meta or para position resulted in improved affinities following the meta > para > ortho order; however, the affinities remained lower than 10 nM (**17**, 13nM; **23**, 21 nM), with no improvement over **9**. This is consistent with functional data reported in the patent by Bengtsson *et al.*, where similar compounds with a methoxybenzyl moiety displayed a loss of CCR2 activity compared to the unsubstituted-phenyl analogue.<sup>22</sup> Substitution of the meta methoxy group by an electron-withdrawing  $CF_3$  group resulted in improved affinity over **17** (**18**, 6 nM), but no improvement over the unsubstituted **9**.

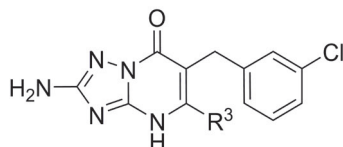
**Table 1. Characterization of compounds 6 – 23 in hCCR2 and hCCR5**



Compound	R <sup>1</sup>	R <sup>2</sup>	hCCR2	hCCR5
			pK <sub>i</sub> ± SEM (K <sub>i</sub> , nM) <sup>a</sup>	pIC <sub>50</sub> ± SEM (IC <sub>50</sub> , nM) or inhibition at 1 μM (%) <sup>b</sup>
<b>6</b>	3-Cl	H	8.76 ± 0.01 (1.7)	60%
<b>7</b>	3-Cl	Me	8.46 ± 0.05 (3.5)	35%
<b>8</b>	3-Cl	NH <sub>2</sub>	8.90 ± 0.04 (1.3)	6.24 ± 0.004 (571)
<b>9</b>	H	NH <sub>2</sub>	8.27 ± 0.10 (5.9)	35%
<b>10</b>	2-Me	NH <sub>2</sub>	7.81 ± 0.05 (15.7)	28%
<b>11</b>	2-Cl	NH <sub>2</sub>	7.84 ± 0.03 (14.5)	27%
<b>12</b>	2-OMe	NH <sub>2</sub>	6.98 ± 0.04 (104.6)	-20% <sup>c</sup>
<b>13</b>	3-Me	NH <sub>2</sub>	8.61 ± 0.03 (2.5)	62%
<b>14</b>	3-F	NH <sub>2</sub>	8.53 ± 0.18 (3.4)	43%
<b>15</b>	3-Br	NH <sub>2</sub>	9.08 ± 0.06 (0.9)	60%
<b>16</b>	3-I	NH <sub>2</sub>	9.06 ± 0.02 (0.9)	66%
<b>17</b>	3-OMe	NH <sub>2</sub>	7.89 ± 0.07 (13.0)	-27% <sup>c</sup>
<b>18</b>	3-CF <sub>3</sub>	NH <sub>2</sub>	8.26 ± 0.09 (5.9)	36%
<b>19</b>	4-Me	NH <sub>2</sub>	8.46 ± 0.03 (3.5)	-57% <sup>c</sup>
<b>20</b>	4-F	NH <sub>2</sub>	8.39 ± 0.03 (4.1)	31%
<b>21</b>	4-Cl	NH <sub>2</sub>	8.74 ± 0.05 (1.8)	31%
<b>22</b>	4-Br	NH <sub>2</sub>	8.84 ± 0.02 (1.5)	14%
<b>23</b>	4-OMe	NH <sub>2</sub>	7.68 ± 0.05 (20.9)	-28%

Data are presented as mean pK<sub>i</sub>/pIC<sub>50</sub> ± standard error of the mean (SEM) and mean K<sub>i</sub>/IC<sub>50</sub> (nM) of at least three independent experiments performed in duplicate. <sup>a</sup>pK<sub>i</sub> values from the displacement of ~6 nM [<sup>3</sup>H]-CCR2-RA-[R] from U2OS cells stably expressing CCR2, at 25°C. <sup>b</sup>Percent inhibition of β-arrestin recruitment in U2OS cells stably expressing CCR5 by 1 μM compound, in presence of CCL3 (pEC<sub>80</sub> = 7.9). pIC<sub>50</sub> values were determined for compounds displaying more than 70% inhibition. % Inhibition values are presented as means of at least two independent experiments, performed in duplicate. <sup>c</sup>No inhibition was observed at the concentration of 1 μM, instead some CCL3 stimulation was measured.

**Table 2. Characterization of compounds 24 – 36 in hCCR2 and hCCR5**



Compound	R <sup>3</sup>	hCCR2	hCCR5
		pK <sub>i</sub> ± SEM (K <sub>i</sub> , nM) <sup>a</sup>	pIC <sub>50</sub> ± SEM (IC <sub>50</sub> , nM) or inhibition at 1 μM (%) <sup>b</sup>
<b>8</b>	<i>c</i> Pr	8.90 ± 0.04 (1.3)	6.24 ± 0.004 (571)
<b>24</b>	Me	7.78 ± 0.07 (17.2)	-35%
<b>25</b>	Et	8.40 ± 0.07 (4.0)	29%
<b>26</b>	Pr	8.46 ± 0.07 (3.6)	64%
<b>27</b>	<i>i</i> Pr	8.72 ± 0.05 (1.9)	6.56 ± 0.05 (281)
<b>28</b>	Bu	8.64 ± 0.03 (2.3)	6.29 ± 0.05 (519)
<b>29</b>	2-EtBu	8.20 ± 0.04 (6.4)	29%
<b>30</b>	Pent	8.14 ± 0.03 (7.2)	38%
<b>31</b>	<i>c</i> Pent	8.81 ± 0.04 (1.6)	6.43 ± 0.08 (388)
<b>32</b>	Hex	7.66 ± 0.02 (22.0)	-63% <sup>c</sup>
<b>33</b>	Hept	6.76 ± 0.05 (178.1)	-265% <sup>c</sup>
<b>34</b>	Ph	7.64 ± 0.17 (26.7)	-41% <sup>c</sup>
<b>35</b>	4-MePh	6.81 ± 0.07 (158.8)	-13% <sup>c</sup>
<b>36</b>	CH <sub>2</sub> CH <sub>2</sub> Ph	7.29 ± 0.05 (52.3)	-42% <sup>c</sup>

Data are presented as mean pK<sub>i</sub>/pIC<sub>50</sub> ± standard error of the mean (SEM) and mean K<sub>i</sub>/IC<sub>50</sub> (nM) of at least three independent experiments performed in duplicate. <sup>a</sup>pK<sub>i</sub> values from the displacement of ~6 nM [<sup>3</sup>H]-CCR2-RA-[R] from U2OS cells stably expressing CCR2, at 25°C. <sup>b</sup>Percent inhibition of β-arrestin recruitment in U2OS cells stably expressing CCR5 by 1 μM compound, in presence of CCL3 (pEC<sub>80</sub> = 7.9). pIC<sub>50</sub> values were determined for compounds displaying more than 70% inhibition. % Inhibition values are presented as means of at least two independent experiments, performed in duplicate. <sup>c</sup>No inhibition was observed at the concentration of 1 μM, instead some CCL3 stimulation was measured.

The effect of introducing different halogen groups was first investigated in meta position. Overall, an increase in size and lipophilicity from fluoro to iodo resulted in improved binding affinities towards CCR2 (F, **14** < Cl, **8** < Br, **15** ≈ I, **16**). In fact, compounds **15** and **16** displayed the highest affinities in this series of derivatives (**15**, 0.8 nM; **16**, 0.9 nM). Moving the halogen substituents to the para position resulted in a similar trend in affinity (F, **20** < Cl, **21** < Br, **22**); however, their affinities were lower compared to the meta-substituted analogues. Of note, compounds with a fluorine atom in meta (**14**) or para (**20**) position displayed lower affinities than compounds with a methyl group in the equivalent position

(**13** and **19**). To gain more insight in a potential relationship between affinity and lipophilicity as observed in the halogen series, calculated log P values (cLogP) of compounds **8** – **23**, with R<sup>1</sup> modifications, were plotted against their pK<sub>i</sub> values in CCR2. This analysis revealed only a slight correlation between these two parameters for this set of compounds (Fig S2a); however, this correlation was lost when all synthesized derivatives were included in this plot (Fig S2b), indicating that this is not a general trend.

In the case of CCR5, meta-substituted derivatives also outperformed their ortho- and para-substituted analogues, with some compound displaying > 60% inhibition at 1 μM; in contrast, ortho- and para-substitution resulted in compounds with low (≤ 31%) to marginal efficacy in CCR5, suggesting that substituents in ortho or para position are not tolerated in CCR5. Similarly as in CCR2, the introduction of a methoxy group was unfavourable, as it led to a complete loss of activity in CCR5 when tested at 1 μM (**12**, **17** and **23**), regardless of the position; whereas electron-withdrawing groups in meta position (**18**, R<sup>2</sup> = CF<sub>3</sub>) did not bring any improvement over the unsubstituted **9**. Except for compound **14** bearing a meta-fluoro, which showed less than 45% inhibition, all other compounds bearing halogens in meta position led to > 60% inhibition; the same was achieved when a methyl group was placed in this position (**13**). Overall, these data indicate that meta-substituents, especially halogens, are preferred to achieve dual CCR2/CCR5 activity, while ortho- and para-substituents lead to a lower affinity but higher selectivity towards CCR2.

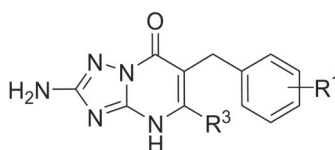
As none of the other substituents in R<sup>2</sup> led to a significant improvement in CCR5 activity over compound **8**, we decided to continue with this compound and investigate the effect of replacing the cyclopropyl moiety in R<sup>3</sup>. Based on the chemical structure of **8** and CCR2-RA-[R] (Figure 1), we hypothesized that the cyclopropyl group in **8** interacts with Val244<sup>6x36</sup> in CCR2, in a similar manner as the cyclohexyl group of CCR2-RA-[R].<sup>14</sup> Thus, several triazolopyrimidinone derivatives were synthesized with different alkyl chains and aromatic groups in this position, in order to investigate their SAR (Table 2). Starting with the effect of alkyl substituents, we observed that increasing the size and flexibility of the alkyl chain from n = 1 (methyl) to n = 4 (butyl) resulted in a parallel increase in CCR2 affinity (17 nM for R<sup>3</sup> = Me (**24**); ~4 nM for R<sup>3</sup> = Et (**25**) and R<sup>3</sup> = Pr (**26**); 2 nM for R<sup>3</sup> = Bu (**28**)). However, further elongation of the chain length (n = 5 – 7) led to a progressive drop in affinity (7 nM for R<sup>3</sup> = Pent (**30**); 22 nM for R<sup>3</sup> = Hex (**32**); 178 nM for R<sup>3</sup> = Hept (**28**)), indicating that linear alkyl chains longer than five carbons might not fit in this hydrophobic pocket. The same trend was observed for CCR5 activity, as only the *n*-propyl (**26**) and *n*-butyl (**28**) substituted compound led to > 60% inhibition, albeit without improvement over **8** (**28**, 519 nM). Moreover, introduction of a hexyl or heptyl group resulted in CCL3 stimulation instead of inhibition, which was not further investigated. Increasing bulkiness via branching of alkyl groups or substitution with aliphatic rings enhanced the affinity towards CCR2, indicating that these substituents

might provide a better interaction with the receptor. For instance, the introduction of both isopropyl (**27**) and cyclopropyl (**8**) groups led to an improvement in CCR2 affinity compared to the linear analogue **26**. Moreover, compound **27** with an isopropyl substituent also yielded a 2-fold increase in CCR5 potency compared to the cyclic analogue **8**, displaying the highest potency in this series of compounds (**27**, 281 nM). In line with this trend, we observed that replacing the linear pentyl group (**30**) with a cyclopentyl group (**31**) was also beneficial for CCR2, as this derivative showed a 4.5-fold increased affinity compared to **30** (**31**, 1.6 nM). In CCR5, **31** inhibited the CCL3-induced response with a potency of 388 nM, showing a slight improvement over compound **8**. In contrast, the introduction of a 2-ethyl butyl group (**29**) resulted in reduced affinity/activity towards both CCR2 and CCR5. These data suggest that the isopropyl group is the preferred R<sup>3</sup> substituent when designing CCR2/CCR5 dual antagonists, as this substituent led to the highest potency in CCR5 while maintaining a high affinity for CCR2. Next, inspired by our work on CCR1/CCR2 selectivity of pyrrolone derivatives,<sup>18</sup> we investigated whether aromatic substituents are tolerated in this position. As expected from previous studies,<sup>18, 29</sup> the introduction of aromatic groups decreased 20-fold (**34**, 27 nM), 40-fold (**36**, 52 nM) and 122-fold (**35**, 159 nM) the affinity for CCR2 compared to **8**. When tested in CCR5, all derivatives showed a complete loss of activity at 1  $\mu$ M, indicating that aromatic groups are not favourable for selectivity or dual activity.

With the aim of finding dual CCR2/CCR5 intracellular inhibitors, we kept the isopropyl moiety in R<sup>3</sup> and investigated the effect of having a di-substituted phenyl moiety in R<sup>1</sup>, by exploring different positions and combinations of chlorine and bromine atoms (Table 3). First, and similar as **8**, we kept the cyclopropyl moiety in R<sup>3</sup> and combined it with di-chlorination in meta and para position (**37**). Compared to the mono-substituted analogues **8** and **21**, this compound yielded an even higher affinity to CCR2 (**37**, 0.4 nM); moreover, its ability to inhibit CCL3-induced response in CCR5 was also improved, as the potency increased to 214 nM. By replacing the cyclopropyl of **37** with an isopropyl group (**38**), we retained affinity for CCR2 (0.6 nM), but the potency for CCR5 increased by almost 2-fold (132 nM), in agreement with the higher potency observed in **27** versus **8** (Table 2). Moving one chlorine atom to ortho position, while keeping one in the adjacent meta position, yielded compound **39** with slightly lower affinity for CCR2 but even higher potency in CCR5 (**39**, 84 nM), indicating that although ortho substituents are not preferred in mono-substituted derivatives, they are still tolerated when placed in combination with halogens in other positions. However, placing the two halogens in the second and fifth position was clearly detrimental for both receptors (**40**); in CCR2, the affinity decreased by almost 40-fold, while in CCR5, the compound was only able to inhibit 20% of the CCR5 response. Placing the two halogens in the symmetrical third and fifth positions restored the affinity/activity in both receptors (**41**, 2.2 nM in CCR2 and 336 nM in CCR5). Replacing the two chlorine atoms of **41** by bromine atoms yielded derivative **42**, which retained affinity towards CCR2 but led to decrease in CCR5 activity,

as this compound was not able to inhibit > 70% of the CCL3-induced response. Finally, the combination of a bromo in meta position with a chloro in para position (**42**) improved both the affinity and activity to both receptors to similar levels as **37**, in the case of CCR2, and **38** in the case of CCR5, indicating that halogens in adjacent positions are more favourable for activity in these receptors. Of note, compounds **37**, **38** and **43** displayed the highest affinities to CCR2 in this study, while **38**, **39** and **43** displayed the highest potencies to CCR5.

**Table 3. Characterization of compounds 37 – 43 in hCCR2 and hCCR5**



Compound	R <sup>1</sup>	R <sup>3</sup>	hCCR2	hCCR5
			pK <sub>i</sub> ± SEM (K <sub>r</sub> , nM) <sup>a</sup>	pIC <sub>50</sub> ± SEM (IC <sub>50</sub> , nM) or inhibition at 1 μM (%) <sup>b</sup>
<b>37</b>	3,4-diCl	<i>c</i> Pr	9.35 ± 0.05 (0.4)	6.67 ± 0.03 (214)
<b>38</b>	3,4-diCl	<i>i</i> Pr	9.22 ± 0.05 (0.6)	6.91 ± 0.09 (132)
<b>39</b>	2,3-diCl	<i>i</i> Pr	8.81 ± 0.07 (1.6)	7.09 ± 0.07 (84)
<b>40</b>	2,5-diCl	<i>i</i> Pr	7.65 ± 0.03 (22.5)	20%
<b>41</b>	3,5-diCl	<i>i</i> Pr	8.66 ± 0.05 (2.2)	6.49 ± 0.06 (336)
<b>42</b>	3,5-diBr	<i>i</i> Pr	8.68 ± 0.01 (2.1)	64%
<b>43</b>	3-Br, 4-Cl	<i>i</i> Pr	9.42 ± 0.02 (0.4)	6.95 ± 0.04 (115)

Data are presented as mean pK<sub>i</sub>/pIC<sub>50</sub> ± standard error of the mean (SEM) and mean K<sub>r</sub>/IC<sub>50</sub> (nM) of at least three independent experiments performed in duplicate. <sup>a</sup>pK<sub>i</sub> values from the displacement of ~6 nM [<sup>3</sup>H]-CCR2-RA-[R] from U2OS cells stably expressing CCR2, at 25°C. <sup>b</sup>Percent inhibition of β-arrestin recruitment in U2OS cells stably expressing CCR5 by 1 μM compound, in presence of CCL3 (pEC<sub>80</sub> = 7.9). pIC<sub>50</sub> values were determined for compounds displaying more than 70% inhibition. % Inhibition values are presented as means of at least two independent experiments, performed in duplicate.

It is important to note that so far we are comparing data not only between two different receptors, but also between two different assays: i) a radioligand binding assay for CCR2, in the absence of agonist, which allows the determination of true affinities (pK<sub>i</sub> values); ii) a functional assay for CCR5 in the presence of an EC<sub>80</sub> concentration of CCL3, without further correction of their IC<sub>50</sub> values. To better compare the activities in both receptors, we selected compounds **39** and **43**—with the highest potency on CCR5 and the highest affinity for CCR2, respectively—and tested these in a previously described β-arrestin recruitment assay for CCR2.<sup>19</sup> In this assay, compound **39** inhibited CCL2-stimulated β-arrestin recruitment with a



potency of 21 nM, while compound **43** displayed a higher potency of 4 nM, consistent with their affinities. In addition, their Hill slopes ( $n_H = -2.5$  for **39**;  $n_H = -3.4$  for **43**) are indicative of a non-competitive form of inhibition, a further confirmation of their allosteric binding site located in the intracellular region of CCR2 (Figure 2b and Table S3). Of note, the Hill slopes in CCR5 were comparable to those in CCR2 ( $n_H = -3.7$  for **39**;  $n_H = -4.4$  for **43**), i.e. indicating an allosteric interaction at CCR5 as well. Comparing the  $IC_{50}$  values obtained with the functional assays in both receptors, we observe a 4-fold difference between CCR2 and CCR5 in the case of **39**, making it a potential dual-antagonist for both receptors. However, the potencies in CCR2 and CCR5 differ by 29-fold in the case of **43**, indicating that this compound is one of the more selective compounds towards CCR2.

## Mechanism of inhibition of selected compounds

Selected compounds **39** and **43** were also tested in a [ $^{35}$ S]GTP $\gamma$ S binding assay in both CCR2 and CCR5, in order to determine their mechanism of inhibition. In the case of CCR2, we have shown that these ligands fully displace radiolabelled [ $^3$ H]-CCR2-RA-[R], indicating that triazolo-pyrimidinone derivatives bind in the same intracellular binding site. Thus, these compounds were expected to show non-competitive, insurmountable antagonism to (orthosteric) chemokine ligands, as previously demonstrated in CCR2 with CCR2-RA-[R]<sup>19</sup> and JNJ-27141491<sup>30</sup>. To verify this, **39** and **43** were characterized in a previously described [ $^{35}$ S]GTP $\gamma$ S binding assay on U2OS-CCR2 membranes.<sup>19</sup> In this assay, CCL2-stimulation of [ $^{35}$ S]GTP $\gamma$ S binding in CCR2 was examined in the absence or presence of fixed concentrations of **39** and **43** (Table 4 and Figure 3a,b). In the absence of antagonist, increasing concentrations of CCL2 induced [ $^{35}$ S]GTP $\gamma$ S binding with an  $EC_{50}$  of 8 nM, in line with previously described parameters.<sup>18,19</sup> Co-incubation of CCL2 with **39** or **43** caused a significant reduction in the maximal response of CCL2 ( $E_{max}$ ) at all three antagonist concentrations tested. The lowest concentrations of antagonist did not affect the potency of CCL2, while higher concentrations significantly reduced the potency of CCL2 (Table 4 and Figures 3a,b).

To confirm our hypothesis that these two compounds also bind to an allosteric site in CCR5, i.e. the intracellular binding site, we next analysed the effect of **39** and **43** on CCL3-induced [ $^{35}$ S]GTP $\gamma$ S binding in U2OS-CCR5 membranes. In agreement with previous studies, CCL3 stimulated [ $^{35}$ S]GTP $\gamma$ S binding in CCR5 with a potency of 4 nM.<sup>27</sup> Similarly as in CCR2, the two compounds were able to significantly suppress the maximal response induced by CCL3 at all concentrations tested (Table 4 and Figures 3c,d). However, in contrast to CCR2, the potency of CCL3 was only significantly reduced with the highest concentration of **43** (Table 4). Such depression of the maximal response with or without a decrease of agonist potency is typical of insurmountable antagonists,<sup>31</sup> indicating that **39** and **43** behave as insurmountable

antagonists at both CCR2 and CCR5. Of note, insurmountable antagonism can be generally achieved by two different mechanisms: allosteric binding or slow binding kinetics, i.e. slow equilibration, of a competitive antagonist.<sup>31</sup> However, insurmountable inhibition due to a hemi-equilibrium is only evident in pre-incubation experiments, where the receptor is pre-incubated with the antagonist before exposure to the agonist.<sup>31</sup> In contrast, allosteric binding leads to insurmountable inhibition in co-incubation experiments, as performed in this study. These data further support our hypothesis that **39** and **43** bind to an allosteric binding site in CCR5, most probably located intracellularly.

**Table 4. Effects of compounds 39 and 43 in chemokine-stimulated [<sup>35</sup>S]GTPγS binding**

Receptor	Compound	pEC <sub>50</sub> ± SEM (EC <sub>50</sub> , nM)	E <sub>max</sub> ± SEM (%) <sup>a</sup>
<b>hCCR2</b>	CCL2	8.10 ± 0.06 (8)	107 ± 2
	CCL2 + 10 nM <b>39</b>	7.89 ± 0.04 (13)	91 ± 1**
	CCL2 + 30 nM <b>39</b>	7.60 ± 0.07 (26)**	75 ± 4****
	CCL2 + 100 nM <b>39</b>	7.27 ± 0.10 (56)****	50 ± 3****
	CCL2 + 1 nM <b>43</b>	7.91 ± 0.10 (13)	72 ± 4****
	CCL2 + 3 nM <b>43</b>	7.53 ± 0.12 (32)***	51 ± 5****
	CCL2 + 10 nM <b>43</b>	6.87 ± 0.13 (148)****	33 ± 3****
<b>hCCR5</b>	CCL3	8.42 ± 0.06 (4)	108 ± 2
	CCL3 + 100 nM <b>39</b>	8.35 ± 0.09 (5)	79 ± 5****
	CCL3 + 300 nM <b>39</b>	8.14 ± 0.12 (8)	56 ± 2****
	CCL3 + 1000 nM <b>39</b>	8.14 ± 0.17 (9)	25 ± 4****
	CCL3 + 30 nM <b>43</b>	8.30 ± 0.05 (5)	81 ± 3****
	CCL3 + 100 nM <b>43</b>	8.21 ± 0.05 (6)	58 ± 1****
	CCL3 + 300 nM <b>43</b>	8.05 ± 0.06 (9)*	35 ± 2****

Data represent the mean ± standard error of the mean (SEM) of three independent experiments performed in duplicate. One-way ANOVA with Dunnett's posthoc test was used to analyze differences in pEC<sub>50</sub> and E<sub>max</sub> values against CCL2 or CCL3 controls. <sup>a</sup>Maximum effect (E<sub>max</sub>) of CCL2 or CCL3 measured in the absence or presence of fixed concentrations of compound **39** and **43** in CCR2 or CCR5, respectively.

## Docking study


To further investigate the binding mode of triazolo-pyrimidinone derivatives, compound **43** was docked into a CCR2b model based on the crystal structure of CCR2 (PDB 5T1A, **Chapter 3**).<sup>14</sup> Due to the close proximity to the intracellular binding site, several residues from the intracellular loop 3 (ICL3) had to be modelled based on the crystal structure of CCR5 (PDB

4MBS),<sup>32</sup> since they were mutated in the original CCR2 crystal structure to further stabilize the receptor. As seen in Figure 4a, **43** was predicted to adopt a similar binding pose as that of the previously co-crystallized CCR2-RA-[R].<sup>14</sup> The di-substituted phenyl group of **43** was constrained to overlap with the corresponding phenyl group of CCR2-RA-[R], since the di-substituted aromatic rings of JNJ-27141491 and SD-24 (Figure 1) were also predicted to overlay with the phenyl group of CCR2-RA-[R] in a previous study.<sup>20</sup> However, the bromine group of compound **43** is predicted to form a halogen bond with the backbone of Val<sup>1x53</sup>, which might contribute to the higher affinity of **43** versus CCR2-RA-[R] (Figure 4b). This data suggests that all intracellular ligands share similar interactions between the aromatic group and the receptor (Figure 4a), and implies that this aromatic moiety is not responsible for the differences in CCR5 activity observed between the reference ligands<sup>20</sup> (Figure S1b).

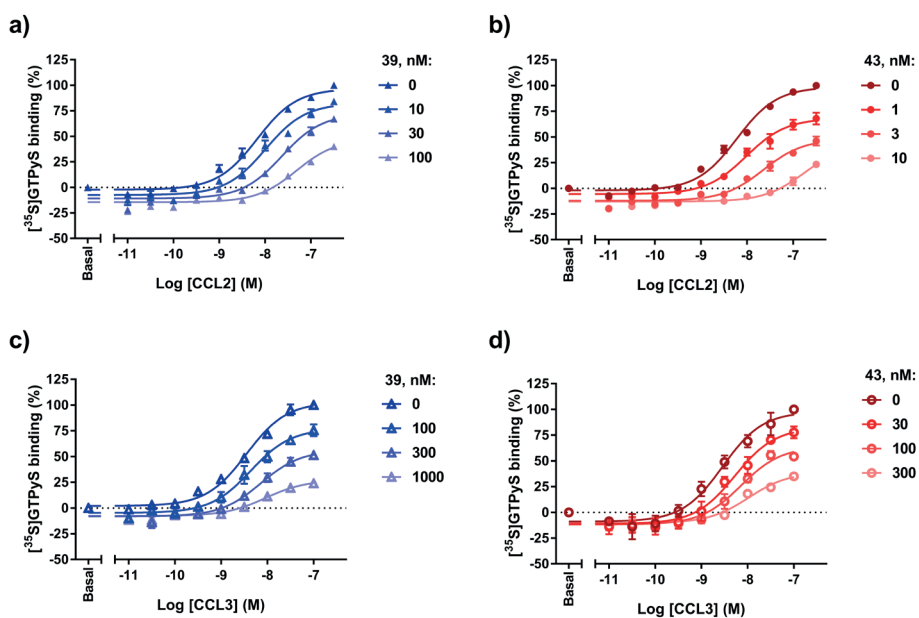


**Figure 3.** Characterization of compounds **39** and **43** as insurmountable, negative allosteric modulators using a [<sup>35</sup>S]GTP $\gamma$ S binding assay in hCCR2 and hCCR5. Effect of increasing concentrations of **39** and **43** in a CCL2-stimulated [<sup>35</sup>S]GTP $\gamma$ S binding in U2OS-CCR2 (a, b), or in a CCL3-stimulated [<sup>35</sup>S]GTP $\gamma$ S binding in U2OS-CCR5 (c, d), at 25 °C. Parameters obtained from the concentration-response curves ( $pEC_{50}$ ,  $E_{max}$ ) are summarized in Table 4. Data are presented as mean  $\pm$  SEM values of three experiments performed in duplicate.

In addition, the isopropyl group of **43** is predicted to bind in the same position as the cyclohexyl moiety of CCR2-RA-[R], although it seems to make less interactions with Val<sup>6x36</sup> perhaps due to the slightly different ligand orientation (Figure 4b). Previous studies have confirmed the crucial role of Val<sup>6x36</sup> for binding affinity of some intracellular ligands in CCR2,



as mutation of this residue to alanine completely abolished binding of CCR2-RA-[R] to the receptor.<sup>20</sup> Moreover, this residue might be involved in target selectivity, as the main difference between the intracellular pockets of CCR2 and CCR5 is the single substitution of Val<sup>6x36</sup> by Leu<sup>6x36</sup>. The steric hindrance introduced by this substitution might be thus responsible for the reduction in affinity of CCR2-RA-[R] towards CCR5 compared to CCR2.<sup>20</sup> Indeed, in the case of CCR5, only small aliphatic groups were tolerated in R<sup>3</sup> position, such as cyclopropyl or isopropyl (Table 2), while bigger aliphatic groups resulted in improved selectivity towards CCR2. However, a previous SAR analysis of pyrrolone derivatives in CCR1, which also contains a leucine in position 6x36, showed that aromatic groups in the equivalent R<sup>3</sup> position provide CCR1 selectivity versus CCR2, as aromatic groups are not tolerated in this position in CCR2<sup>18</sup> (Table 2).

The binding pose of **43** seems to be stabilized by a network of hydrogen bonds between the triazolo-pyrimidinone core and residues E<sup>8x48</sup>, Lys<sup>8x49</sup>, F<sup>8x50</sup> and R<sup>3x50</sup> (Figure 4b). Although the core of CCR2-RA-[R] and **43** binds with a different orientation, the carboxy group of both overlay in the same position, interacting with the backbones of Lys<sup>8x49</sup> and F<sup>8x50</sup>. Moreover, the secondary and tertiary amino groups present in the triazolo-pyrimidinone core also form hydrogen bonds with the backbones of Lys<sup>8x49</sup> and Glu<sup>8x48</sup>, as well as with the side chains of Arg<sup>3x50</sup>. Finally, the primary amino group in position R<sup>2</sup> of compound **43** also makes an extra hydrogen bond with the side chain of E<sup>8x48</sup>. Such extended network of hydrogen bond interactions is not present with CCR2-RA-[R], and thus it might be responsible for the higher affinity of **43** in CCR2, compared to CCR2-RA-[R]. Previous studies have confirmed the importance of residues 8x49 and/or 8x50 in chemokine receptors for the binding of several intracellular ligands. For example, alanine mutations of Lys<sup>8x49</sup> and F<sup>8x50</sup> in CCR2 caused a 10-fold reduction or a complete loss of affinity of intracellular ligands, respectively, compared to the wild-type receptor.<sup>20</sup> In CXCR2, alanine mutation of Lys<sup>8x49</sup> led to a reduced affinity of three different intracellular ligands, while the mutation F<sup>8x50</sup>A only affected one of the ligands tested, indicating a different binding mode.<sup>33</sup> Moreover, Lys<sup>8x49</sup> has been suggested as a key residue for target selectivity between CXCR1 and CXCR2, as it is exchanged by Asn<sup>8x49</sup> in CXCR1.<sup>34</sup> In addition, the crystal structure of CCR9 in complex with vercirnon<sup>15</sup> also shows a binding interaction between the ligand and Arg323<sup>8x49</sup> and Phe324<sup>8x50</sup>. Overall, these data suggest that although the intracellular pockets of CCR2 and CCR5 are quite conserved, the design of multitarget compounds is not quite straightforward. Moreover, several of these residues have been shown to be involved in G<sub>α</sub> coupling in recent cryo-electron microscopy (cryo-EM)-derived GPCR structures, including residues 3x50, 6x29, 6x32 to 6x37, 8x47 and 8x49.<sup>35-37</sup> Similarly, homologous residues are also involved in direct interactions between rhodopsin and arrestin,<sup>38</sup> suggesting a direct interference of these intracellular ligands with the G<sub>α</sub> protein and β-arrestin binding site, and the possibility of fine-tuning residue interactions for the design of biased ligands.

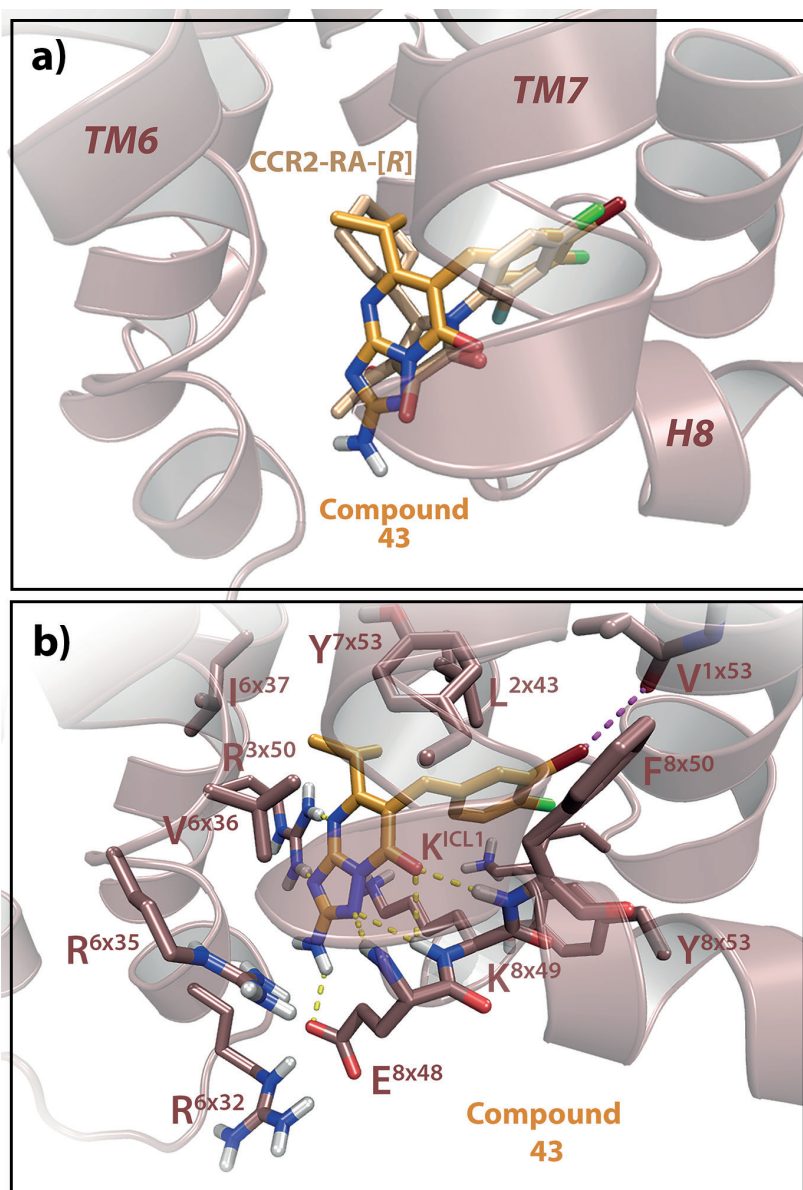


**Figure 4. Proposed binding mode of 43 in hCCR2b.** (a) Overlay of **43** with the CCR2 intracellular ligand CCR2-RA-[R], showing that **43** interacts in a similar manner as CCR2-RA-[R]. (b) Docking of **43**, displaying the interactions with CCR2. The amino group in R<sup>2</sup> makes an extra hydrogen-bond interaction with E<sup>8x48</sup>, while the bromine group in R<sup>1</sup> makes an extra halogen bond with the backbone of V<sup>1x53</sup>, which might contribute to the improved affinity to this receptor. Model of hCCR2 is based on the crystal structure of CCR2 (PDB 5T1A),<sup>14</sup> and amino acid residues are labeled according to their structure-based Ballesteros-Weinstein numbers.<sup>24</sup>



## CONCLUSIONS

In this study we first confirmed that the triazolo-pyrimidinone derivative **8** binds to the intracellular pocket of CCR2, in a similar manner as the reference intracellular ligand CCR2-RA-[R]. Moreover, compound **8** was also able to inhibit CCR5 in a functional  $\beta$ -arrestin recruitment assay; thus, we took this compound as a starting point for the synthesis of a series of novel and previously described triazolo-pyrimidinone derivatives. Using [ $^3\text{H}$ ]-CCR2-RA-[R] binding assays and functional  $\beta$ -arrestin recruitment assays, we explored structure-affinity/activity relationships (SAR) in both receptors. Overall, these compounds were mostly selective towards CCR2; however, CCR5 activity was increased with the combination of isopropyl in R<sup>3</sup> position and two halogens placed in adjacent positions at the phenyl group in R<sup>1</sup>. Overall, these findings indicate that even though the intracellular pockets of CCR2 and CCR5 are highly conserved, selectivity of intracellular ligands can be fine-tuned, allowing the design of either selective or multitarget ligands. Evaluation of compounds **39** and **43** in a [ $^{35}\text{S}$ ]GTP $\gamma$ S binding assay indicates that both compounds display a noncompetitive, insurmountable mode of inhibition in CCR2 and CCR5, which might represent a therapeutic advantage in inflammatory diseases characterized by a high local concentration of endogenous chemokines, such as multiple sclerosis and rheumatoid arthritis. Thus, in diseases where selective chemokine receptor antagonists have been largely unsuccessful, the development of multitarget, intracellular ligands for CCR2 and CCR5 may represent a novel therapeutic option.

## EXPERIMENTAL SECTION

### Chemistry

#### General methods

All solvents and reagents used were of analytical grade and from commercial sources. Demineralized water was used in all cases, unless stated otherwise, and is simply referred to as H<sub>2</sub>O. Microwave-based synthesis was carried out using a Biotage Initiator® equipment (Biotage, Sweden). All reactions were monitored by thin-layer chromatography (TLC) using aluminum plates coated with silica gel 60 F<sub>254</sub> (Merck), and compounds were visualized under ultraviolet light at 254 nm or via KMnO<sub>4</sub> staining. Column chromatography for compound purification was performed using silica gel (Merck millipore) with particle size 0.04-0.63 mm. Chemical identity of final compounds was established using <sup>1</sup>H NMR and Liquid chromatography–mass spectrometry (LC–MS). <sup>1</sup>H NMR spectra were recorded on a Bruker AV 400 liquid spectrometer (<sup>1</sup>H NMR, 400 MHz) at room temperature (rt). Chemical shifts ( $\delta$ ) are reported in parts per million (ppm), and coupling-constants (J) in Hz. Liquid chromatography–mass spectrometry (LC–MS) of final compounds was performed using a Thermo Finnigan Surveyor LCQ Advantage Max LC-MS system and a Gemini C18 Phenomenex column (50 × 4.6 mm, 3  $\mu$ m). Analytical purity of the compounds was determined using a Shimadzu high pressure liquid chromatography (HPLC) equipment with a Phenomenex Gemini column (3 × C18 110A column, 50 × 4.6 mm, 3  $\mu$ m). A flow rate of 1.3 mL/min, and an elution gradient of 10-90% MeCN/H<sub>2</sub>O (0.1% TFA) was used. The absorbance of the UV spectrophotometer was set at 254 nm. All compounds tested in biological assays showed a single peak at the designated retention time and were  $\geq$  95% pure. Sample preparation for HPLC and LC-MS were as follows, unless stated otherwise: 0.3 mg/mL of compound was dissolved in a 1:1:1 mixture of H<sub>2</sub>O:MeOH:tBuOH. Of note, some compounds required DMSO and heat to ensure proper dissolution. None of the final compounds were identified as potential pan-assay interference compounds (PAINS) after assessment with the Free ADME-Tox Filtering Tool (FAF-Drugs4),<sup>39, 40</sup> which uses three different PAINS filters based on Baell et al.<sup>41</sup>

#### General procedure 1: Synthesis of $\beta$ - keto esters 1f-h,j,k,n.<sup>42</sup>

In a flame-dried round bottom flask under a nitrogen atmosphere, ethyl acetoacetate (2.53 mL, 20.0 mmol, 1.00 eq.) was added drop wise to a suspension of NaH (880 mg, 22.1 mmol 1.10 eq.) in dry THF (5 mL) at 0°C while stirring. After 20 min, n-butyl lithium (20 .0 mmol, 2.50 M solution in pentane,1.00 eq.) was added drop wise to the mixture and stirred for



further 30 min. The respective alkyl halide **2f-h,j,k** or benzyl bromide **2n** (1.20 eq.) was subsequently added drop wise over a period of 10 min to the dianion solution after which the solution was allowed to reach rt. After 14 hours, the reaction was quenched by the addition of saturated  $\text{NH}_4\text{Cl}$  (aq., 80 mL). The mixture was subsequently extracted with diethyl ether (2 X 120 mL). The combined organic fractions were washed with brine (80 mL) and dried over  $\text{MgSO}_4$  followed by concentration in vacuo. The crude products were purified by flash chromatography ( $\text{CH}_2\text{Cl}_2$ /petroleum ether and/or EtOAc/petroleum ether as the eluent) to give the title compounds **1f-h,j,k,n** as oils. Compounds **1a-e,i,l,m** were commercially available.

**Ethyl-3-oxoheptanoate (1f).**<sup>42</sup> Synthesized according to general procedure 1. Started from 1-bromopropane (**2f**) (2.00 mL, 22.0 mmol, 1.10 eq.) and purified by silica column chromatography (1% – 30% EtOAc in petroleum ether). Yield: 36% (1.25 g) as a colourless oil.  $^1\text{H}$  NMR (400 MHz,  $\text{CDCl}_3$ )  $\delta$  4.19 (q,  $J = 7.2$  Hz, 2H), 3.44 (s, 2H), 2.54 (t,  $J = 7.4$  Hz, 2H), 1.65-1.55 (m, 2H), 1.38-1.25 (m, 7H), 0.88 (t,  $J = 6.8$  Hz, 3H) ppm.

**Ethyl 5-ethyl-3-oxoheptanoate (1g).** Synthesized according to the general procedure 1. Started from 3-bromopentane (**2g**) (3.00 mL, 24.2 mmol, 1.21 eq.) and purified by silica column chromatography (1% – 30% EtOAc in petroleum ether). Yield: 18% (630 mg) as a yellow oil.  $^1\text{H}$  NMR (400 MHz,  $\text{CDCl}_3$ )  $\delta$  4.17 (q,  $J = 7.2$  Hz, 2H), 3.40 (s, 2H), 2.43 (d,  $J = 6.8$  Hz, 2H), 1.88-1.73 (m, 1H), 1.33-1.21 (m, 7H), 0.82 (t,  $J = 7.4$  Hz, 6H) ppm.

**Ethyl 3-oxooctanoate (1h).**<sup>42</sup> Synthesized according to general procedure 1. Started from 1-bromobutane (**2h**) (2.59 mL, 24.1 mmol, 1.21 eq.) and purified by silica column chromatography (1% – 30% EtOAc in petroleum ether). Yield: 38% (1.41 g) as a yellow oil.  $^1\text{H}$  NMR (400 MHz,  $\text{CDCl}_3$ )  $\delta$  4.19 (q,  $J = 7.2$  Hz, 2H), 3.43 (s, 2H), 2.53 (t,  $J = 7.2$  Hz, 2H), 1.65-1.55 (m, 2H), 1.37-1.12 (m, 7H), 0.89 (t,  $J = 7.2$  Hz, 3H) ppm.

**Ethyl 3-oxononanoate (1i).**<sup>42</sup> Synthesized according to the general procedure 1. Started from 1-iodopentane (**2i**) (3.13 mL, 24.0 mmol, 1.20 eq.) and purified by silica column chromatography (1% – 30% EtOAc in petroleum ether). Yield: 44% (1.76 g) as a yellow oil.  $^1\text{H}$  NMR (400 MHz,  $\text{CDCl}_3$ )  $\delta$  4.19 (q,  $J = 7.2$  Hz, 2H), 3.43 (s, 2H), 2.53 (t,  $J = 7.4$  Hz, 2H), 1.54-1.64 (m, 2H), 1.33-1.24 (m, 9H), 0.88 (t,  $J = 6.8$  Hz, 3H) ppm.

**Ethyl 3-oxodecanoate (1k).**<sup>43</sup> Synthesized according to the general procedure 1. Started from 1-bromohexane (**2k**) (3.36 mL, 25.0 mmol, 1.24 eq.) and purified by silica column chromatography (30%  $\text{CH}_2\text{Cl}_2$  in Petroleum ether to 100%  $\text{CH}_2\text{Cl}_2$ ). Yield: 15% (625 mg) as a yellow oil.  $^1\text{H}$  NMR (400 MHz,  $\text{CDCl}_3$ )  $\delta$  4.19 (q,  $J = 7.2$  Hz, 2H), 3.43 (s, 2H), 2.53 (t,  $J = 7.4$  Hz, 2H), 1.64-1.53 (m, 2H), 1.33-1.24 (m, 11H), 0.88 (t,  $J = 7.5$  Hz, 3H) ppm.

**Ethyl 3-oxo-5-phenylpentanoate (1n).**<sup>44</sup> Synthesized according to the general procedure 1. Started from benzyl bromide (**2n**) (2.90 mL, 24.4 mmol, 1.22 eq.) and purified by silica column chromatography (1% – 30% EtOAc in petroleum ether). Yield: 20% (1.06 g) as a colorless oil.  $^1\text{H}$  NMR (400 MHz,  $\text{CDCl}_3$ )  $\delta$  7.33-7.23 (m, 2H), 7.23-7.12 (m, 3H), 4.17 (q,  $J = 7.2$  Hz, 2H), 3.42 (s, 2H), 2.98-2.81 (m, 4H), 1.26 (t,  $J = 7.2$  Hz, 3H) ppm.



## General procedure 2. Benzylated $\beta$ -keto esters **4aa-na**, **4bb-bq**, **4eq-ev**.<sup>22</sup>

LiCl (1.00 eq.) was slurried in anhydrous THF (1 mL/mmol **1a-n**) in a flame dried round bottom flask and under an atmosphere of nitrogen. The desired  $\beta$ -keto ester **1a-n** (1.00 eq.) was added and followed by DIPEA (2.00 eq.) and the respective benzylic halide **3a-v** (1.20 eq.). The reaction mixture was reflux for 20 hours, after which the reaction was completed as indicated by TLC (5-10% EtOAc in Petroleum ether). THF was removed in vacuo, the crude dissolved EtOAc (30 mL) and this organic layer was washed with citric acid (5%, 25 mL) followed by saturated NaHCO<sub>3</sub> (25 mL) and brine (25 mL). The organic layer was subsequently dried over MgSO<sub>4</sub>, concentrated in vacuo to afford the crude product. The crude product was purified by flash column chromatography (5%-10% EtOAc/petroleum ether) to yield the corresponding benzylated  $\beta$ -keto esters **4aa-na**, **4bb-bq**, **4eq-ev**.

**Ethyl 2-(3-chlorobenzyl)-3-oxobutanoate (4aa)**.<sup>22</sup> Synthesis according to general procedure 2. Reagents: Ethyl 3-oxobutanoate **1a** (0.37 mL, 2.92 mmol, 1.20 eq.), 3-chlorobenzyl bromide **3a** (0.32 mmol, 2.43 mmol, 1.00 eq.), DIPEA (0.85 mL, 4.86 mmol, 2.00 eq.), LiCl (103 mg, 2.43 mmol, 1.00 eq.), 5 mL dry THF. Yield: 70% (433 mg) as a colourless oil. <sup>1</sup>H NMR: (400 MHz, CDCl<sub>3</sub>):  $\delta$  7.21-7.14 (m, 3H), 7.09-7.04 (m, 1H), 4.16 (q,  $J = 7.2$  Hz, 2H), 3.75 (t,  $J = 8.0$  Hz, 1H), 3.17-3.07 (m, 2H), 2.21 (s, 3H), 1.21 (t,  $J = 7.2$  Hz, 3H) ppm.

**Ethyl 3-cyclopropyl-2-(3-chlorobenzyl)-3-oxopropanoate (4ba)**.<sup>22</sup> Synthesis according to general procedure 2. Reagents: Ethyl 3-cyclopropyl-3-oxopropanoate **1b** (7.56 mL, 51.2 mmol, 1.00 eq.), 3-chlorobenzyl bromide **3a** (7.06 mL, 53.8 mmol, 1.05 eq.), DIPEA (17.8 mL, 102 mmol, 2.00 eq.), LiCl (2.17 g, 51.22 mmol, 1.00 eq.), 5 mL dry THF. Yield: 71% (10.2 g) as a colorless oil. <sup>1</sup>H NMR (400 MHz, CDCl<sub>3</sub>)  $\delta$  7.21-7.16 (m, 3H), 7.10-7.05 (m, 1H), 4.17 (qd,  $J = 7.2, 1.6$  Hz, 2H), 3.89 (t,  $J = 7.6$  Hz, 1H), 3.15 (dd,  $J = 7.2$  Hz, 2H), 2.08-2.02 (m, 1H), 1.22 (t,  $J = 7.2$  Hz, 3H), 1.11-1.01 (m, 2H), 0.98-0.88 (m, 2H) ppm.

**Ethyl 2-benzyl-3-cyclopropyl-3-oxopropanoate (4bb)**.<sup>23</sup> Synthesis according to general procedure 2. Reagents: Ethyl 3-cyclopropyl-3-oxopropanoate **1b** (0.52 mL, 3.51 mmol, 1.20 eq.), benzylbromide **3b** (0.347 mL, 2.92 mmol, 1.00 eq.), DIPEA (1.02 mL, 5.84 mmol, 2.00 eq.), LiCl (124 mg, 2.92 mmol, 1.00 eq.), 4 mL dry THF. Yield: 26% (105 mg) as a colourless oil. <sup>1</sup>H NMR (400 MHz, CDCl<sub>3</sub>)  $\delta$  7.29-7.25 (m, 2H), 7.22-7.18 (m, 3H), 4.20-4.12 (m, 2H), 3.91 (t,  $J = 7.6$  Hz, 1H), 3.20 (d,  $J = 7.6$  Hz, 2H), 2.08-2.02 (m, 1H), 1.20 (t,  $J = 7.2$  Hz, 3H), 1.06-1.03 (m, 2H), 0.94-0.84 (m, 2H) ppm.

**Ethyl 3-cyclopropyl-2-(2-methylbenzyl)-3-oxopropanoate (4bc)**. Synthesis according to general procedure 2. Reagents: Ethyl 3-cyclopropyl-3-oxopropanoate **1b** (0.63 mL, 4.27 mmol, 1.20 eq.), 2-methylbenzyl chloride **3c** (0.48 mL, 3.56 mmol, 1.00 eq.), DIPEA (1.24 mL, 7.12 mmol, 2.00 eq.), LiCl (151 mg, 3.56 mmol, 1.00 eq.), 4 mL dry THF. Yield: 80% (742 mg) as a colourless oil. <sup>1</sup>H NMR (400 MHz, CDCl<sub>3</sub>)  $\delta$  7.15-7.09 (m, 4H), 4.16 (qd,  $J = 7.2, 1.2$  Hz, 2H), 3.91 (t,  $J = 7.2$  Hz, 1H), 3.20 (d,  $J = 7.6$  Hz, 2H), 2.34 (s, 3H), 2.05-2.00 (m, 1H), 1.20 (t,  $J = 7.2$  Hz, 3H), 1.07-1.02 (m, 2H), 0.95-0.84 (m, 2H) ppm.

**Ethyl 3-cyclopropyl-2-(2-chlorobenzyl)-3-oxopropanoate (4bd)**. Synthesis according to general procedure 2. Reagents: Ethyl 3-cyclopropyl-3-oxopropanoate **1b** (0.43 mL, 2.92 mmol, 1.20 eq.), 2-chlorobenzyl bromide **3d** (0.32 mL, 2.43 mmol, 1.00 eq.), DIPEA (0.85 mL, 4.86 mmol, 2.00 eq.), LiCl (103 mg, 2.43 mmol, 1.00 eq.), 5 mL dry THF. Yield: 78% (532 mg) as a colourless oil. <sup>1</sup>H NMR (400 MHz, CDCl<sub>3</sub>)  $\delta$  7.36-7.33 (m, 1H), 7.26-7.24 (m, 1H), 7.18-7.14 (m, 2H), 4.20-4.08 (m, 3H), 3.37-3.22 (m, 2H),

2.10-2.03 (m, 1H), 1.21 (t,  $J = 7.2$  Hz, 3H), 1.09-1.01 (m, 2H), 0.97-0.87 (m, 2H) ppm.

**Ethyl 3-cyclopropyl-2-(2-methoxybenzyl)-3-oxopropanoate (4be).** Synthesis according to general procedure 2. Reagents: Ethyl 3-cyclopropyl-3-oxopropanoate **1b** (0.33 mL, 2.26 mmol, 1.20 eq.), 2-methoxybenzyl bromide<sup>45</sup> **3e** (378 mg, 1.88 mmol, 1.00 eq.), DIPEA (0.66 mL, 3.76 mmol, 2.00 eq.), LiCl (79.7 mg, 1.88 mmol, 1.00 eq.), 5 mL dry THF. Silica column chromatography in 8:1:1 petroleum ether:EtOAc:CH<sub>2</sub>Cl<sub>2</sub>. Yield: 36% (185 mg) as a colourless oil. <sup>1</sup>H NMR (400 MHz, CDCl<sub>3</sub>)  $\delta$  7.20 (td,  $J = 6.4, 1.6$  Hz, 1H), 7.13 (dd,  $J = 6.0, 1.2$  Hz, 1H), 6.86-6.26 (m, 2H), 4.17-4.09 (m, 2H), 4.04 (dd,  $J = 6.8, 1.6$  Hz, 1H), 3.84 (s, 3H), 3.42-3.11 (m, 2H), 2.07-2.02 (m, 1H), 1.19 (t,  $J = 6.0$  Hz, 3H), 1.05-1.02 (m, 2H), 0.92-0.85 (m, 2H) ppm.

**Ethyl 3-cyclopropyl-2-(3-methylbenzyl)-3-oxopropanoate (4bf).** Synthesis according to general procedure 2. Reagents: Ethyl 3-cyclopropyl-3-oxopropanoate **1b** (0.47 mL, 3.24 mmol, 1.20 eq.), 3-methylbenzyl bromide **3f** (0.36 mL, 2.70 mmol, 1.00 eq.), DIPEA (0.94 mL, 5.40 mmol, 2.00 eq.), LiCl (114 mg, 2.70 mmol, 1.00 eq.), 5 mL dry THF. Yield: 74% (521 mg) as a colourless oil. <sup>1</sup>H NMR (400 MHz, CDCl<sub>3</sub>)  $\delta$  7.17 (t,  $J = 7.6$  Hz, 1H), 7.02-6.96 (m, 3H), 4.19-4.10 (m, 2H), 3.90 (t,  $J = 7.6$  Hz, 1H), 3.15 (d,  $J = 7.6$  Hz, 2H), 2.30 (s, 3H), 2.07-2.01 (m, 1H), 1.19 (t,  $J = 7.2$  Hz, 3H), 1.04-0.99 (m, 2H), 0.93-0.82 (m, 2H) ppm.

**Ethyl 3-cyclopropyl-2-(3-fluorobenzyl)-3-oxopropanoate (4bg).**<sup>22</sup> Synthesis according to general procedure 2. Reagents: Ethyl 3-cyclopropyl-3-oxopropanoate **1b** (0.550 mL, 3.73 mmol, 1.31 eq.), 3-fluorobenzyl bromide **3g** (0.350 mL, 2.85 mmol, 1.00 eq.), DIPEA (0.940 mL, 5.39 mmol, 1.89 eq.), LiCl (0.140 g, 2.70 mmol, 0.947 eq.), 5 mL dry THF. Yield: 100% (770 mg) as a yellow oil. <sup>1</sup>H NMR (400 MHz, CDCl<sub>3</sub>)  $\delta$  7.26-7.16 (m, 1H), 6.97 (d,  $J = 8.0$  Hz, 1H), 6.94-6.84 (m, 2H), 4.19-4.11 (m, 2H), 3.92 (t,  $J = 7.6$  Hz, 1H), 3.18 (dd,  $J = 7.6, 1.6$  Hz, 2H), 2.10-2.04 (m, 1H), 1.20 (t,  $J = 7.2$  Hz, 3H), 1.07-0.98 (m, 2H), 0.93 – 0.83 (m, 2H) ppm.

**Ethyl 2-(3-bromobenzyl)-3-cyclopropyl-3-oxopropanoate (4bh).** Synthesis according to general procedure 2. Reagents: Ethyl 3-cyclopropyl-3-oxopropanoate **1b** (0.35 mL, 2.40 mmol, 1.20 eq.), 3-bromobenzyl bromide **3h** (500 mg, 2.00 mmol, 1.00 eq.), DIPEA (0.70 mL, 4.00 mmol, 2.00 eq.), LiCl (85 mg, 2.00 mmol, 1.00 eq.), 5 mL dry THF. Yield: 47% (303 mg) as a colourless oil. <sup>1</sup>H NMR (400 MHz, CDCl<sub>3</sub>)  $\delta$  7.36-7.32 (m, 2H), 7.17-7.10 (m, 2H), 4.17 (q,  $J = 7.2$  Hz, 2H), 3.89 (t,  $J = 7.2$  Hz, 1H), 3.15 (d,  $J = 8.0$  Hz, 2H), 2.08-2.01 (m, 1H), 1.22 (t,  $J = 7.2$  Hz, 3H), 1.11-1.01 (m, 2H), 0.98-0.86 (m, 2H) ppm.

**Ethyl 3-cyclopropyl-2-(3-iodobenzyl)-3-oxopropanoate (4bi).** Synthesis according to general procedure 2. Reagents: Ethyl 3-cyclopropyl-3-oxopropanoate **1b** (0.550 mL, 3.73 mmol, 1.38 eq.), 3-iodobenzyl bromide **3i** (0.802 g, 2.70 mmol, 1.00 eq.), DIPEA (0.940 mL, 5.39 mmol, 2.00 eq.), LiCl (0.150 g, 2.70 mmol, 1.00 eq.), 5 mL dry THF. Yield: quantitative (1.28 g) as a yellow oil. <sup>1</sup>H NMR (400 MHz, CDCl<sub>3</sub>)  $\delta$  7.55-7.51 (m, 2H), 7.15 (d,  $J = 7.6$  Hz, 1H), 6.99 (t,  $J = 7.6$  Hz, 1H), 4.16 (qd,  $J = 7.2, 1.6$  Hz, 2H), 3.87 (t,  $J = 7.2$  Hz, 1H), 3.11 (dd,  $J = 8.0, 2.0$  Hz, 2H), 2.06-2.00 (m, 1H), 1.20 (t,  $J = 6.8$  Hz, 3H), 1.11-1.00 (m, 2H), 0.98-0.81 (m, 2H) ppm.

**Ethyl 3-cyclopropyl-2-(3-methoxybenzyl)-3-oxopropanoate (4bj).**<sup>46</sup> Synthesis according to general procedure 2. Reagents: Ethyl 3-cyclopropyl-3-oxopropanoate **1b** (0.44 mL, 3.00 mmol, 1.20 eq.), 3-methoxybenzyl bromide **3j** (0.35 mL, 2.50 mmol, 1.00 eq.), DIPEA (0.87 mL, 5.00 mmol, 2.00 eq.), LiCl (106 mg, 2.50 mmol, 1.00 eq.), 5 mL dry THF. Silica column chromatography in 8:1:1 petroleum ether:EtOAc:CH<sub>2</sub>Cl<sub>2</sub>. Yield: 42% (294 mg) as a colourless oil. <sup>1</sup>H NMR (400 MHz, CDCl<sub>3</sub>)  $\delta$  7.19 (td,  $J = 7.2$  Hz, 1.2 Hz, 1H), 6.79-6.74 (m, 3H), 4.21-4.13 (m, 2H), 3.91 (t,  $J = 7.6$  Hz, 1H), 3.78 (s, 3H), 3.17 (d,  $J = 7.6$  Hz, 2H), 2.08-2.02 (m, 1H), 1.22 (t,  $J = 7.2$  Hz, 3H), 1.06-1.01 (m, 2H), 0.96-0.85 (m, 2H) ppm.

**Ethyl 3-cyclopropyl-3-oxo-2-(3-(trifluoromethyl)benzyl)propanoate (4bk).**<sup>23</sup> Synthesis according to general procedure 2. Reagents: Ethyl 3-cyclopropyl-3-oxopropanoate **1b** (0.37 mL, 2.51 mmol, 1.20 eq.), 3-(trifluoromethyl)benzyl bromide **3k** (0.32 mL, 2.09 mmol, 1.00 eq.), DIPEA (0.73 mL, 4.18 mmol, 2.00 eq.), LiCl (89 mg, 2.09 mmol, 1.00 eq.), 5 mL dry THF. Yield: 31% (214 mg) as a

colourless oil.  $^1\text{H}$  NMR (400 MHz,  $\text{CDCl}_3$ )  $\delta$  7.50-7.44 (m, 2H), 7.42-7.38 (m, 2H), 4.17 (q,  $J = 6.8$  Hz, 2H), 3.92 (t,  $J = 8.0$  Hz, 1H), 3.25 (d,  $J = 7.2$  Hz, 2H), 2.10-2.02 (m, 1H), 1.21 (t,  $J = 7.2$  Hz, 3H), 1.12-1.01 (m, 2H), 0.99-0.86 (m, 2H) ppm.

**Ethyl 3-cyclopropyl-2-(4-methylbenzyl)-3-oxopropanoate (4bl).** Synthesis according to general procedure 2. Reagents: Ethyl 3-cyclopropyl-3-oxopropanoate **1b** (0.48 mL, 3.24 mmol, 1.20 eq.), 4-methylbenzyl bromide **3l** (500 mg, 2.70 mmol, 1.00 eq.), DIPEA (0.94 mL, 5.40 mmol, 2.00 eq.), LiCl (114 mg, 2.70 mmol, 1.00 eq.), 5 mL dry THF. Yield: 74% (521 mg) as a colourless oil.  $^1\text{H}$  NMR (400 MHz,  $\text{CDCl}_3$ )  $\delta$  7.08 (s, 4H), 4.22-4.09 (m, 2H), 3.88 (t,  $J = 7.6$  Hz, 1H), 3.15 (d,  $J = 7.6$  Hz, 2H), 2.30 (s, 3H), 2.07-2.02 (m, 1H), 1.21 (t,  $J = 7.2$  Hz, 3H), 1.07-1.02 (m, 2H), 0.96-0.83 (m, 2H) ppm.

**Ethyl 3-cyclopropyl-2-(4-fluorobenzyl)-3-oxopropanoate (4bm).** Synthesis according to general procedure 2. Reagents: Ethyl 3-cyclopropyl-3-oxopropanoate **1b** (0.890 mL, 6.04 mmol, 1.14 eq.), 1-(bromomethyl)-4-fluorobenzene **3m** (1.57 g, 5.29 mmol, 1.00 eq.), DIPEA (1.05 mL, 6.00 mmol, 1.13 eq.), LiCl (0.130 g, 3.00 mmol, 0.58 eq.), 5 mL dry THF. Yield: 56% (780 mg) as a yellow oil.  $^1\text{H}$  NMR (400 MHz,  $\text{CDCl}_3$ )  $\delta$  7.18-7.12 (m, 2H), 6.96 (tt,  $J = 8.8, 2.0$  Hz, 2H), 4.22-4.10 (m, 2H), 3.87 (t,  $J = 8.0$  Hz, 1H), 3.16 (d,  $J = 7.6$  Hz, 2H), 2.08-2.00 (m, 1H), 1.21 (t,  $J = 7.2$  Hz, 3H), 1.09-0.99 (m, 2H), 0.97-0.84 (m, 2H) ppm.

**Ethyl 2-(4-chlorobenzyl)-3-cyclopropyl-3-oxopropanoate (4bn).** Synthesis according to general procedure 2. Reagents: Ethyl 3-cyclopropyl-3-oxopropanoate **1b** (0.43 mL, 2.92 mmol, 1.20 eq.), 4-chlorobenzyl bromide **3n** (500 mg, 2.43 mmol, 1.00 eq.), DIPEA (0.85 mL, 4.86 mmol, 2.00 eq.), LiCl (103 mg, 2.43 mmol, 1.00 eq.), 5 mL dry THF. Yield: 66% (451 mg) as a colourless oil.  $^1\text{H}$  NMR (400 MHz,  $\text{CDCl}_3$ )  $\delta$  7.24 (dt,  $J = 8.8, 2.0$  Hz, 2H), 7.13 (dt,  $J = 8.4, 2.0$  Hz, 2H), 4.21-4.11 (m, 2H), 3.87 (dd,  $J = 8.0, 0.8$  Hz, 1H), 3.15 (dd,  $J = 6.8, 1.2$  Hz, 2H), 2.08-2.01 (m, 1H), 1.21 (t,  $J = 7.2$  Hz, 3H), 1.09-1.01 (m, 2H), 0.97-0.86 (m, 2H) ppm.

**Ethyl 2-(4-bromobenzyl)-3-cyclopropyl-3-oxopropanoate (4bo).** Synthesis according to general procedure 2. Reagents: Ethyl 3-cyclopropyl-3-oxopropanoate **1b** (0.880 mL, 5.97 mmol, 1.49 eq.), 1-(bromomethyl)-4-bromobenzene **3o** (1.00 g, 4.00 mmol, 1.00 eq.), DIPEA (1.39 mL, 8.00 mmol, 2.00 eq.), LiCl (0.170 g, 4.00 mmol, 1.00 eq.), 5 mL dry THF. Yield: 67% (0.880 g) as a yellow oil.  $^1\text{H}$  NMR (400 MHz,  $\text{CDCl}_3$ )  $\delta$  7.39 (d,  $J = 8.4$  Hz, 2H), 7.07 (d,  $J = 8.4$  Hz, 2H), 4.22-4.10 (m, 2H), 3.87 (t,  $J = 8.0$  Hz, 1H), 3.14 (d,  $J = 8.2$  Hz, 2H), 2.08-1.96 (m, 1H), 1.22 (t,  $J = 7.2$  Hz, 3H), 1.10-0.99 (m, 2H), 0.99-0.85 (m, 2H) ppm.

**Ethyl 3-cyclopropyl-2-(4-methoxybenzyl)-3-oxopropanoate (4bp).** Synthesis according to general procedure 2. Reagents: Ethyl 3-cyclopropyl-3-oxopropanoate **1b** (0.57 mL, 3.83 mmol, 1.20 eq.), 4-methoxybenzyl bromide **3p** (0.46 mL, 3.19 mmol, 1.00 eq.), DIPEA (1.11 mL, 6.38 mmol, 2.00 eq.), LiCl (135 mg, 3.19 mmol, 1.00 eq.), 5 mL dry THF. Silica column chromatography in 7:1:2 petroleum ether:EtOAc: $\text{CH}_2\text{Cl}_2$ . Yield: 52% (454 mg) as a colourless oil.  $^1\text{H}$  NMR (400 MHz,  $\text{CDCl}_3$ )  $\delta$  7.10 (dt,  $J = 8.8, 2.0$  Hz, 2H), 6.81 (dt,  $J = 8.8, 2.4$  Hz, 2H), 4.20-4.10 (m, 2H), 3.86 (t,  $J = 7.6$  Hz, 1H), 3.78 (s, 3H), 3.13 (d,  $J = 7.6$  Hz, 2H), 2.07-2.01 (m, 1H), 1.21 (t,  $J = 7.2$  Hz, 3H), 1.08-1.01 (m, 2H), 0.95-0.83 (m, 2H) ppm.

**Ethyl 3-cyclopropyl-2-(3,4-dichlorobenzyl)-3-oxopropanoate (4bq).**<sup>22</sup> Synthesis according to general procedure 2. Reagents: Ethyl 3-cyclopropyl-3-oxopropanoate **1b** (0.60 mL, 4.06 mmol, 1.00 eq.), 3,4-dichlorobenzyl bromide **3q** (0.62 mL, 4.27 mmol, 1.05 eq.), DIPEA (1.42 mL, 8.13 mmol, 2.00 eq.), LiCl (172 mg, 4.06 mmol, 1.00 eq.), 5 mL dry THF. Yield: 39% (493 mg) as a colourless oil.  $^1\text{H}$  NMR (400 MHz,  $\text{CDCl}_3$ )  $\delta$  7.33 (d,  $J = 8.4$  Hz, 1H), 7.30 (d,  $J = 1.6$  Hz, 1H), 7.03 (dd,  $J = 8.4, 2.0$  Hz, 1H), 4.22-4.12 (m, 2H), 3.87 (t,  $J = 7.6$  Hz, 1H), 3.18-3.09 (m, 2H), 2.09-2.02 (m, 1H), 1.23 (t,  $J = 7.2$  Hz, 3H), 1.09-1.01 (m, 2H), 0.95-0.85 (m, 2H) ppm.

**Ethyl 2-(3-chlorobenzyl)-3-oxopentanoate (4ca).**<sup>47</sup> Synthesis according to general procedure 2. Reagents: Ethyl 3-oxopentanoate **1c** (0.42 mL, 2.92 mmol, 1.20 eq.), 3-chlorobenzyl bromide **3a** (0.32 mL, 2.43 mmol, 1.00 eq.), NaH (117 mg, 4.86 mmol, 2.00 eq.), 5 mL dry THF. Yield: 52% (340 mg) as a

colourless oil.  $^1\text{H}$  NMR (500 MHz,  $\text{CDCl}_3$ ):  $\delta$  7.20-7.14 (m, 3H), 7.09-7.03 (m, 1H), 4.15 (qd,  $J = 7.5$ , 0.8 Hz, 2H), 3.76 (t,  $J = 7.5$  Hz, 1H), 3.17-3.08 (m, 2H), 2.60 (dq,  $J = 18.0$ , 7.0, 1.0 Hz, 1H), 2.37 (dq,  $J = 18.5$ , 7.0, 0.5 Hz, 1H), 1.20 (td,  $J = 7.0$ , 1.0 Hz, 3H), 1.01 (td,  $J = 7.5$ , 1.0 Hz, 3H) ppm.

**Ethyl 2-(3-chlorobenzyl)-3-oxohexanoate (4da).**<sup>22</sup> Synthesis according to general procedure 1. Reagents: Ethyl 3-oxohexanoate **1d** (0.46 mL, 2.92 mmol, 1.20 eq.), 2.43 mmol 3-chlorobenzyl bromide **3a**, DIPEA (0.85 mmol, 4.86 mmol, 2.00 eq.), LiCl (103 mg, 2.43 mmol, 1.00 eq.), 5 mL dry THF. Yield: 76% (522 mg) as a colourless oil.  $^1\text{H}$  NMR (400 MHz,  $\text{CDCl}_3$ ):  $\delta$  7.22-7.14 (m, 3H), 7.08-7.04 (m, 1H), 4.15 (q,  $J = 7.2$  Hz, 2H), 3.75 (t,  $J = 7.6$  Hz, 1H), 3.18-3.07 (m, 2H), 2.54 (dt,  $J = 17.6$ , 7.2 Hz, 1H), 2.35 (dt,  $J = 17.2$ , 7.2 Hz, 1H), 1.57 (sextet,  $J = 7.2$  Hz, 2H), 1.21 (t,  $J = 7.2$  Hz, 3H), 0.85 (t,  $J = 7.6$  Hz, 3H) ppm.

**Ethyl 2-(3-chlorobenzyl)-4-methyl-3-oxopentanoate (4ea).**<sup>22</sup> Synthesis according to general procedure 2. Reagents: Ethyl 4-methyl-3-oxopentanoate **1e** (0.51 mL, 3.16 mmol, 1.20 eq.), 3-chlorobenzyl bromide **3a** (0.35 mL, 2.63 mmol, 1.00 eq.), DIPEA (0.95 mL, 5.26 mmol, 2.00 eq.), LiCl (111 mg, 2.63 mmol, 1.00 eq.), 5 mL dry THF. Yield: 86% (640 mg) as a colourless oil.  $^1\text{H}$  NMR (400 MHz,  $\text{CDCl}_3$ ):  $\delta$  7.20-7.14 (m, 3H), 7.07-7.04 (m, 1H), 4.14 (qd,  $J = 7.2$ , 0.8 Hz, 2H), 3.91 (t,  $J = 7.6$  Hz, 1H), 3.17-3.07 (m, 2H), 2.66 (septet,  $J = 6.8$  Hz, 1H), 1.21 (t,  $J = 7.2$  Hz, 3H), 1.07 (d,  $J = 6.8$  Hz, 3H), 0.91 (d,  $J = 7.2$  Hz, 3H) ppm.

**Ethyl 2-(3,4-dichlorobenzyl)-4-methyl-3-oxopentanoate (4eq).**<sup>23</sup> Synthesis according to general procedure 2. Reagents: Ethyl 4-methyl-3-oxopentanoate **1e** (5.00 mL, 31.0 mmol, 1.00 eq.), 3,4-dichlorobenzyl bromide **3q** (5.41 mL, 37.2 mmol, 1.20 eq.), DIPEA (10.8 mL, 62.0 mmol, 2.00 eq.), LiCl (1.31 g, 30.9 mmol, 1.00 eq.), 50 mL dry THF. Yield: 33% (3.20 g) as a yellow oil.  $^1\text{H}$  NMR (400 MHz,  $\text{CDCl}_3$ )  $\delta$  7.33 (d,  $J = 8.4$  Hz, 1H), 7.29-7.25 (m, 1H), 7.01 (dd,  $J = 8.0$ , 2.0 Hz, 1H), 4.15 (qd,  $J = 7.2$ , 1.6 Hz, 2H), 3.89 (t,  $J = 7.6$  Hz, 1H), 3.16-3.04 (m, 2H), 2.69 (heptet,  $J = 6.8$  Hz, 1H), 1.22 (t,  $J = 7.2$  Hz, 3H), 1.07 (d,  $J = 6.4$  Hz, 3H), 0.93 (d,  $J = 7.2$  Hz, 3H) ppm.

**Ethyl 2-(2,3-dichlorobenzyl)-4-methyl-3-oxopentanoate (4er).** Synthesis according to general procedure 2. Reagents: Ethyl 4-methyl-3-oxopentanoate **1e** (0.670 mL, 4.61 mmol, 1.00 eq.), 2,3-dichlorobenzyl bromide **3r** (1.00 g, 4.17 mmol, 0.90 eq.), DIPEA (1.45 mL, 8.34 mmol, 1.81 eq.), LiCl (180 mg, 0.90 mmol, 1.00 eq.), 5 mL dry THF. Yield: 8% (110 mg) as a yellow oil.  $^1\text{H}$  NMR (400 MHz,  $\text{CDCl}_3$ )  $\delta$  7.34 (dd,  $J = 7.6$ , 1.6 Hz, 1H), 7.15 (dd,  $J = 7.6$ , 1.6 Hz, 1H), 7.09 (t,  $J = 7.6$  Hz, 1H), 4.20-4.03 (m, 3H), 3.34-3.22 (m, 2H), 2.71 (heptet,  $J = 6.8$  Hz, 1H), 1.19 (t,  $J = 7.2$  Hz, 3H), 1.07 (d,  $J = 6.8$  Hz, 3H), 0.90 (d,  $J = 6.8$  Hz, 3H) ppm.

**Ethyl 2-(2,5-dichlorobenzyl)-4-methyl-3-oxopentanoate (4es).** Synthesis according to general procedure 2. Reagents: Ethyl 4-methyl-3-oxopentanoate **1e** (0.204 mL, 1.39 mmol, 1.00 eq.), 2,5-dichlorobenzyl bromide **3s** (500 mg, 2.08 mmol, 1.5 eq.), DIPEA (0.242 mL, 1.39 mmol, 1.00 eq.), LiCl (60 mg, 1.39 mmol, 1.00 eq.), 5 mL dry THF. Yield: 71% (315 mg) as a colorless oil.  $^1\text{H}$  NMR (400 MHz,  $\text{CDCl}_3$ )  $\delta$  7.27 (d,  $J = 8.8$  Hz, 1H), 7.22 (d,  $J = 2.4$  Hz, 1H), 7.15 (dd,  $J = 8.4$ , 2.4 Hz, 1H), 4.18-4.12 (m, 2H), 4.10 (t,  $J = 7.2$  Hz, 1H), 3.26-3.16 (m, 2H), 2.73 (heptet,  $J = 6.8$  Hz, 1H), 1.22 (t,  $J = 7.2$  Hz, 3H), 1.08 (d,  $J = 6.8$  Hz, 3H), 0.93 (d,  $J = 7.2$  Hz, 3H) ppm.

**Ethyl 2-(3,5-dichlorobenzyl)-4-methyl-3-oxopentanoate (4et).**<sup>23</sup> Synthesis according to general procedure 2. Reagents: Ethyl 4-methyl-3-oxopentanoate **1e** (0.480 mL, 3.30 mmol, 1.00 eq.), 3,5-dichlorobenzyl bromide **3t** (0.440 mL, 3.12 mmol, 1.00 eq.), DIPEA (1.05 mL, 6.00 mmol, 1.82 eq.), LiCl (0.310 g, 3.00 mmol, 0.91 eq.), 5 mL dry THF. Yield: 16% (150 mg) as a yellow oil.  $^1\text{H}$  NMR (400 MHz,  $\text{CDCl}_3$ )  $\delta$  7.13 (t,  $J = 2.0$  Hz, 1H), 6.99 (d,  $J = 2.0$  Hz, 2H), 4.08 (q,  $J = 7.2$  Hz, 2H), 3.81 (t,  $J = 7.6$  Hz, 1H), 3.07-2.97 (m, 2H), 2.63 (heptet,  $J = 6.8$  Hz, 1H), 1.15 (t,  $J = 7.2$  Hz, 3H), 1.00 (d,  $J = 6.8$  Hz, 3H), 0.87 (d,  $J = 6.8$  Hz, 3H) ppm.

**Ethyl 2-(3,5-dibromobenzyl)-4-methyl-3-oxopentanoate (4eu).** Synthesis according to general procedure 2. Reagents: Ethyl 4-methyl-3-oxopentanoate **1e** (0.480 mL, 3.30 mmol, 1.00 eq.), 3,5-dibromobenzyl bromide **3u** (1.04 g, 3.16 mmol, 0.958 eq.), DIPEA (1.05 mL, 6.00 mmol, 1.82 eq.), LiCl (0.130 g, 3.00 mmol, 0.909 eq.), 5 mL dry THF. Yield: 29% (0.350 g) as a yellow oil.  $^1\text{H}$  NMR (400 MHz,

$\text{CDCl}_3$ )  $\delta$  7.27 (s, 3H), 4.15 (q,  $J = 7.2$  Hz, 2H), 3.87 (t,  $J = 7.2$  Hz, 1H), 3.13-3.05 (m, 2H), 2.70 (heptet,  $J = 6.8$  Hz, 1H), 1.24 (t,  $J = 6.4$  Hz, 3H), 1.08 (d,  $J = 6.8$  Hz, 3H), 0.95 (d,  $J = 6.8$  Hz, 3H) ppm.

**Ethyl 2-(3-bromo-4-chlorobenzyl)-4-methyl-3-oxopentanoate (4ev).** Synthesis according to general procedure 2. Reagents: Ethyl 4-methyl-3-oxopentanoate **1e** (0.480 mL, 3.30 mmol, 1.00 eq.), 3-bromo-4-chlorobenzyl bromide **3v** (0.900 g, 3.16 mmol, 0.958 eq.), DIPEA (1.05 mL, 6.00 mmol, 1.82 eq.), LiCl (0.130 g, 3.00 mmol, 0.909 eq.), 5 mL dry THF. Yield: 34% (0.360 g) as a yellow oil.  $^1\text{H}$  NMR (400 MHz,  $\text{CDCl}_3$ )  $\delta$  7.44 (d,  $J = 2.0$  Hz, 1H), 7.33 (d,  $J = 8.0$  Hz, 1H), 7.06 (dd,  $J = 8.0, 2.0$  Hz, 1H), 4.15 (qd,  $J = 7.2, 1.6$  Hz, 2H), 3.88 (t,  $J = 7.6$  Hz, 1H), 3.14-3.04 (m, 2H), 2.69 (heptet,  $J = 6.8$  Hz, 1H), 1.22 (t,  $J = 7.2$  Hz, 3H), 1.08 (d,  $J = 6.8$  Hz, 3H), 0.94 (d,  $J = 6.8$  Hz, 3H) ppm.

**Ethyl 2-(3-chlorobenzyl)-3-oxoheptanoate (4fa).** Synthesis according to general procedure 2. Reagents: Ethyl 3-oxoheptanoate **1f** (0.47 g, 2.72 mmol, 1.00 eq.), 3-chlorobenzyl bromide **3a** (0.33 mL, 2.51 mmol, 0.922 eq.), DIPEA (1.05 mL, 6.00 mmol, 2.21 eq.), LiCl (0.130 g, 3.00 mmol, 1.10 eq.), 5 mL dry THF. Yield: 67% (0.550 g) as a colorless oil.  $^1\text{H}$  NMR (400 MHz,  $\text{CDCl}_3$ )  $\delta$  7.20-7.15 (m, 3H), 7.07-7.03 (m, 1H), 7.17-4.10 (m, 2H), 3.75 (t,  $J = 7.6$  Hz, 1H), 3.16-3.06 (m, 2H), 2.55 (dt,  $J = 17.2, 7.2$  Hz, 1H), 2.35 (dt,  $J = 17.6, 7.2$  Hz, 1H), 1.50 (pentet,  $J = 7.6$  Hz, 2H), 1.28-1.19 (m, 5H), 0.85 (t,  $J = 7.2$  Hz, 3H) ppm.

**Ethyl 2-(3-chlorobenzyl)-5-ethyl-3-oxoheptanoate (4ga).** Synthesis according to general procedure 2. Reagents: Ethyl 5-ethyl-3-oxoheptanoate **1g** (0.600 g, 3.00 mmol, 1.00 eq.), 3-chlorobenzyl bromide **3a** (0.470 mL, 3.57 mmol, 1.19 eq.), DIPEA (1.05 mL, 6.00 mmol, 2.00 eq.), LiCl (0.130 g, 3.00 mmol, 1.00 eq.), 5 mL dry THF. Yield: 31% (0.300 g) as a yellow oil.  $^1\text{H}$  NMR (400 MHz,  $\text{CDCl}_3$ )  $\delta$  7.20-7.14 (m, 3H), 7.06-7.05 (m, 1H), 4.18-4.12 (m, 2H), 3.75 (t,  $J = 7.6$  Hz, 1H), 3.17-3.06 (m, 2H), 2.45 (dd,  $J = 17.2, 6.8$  Hz, 1H), 2.29 (dd,  $J = 17.2, 6.0$  Hz, 1H), 1.76 (heptet,  $J = 6.4$  Hz, 1H), 1.30-1.17 (m, 7H), 0.78 (t,  $J = 7.6$  Hz, 6H) ppm.

**Ethyl 2-(3-chlorobenzyl)-3-oxooctanoate (4ha).** Synthesis according to general procedure 2. Reagents: Ethyl 3-oxooctanoate **1h** (0.560 g, 3.01 mmol, 1.00 eq.), 3-chlorobenzyl bromide **3a** (0.470 mL, 3.57 mmol, 1.18 eq.), DIPEA (1.05 mL, 6.00 mmol, 1.99 eq.), LiCl (0.130 g, 3.00 mmol, 1.00 eq.), 5 mL dry THF. Yield: 21% (0.197 g) as a yellow oil.  $^1\text{H}$  NMR (400 MHz,  $\text{CDCl}_3$ )  $\delta$  7.22-7.15 (m, 3H), 7.07-7.04 (m, 1H), 4.15 (q,  $J = 7.2$  Hz, 2H), 3.75 (t,  $J = 7.6$  Hz, 1H), 3.17-3.07 (m, 2H), 2.54 (dt,  $J = 17.2, 7.2$  Hz, 1H), 2.36 (dt,  $J = 17.2, 7.2$  Hz, 1H), 1.52 (pentet,  $J = 7.4$  Hz, 2H), 1.31-1.13 (m, 7H), 0.86 (t,  $J = 7.2$  Hz, 3H) ppm.

**Ethyl 2-(3-chlorobenzyl)-3-cyclopentyl-3-oxopropanoate (4ia).**<sup>22</sup> Synthesis according to general procedure 2. Reagents: Ethyl 3-cyclopentyl-3-oxopropanoate **1i** (0.376 g, 2.04 mmol, 1.00 eq.), 3-chlorobenzyl bromide **3a** (0.240 mL, 1.83 mmol, 0.888 eq.), DIPEA (0.530 mL, 3.03 mmol, 1.47 eq.), LiCl (0.067 g, 1.57 mmol, 0.772 eq.), 5 mL dry THF. Silica column chromatography (20-50%  $\text{CH}_2\text{Cl}_2$ /Petroleum ether). Yield: 85% (0.483 g) as a colourless oil.  $^1\text{H}$  NMR (400 MHz,  $\text{CDCl}_3$ )  $\delta$  7.20-7.15 (m, 3H), 7.08-7.02 (m, 1H), 4.13 (q,  $J = 7.2$  Hz, 2H), 3.85 (t,  $J = 7.6$  Hz, 1H), 3.15-3.05 (m, 2H), 2.94 (pentet,  $J = 8.0$  Hz, 1H), 1.87-1.35 (m, 8H), 1.20 (t,  $J = 7.2$  Hz, 3H) ppm.

**Ethyl 2-(3-chlorobenzyl)-3-oxononanoate (4ja).** Synthesis according to general procedure 2. Reagents: Ethyl 3-oxononanoate **1j** (0.601 g, 3.00 mmol, 1.00 eq.), 3-chlorobenzyl bromide **3a** (0.325 mL, 2.48 mmol, 0.825 eq.), DIPEA (1.05 mL, 6.00 mmol, 2.00 eq.), LiCl (0.130 g, 3.00 mmol, 1.00 eq.), 5 mL dry THF. Yield: 97% (0.780 g) as a colourless oil.  $^1\text{H}$  NMR (400 MHz,  $\text{CDCl}_3$ )  $\delta$  7.20-7.15 (m, 3H), 7.07-7.01 (m, 1H), 4.14 (q,  $J = 6.8$  Hz, 2H), 3.75 (t,  $J = 7.6$  Hz, 1H), 3.17-3.06 (m, 2H), 2.53 (dt,  $J = 17.6, 7.2$  Hz, 1H), 2.35 (dt,  $J = 17.6, 7.2$  Hz, 1H), 1.50 (pentet,  $J = 7.2$  Hz, 2H), 1.30-1.15 (m, 9H), 0.85 (t,  $J = 7.2$  Hz, 3H) ppm.

**Ethyl 2-(3-chlorobenzyl)-3-oxodecanoate (4ka).** Synthesis according to general procedure 2. Reagents: Ethyl 3-oxodecanoate **1k** (0.650 g, 3.03 mmol, 1.00 eq.), 3-chlorobenzyl bromide **3a** (0.475 mL, 3.60 mmol, 1.20 eq.), DIPEA (1.05 mL, 6.00 mmol, 2.00 eq.), LiCl (0.128 g, 3.00 mmol, 1.00 eq.), 5 mL dry THF. Yield: 50% (0.511 g) as a yellow oil.  $^1\text{H}$  NMR (400 MHz,  $\text{CDCl}_3$ )  $\delta$  7.21-7.16 (m, 3H),

7.07-7.04 (m, 1H), 4.15 (q,  $J = 7.2$  Hz, 2H), 3.75 (t,  $J = 7.6$  Hz, 1H), 3.18-3.06 (m, 2H), 2.54 (dt,  $J = 17.6$ , 7.2 Hz, 1H), 2.36 (dt,  $J = 17.6$ , 7.6 Hz, 1H), 1.51 (pentet,  $J = 6.8$  Hz, 2H), 1.31-1.17 (m, 11H), 0.87 (t,  $J = 6.8$  Hz, 3H) ppm.

**Ethyl 2-(3-chlorobenzyl)-3-oxo-3-phenylpropanoate (4la).**<sup>22</sup> Synthesis according to general procedure 2. Reagents: Ethyl 3-oxo-3-phenylpropanoate **1l** (0.498 mL, 2.92 mmol, 1.20 eq.), 3-chlorobenzyl bromide **3a** (0.320 mL, 2.43 mmol, 1.00 eq.), DIPEA (0.847 mL, 4.86, 2.00 eq.), LiCl (103 mg; 2.43 mmol, 1.00 eq.), 5 mL dry THF. Yield: 85% (686 mg) as a colourless oil. <sup>1</sup>H NMR (400 MHz, CDCl<sub>3</sub>):  $\delta$  7.92 (dd,  $J = 8.0$ , 0.8, 2H), 7.46 (td,  $J = 7.6$ , 1.2 Hz, 1H), 7.35 (t,  $J = 7.6$  Hz, 2H), 7.20 (s, 1H), 7.10-7.05 (m, 3H), 4.62 (t,  $J = 7.2$  Hz, 1H), 4.05-3.95 (m, 2H), 3.31-3.20 (m, 2H), 1.01 (t,  $J = 7.2$ , 0.8 Hz, 3H) ppm.

**Ethyl 2-(3-chlorobenzyl)-3-oxo-3-(*p*-tolyl)propanoate (4ma).** Synthesis according to general procedure 2. Reagents: Ethyl 3-oxo-3-(*p*-tolyl)propanoate **1m** (2.30 g, 11.15 mmol, 1.00 eq.), 3-chlorobenzyl bromide **3a** (2.29 mL, 11.15 mmol, 1.00 eq.), DIPEA (3.88 mL, 22.3 mmol, 2.00 eq.), LiCl (473 mg; 11.15 mmol, 1.00 eq.), 30 mL dry THF. Yield: 86% (3.18 g) as a white solid. <sup>1</sup>H NMR (400 MHz, CDCl<sub>3</sub>):  $\delta$  7.87 (d,  $J = 8.0$  Hz, 2H), 7.28-7.22 (m, 3H), 7.19-7.14 (m, 2H), 7.12-7.09 (m, 1H), 4.57 (t,  $J = 7.6$  Hz, 1H), 4.13-4.05 (m, 2H), 3.33-3.23 (m, 2H), 2.41 (s, 3H), 1.12 (t,  $J = 7.2$  Hz, 3H) ppm.

**Ethyl 2-(3-chlorobenzyl)-3-oxo-5-phenylpentanoate (4na).** Synthesis according to general procedure 2. Reagents: Ethyl 3-oxo-5-phenylpentanoate **1n** (0.661 g, 3.00 mmol, 1.00 eq.), 3-chlorobenzyl bromide **3a** (0.475 mL, 3.65 mmol, 1.20 eq.), DIPEA (1.05 mL, 6.00 mmol, 2.00 eq.), LiCl (0.128 g, 3.00 mmol, 1.00 eq.), 5 mL dry THF. Yield: 67% (0.690 g) as a white solid. <sup>1</sup>H NMR (400 MHz, CDCl<sub>3</sub>)  $\delta$  7.32-7.26 (m, 2H), 7.24-7.19 (m, 3H), 7.16 (t,  $J = 7.2$  Hz, 3H), 4.13 (q,  $J = 7.2$  Hz, 2H), 3.75 (t,  $J = 7.6$  Hz, 1H), 3.13 (d,  $J = 7.6$  Hz, 2H), 2.99-2.85 (m, 3H), 2.75-2.67 (m, 1H), 1.20 (t,  $J = 7.2$  Hz, 3H) ppm.

**Procedure for the synthesis of 6-(3-Chlorobenzyl)-5-cyclopropyl-[1,2,4]triazolo[1,5-a]pyrimidin-7(4H)-one (6).**<sup>22, 23</sup> In a sealed microwave tube 3-amino-1,2,4-triazole **5a** (66 mg, 0.78 mmol, 1.1 eq.), **4ba** (200 mg, 0.71 mmol, 1.00 eq.) and H<sub>3</sub>PO<sub>4</sub> (96  $\mu$ l, 1.42 mmol, 2.00 eq.) were heated at 170°C in 1 mL of EtOH in the microwave for 10 hours. The reaction mixture was poured in water (30 mL), the pH was adjusted to pH=12 (1M NaOH aq.) and the organics were extracted with EtOAc (3x 30 mL). The combined extracts were dried over MgSO<sub>4</sub> and the solvents evaporated in vacuo, resulting in 165 mg crude mixture. The pure product was obtained by column chromatography (5% CH<sub>3</sub>OH in CH<sub>2</sub>Cl<sub>2</sub>) followed by prep HPLC gradient 10-90% CH<sub>3</sub>CN/water+0.1%TFA yielding 4% (9 mg) as a white solid. <sup>1</sup>H NMR (400 MHz, CDCl<sub>3</sub>):  $\delta$  8.14 (s, 1H), 7.28-7.25 (m, 1H), 7.22-7.15 (m, 3H), 7.17-7.08 (m, 3H), 4.16 (s, 2H), 2.22-2.13 (m, 1H), 1.36-1.30 (m, 2H), 1.20-1.15 (m, 2H) ppm. LC-MS (ESI)  $m/z$  calcd for C<sub>15</sub>H<sub>13</sub>ClN<sub>4</sub>O [M+H]<sup>+</sup> 301.09, found 301.1. Purity by HPLC: 97%.

**Procedure for the synthesis of 6-(3-Chlorobenzyl)-5-cyclopropyl-2-methyl-[1,2,4]triazolo[1,5-a]pyrimidin-7(4H)-one (7).** In a sealed microwave tube 3-amino-5-methyl-1,2,4-triazole **5b** (126 mg, 1.28 mmol, 1.2 eq.), **4ba** (300 mg, 1.07 mmol, 1.0 eq.) and *p*-toluenesulfonic acid monohydrate (102 mg, 0.53 mmol, 0.5 eq.) were heated for 30 minutes at 180°C in the microwave. As visualised by TLC **4ba** was consumed and mainly one product was formed (Rf 0.5 in 5% CH<sub>3</sub>OH in CH<sub>2</sub>Cl<sub>2</sub>). The crude product was purified by column chromatography (3% CH<sub>3</sub>OH in CH<sub>2</sub>Cl<sub>2</sub>) yielding 31% (96 mg) as a white solid. <sup>1</sup>H NMR (400 MHz, CDCl<sub>3</sub> + drop MeOD):  $\delta$  7.23 (s, 1H), 7.21-7.13 (m, 3H), 6.26 (br s, 2H), 4.11 (s, 2H), 2.47 (s, 2H), 2.05-1.96 (m, 1H), 1.14-1.07 (m, 2H), 1.05-1.01 (m, 2H) ppm. LC-MS (ESI)  $m/z$  calcd for C<sub>16</sub>H<sub>15</sub>ClN<sub>4</sub>O [M+H]<sup>+</sup> 315.10, found 315.1. Purity by HPLC: 96%.



## General procedure 3. Triazolo-pyrimidinones 8-43.<sup>22</sup>

The synthesis of compounds **8-43** was according to the following procedure: In a microwave tube a mixture of the corresponding benzylated beta keto ester **4aa-na**, **4bb-bq**, **4eq-ev** (1.00 eq.), triazole **5c** (2.00 eq.) and 1-butyl-3-methylimidazolium hexafluorophosphate (BMIM-PF6, 1 mL or 6.00 eq.) was heated at 200 °C in a microwave reactor for an hour. Afterwards, the reaction was allowed to cool to room temperature and stirred in a mixture of CH<sub>2</sub>Cl<sub>2</sub> (30 mL), H<sub>2</sub>O (10 mL) and 5 - 10% aqueous citric acid (1 mL) for 20 - 30 min. The resulting mixture was filtered over a glass filter and the residue was washed with hot methanol. Finally, the precipitate was collected and dried *in vacuo* to yield the pure compounds.

**2-Amino-6-(3-chlorobenzyl)-5-cyclopropyl-[1,2,4]triazolo[1,5-a]pyrimidin-7(4H)-one (8).**<sup>22</sup> Synthesis according to general procedure 3. Reagents: 3,5-diamino-4*H*-1,2,4-triazole **5c** (216 mg, 2.18 mmol, 2.00 eq.), **4ba** (306 mg, 1.09 mmol, 1.00 eq.) and BMIM-PF6 (1.35 mL, 6.54 mmol, 6.00 eq.). Yield: 36% (125 mg) as a white solid. <sup>1</sup>H NMR (400 MHz, DMSO): δ 12.16 (br s, 1H), 7.35-7.24 (m, 2H), 7.24-7.14 (m, 2H), 6.24 (br s, 2H), 3.96 (s, 2H), 2.14-2.01 (m, 1H), 1.07-0.94 (m, 2H), 0.94-0.81 (m, 2H) ppm. LC-MS (ESI) *m/z* calcd for C<sub>15</sub>H<sub>14</sub>ClN<sub>5</sub>O [M+H]<sup>+</sup> 316.10, found 316.13. Purity by HPLC: 98%.

**2-Amino-6-benzyl-5-cyclopropyl-[1,2,4]triazolo[1,5-a]pyrimidin-7(4H)-one (9).** Synthesis according to general procedure 3. Reagents: 3,5-diamino-4*H*-1,2,4-triazole **5c** (276 mg, 2.84 mmol, 2.00 eq.), **4bb** (350 mg, 1.42 mmol, 1.00 eq.) and BMIM-PF6 (1.75 mL, 8.52 mmol, 6.00 eq.). Yield: 26% (105 mg) as a white solid. <sup>1</sup>H NMR (400 MHz, DMSO): δ 12.11 (br s, 1H), 7.26-7.20 (m, 4H), 7.17-7.10 (m, 1H), 6.20 (br s, 2H), 3.96 (s, 2H), 2.10-2.03 (m, 1H), 1.04-0.95 (m, 2H), 0.94-0.88 (m, 2H) ppm. LC-MS (ESI) *m/z* calcd for C<sub>15</sub>H<sub>15</sub>N<sub>5</sub>O [M+H]<sup>+</sup> 282.14, found 282.13. Purity by HPLC: 97%.

**2-Amino-5-cyclopropyl-6-(2-methylbenzyl)-[1,2,4]triazolo[1,5-a]pyrimidin-7(4H)-one (10).** Synthesis according to general procedure 3. Reagents: 3,5-diamino-4*H*-1,2,4-triazole **5c** (190 mg, 1.96 mmol, 2.00 eq.), **4bc** (255 mg, 0.98 mmol, 1.00 eq.) and BMIM-PF6 (1.21 mL, 5.88 mmol, 6.00 eq.). Yield: 32% (93 mg) as a white solid. <sup>1</sup>H NMR (400 MHz, DMSO): δ 12.17 (br s, 1H), 7.15 (d, *J* = 6.8 Hz, 1H), 7.08-6.99 (m, 2H), 6.81 (d, *J* = 6.8 Hz, 1H), 6.21 (br s, 2H), 3.86 (s, 2H), 2.36 (s, 3H), 1.90-1.81 (m, 1H), 1.04-0.94 (m, 2H), 0.88-0.81 (m, 2H) ppm. LC-MS (ESI) *m/z* calcd for C<sub>16</sub>H<sub>17</sub>N<sub>5</sub>O [M+H]<sup>+</sup> 296.15, found 296.13. Purity by HPLC: 98%.

**2-Amino-6-(2-chlorobenzyl)-5-cyclopropyl-[1,2,4]triazolo[1,5-a]pyrimidin-7(4H)-one (11).** Synthesis according to general procedure 3. Reagents: 3,5-diamino-4*H*-1,2,4-triazole **5c** (173 mg, 1.78 mmol, 2.00 eq.), **4bd** (250 mg, 0.89 mmol, 1.00 eq.) and BMIM-PF6 (1.01 mL, 5.34 mmol, 6.00 eq.). Yield: 37% (104 mg) as a white solid. <sup>1</sup>H NMR (400 MHz, DMSO): δ 12.14 (br s, 1H), 7.47-7.42 (m, 1H), 7.24-7.17 (m, 2H), 7.01-6.96 (m, 1H), 6.20 (br s, 2H), 4.00 (s, 2H), 1.90-1.80 (m, 1H), 0.99-0.93 (m, 2H), 0.89-0.80 (m, 2H) ppm. LC-MS (ESI) *m/z* calcd for C<sub>15</sub>H<sub>14</sub>ClN<sub>5</sub>O [M+H]<sup>+</sup> 316.10, found 316.13. Purity by HPLC: 95%.

**2-Amino-5-cyclopropyl-6-(2-methoxybenzyl)-[1,2,4]triazolo[1,5-a]pyrimidin-7(4H)-one (12).** Synthesis according to general procedure 3. Reagents: 3,5-diamino-4*H*-1,2,4-triazole **5c** (130 mg, 1.34 mmol, 2.00 eq.), **4be** (185 mg, 0.67 mmol, 1.00 eq.) and BMIM-PF6 (0.83 mL, 4.02 mmol, 6.00 eq.). Yield: 43% (89 mg) as a white solid. <sup>1</sup>H NMR (400 MHz, DMSO): δ 12.11 (br s, 1H), 7.15 (t, *J* = 6.0 Hz, 1H), 6.95 (d, *J* = 6.4 Hz, 1H), 6.86 (d, *J* = 5.6 Hz, 1H), 6.78 (t, *J* = 5.6 Hz, 1H), 6.18 (br s, 2H), 3.86 (s, 2H), 3.83 (s, 3H), 1.98-1.86 (m, 1H), 1.03-0.91 (m, 2H), 0.90-0.79 (m, 2H) ppm. LC-MS (ESI) *m/z* calcd for C<sub>16</sub>H<sub>17</sub>N<sub>5</sub>O<sub>2</sub> [M+H]<sup>+</sup> 312.15, found 312.2. Purity by HPLC: 98%.

**2-Amino-5-cyclopropyl-6-(3-methylbenzyl)-[1,2,4]triazolo[1,5-a]pyrimidin-7(4H)-one (13).** Synthesis according to general procedure 3. Reagents: 3,5-diamino-4H-1,2,4-triazole **5c** (216 mg, 2.22 mmol, 2.00 eq.), **4bf** (289 mg, 1.11 mmol, 1.00 eq.) and BMIM-PF6 (1.37 mL, 6.66 mmol, 6.00 eq.). Yield: 35% (114 mg) as a white solid. <sup>1</sup>H NMR (400 MHz, DMSO): δ 11.98 (br s, 1H), 7.12 (t, *J* = 7.6 Hz, 1H), 7.04 (s, 1H), 7.01 (d, *J* = 7.2 Hz, 1H), 6.95 (d, *J* = 7.2 Hz, 1H), 6.17 (br s, 2H), 3.91 (s, 2H), 2.23 (s, 3H), 2.10-2.00 (m, 1H), 1.04-0.94 (m, 2H), 0.94-0.83 (m, 2H) ppm. LC-MS (ESI) *m/z* calcd for C<sub>16</sub>H<sub>17</sub>N<sub>5</sub>O [M+H]<sup>+</sup> 296.15, found 296.13. Purity by HPLC: 97%

**2-Amino-5-cyclopropyl-6-(3-fluorobenzyl)-[1,2,4]triazolo[1,5-a]pyrimidin-7(4H)-one (14).** Synthesis according to general procedure 3. Reagents: 3,5-diamino-4H-1,2,4-triazole **5c** (190 mg, 1.92 mmol, 1.45 eq.), **4bg** (350 mg, 1.32 mmol, 1.00 eq.) and BMIM-PF6 (1.14 mL, 5.54 mmol, 4.19 eq.). Yield: 15% (61mg) as a white solid. <sup>1</sup>H NMR (400 MHz, DMSO): δ 7.40-7.20 (m, 1H), 7.16-6.85 (m, 3H), 5.81 (br s, 2H), 4.01 (s, 2H), 2.12-1.95 (m, 1H), 1.10-0.85 (m, 4H) ppm. LC-MS (ESI) *m/z* calcd for C<sub>15</sub>H<sub>14</sub>FN<sub>5</sub>O [M+H]<sup>+</sup> 300.13, found 300.1. Purity by HPLC 97%.

**2-Amino-6-(3-bromobenzyl)-5-cyclopropyl-[1,2,4]triazolo[1,5-a]pyrimidin-7(4H)-one (15).** Synthesis according to general procedure 3. Reagents: 3,5-diamino-4H-1,2,4-triazole **5c** (169 mg, 1.74 mmol, 2.00 eq.), **4bh** (283 mg, 0.87 mmol, 1.00 eq.) and BMIM-PF6 (1.07 mL, 5.22 mmol, 6.00 eq.). Yield: 43% (135 mg) as a white solid. <sup>1</sup>H NMR (400 MHz, DMSO): δ 12.21 (br s, 1H), 7.43 (s, 1H), 7.34 (d, *J* = 7.2 Hz, 1H), 7.25 (d, *J* = 7.6 Hz, 1H), 7.20 (t, *J* = 7.6 Hz, 1H), 6.26 (br s, 2H), 3.96 (s, 2H), 2.12-2.04 (m, 1H), 1.04-0.94 (m, 2H), 0.94-0.85 (m, 2H) ppm. LC-MS (ESI) *m/z* calcd for C<sub>15</sub>H<sub>14</sub>BrN<sub>5</sub>O [M+H]<sup>+</sup> 360.05, found 360.2. Purity by HPLC: 99%.

**2-Amino-5-cyclopropyl-6-(3-iodobenzyl)-[1,2,4]triazolo[1,5-a]pyrimidin-7(4H)-one (16).** Synthesis according to general procedure 3. Reagents: 3,5-diamino-4H-1,2,4-triazole **5c** (190 mg, 1.92 mmol, 2.32 eq.), **4bi** (320 mg, 0.86 mmol, 1.00 eq.) and BMIM-PF6 (1.14 mL, 4.25 mmol, 6.00 eq.). Yield: 26% (92 mg) as a white solid. <sup>1</sup>H NMR (400 MHz, DMSO): δ 12.18 (br s, 1H), 7.62 (s, 4H), 7.51 (d, *J* = 7.6 Hz, 1H), 7.25 (d, *J* = 7.6 Hz, 1H), 7.05 (t, *J* = 7.6 Hz, 1H), 6.22 (br s, 2H), 3.92 (s, 2H), 2.12-2.07 (m, 1H), 1.01-0.94 (m, 2H), 0.93-0.86 (m, 2H). LC-MS (ESI) *m/z* calcd for C<sub>15</sub>H<sub>14</sub>IN<sub>5</sub>O [M+H]<sup>+</sup> 408.03, found 408.1. Purity by HPLC: 96%.

**2-Amino-5-cyclopropyl-6-(3-methoxybenzyl)-[1,2,4]triazolo[1,5-a]pyrimidin-7(4H)-one (17).** Synthesis according to general procedure 3. Reagents: 3,5-diamino-4H-1,2,4-triazole **5c** (146 mg, 1.50 mmol, 2.00 eq.), **4bj** (207 mg, 0.75 mmol, 1.00 eq.), BMIM-PF6 (0.93 mL, 4.50 mmol, 6.00 eq.). Yield: 21% (48 mg) as a white solid. <sup>1</sup>H NMR (400 MHz, DMSO): δ 11.94 (br s, 1H), 7.15 (t, *J* = 8.0 Hz, 1H), 6.82-6.77 (m, 2H), 6.72 (d, *J* = 7.6 Hz, 1H), 6.16 (br s, 2H), 3.93 (s, 2H), 3.69 (s, 3H), 2.11-2.03 (m, 1H), 1.04-0.96 (m, 2H), 0.96-0.85 (m, 2H) ppm. LC-MS (ESI) *m/z* calcd for C<sub>16</sub>H<sub>17</sub>N<sub>5</sub>O<sub>2</sub> [M+H]<sup>+</sup> 312.15, found 312.13. Purity by HPLC: 96%.

**2-Amino-5-cyclopropyl-6-(3-(trifluoromethyl)benzyl)-[1,2,4]triazolo[1,5-a]pyrimidin-7(4H)-one (18).** Synthesis according to general procedure 3. Reagents: 3,5-diamino-4H-1,2,4-triazole **5c** (150 mg, 1.54 mmol, 2.00 eq.), **4bk** (242 mg, 0.77 mmol, 1.00 eq.) and BMIM-PF6 (0.95 mL, 4.62 mmol, 6.00 eq.). Yield 6% (17 mg) as a white solid. <sup>1</sup>H NMR (400 MHz, DMSO): δ 12.18 (br s, 1H), 7.61 (s, 1H), 7.57-7.46 (m, 3H), 6.24 (br s, 2H), 4.06 (s, 2H), 2.17-2.08 (m, 1H), 1.03-0.95 (m, 2H), 0.94-0.86 (m, 2H) ppm. LC-MS (ESI) *m/z* calcd for C<sub>16</sub>H<sub>14</sub>F<sub>3</sub>N<sub>5</sub>O [M+H]<sup>+</sup> 350.13, found 350.27. Purity by HPLC: 97%.

**2-Amino-5-cyclopropyl-6-(4-methylbenzyl)-[1,2,4]triazolo[1,5-a]pyrimidin-7(4H)-one (19).** Synthesis according to general procedure 3. Reagents: 3,5-diamino-4H-1,2,4-triazole **5c** (197 mg, 2.03 mmol, 2.00 eq.), **4bl** (266 mg, 1.02 mmol, 1.00 eq.) and BMIM-PF6 (1.25 mL, 6.09 mmol, 6.00 eq.). Yield: 39% (115 mg) as a white solid. <sup>1</sup>H NMR (400 MHz, DMSO): δ 12.06 (br s, 1H), 7.10 (d, *J* = 8.0 Hz, 2H), 7.03 (d, *J* = 8.0 Hz, 2H), 6.18 (br s, 2H), 3.90 (s, 2H), 2.23 (s, 3H), 2.08-2.01 (m, 1H), 1.01-0.94 (m, 2H), 0.94-0.87 (m, 2H) ppm. LC-MS (ESI) *m/z* calcd for C<sub>16</sub>H<sub>17</sub>N<sub>5</sub>O [M+H]<sup>+</sup> 296.15, found 296.13. Purity by HPLC: 97%.



**2-Amino-5-cyclopropyl-6-(4-fluorobenzyl)-[1,2,4]triazolo[1,5-a]pyrimidin-7(4H)-one (20).**

Synthesis according to general procedure 3. Reagents: 3,5-diamino-4*H*-1,2,4-triazole **5c** (150 mg, 1.51 mmol, 2.00 eq.), **4bm** (200 mg, 0.756 mmol, 1.00 eq.) and BMIM-PF6 (1.00 mL, 4.86 mmol, 6.39 eq.). Yield: 35% (79 mg) as a white solid. <sup>1</sup>H NMR (400 MHz, DMSO): δ 12.13 (s, 1H), 7.28 (dd, *J* = 9.6, 2.4 Hz, 2H), 7.07 (t, *J* = 8.8 Hz, 2H), 6.21 (s br, 2H), 3.95 (s, 2H), 2.15-2.02 (m, 1H), 1.05-0.85 (m, 4H) ppm. LC-MS (ESI) *m/z* calcd for C<sub>15</sub>H<sub>14</sub>FN<sub>5</sub>O [M+H]<sup>+</sup> 300.13, found 300.2. Purity by HPLC: 95%.

**2-Amino-6-(4-chlorobenzyl)-5-cyclopropyl-[1,2,4]triazolo[1,5-a]pyrimidin-7(4H)-one (21).**

Synthesis according to general procedure 3. Reagents: 3,5-diamino-4*H*-1,2,4-triazole **5c** (179 mg, 1.84 mmol, 2.00 eq.), **4bn** (258 mg, 0.92 mmol, 1.00 eq.) and BMIM-PF6 (1.14 mL, 5.52 mmol, 6.00 eq.). Yield: 33% (105 mg) as a white solid. <sup>1</sup>H NMR (400 MHz, DMSO): δ 12.18 (br s, 1H), 7.28 (d, *J* = 8.4 Hz, 2H), 7.25 (d, *J* = 8.4 Hz, 2H), 6.24 (br s, 2H), 3.94 (s, 2H), 2.10-2.00 (m, 1H), 1.04-0.94 (m, 2H), 0.93-0.81 (m, 2H) ppm. LC-MS (ESI) *m/z* calcd for C<sub>15</sub>H<sub>14</sub>ClN<sub>5</sub>O [M+H]<sup>+</sup> 316.10, found 316.13. Purity by HPLC: 96%.

**2-Amino-5-cyclopropyl-6-(4-bromobenzyl)-[1,2,4]triazolo[1,5-a]pyrimidin-7(4H)-one (22).**

Synthesis according to general procedure 3. Reagents: 3,5-diamino-4*H*-1,2,4-triazole **5c** (120 mg, 1.21 mmol, 2.00 eq.), **4bo** (200 mg, 0.615 mmol, 1.00 eq.) and BMIM-PF6 (1.00 mL, 4.86 mmol, 7.90 eq.). Yield: 21% (47 mg) as an off-white solid. <sup>1</sup>H NMR (400 MHz, DMSO): δ 12.15 (s, 1H), 7.42 (d, *J* = 8.4 Hz, 2H), 7.20 (d, *J* = 8.0 Hz, 2H), 6.24 (br s, 2H), 3.92 (s, 2H), 2.10-2.00 (m, 1H), 1.08-0.75 (m, 4H) ppm. LC-MS (ESI) *m/z* calcd for C<sub>15</sub>H<sub>14</sub>BrN<sub>5</sub>O [M+H]<sup>+</sup> 360.05, found 360.1. Purity by HPLC: 96%.

**2-amino-5-cyclopropyl-6-(4-methoxybenzyl)-[1,2,4]triazolo[1,5-a]pyrimidin-7(4H)-one (23).**

Synthesis according to general procedure 3. Reagents: 3,5-diamino-4*H*-1,2,4-triazole **5c** (165 mg, 1.70 mmol, 2.00 eq.), **4bp** (235 mg, 0.85 mmol, 1.00 eq.) and BMIM-PF6 (1.05 mL, 5.10 mmol, 6.00 eq.). Yield: 41% (109 mg) as a white solid. <sup>1</sup>H NMR (400 MHz, DMSO): δ 12.07 (br s, 1H), 7.15 (d, *J* = 8.4 Hz, 2H), 6.80 (d, *J* = 8.8 Hz, 2H), 6.19 (br s, 2H), 3.88 (s, 2H), 3.69 (s, 3H), 2.12-2.01 (m, 1H), 1.04-0.95 (m, 2H), 0.94-0.86 (m, 2H) ppm. LC-MS (ESI) *m/z* calcd for C<sub>16</sub>H<sub>17</sub>N<sub>5</sub>O<sub>2</sub> [M+H]<sup>+</sup> 312.15, found 312.07. Purity by HPLC: 96%.

**2-Amino-6-(3-chlorobenzyl)-5-methyl-[1,2,4]triazolo[1,5-a]pyrimidin-7(4H)-one (24).<sup>22</sup>**

Synthesis according to general procedure 3. Reagents: 3,5-diamino-4*H*-1,2,4-triazole **5c** (94 mg, 0.95 mmol, 2.00 eq.), **4aa** (120 mg, 0.47 mmol, 1.00 eq.) and BMIM-PF6 (0.58 mL, 2.82 mmol, 6.00 eq.). Yield: 57% (77 mg) as a white solid. <sup>1</sup>H NMR (400 MHz, DMSO): δ 12.56 (s, 1H), 7.30-7.21 (m, 3H), 7.17 (d, *J* = 7.2 Hz, 1H), 5.99 (s, 2H), 3.78 (s, 2H), 2.25 (s, 3H) ppm. LC-MS (ESI) *m/z* calcd for C<sub>13</sub>H<sub>12</sub>ClN<sub>5</sub>O [M+H]<sup>+</sup> 290.08, found 290.1. Purity by HPLC: 99%.

**2-Amino-6-(3-chlorobenzyl)-5-ethyl-[1,2,4]triazolo[1,5-a]pyrimidin-7(4H)-one (25).<sup>22</sup>**

Synthesis according to general procedure 3. Reagents: 3,5-diamino-4*H*-1,2,4-triazole **5c** (141 mg, 1.43 mmol, 2.00 eq.), **4ca** (192 mg, 0.71 mmol, 1.00 eq.) and BMIM-PF6 (0.88 mL, 4.28 mmol, 6.00 eq.). Yield: 21% (46 mg) as a white solid. <sup>1</sup>H NMR (500 MHz, DMSO): δ 12.57 (s, 1H) 7.29-7.51 (m, 2H), 7.22 (d, *J* = 8.0 Hz, 1H), 7.16 (d, *J* = 7.5 Hz, 1H), 6.02 (s, 2H), 3.81 (s, 2H), 2.57 (q, *J* = 7.5 Hz, 2H), 1.05 (t, *J* = 7.5 Hz, 3H) ppm. LC-MS (ESI) *m/z* calcd for C<sub>14</sub>H<sub>14</sub>ClN<sub>5</sub>O [M+H]<sup>+</sup> 304.10, found 304.2. Purity by HPLC: 95%.

**2-Amino-6-(3-chlorobenzyl)-5-propyl-[1,2,4]triazolo[1,5-a]pyrimidin-7(4H)-one (26).<sup>22</sup>**

Synthesis according to general procedure 3. Reagents: 3,5-diamino-4*H*-1,2,4-triazole **5c** (210 mg, 2.12 mmol, 2.00 eq.), **4da** (300 mg, 1.06 mmol, 1.00 eq.) and BMIM-PF6 (1.31 mL, 6.36 mmol, 6.00 eq.). Yield: 22% (76 mg) as a white solid. <sup>1</sup>H NMR (400 MHz, DMSO): δ 12.56 (s, 1H), 7.29-7.20 (m, 3H), 7.16 (d, *J* = 7.6 Hz, 1H), 6.01 (s, 2H), 3.81 (s, 2H), 2.53 (t, *J* = 7.6 Hz, 2H), 1.45 (sextet, *J* = 7.6 Hz, 2H), 0.85 (t, *J* = 7.2 Hz, 3H) ppm. LC-MS (ESI) *m/z* calcd for C<sub>15</sub>H<sub>16</sub>ClN<sub>5</sub>O [M+H]<sup>+</sup> 318.11, found 318.2. Purity by HPLC: 99%.

**2-Amino-6-(3-chlorobenzyl)-5-isopropyl-[1,2,4]triazolo[1,5-a]pyrimidin-7(4H)-one (27).<sup>22</sup>**

Synthesis according to general procedure 3. Reagents: 3,5-diamino-4*H*-1,2,4-triazole **5c** (284 mg, 2.87 mmol, 2.00 eq.), **1ea** (407 mg, 1.44 mmol, 1.00 eq.) and BMIM-PF6 (1.76 mL, 8.63 mmol, 6.00 eq.). Yield: 21% (96 mg) as a white solid. <sup>1</sup>H NMR (400 MHz, DMSO): δ 12.33 (s, 1H), 7.28 (t, *J* = 8.0 Hz, 1H),

7.35 (s, 1H), 7.21 (d,  $J = 8.0$  Hz, 1H), 7.14 (d,  $J = 7.6$  Hz, 1H), 6.04 (s, 2H) 3.89 (s, 2H), 3.18 (septet,  $J = 6.8$  Hz, 1H), 1.12 (d,  $J = 6.8$  Hz, 6H) ppm. LC-MS (ESI)  $m/z$  calcd for  $C_{15}H_{16}ClN_5O$   $[M+H]^+$  318.11, found 318.2. Purity by HPLC: 99%.

**2-Amino-5-butyl-6-(3-chlorobenzyl)-[1,2,4]triazolo[1,5-a]pyrimidin-7(4H)-one (28).<sup>22</sup>**

Synthesis according to general procedure 3. Reagents: 3,5-diamino-4H-1,2,4-triazole **5c** (250 mg, 1.51 mmol, 2.14 eq.), **1fa** (210 mg, 0.708 mmol, 1.00 eq.) and BMIM-PF6 (1.00 mL, 4.86 mmol, 6.86 eq.). Yield: 20% (47 mg) as a white solid. Purity: 98%. <sup>1</sup>H NMR (400 MHz, DMSO)  $\delta$  12.54 (s, 1H), 7.33-7.19 (m, 3H), 7.16 (d,  $J = 7.3$  Hz, 1H), 6.02 (s, 2H), 3.82 (s, 2H), 2.60-2.50 (m, 2H), 1.45-1.32 (m, 2H), 1.32-1.20 (m, 2H), 0.81 (t,  $J = 7.1$  Hz, 3H) ppm. LC-MS (ESI)  $m/z$  calcd for  $C_{16}H_{18}ClN_5O$   $[M+H]^+$  332.13, found 332.3. Purity by HPLC: 98%.

**2-Amino-6-(3-chlorobenzyl)-5-(2-ethylbutyl)-[1,2,4]triazolo[1,5-a]pyrimidin-7(4H)-one (29).**

Synthesis according to general procedure 3. Reagents: 3,5-diamino-4H-1,2,4-triazole **5c** (130 mg, 1.31 mmol, 2.13 eq.), **4ga** (200 mg, 0.616 mmol, 1.00 eq.) and BMIM-PF6 (1.00 mL, 4.86 mmol, 7.89 eq.) Yield: 9% (20 mg) as a white solid. <sup>1</sup>H NMR (400 MHz, DMSO):  $\delta$  12.49 (br s, 1H), 7.28 (t,  $J = 7.2$  Hz, 1H), 7.24-7.18 (m, 2H), 7.14 (d,  $J = 7.2$  Hz, 1H), 5.91 (br s, 2H), 3.82 (s, 2H), 1.58 (s, 2H), 1.30-1.15 (m, 5H), 0.77 (t,  $J = 6.8$  Hz, 6H) ppm. LC-MS (ESI)  $m/z$  calcd for  $C_{18}H_{22}ClN_5O$   $[M+H]^+$  360.16, found 360.3. Purity by HPLC: 97%.

**2-Amino-6-(3-chlorobenzyl)-5-pentyl-[1,2,4]triazolo[1,5-a]pyrimidin-7(4H)-one (30).**

Synthesis according to general procedure 3. Reagents: 3,5-diamino-4H-1,2,4-triazole **5c** (120 mg, 1.21 mmol, 1.88 eq.), **4ha** (200 mg, 0.643 mmol; 1.00 eq.) and BMIM-PF6 (1.00 mL, 4.86 mmol, 7.56 eq.). Yield: 24% (52 mg) as a white solid. <sup>1</sup>H NMR (400 MHz, DMSO):  $\delta$  12.43 (br s, 1H), 7.35-7.10 (m, 4H), 6.02 (br s, 2H), 3.82 (s, 2H), 1.45-1.15 (m, 6H), 0.79 (s, 3H) ppm. LC-MS (ESI)  $m/z$  calcd for  $C_{17}H_{20}ClN_5O$   $[M+H]^+$  346.15, found 346.2. Purity by HPLC: 98%.

**2-Amino-6-(3-chlorobenzyl)-5-cyclopentyl-[1,2,4]triazolo[1,5-a]pyrimidin-7(4H)-one (31).**

Synthesis according to general procedure 3. Reagents: 3,5-diamino-4H-1,2,4-triazole **5c** (130 mg, 1.31 mmol, 2.00 eq.), **4ia** (200 mg, 0.647 mmol, 1.00 eq.) and BMIM-PF6 (1.00 mL, 4.86 mmol, 7.51 eq.). Yield: 38% (86 mg) as a white solid. <sup>1</sup>H NMR (400 MHz, DMSO):  $\delta$  12.36 (br s, 1H), 7.38-7.07 (m, 4H), 6.07 (br s, 2H), 3.90 (s, 2H), 3.23 (m, 1H), 1.90-1.45 (m, 8H) ppm. LC-MS (ESI)  $m/z$  calcd for  $C_{17}H_{18}ClN_5O$   $[M+H]^+$  344.13, found 344.1. Purity by HPLC: 99%.

**2-Amino-6-(3-chlorobenzyl)-5-hexyl-[1,2,4]triazolo[1,5-a]pyrimidin-7(4H)-one (32).**

Synthesis according to general procedure 3. Reagents: 3,5-diamino-4H-1,2,4-triazole **5c** (86 mg, 0.86 mmol, 2.00 eq.), **4ja** (140 mg, 0.431 mmol, 1.00 eq.) and BMIM-PF6 (1.00 mL, 4.86 mmol, 11.3 eq.). Yield: 83% (128 mg) as a white solid. <sup>1</sup>H NMR (400 MHz, DMSO):  $\delta$  12.50 (s, 1H), 7.33-7.19 (m, 3H), 7.15 (d,  $J = 6.8$  Hz, 1H), 6.02 (s, 2H), 3.82 (s, 2H), 2.60-2.40 (m, 2H), 1.44-1.32 (m, 2H), 1.30-1.08 (m, 6H), 0.82 (t,  $J = 6.5$  Hz, 3H) ppm. LC-MS (ESI)  $m/z$  calcd for  $C_{18}H_{22}ClN_5O$   $[M+H]^+$  360.16, found 360.3. Purity by HPLC: 97%.

**2-Amino-6-(3-chlorobenzyl)-5-heptyl-[1,2,4]triazolo[1,5-a]pyrimidin-7(4H)-one (33).**

Synthesis according to general procedure 3. Reagents: 3,5-diamino-4H-1,2,4-triazole **5c** (116 mg, 1.18 mmol, 2.00 eq.), **4ka** (200 mg, 0.591 mmol, 1.00 eq.) and BMIM-PF6 (1.00 mL, 4.86 mmol, 8.22 eq.). Yield: 50% (108 mg) as a white solid. <sup>1</sup>H NMR (400 MHz, DMSO):  $\delta$  12.55 (s, 1H), 7.30-7.19 (m, 3H), 7.15 (d,  $J = 6.4$  Hz, 1H), 6.01 (s, 1H), 3.82 (s, 2H), 1.46-1.32 (m, 2H), 1.27-1.10 (m, 8H), 0.83 (t,  $J = 6.4$  Hz, 3H) ppm. LC-MS (ESI)  $m/z$  calcd for  $C_{19}H_{24}ClN_5O$   $[M+H]^+$  374.18, found 374.3. Purity by HPLC: 98%.

**2-Amino-6-(3-chlorobenzyl)-5-phenyl-[1,2,4]triazolo[1,5-a]pyrimidin-7(4H)-one (34).**

Synthesis according to general procedure 3. Reagents: 3,5-diamino-4H-1,2,4-triazole **5c** (177 mg, 1.79 mmol, 2.00 eq.), **4la** (296 mg, 0.89 mmol, 1.00 eq.) and BMIM-PF6 (1.11 mL, 5.36 mmol, 6.00 eq.). Yield: 30% (95 mg) as a white solid. <sup>1</sup>H NMR (500 MHz, DMSO):  $\delta$  12.83 (s, 1H), 7.53-7.47 (m, 3H), 7.42 (dd,  $J = 8.0, 1.5$  Hz, 2H), 7.20 (t,  $J = 8.0$  Hz, 1H), 7.17 (d,  $J = 7.0$  Hz, 1H), 7.03 (s, 1H), 6.94 (d,  $J = 7.0$  Hz, 1H), 6.12 (s, 2H), 3.64 (s, 2H) ppm. LC-MS (ESI)  $m/z$  calcd for  $C_{18}H_{14}ClN_5O$   $[M+H]^+$  352.10, found 352.2.

Purity by HPLC: 99%

**2-Amino-6-(3-chlorobenzyl)-5-(p-tolyl)-[1,2,4]triazolo[1,5-a]pyrimidin-7(4H)-one (35).**

Synthesis according to general procedure 3. Reagents: 3,5-diamino-4*H*-1,2,4-triazole **5c** (181 mg, 1.82 mmol, 2.00 eq.), **4ma** (314 mg, 0.937 mmol, 1.00 eq.) and BMIM-PF<sub>6</sub> (1.5 mL, 7.28 mmol, 7.77 eq.). Yield: 33% (108 mg) as a white solid. <sup>1</sup>H NMR (400 MHz, DMSO): δ 12.80 (s, 1H), 7.33-7.28 (m, 4H), 7.26-7.14 (m, 2H), 7.05 (s, 1H), 6.96 (d, *J* = 7.1 Hz, 1H), 6.11 (s, 2H), 3.64 (s, 2H), 2.36 (s, 3H) ppm. LC-MS (ESI) *m/z* calcd for C<sub>19</sub>H<sub>16</sub>ClN<sub>5</sub>O [M+H]<sup>+</sup> 366.20, found 366.2. Purity by HPLC: 98%.

**Procedure for the synthesis of 2-Amino-6-(3-chlorobenzyl)-5-phenethyl-[1,2,4]triazolo[1,5-a]pyrimidin-7(4H)-one (36).** A mixture of **4na** (213 mg, 0.57 mmol, 1.00 eq.), 3,5-diamino-4*H*-1,2,4-triazole **5c** (116 mg, 1.16 mmol, 2.00 eq.) and ortho-phosphoric acid 85% (59.6 μL, 0.906 mmol, 1.58 eq.) in EtOH (1 mL) was stirred for 1 minute at 20°C and then heated at 175°C under microwave irradiation for 3 hours. The reaction mixture was allowed to cool to room temperature and CH<sub>2</sub>Cl<sub>2</sub> (30 mL), water (10 mL) and aqueous citric acid (5%, 1 mL) was added. The resulting precipitate was stirred for 20 min, filtered and the residue was washed with hot methanol, collected and dried in vacuo to afford the title compound. Yield: 22% (49 mg) as a white solid. <sup>1</sup>H NMR (400 MHz, DMSO): δ 12.67 (s, 1H), 7.32-7.18 (m, 6H), 7.17-7.10 (m, 3H), 6.06 (br s, 2H), 3.76 (s, 2H), 2.84-2.78 (m, 2H), 2.70-2.66 (m, 2H) ppm. LC-MS (ESI) *m/z* calcd for C<sub>20</sub>H<sub>18</sub>ClN<sub>5</sub>O [M+H]<sup>+</sup> 380.13, found 380.2. Purity by HPLC: 97%.

**2-Amino-5-cyclopropyl-6-(3,4-dichlorobenzyl)-[1,2,4]triazolo[1,5-a]pyrimidin-7(4H)-one (37).**<sup>22</sup> Synthesis according to general procedure 3. Reagents: 3,5-diamino-4*H*-1,2,4-triazole **5c** (157 mg, 1.58 mmol, 2.00 eq.), **4bq** (250 mg, 0.79 mmol, 1.00 eq.) and BMIM-PF<sub>6</sub> (1.3 mL, 4.74 mmol, 6.00 eq.). Yield: 31% (86 mg) as a white solid. <sup>1</sup>H NMR (400 MHz, DMSO): δ 12.26 (br s, 1H), 7.52-7.47 (m, 2H), 7.22 (d, *J* = 8.4 Hz, 2H), 6.26 (br s, 2H), 3.95 (s, 2H), 2.12-2.01 (m, 1H), 1.01-0.85 (m, 4H) ppm. LC-MS (ESI) *m/z* calcd for C<sub>15</sub>H<sub>13</sub>Cl<sub>2</sub>N<sub>5</sub>O [M+H]<sup>+</sup> 350.06, found 350.1. Purity by HPLC: 96%.

**2-Amino-6-(3,4-dichlorobenzyl)-5-isopropyl-[1,2,4]triazolo[1,5-a]pyrimidin-7(4H)-one (38).** Synthesis according to general procedure 3. Reagents: 3,5-diamino-4*H*-1,2,4-triazole **5c** (125 mg, 1.26 mmol, 2.00 eq.), **4eq** (200 mg, 0.63 mmol, 1.00 eq.) and BMIM-PF<sub>6</sub> (1.00 mL, 4.86 mmol, 7.71 eq.). Yield: 34% (76 mg), as a white solid. <sup>1</sup>H NMR (400 MHz, DMSO): δ 12.23 (br s, 1H), 7.54-7.43 (m, 2H), 7.17 (d, *J* = 8.0 Hz, 1H), 6.09 (s, 2H), 3.88 (s, 2H), 3.22-3.13 (m, 1H), 1.12 (d, *J* = 6.4 Hz, 6H) ppm. LC-MS (ESI) *m/z* calcd for C<sub>15</sub>H<sub>15</sub>Cl<sub>2</sub>N<sub>5</sub>O [M+H]<sup>+</sup> 352.08, found 352.3. Purity by HPLC: 97%.

**2-Amino-6-(2,3-dichlorobenzyl)-5-isopropyl-[1,2,4]triazolo[1,5-a]pyrimidin-7(4H)-one (39).** Synthesis according to general procedure 3. Reagents: 3,5-diamino-4*H*-1,2,4-triazole **5c** (125 mg, 1.26 mmol, 2.00 eq.), **4er** (200 mg, 0.630 mmol, 1.00 eq.) and BMIM-PF<sub>6</sub> (1.00 mL, 4.86 mmol, 7.71 eq.). Yield: 48% (106 mg) as a white solid. <sup>1</sup>H NMR (400 MHz, DMSO): δ 12.27 (br s, 1H), 7.49 (dd, *J* = 8.0, 1.6 Hz, 1H), 7.21 (t, *J* = 8.0 Hz, 1H), 6.96 (d, *J* = 7.2 Hz, 1H), 3.93 (s, 2H), 2.93 (septet, *J* = 6.8 Hz, 1H), 1.14 (d, *J* = 6.8 Hz, 6H) ppm. LC-MS (ESI) *m/z* calcd for C<sub>15</sub>H<sub>15</sub>Cl<sub>2</sub>N<sub>5</sub>O [M+H]<sup>+</sup> 352.08, found 352.2. Purity by HPLC: 97%.

**2-Amino-6-(2,5-dichlorobenzyl)-5-isopropyl-[1,2,4]triazolo[1,5-a]pyrimidin-7(4H)-one (40).** Synthesis according to general procedure 3. Reagents: 3,5-diamino-4*H*-1,2,4-triazole **5c** (125 mg, 1.26 mmol, 2.00 eq.), **4es** (200 mg, 0.630 mmol, 1.00 eq.) and BMIM-PF<sub>6</sub> (1.00 mL, 4.86 mmol, 7.71 eq.). Yield: 24% (54 mg) as a white solid. <sup>1</sup>H NMR (400 MHz, DMSO): δ 12.41 (br s, 1H), 7.70-7.42 (m, 1H), 7.40-7.19 (m, 1H), 7.16-6.85 (m, 1H), 6.08 (br s, 2H), 3.88 (s, 2H), 3.01-2.83 (m, 1H), 1.14 (s, 6H) ppm. LC-MS (ESI) *m/z* calcd for C<sub>15</sub>H<sub>15</sub>Cl<sub>2</sub>N<sub>5</sub>O [M+H]<sup>+</sup> 352.08, found 352.2. Purity by HPLC: 96%.

**2-amino-6-(3,5-dichlorobenzyl)-5-isopropyl-[1,2,4]triazolo[1,5-a]pyrimidin-7(4H)-one (41).** Synthesis according to general procedure 3. Reagents: 3,5-diamino-4*H*-1,2,4-triazole **5c** (96 mg, 0.97 mmol, 2 eq.), **4et** (153 mg, 0.48 mmol, 1.00 eq.) and BMIM-PF<sub>6</sub> (1.00 mL, 4.86 mmol, 10 eq.) Yield: 18% (31 mg) as a white solid. <sup>1</sup>H NMR (400 MHz, DMSO): δ 12.33 (s, 1H), 7.41 (s, 1H), 7.26 (s, 2H), 6.07 (br s, 2H), 3.89 (s, 2H), 1.13 (s, 6H) ppm. LC-MS (ESI) *m/z* calcd for C<sub>15</sub>H<sub>15</sub>Cl<sub>2</sub>N<sub>5</sub>O [M+H]<sup>+</sup> 352.08, found 352.1. Purity by HPLC: 98%.

**2-Amino-6-(3,5-dibromobenzyl)-5-isopropyl-[1,2,4]triazolo[1,5-a]pyrimidin 7(4H)-one (42).** Synthesis according to general procedure 3. Reagents: 3,5-diamino-4*H*-1,2,4-triazole **5c** (97 mg, 0.98 mmol, 2.00 eq.), **4eu** (200 mg, 0.49 mmol, 1.00 eq.), and BMIM-PF<sub>6</sub> (1.00 mL, 4.86 mmol, 9.91 eq.). Yield: 7% (14 mg) as a white solid. <sup>1</sup>H NMR (400 MHz, DMSO): δ 12.33 (br s, 1H), 7.63 (s, 1H), 7.42 (s, 2H), 6.07 (br s, 2H), 3.88 (s, 2H), 1.13 (s, 6H) ppm. LC-MS (ESI) *m/z* calcd for C<sub>15</sub>H<sub>15</sub>Br<sub>2</sub>N<sub>5</sub>O [M+H]<sup>+</sup> 439.97, found 440.1. Purity by HPLC: 98%.

**2-amino-6-(3-bromo-4-chloro-benzyl)-5-isopropyl-[1,2,4]triazolo[1,5-a]pyrimidin-7(4H)-one (43).** Synthesis according to general procedure 3. Reagents: 3,5-diamino-4*H*-1,2,4-triazole **5c** (109 mg, 1.10 mmol, 2.00 eq.), **4ev** (200 mg, 0.553 mmol, 1.00 eq.), and BMIM-PF<sub>6</sub> (1.00 mL, 4.86 mmol, 8.83 eq.). Yield: 24% (53 mg) as a white solid. <sup>1</sup>H NMR (400 MHz, DMSO): δ 7.60 (d, *J* = 2.0 Hz, 1H), 7.49 (d, *J* = 8.0 Hz, 1H), 7.21 (dd, *J* = 8.0, 2.0 Hz, 1H), 6.08 (br s, 2H), 3.87 (s, 2H), 3.22-3.11 (m, 1H), 1.12 (d, *J* = 7.2 Hz, 6H) ppm. LC-MS (ESI) *m/z* calcd for C<sub>15</sub>H<sub>15</sub>BrClN<sub>5</sub>O [M+H]<sup>+</sup> 396.02, found 396.1. Purity by HPLC: 98%.

## Biology

### Chemicals and reagents

The human recombinant chemokines CCL2 and CCL3 were purchased from PeproTech (Rocky Hill, NJ). TAK-779 was obtained from NIH AIDS reagent program (Germantown, MD, catalogue number 4983). All triazolo-pyrimidinone derivatives were synthesized in-house. Guanosine 5'-*O*-[gamma-thio]triphosphate ([<sup>35</sup>S]GTPγS) (specific activity 1250 Ci/mmol) was purchased from PerkinElmer (Waltham, MA), while [<sup>3</sup>H]-CCR2-RA-[*R*] (specific activity 59.6 Ci mmol<sup>-1</sup>) was custom-labelled by Vitrox (Placentia, CA). Bovine serum albumin was purchased from Sigma-Aldrich (St. Louis, MO). Bicinchoninic acid (BCA) and Pierce™ BCA protein assay kit were purchased from Pierce Biotechnology (Thermo Scientific, Rockford, IL). Tango™ U2OS cells stably expressing human CCR2b (U2OS-CCR2) or human CCR5 (U2OS-CCR5) were purchased from Invitrogen (Carlsbad, CA). All other chemicals were obtained from standard commercial sources.

### Cell culture

Both U2OS-CCR2b and U2OS-CCR5 cells were cultured in McCoy's 5A medium supplemented with 10% (v/v) fetal calf serum, 2 mM glutamine, 0.1 mM non-essential amino acids, 25 mM HEPES, 1 mM sodium pyruvate, 200 IU/mL penicillin, 200 μg/mL streptomycin, 100 μg/mL G418, 40-50 μg/mL hygromycin and 125 μg/mL zeocin. Cells were grown until 80% confluence and cultured twice-weekly on 10 or 15 cm Ø plates by trypsinization. Dialyzed fetal calf serum was used when culturing cells for functional assays or as a last step before membrane preparation.

## Membrane preparation


Membranes from U2OS-CCR2 or U2OS-CCR5 cells were prepared as previously described for CCR2.<sup>19</sup> Briefly, U2OS-CCR2 or U2OS-CCR5 cells were scraped from confluent 15 cm Ø plates using phosphate-buffered saline (PBS) and subsequently centrifuged at 3000 rpm for 5 minutes. Pellets were then resuspended in ice-cold Tris buffer (50 mM Tris-HCl, 5 mM MgCl<sub>2</sub>, pH 7.4) before homogenization with an Ultra Turrax homogenizer (IKA-Werke GmbH & Co. KG, Staufen, Germany). Membranes and cytosolic contents were separated using an Optima LE-80 K ultracentrifuge (Beckman Coulter, Inc., Fullerton, CA) at 31000 rpm for 20 minutes at 4 °C. After a second cycle of homogenization and centrifugation, the final pellet was resuspended and homogenized in ice-cold Tris buffer, aliquoted and stored at -80 °C. Finally, membrane protein concentrations were determined using a BCA protein determination assay, as described by the manufacturer (Pierce™ BCA protein assay kit).<sup>48</sup>

## [<sup>3</sup>H]-CCR2-RA-[R] binding assays

For [<sup>3</sup>H]-CCR2-RA-[R] displacement assays, U2OS-CCR2b membrane homogenates (15 - 20 µg of total protein) were incubated with ~6 nM [<sup>3</sup>H]-CCR2-RA-[R] and at least 6 increasing concentrations of competing ligand in a final volume of 100 µL assay buffer (50 mM Tris-HCl, 5 mM MgCl<sub>2</sub>, 0.1% CHAPS, pH 7.4). Ligands were diluted to the desired concentration with an HP D300 digital dispenser (Tecan, Giessen, The Netherlands). Total radioligand binding did not exceed 10% of the amount added to prevent ligand depletion, and nonspecific binding was determined using 10 µM CCR2-RA-[R]. After 2 hours at 25 °C, incubation was terminated by rapid filtration through a 96-well GF/B filterplate on a PerkinElmer FilterMate harvester, using ice-cold wash buffer (50 mM Tris-HCl buffer supplemented with 5 mM MgCl<sub>2</sub> and 0.05% CHAPS, pH 7.4). Filters were washed 10 times with ice-cold wash buffer, and subsequently dried at 55 °C for 30 min. After addition of 25 µl Microscint scintillation cocktail (PerkinElmer), the filter-bound radioactivity was measured by scintillation spectrometry using the P-E 2450 Microbeta<sup>2</sup> counter (PerkinElmer).

## Tango β-arrestin recruitment assay

β-arrestin recruitment was measured using the Tango™ CCR2-*bla* or CCR5-*bla* U2OS cell-based assay (Invitrogen) according to the manufacturer's protocol. Briefly, U2OS-CCR2b or U2OS-CCR5 cells were grown until approximately 80% confluence and detached by trypsinization. Cells were recovered by centrifugation at 1000 rpm for 5 minutes before resuspending in assay medium (FreeStyle™ Expression Medium, Invitrogen) to a density



of 10,000 cells per well and seeded into black-wall, clear-bottom, 384-well assay plates (Corning). For agonist assays, cells were exposed to increasing concentrations of CCL2 or CCL3, for CCR2 or CCR5 respectively, for 16 hours at 37 °C and 5% CO<sub>2</sub>. For antagonist assays, compounds were first diluted in assay medium containing a final dimethylsulfoxide (DMSO) concentration of 0.5% or lower. Cells were then pre-incubated with either 1 μM (for single-point inhibition experiments) or increasing concentrations of antagonist for 30 minutes at room temperature, before a 16 hour co-incubation with an EC<sub>80</sub> concentration of CCL2 (5 nM) or CCL3 (14 nM) at 37 °C and 5% CO<sub>2</sub>. After 16h cells were loaded in the dark with 8 μl of LiveBLAzer™-FRET B/G substrate (Invitrogen) and incubated for 2 hours at room temperature. Finally, fluorescence emission at 460 nm and 535 nm was measured in an EnVision multilabel plate reader (PerkinElmer) after excitation at 400 nm. The ratio of emission at 460 and 535 nm was calculated for each well.

## [<sup>35</sup>S]GTPγS binding assay

To determine the mechanism of inhibition [<sup>35</sup>S]GTPγS binding assays were performed. In CCR2 the [<sup>35</sup>S]GTPγS binding assay was performed as previously described.<sup>18,19</sup> In the case of CCR5 10 μg U2OS-CCR5 membranes with 0.25 mg/mL saponin were pre-incubated with 5 μM GDP, increasing concentrations of CCL3 and three different antagonist concentrations for 30 minutes at 25 °C. All dilutions were made in assay buffer containing 50 mM Tris-HCl (pH 7.4), 10 mM MgCl<sub>2</sub>, 10 mM NaCl, 1 mM EDTA, and 0.05% BSA. [<sup>35</sup>S]GTPγS (0.3 nM) was added and the mixture was co-incubated for an additional 90 minutes at 25 °C before harvesting. Incubation was stopped by dilution with ice-cold 50 mM Tris-HCl buffer with 5 mM MgCl<sub>2</sub>. Separation of bound and unbound radioligand was performed by rapid filtration through a 96-well GF/B filter plate as described in “[<sup>3</sup>H]-CCR2-RA-[R] binding assays”.

## Data analysis

All experiments were analyzed using non-linear regression curve fitting program Prism 7 (Graphpad, San Diego, CA). EC<sub>50</sub>, EC<sub>80</sub>, E<sub>max</sub> and IC<sub>50</sub> values from functional assays were obtained by nonlinear regression analysis. All values obtained are means ± S.E.M. of at least three separate experiments performed in duplicate, unless stated otherwise. For radioligand binding assays, K<sub>i</sub> values were determined using the Cheng-Prussoff equation using a K<sub>D</sub> of 6.3 nM for the radioligand.<sup>18</sup>

## Computational modelling

The inactive crystal structure of hCCR2b with BMS-681 and CCR2-RA-[R] (PDB: 5T1A)<sup>14</sup> was used as the basis for docking compound **43**. Docking was performed in the Schrodinger suite,<sup>49</sup> as previously described for the docking of CCR2-RA-[R].<sup>18</sup> Before docking, the CCR2b crystal structure was prepared by replacing the residues between L226<sup>5x62</sup> and R240<sup>6x32</sup>, which correspond to the M2 muscarinic acetylcholine receptor, with the CCR2b sequence using prime<sup>50-52</sup> and CCR5 as template (PDB ID: 4MBS).<sup>32</sup> Induced fit docking, with a substructure restraint on the right hand phenyl (R<sup>1</sup>, SMARTS: "c1ccccc1") was used to dock compound **43** in the hCCR2b model.<sup>53, 54</sup> Figures 4a and 4b were rendered using PyMOL.<sup>55</sup>



## REFERENCES

1. Bachelier, F.; Ben-Baruch, A.; Burkhardt, A. M.; Combadiere, C.; Farber, J. M.; Graham, G. J.; Horuk, R.; Sparre-Ulrich, A. H.; Locati, M.; Luster, A. D.; Mantovani, A.; Matsushima, K.; Murphy, P. M.; Nibbs, R.; Nomiyama, H.; Power, C. A.; Proudfoot, A. E.; Rosenkilde, M. M.; Rot, A.; Sozzani, S.; Thelen, M.; Yoshie, O.; Zlotnik, A. International union of basic and clinical pharmacology. LXXXIX. Update on the extended family of chemokine receptors and introducing a new nomenclature for atypical chemokine receptors. *Pharmacol. Rev.* **2014**, *66*, 1-79.
2. Lopez-Cotarelo, P.; Gomez-Moreira, C.; Criado-Garcia, O.; Sanchez, L.; Rodriguez-Fernandez, J. L. Beyond chemoattraction: multifunctionality of chemokine receptors in leukocytes. *Trends Immunol* **2017**, *38*, 927 - 941.
3. Schall, T. J.; Proudfoot, A. E. Overcoming hurdles in developing successful drugs targeting chemokine receptors. *Nat Rev Immunol* **2011**, *11*, 355-363.
4. Zweemer, A. J.; Toraskar, J.; Heitman, L. H.; IJzerman, A. P. Bias in chemokine receptor signalling. *Trends Immunol* **2014**, *35*, 243-252.
5. Koelink, P. J.; Overbeek, S. A.; Braber, S.; de Kruijff, P.; Folkerts, G.; Smit, M. J.; Kraneveld, A. D. Targeting chemokine receptors in chronic inflammatory diseases: an extensive review. *Pharmacol Ther* **2012**, *133*, 1-18.
6. White, G. E.; Iqbal, A. J.; Greaves, D. R. CC chemokine receptors and chronic inflammation—therapeutic opportunities and pharmacological challenges. *Pharmacol. Rev.* **2013**, *65*, 47-89.
7. Woollard, S. M.; Kanmogne, G. D. Maraviroc: a review of its use in HIV infection and beyond. *Drug Des. Devel. Ther.* **2015**, *9*, 5447-5468.
8. Horuk, R. Chemokine receptor antagonists: overcoming developmental hurdles. *Nat Rev Drug Discov* **2009**, *8*, 23-33.
9. Horuk, R. Promiscuous drugs as therapeutics for chemokine receptors. *Expert Rev. Mol. Med.* **2009**, *11*, e1.
10. Friedman, S. L.; Ratziu, V.; Harrison, S. A.; Abdelmalek, M. F.; Aithal, G. P.; Caballeria, J.; Francque, S.; Farrell, G.; Kowdley, K. V.; Craxi, A. A randomized, placebo-controlled trial of ceniciviroc for treatment of nonalcoholic steatohepatitis with fibrosis. *Hepatology* **2018**, *67*, 1754-1767.
11. Zhao, Q. Dual targeting of CCR2 and CCR5: therapeutic potential for immunologic and cardiovascular diseases. *J. Leukoc. Biol.* **2010**, *88*, 41-55.
12. Junker, A.; Kokornaczyk, A. K.; Strunz, A. K.; Wunsch, B. Selective and dual targeting of CCR2 and CCR5 receptors: a current overview. In *Chemokines: Chemokines and Their Receptors in Drug Discovery*, Tschammer, N., Ed. Springer International Publishing: Cham, 2015; pp 187-241.
13. Kothandan, G.; Gadhe, C. G.; Cho, S. J. Structural insights from binding poses of CCR2 and CCR5 with clinically important antagonists: a combined in silico study. *PLoS One* **2012**, *7*, e32864.
14. Zheng, Y.; Qin, L.; Ortiz Zacarias, N. V.; de Vries, H.; Han, G. W.; Gustavsson, M.; Dabros, M.; Zhao, C.; Cherney, R. J.; Carter, P.; Stamos, D.; Abagyan, R.; Cherezov, V.; Stevens, R. C.; IJzerman, A. P.; Heitman, L. H.; Tebben, A.; Kufareva, I.; Handel, T. M. Structure of CC chemokine receptor 2 with orthosteric and allosteric antagonists. *Nature* **2016**, *540*, 458-461.
15. Oswald, C.; Rappas, M.; Kean, J.; Dore, A. S.; Errey, J. C.; Bennett, K.; Deflorian, F.; Christopher, J. A.; Jazayeri, A.; Mason, J. S.; Congreve, M.; Cooke, R. M.; Marshall, F. H. Intracellular allosteric antagonism of the CCR9 receptor. *Nature* **2016**, *540*, 462-465.
16. Turner, M. D.; Nedjai, B.; Hurst, T.; Pennington, D. J. Cytokines and chemokines: at the crossroads of cell signalling and inflammatory disease. *Biochim Biophys Acta* **2014**, *1843*, 2563-2582.
17. Ortiz Zacarias, N. V.; Lenselink, E. B.; IJzerman, A. P.; Handel, T. M.; Heitman, L. H. Intracellular receptor modulation: novel approach to target GPCRs. *Trends Pharmacol Sci* **2018**, *39*, 547-559.



18. Ortiz Zacarías, N. V.; van Veldhoven, J. P. D.; Portner, L.; van Spronsen, E.; Ullo, S.; Veenhuizen, M.; van der Velden, W. J. C.; Zweemer, A. J. M.; Kreekel, R. M.; Oenema, K.; Lenselink, E. B.; Heitman, L. H.; IJzerman, A. P. Pyrrolone derivatives as intracellular allosteric modulators for chemokine receptors: selective and dual-targeting inhibitors of CC chemokine receptors 1 and 2. *J. Med. Chem.* **2018**, *61*, 9146-9161.
19. Zweemer, A. J.; Nederpelt, I.; Vrieling, H.; Hafith, S.; Doornbos, M. L.; de Vries, H.; Abt, J.; Gross, R.; Stamos, D.; Saunders, J.; Smit, M. J.; IJzerman, A. P.; Heitman, L. H. Multiple binding sites for small-molecule antagonists at the CC chemokine receptor 2. *Mol. Pharmacol.* **2013**, *84*, 551-561.
20. Zweemer, A. J.; Bunnik, J.; Veenhuizen, M.; Miraglia, F.; Lenselink, E. B.; Vilums, M.; de Vries, H.; Gibert, A.; Thiele, S.; Rosenkilde, M. M.; IJzerman, A. P.; Heitman, L. H. Discovery and mapping of an intracellular antagonist binding site at the chemokine receptor CCR2. *Mol. Pharmacol.* **2014**, *86*, 358-368.
21. Andrews, G.; Jones, C.; Wreggett, K. A. An intracellular allosteric site for a specific class of antagonists of the CC chemokine G protein-coupled receptors CCR4 and CCR5. *Mol. Pharmacol.* **2008**, *73*, 855-867.
22. Bengtsson, B. A.; Blackaby, W.; Cumming, J.; Faull, A. W.; Larsson, J.; Nash, I. A.; Oldham, K.; Pape, A. 4H-[1, 2, 4] Triazololo [5, 1-b] Pyrimidin-7-one Derivatives As CCR2b Receptor Antagonists. Patent WO 2011/114148-A1. **2011**.
23. Boyd, J. W.; Meo, P.; Higginbottom, M.; Simpson, I.; Mountford, D.; Savory, E. D. 7-Hydroxy-Pyrazolo [1,5-a] Pyrimidine Compounds And Their Use As CCR2 Receptor Antagonists. Patent WO 2012/041817-A1. **2012**.
24. Isberg, V.; de Graaf, C.; Bortolato, A.; Cherezov, V.; Katritch, V.; Marshall, F. H.; Mordalski, S.; Pin, J.-P.; Stevens, R. C.; Vriend, G.; Gloriam, D. E. Generic GPCR residue numbers – aligning topology maps while minding the gaps. *Trends Pharmacol. Sci.* **2015**, *36*, 22-31.
25. Baba, M.; Nishimura, O.; Kanzaki, N.; Okamoto, M.; Sawada, H.; Iizawa, Y.; Shiraishi, M.; Aramaki, Y.; Okonogi, K.; Ogawa, Y.; Meguro, K.; Fujino, M. A small-molecule, nonpeptide CCR5 antagonist with highly potent and selective anti-HIV-1 activity. *Proc. Natl. Acad. Sci. USA* **1999**, *96*, 5698-5703.
26. Thum, S.; Kokornaczyk, A. K.; Seki, T.; De Maria, M.; Ortiz Zacarias, N. V.; de Vries, H.; Weiss, C.; Koch, M.; Schepmann, D.; Kitamura, M.; Tschammer, N.; Heitman, L. H.; Junker, A.; Wunsch, B. Synthesis and biological evaluation of chemokine receptor ligands with 2-benzazepine scaffold. *Eur. J. Med. Chem.* **2017**, *135*, 401-413.
27. Corbisier, J.; Gales, C.; Huszagh, A.; Parmentier, M.; Springael, J. Y. Biased signaling at chemokine receptors. *J Biol Chem* **2015**, *290*, 9542-9554.
28. Prinz, H. Hill coefficients, dose-response curves and allosteric mechanisms. *J. Chem. Biol.* **2010**, *3*, 37-44.
29. Zou, D.; Zhai, H.-X.; Eckman, J.; Higgins, P.; Gillard, M.; Knerr, L.; Carre, S.; Pasau, P.; Collart, P.; Grassi, J. Novel, acidic CCR2 receptor antagonists: from hit to lead. *Lett. Drug. Des. Discov.* **2007**, *4*, 185-191.
30. Buntinx, M.; Hermans, B.; Goossens, J.; Moechars, D.; Gilissen, R. A.; Doyon, J.; Boeckx, S.; Coesemans, E.; Van Lommen, G.; Van Wauwe, J. P. Pharmacological profile of JNJ-27141491 [(S)-3-[3, 4-difluorophenyl]-propyl]-5-isoxazol-5-yl-2-thioxo-2, 3-dihydro-1H-imidazole-4-carboxyl acid methyl ester], as a noncompetitive and orally active antagonist of the human chemokine receptor CCR2. *J. Pharmacol. Exp. Ther.* **2008**, *327*, 1-9.
31. Vauquelin, G.; Szczuka, A. Kinetic versus allosteric mechanisms to explain insurmountable antagonism and delayed ligand dissociation. *Neurochem. Int.* **2007**, *51*, 254-260.
32. Tan, Q.; Zhu, Y.; Li, J.; Chen, Z.; Han, G. W.; Kufareva, I.; Li, T.; Ma, L.; Fenalti, G.; Li, J. Structure of the CCR5 chemokine receptor–HIV entry inhibitor maraviroc complex. *Science* **2013**, *341*, 1387-1390.
33. Salchow, K.; Bond, M. E.; Evans, S. C.; Press, N. J.; Charlton, S. J.; Hunt, P. A.; Bradley, M. E. A common intracellular allosteric binding site for antagonists of the CXCR2 receptor. *Br J Pharmacol* **2010**, *159*, 1429-1439.
34. Nicholls, D. J.; Tomkinson, N. P.; Wiley, K. E.; Brammall, A.; Bowers, L.; Grahames, C.; Gaw, A.; Meghani, P.; Shelton, P.; Wright, T. J.; Mallinder, P. R. Identification of a putative intracellular allosteric antagonist binding-site in the CXC chemokine receptors 1 and 2. *Mol. Pharmacol.* **2008**, *74*, 1193-1202.
35. Draper-Joyce, C. J.; Khoshouei, M.; Thal, D. M.; Liang, Y.-L.; Nguyen, A. T. N.; Furness, S. G. B.; Venugopal, H.; Baltos, J.-A.; Plitzko, J. M.; Danev, R.; Baumeister, W.; May, L. T.; Wootten, D.; Sexton, P. M.; Glukhova, A.; Christopoulos, A. Structure of the adenosine-bound human adenosine A1 receptor–Gi complex. *Nature* **2018**, *558*, 559-563.

36. Koehl, A.; Hu, H.; Maeda, S.; Zhang, Y.; Qu, Q.; Paggi, J. M.; Latorraca, N. R.; Hilger, D.; Dawson, R.; Matile, H.; Schertler, G. F. X.; Granier, S.; Weis, W. I.; Dror, R. O.; Manglik, A.; Skiniotis, G.; Kobilka, B. K. Structure of the  $\mu$ -opioid receptor–Gi protein complex. *Nature* **2018**, *558*, 547–552.
37. Kang, Y.; Kuybeda, O.; de Waal, P. W.; Mukherjee, S.; Van Eps, N.; Dutka, P.; Zhou, X. E.; Bartesaghi, A.; Erramilli, S.; Morizumi, T.; Gu, X.; Yin, Y.; Liu, P.; Jiang, Y.; Meng, X.; Zhao, G.; Melcher, K.; Ernst, O. P.; Kosiakoff, A. A.; Subramaniam, S.; Xu, H. E. Cryo-EM structure of human rhodopsin bound to an inhibitory G protein. *Nature* **2018**, *558*, 553–558.
38. Kang, Y.; Zhou, X. E.; Gao, X.; He, Y.; Liu, W.; Ishchenko, A.; Barty, A.; White, T. A.; Yefanov, O.; Han, G. W.; Xu, Q.; de Waal, P. W.; Ke, J.; Tan, M. H.; Zhang, C.; Moeller, A.; West, G. M.; Pascal, B. D.; Van Eps, N.; Caro, L. N.; Vishnivetskiy, S. A.; Lee, R. J.; Suino-Powell, K. M.; Gu, X.; Pal, K.; Ma, J.; Zhi, X.; Boutet, S.; Williams, G. J.; Messerschmidt, M.; Gati, C.; Zatsepin, N. A.; Wang, D.; James, D.; Basu, S.; Roy-Chowdhury, S.; Conrad, C. E.; Coe, J.; Liu, H.; Lisova, S.; Kupitz, C.; Grotjohann, I.; Fromme, R.; Jiang, Y.; Tan, M.; Yang, H.; Li, J.; Wang, M.; Zheng, Z.; Li, D.; Howe, N.; Zhao, Y.; Standfuss, J.; Diederichs, K.; Dong, Y.; Potter, C. S.; Carragher, B.; Caffrey, M.; Jiang, H.; Chapman, H. N.; Spence, J. C.; Fromme, P.; Weierstall, U.; Ernst, O. P.; Katritch, V.; Gurevich, V. V.; Griffin, P. R.; Hubbell, W. L.; Stevens, R. C.; Cherezov, V.; Melcher, K.; Xu, H. E. Crystal structure of rhodopsin bound to arrestin by femtosecond X-ray laser. *Nature* **2015**, *523*, 561–567.
39. Lagorce, D.; Douguet, D.; Miteva, M. A.; Villoutreix, B. O. Computational analysis of calculated physicochemical and ADMET properties of protein-protein interaction inhibitors. *Sci. Rep.* **2017**, *7*, 46277.
40. Lagorce, D.; Sperandio, O.; Baell, J. B.; Miteva, M. A.; Villoutreix, B. O. FAF-Drugs3: a web server for compound property calculation and chemical library design. *Nucleic Acids Res.* **2015**, *43*, W200–W207.
41. Baell, J. B.; Holloway, G. A. New substructure filters for removal of pan assay interference compounds (PAINS) from screening libraries and for their exclusion in bioassays. *J. Med. Chem.* **2010**, *53*, 2719–2740.
42. Lager, E.; Nilsson, J.; Østergaard Nielsen, E.; Nielsen, M.; Liljefors, T.; Sterner, O. Affinity of 3-acyl substituted 4-quinolones at the benzodiazepine site of GABAA receptors. *Bioorg. Med. Chem.* **2008**, *16*, 6936–6948.
43. Liu, Y.; Zhang, Q.; Chen, L. H.; Yang, H.; Lu, W.; Xie, X.; Nan, F. J. Design and synthesis of 2-alkylpyrimidine-4,6-diol and 6-alkylpyridine-2,4-diol as potent GPR84 agonists. *ACS Med Chem Lett* **2016**, *7*, 579–583.
44. Bowman, R. K.; Johnson, J. S. Nickel-catalyzed rearrangement of 1-acyl-2-vinylcyclopropanes. A mild synthesis of substituted dihydrofurans. *Org Lett* **2006**, *8*, 573–576.
45. Doni, E.; Mondal, B.; O'Sullivan, S.; Tuttle, T.; Murphy, J. A. Overturning established chemoselectivities: selective reduction of arenes over malonates and cyanoacetates by photoactivated organic electron donors. *J. Am. Chem. Soc.* **2013**, *135*, 10934–10937.
46. Amupitan, J. A.; Beddoes, R. L.; Mills, O. S.; Sutherland, J. K. 3-Methylcyclohex-2-enone derivatives as initiators of cyclisation. Part 4. Some bicyclisations. *J. Chem. Soc. Perkin Trans 1* **1983**, 759–763.
47. Sun, X.; Tymianski, M.; Garman, D. Agents And Methods For Treating Ischemic And Other Diseases. Patent WO 2012/174488-A2. **2012**.
48. Smith, P. K.; Krohn, R. I.; Hermanson, G. T.; Mallia, A. K.; Gartner, F. H.; Provenzano, M. D.; Fujimoto, E. K.; Goeke, N. M.; Olson, B. J.; Klenk, D. C. Measurement of protein using bicinchoninic acid. *Anal. Biochem.* **1985**, *150*, 76–85.
49. *Maestro Release 2017-1*; Schrödinger, LLC, New York, 2017.
50. *Prime Release 2017-1*; Schrödinger, LLC, New York, 2017.
51. Jacobson, M. P.; Friesner, R. A.; Xiang, Z.; Honig, B. On the role of the crystal environment in determining protein side-chain conformations. *J. Mol. Biol.* **2002**, *320*, 597–608.
52. Jacobson, M. P.; Pincus, D. L.; Rapp, C. S.; Day, T. J.; Honig, B.; Shaw, D. E.; Friesner, R. A. A hierarchical approach to all-atom protein loop prediction. *Proteins* **2004**, *55*, 351–367.
53. *Glide Release 2017-1; Schrödinger Suite Prime 2017-1 Induced Fit Docking protocol*; Schrödinger, LLC, New York, 2017.
54. Sherman, W.; Day, T.; Jacobson, M. P.; Friesner, R. A.; Farid, R. Novel procedure for modeling ligand/receptor induced fit effects. *J. Med. Chem.* **2006**, *49*, 534–553.
55. *The PyMOL Molecular Graphics System*, version 1.8; Schrödinger, LLC, New York, 2015.

## SUPPORTING INFORMATION

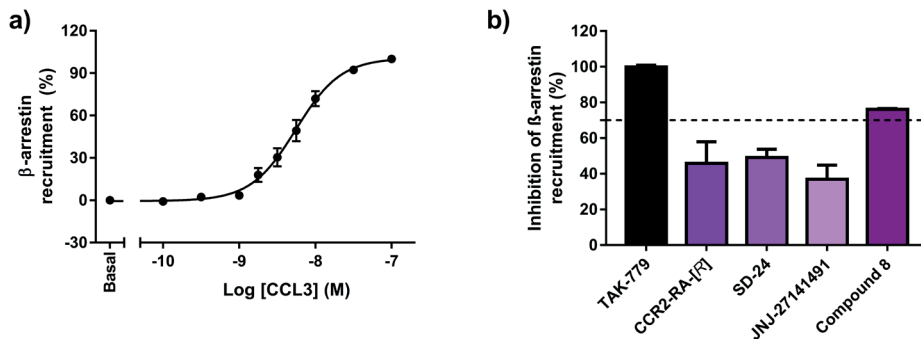


**Figure S1. Characterization of intracellular ligands in a U2OS-CCR5  $\beta$ -arrestin-recruitment assay.** (a) Increasing concentrations of CCL3-induced  $\beta$ -arrestin recruitment in U2OS-CCR5 cells, with a  $pEC_{50}$  value of  $8.3 \pm 0.08$  (6 nM) and a  $pEC_{80}$  of  $7.9 \pm 0.08$  (14 nM). (b) Inhibition of  $\beta$ -arrestin recruitment in U2OS-CCR5 by the orthosteric compound TAK-779 and several intracellular ligands with different chemical structures, all tested at  $1 \mu\text{M}$ , after stimulation with an  $EC_{80}$  concentration of CCL3. The dashed line indicates 70% inhibition. Only TAK-779 and compound **8** were able to inhibit CCL3-induced  $\beta$ -arrestin recruitment more than 70%.

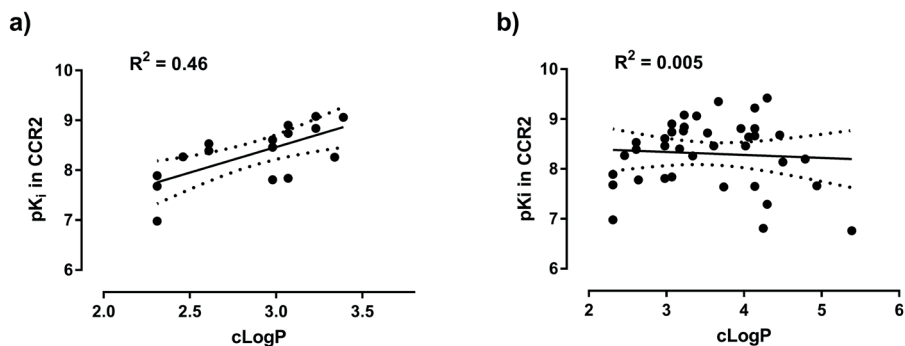


**Figure S2. Correlation between log P (cLogP) and affinity ( $pK_i$ ) values in CCR2.** (a) Correlation shown for compounds **8** – **23** (Table 1), with  $R^2$  modifications. (b) Correlation shown for all triazolo-pyrimidinone derivatives. In all cases, cLogP values were calculated using the calculator plugins in MarvinSketch, version 19.1.0, 2019, developed by ChemAxon (<http://www.chemaxon.com>).  $pK_i$  values were determined from  $[^3\text{H}]\text{-CCR2-RA-[R]}$  displacement assays in U2OS-CCR2 and are shown in Tables 1 – 3.

**Table S1. List of intermediate compounds 4aa-na, 4bb-bq, 4eq-ev.**

Compound	R <sup>3</sup>	R <sup>1</sup>
4aa	Me	3-Cl
4ba	cPr	3-Cl
4bb	cPr	H
4bc	cPr	2-Me
4bd	cPr	2-Cl
4be	cPr	2-OMe
4bf	cPr	3-Me
4bg	cPr	3-F
4bh	cPr	3-Br
4bi	cPr	3-I
4bj	cPr	3-OMe
4bk	cPr	3-CF <sub>3</sub>
4bl	cPr	4-Me
4bm	cPr	4-F
4bn	cPr	4-Cl
4bo	cPr	4-Br
4bp	cPr	4-OMe
4bq	cPr	3,4-diCl
4ca	Et	3-Cl
4da	Pr	3-Cl
4ea	<i>i</i> Pr	3-Cl
4eq	<i>i</i> Pr	3,4-diCl
4er	<i>i</i> Pr	2,3-diCl
4es	<i>i</i> Pr	2,5-diCl
4et	<i>i</i> Pr	3,5-diCl
4eu	<i>i</i> Pr	3,5-diBr
4ev	<i>i</i> Pr	3-Br, 4-Cl
4fa	Bu	3-Cl
4ga	2-EtBu	3-Cl
4ha	Pent	3-Cl
4ia	cPent	3-Cl
4ja	Hex	3-Cl
4ka	Hept	3-Cl
4la	Ph	3-Cl
4ma	4-MePh	3-Cl
4na	CH <sub>2</sub> CH <sub>2</sub> Ph	3-Cl

**Table S2. Functional activity of TAK-779 and CCR2-RA-[R] in hCCR5, using a CCL3-induced  $\beta$ -arrestin recruitment assay.**

Compound	pIC <sub>50</sub> ± SEM (IC <sub>50</sub> , nM)	Hill slope
TAK-779	8.32 ± 0.17 (6)	-1.1 ± 0.1
CCR2-RA-[R]	6.15 ± 0.02 (703)	-2.4 ± 0.2**

Data represent the mean ± standard error of the mean (SEM) of three independent experiments performed in duplicate. \*\*p < 0.01 (p = 0.0038) versus Hill slope (n<sub>H</sub>) of TAK-779, determined with a two-tailed, unpaired Student's t-test.

**Table S3. Functional activity of compounds 39 and 43 in hCCR2, using a CCL2-induced  $\beta$ -arrestin recruitment assay.**

Compound	pIC <sub>50</sub> ± SEM (IC <sub>50</sub> , nM)	Hill slope
<b>39</b>	7.68 ± 0.05 (21)	-2.5 ± 0.2
<b>43</b>	8.40 ± 0.01 (4)	-3.4 ± 0.4

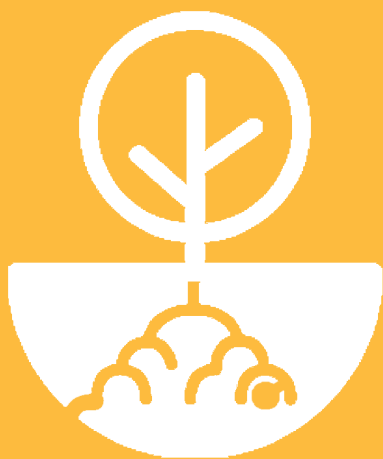
Data represent the mean ± standard error of the mean (SEM) of three independent experiments performed in duplicate.



## Chapter 6

---

# Design and characterization of an intracellular covalent ligand for CC Chemokine Receptor 2 (CCR2)



*Natalia V. Ortiz Zacarías, Julien Louvel, Tereza Šimková, Kirti K. Chahal, Yi Zheng, Emy Theunissen, Lloyd Mallee, Daan van der Es, Tracy Handel, Irina Kufareva, Adriaan P. IJzerman, Laura H. Heitman*

*Manuscript in preparation*



## ABSTRACT

CC chemokine receptor 2 (CCR2) plays a key role in the migration of leukocytes to sites of inflammation; thus, CCR2 represents a potential drug target in many inflammatory and immune diseases. Yet all CCR2 antagonists developed so far have failed in clinical trials (mostly) due to lack of efficacy, rendering the development of novel tools and concepts necessary to better study drug receptor pharmacology in early phases of drug discovery. In this regard, the recent crystal structure of CCR2 has suggested a new manner of pharmaceutical intervention, i.e. using intracellular allosteric modulators. In addition, irreversible or covalent probes represent important pharmacological tools that allow a variety of applications: target crystallization, study of *in vivo* target engagement or target validation, among others. Thus, we aimed to develop and characterize an intracellular covalent ligand for CCR2. Based on the structure of a known CCR2 intracellular ligand, SD-24, we designed and synthesized several potential covalent ligands by incorporating different electrophilic groups as reactive warheads. Next, a combination of radioligand binding and functional assays allowed us to identify compound **14** as an intracellular covalent binder for CCR2. In addition, *in silico* modeling followed by site-directed mutagenesis of CCR2 confirmed that **14** binds to the intracellular pocket of CCR2, where a cysteine residue appears to be one of the target amino acids for the irreversible interaction. To conclude, we report the design, synthesis, pharmacological characterization and binding mode of **14**, a first covalent probe for CCR2. This tool compound might represent a promising approach to further study CCR2, both *in vitro* and *in vivo*.

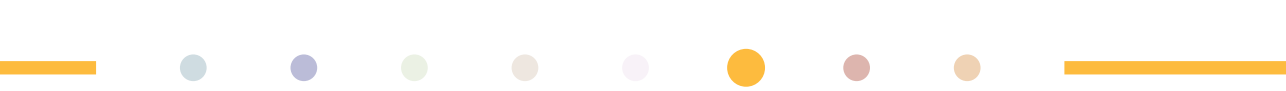


## INTRODUCTION

CC Chemokine receptor 2 (CCR2) is a G protein-coupled receptor (GPCR) expressed on the surface of various immune cells, including monocytes, basophiles and natural killer cells.<sup>1</sup> Activation of CCR2 by its endogenous chemokine ligands, such as CCL2, CCL7 and CCL13, results in leukocyte trafficking towards sites of inflammation as part of the immune response.<sup>2</sup> However, dysregulation of CCR2 signalling can lead to leukocyte accumulation—a hallmark of the inflammatory response—and ultimately to a variety of inflammatory and immune diseases.<sup>3</sup> In this regard, preclinical studies have suggested a critical role of CCR2/CCL2 signalling in atherosclerosis (**Chapter 7**),<sup>4</sup> diabetes,<sup>5</sup> neuropathic pain,<sup>6</sup> and cancer,<sup>7</sup> among others. Although many efforts have been made to bring CCR2 antagonists into the clinic, most clinical candidates have failed due to lack of efficacy.<sup>8</sup> Thus, a better understanding of its structure and biological function, both *in vitro* and *in vivo*, is necessary for the successful development of CCR2 antagonists.

Covalent ligands have recently re-emerged as valuable tool compounds, i.e. covalent probes or affinity-based probes, and as therapeutic agents for several targets and diseases.<sup>9–11</sup> As the name implies, covalent ligands contain a reactive group, or “warhead”, which allows them to bind to their target in an irreversible manner.<sup>12</sup> In the field of GPCRs, covalent ligands have been mostly used as tool compounds due to major safety concerns; however, recent studies have highlighted several potential advantages for the development of covalent drugs, including their insurmountability and prolonged duration of action.<sup>13–15</sup> As tool compounds, covalent ligands have been increasingly used for structure elucidation purposes, as they stabilize the inherently flexible receptor-ligand complexes.<sup>9</sup> Examples include the recent crystal structures of cannabinoid receptor CB<sub>1</sub>,<sup>16</sup> and adenosine A<sub>1</sub> receptor.<sup>17</sup> Furthermore, covalent probes represent valuable starting points for a wide variety of chemical biology and proteomic profiling applications.<sup>9, 12</sup>

Recently, the X-ray structures of CCR2 isoform a (CCR2a)<sup>18</sup> and isoform b (CCR2b, **Chapter 3**)<sup>19</sup> have been solved in complex with small-molecule antagonists. Besides providing structural insight on the antagonists’ binding mode, the crystal structure of CCR2b described in **Chapter 3** has revealed an intracellular binding site for small molecules, which can be used to inhibit CCR2 without directly competing with the binding of chemokines.<sup>19</sup> Due to their noncompetitive manner of inhibition, these intracellular allosteric modulators might be more efficacious in the treatment of inflammatory diseases characterized by high levels of endogenous chemokines, as suggested in **Chapter 2**.<sup>20</sup> An intracellular covalent ligand could represent a valuable tool to further investigate CCR2 pharmacology and intracellular modulation. Thus, based on previously described high-affinity intracellular ligands for CCR2, we aimed to design and synthesize novel putatively covalent intracellular ligands for this



receptor. Biochemical characterization, *in silico* modelling and a mutational study resulted in the identification of compound **14** as a covalent, negative allosteric modulator (NAM) of CCR2, and as a promising starting point for a variety of applications to further study CCR2 pharmacology.

## RESULTS

### Design and apparent affinity of putative covalent ligands for CCR2

As a starting point for the design of putative covalent intracellular ligands for CCR2, we first synthesized sulfonamide **34** by Peace *et al.*,<sup>21</sup> corresponding to compound **7** in our study (Figure 1). In order to covalently target nucleophilic residues present near the intracellular binding pocket of CCR2, four different warheads with different reactivity profiles were envisioned: fluorosulfonyl, acryloyl, isothiocyanate, and thiocyanate. These reactive warheads were incorporated at the position of the carboxyl group of **7**, using an ethylacetamide linker (Figure 1). Lastly, we incorporated a trifluoromethyl group in our design to improve the *in vivo* activity,<sup>22</sup> resulting in compounds **11** – **14** with varying reactive warheads (Figure 1). The binding affinities of compounds **7**, **11** – **14** were determined using a [<sup>3</sup>H]-CCR2-RA displacement assay (Table 1). In this assay, all compounds fully displaced the intracellular radioligand [<sup>3</sup>H]-CCR2-RA in a concentration-dependent manner, displaying high to moderate binding affinities for hCCR2b ( $K_i < 100$  nM). Of note, for compounds **11** – **14**, binding affinities are reported as “apparent (p)K<sub>i</sub>” values due to the putative covalent interaction between these compounds with CCR2, which precludes the determination of equilibrium binding parameters. The non-covalent control **7** displaced [<sup>3</sup>H]-CCR2-RA with a pK<sub>i</sub> value of 8.2 (Table 1). Of note, substitution of the chlorine group in **7** by trifluoromethyl in **11** – **14** does not affect the affinity towards CCR2, indicating that both groups are equally tolerated; thus we continued using compound **7** as non-covalent control (data not shown). Compound **13** with a non-selective fluorosulfonyl warhead exhibited the highest drop in affinity compared to **7**, with a 15-fold difference in apparent affinity (89 nM). Compound **13** was followed by **11** with the isothiocyanate warhead, which showed a 5-fold reduced affinity compared to **7** (31 nM). Compounds containing an acryloyl (**12**) or thiocyanate (**14**) warhead displayed the highest apparent affinities towards CCR2. Compound **12** displaced [<sup>3</sup>H]-CCR2-RA with a pK<sub>i</sub> of 7.7, while **14** displaced it with a pK<sub>i</sub> of 8.4, the highest affinity in this series of compounds (Table 1). Based on the apparent affinities, we decided to continue with compound **14** for further characterization in radioligand binding and functional assays.

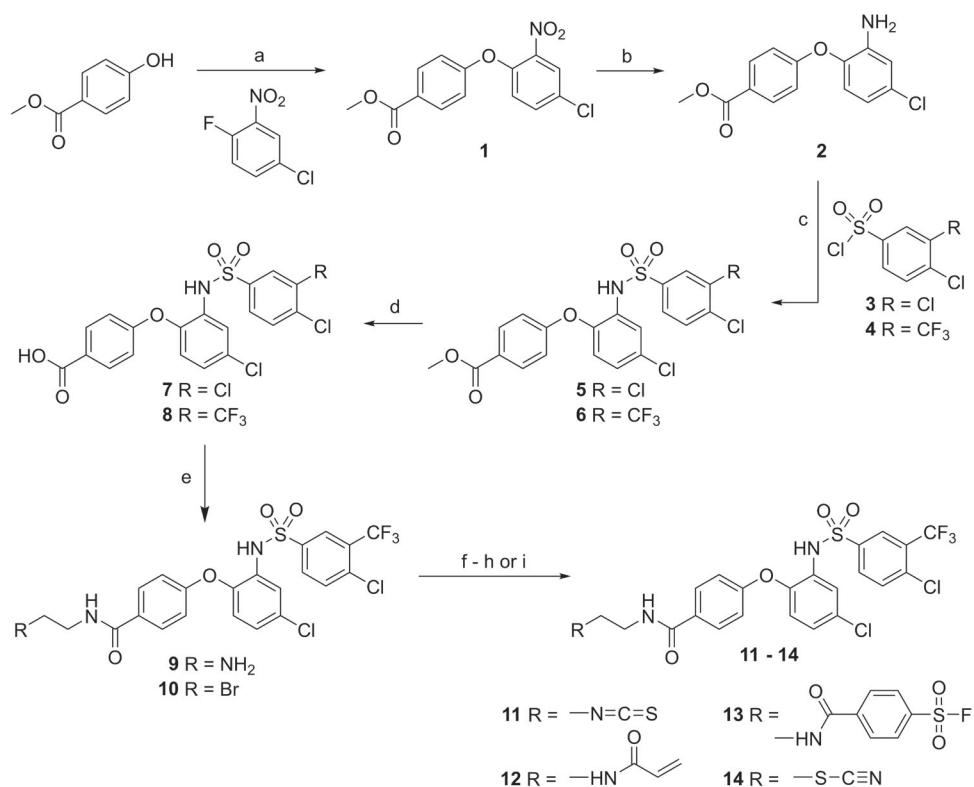


**Figure 1. Synthesis of compounds 7, 11 – 14.** Final compounds were synthesized using the following reagents and conditions: a)  $K_2CO_3$ , DMF, 70°C, 3.5h or overnight; b)  $SnCl_2 \cdot 2H_2O$ , EtOAc, rt, overnight; c) **3**, indium, MeCN, rt, overnight, or **4**, DMAP, pyridine, microwave 95°C, 3h; d) NaOH, dioxane, rt, 2h, or NaOH, dioxane, 60°C, 2.5h; e) i. tert-butyl-N-(2-aminoethyl)carbamate, EDC, HOBT, dioxane, rt; ii. TFA, DCM, rt, for **9**; or 2-bromoethan-1-amine, EDC, HOBT, dioxane, rt for **10**; f) **9**, TEA,  $CS_2$ , TsCl, THF for **11**; g) **9**, acryloyl chloride, TEA, acetonitrile, -78°C to rt for **12**; h) **9**, 4-(fluorosulfonyl) benzoic acid, EDC, HOBT, TEA, dioxane, rt for **13**; i) **10**, KSCN, EtOH, reflux, for **14**.

**Table 1. Binding affinities ( $pK_i$ ) of synthesized sulfonamide derivatives determined in [ $^3H$ ]-CCR2-RA displacement assays.**

Compound	$R_1$	$pK_i \pm S.E.M (K, nM)$
<b>7</b>	-	$8.2 \pm 0.03 (6)$
<b>11</b>	Isothiocyanate	$7.5 \pm 0.04 (31)^a$
<b>12</b>	Acryloylamide	$7.7 \pm 0.14 (22)^a$
<b>13</b>	(Fluorosulfonyl)phenyl amide	$7.2 \pm 0.16 (89)^a$
<b>14</b>	Thiocyanate	$8.4 \pm 0.06 (4)^a$

Data is presented as mean  $\pm$  S.E.M. of at least three individual experiments performed in duplicate.

<sup>a</sup>As these compounds might bind covalently, we only refer to these affinities as apparent affinities.

## Characterization of **14** as covalent probe with radioligand binding assays

### *Time-dependent characterization of affinity*

To determine whether compound **14** binds irreversibly to CCR2, we first determined the time dependency of its affinity, in comparison with the non-covalent control **7**. For this, we measured the affinity of compounds **7** and **14** using a [<sup>3</sup>H]-CCR2-RA-[R] displacement assay, with a short incubation time of 20 min. In addition, their affinity was measured after a 4 hour pre-incubation of U2OS-CCR2 with increasing concentrations of **7** or **14**, followed by a 20 min co-incubation with [<sup>3</sup>H]-CCR2-RA-[R] (Figure 2a,b). It is worth to mention that for practical reasons, we switched to using the *R*-isomer [<sup>3</sup>H]-CCR2-RA-[R] for this and the following assays, instead of the racemic mixture [<sup>3</sup>H]-CCR2-RA used in the previous section. Compared to the co-incubation experiment, the affinity of non-covalent control **7** remained similar after 4 hour pre-incubation, in agreement with its reversible mode of interaction (Figure 2a and Table 2). In contrast, the affinity of compound **14** increased almost 4 times after pre-incubation, from a  $K_i$  of 2.4 nM to 0.7 nM (Table 2), which is apparent as a shift to the left in the concentration-displacement curve (Figure 2b). This indicates that over time, more compound is covalently bound to the receptor, and thus, less of the compound is needed to achieve similar levels of displacement.

**Table 2. Time-dependent characterization of affinity ( $pK_i$ ) of compounds **7** and **14** obtained from [<sup>3</sup>H]-CCR2-RA-[R] displacement assays.**

Compound	$pK_{i,0h} \pm \text{S.E.M} (K_{i,0h}, \text{nM})^a$	$pK_{i,4h} \pm \text{S.E.M} (K_{i,4h}, \text{nM})^b$	$K_i \text{ shift}^c$
<b>7</b>	$8.4 \pm 0.08 (4.4)$	$8.2 \pm 0.02 (6.1)$	$0.7 \pm 0.1$
<b>14</b>	$8.7 \pm 0.10 (2.4)$	$9.2 \pm 0.15 (0.7)^{**}$	$3.8 \pm 0.5$

Data is presented as mean  $\pm$  S.E.M. of at least three individual experiments performed in duplicate. Differences in  $pK_{i,0h}$  versus  $pK_{i,4h}$  values were analyzed using a paired, two-tailed, Student's *t*-test, with differences as: \*\* $p < 0.01$ . <sup>a</sup>Affinity after 20 min co-incubation of unlabeled ligands with [<sup>3</sup>H]-CCR2-RA-[R] and no pre-incubation. <sup>b</sup>Affinity after 4h pre-incubation with unlabeled ligands followed by 20 min co-incubation with radioligand. <sup>c</sup> $K_i$ -shift: Ratio of  $K_{i,4h}/K_{i,0h}$

### *Wash-resistant interaction of compound **14** with hCCR2b*

To assess the irreversibility of the interaction with the receptor, we set up a [<sup>3</sup>H]-CCR2-RA-[R] washout experiment. In this assay we pre-incubated U2OS-CCR2 membranes with  $10 \times IC_{50}$  concentration of **7** or **14** for 2 hours, followed by four extensive washing and centrifugation cycles, in order to remove the non-covalently bound ligands. After the washing steps, [<sup>3</sup>H]-

CCR2-RA-[R] was added and the mix was further incubated for two more hours before measuring radioligand binding. Radioligand binding was compared to the vehicle control, in absence of **7** or **14** (set as 100% binding). [<sup>3</sup>H]-CCR2-RA-[R] binding was fully recovered in membranes pretreated with **7** (116 ± 8% binding), indicating that this compound was completely washed away during the washing and centrifugation cycles (Figure 2c). In contrast, less than 30% binding of [<sup>3</sup>H]-CCR2-RA-[R] was measured in membranes pretreated with compound **14** (27 ± 0.4%), indicating that even after extensive washing this compound was still significantly bound to the receptor, prohibiting radioligand binding (Figure 2c). As the thiocyanate warhead of compound **14** reacts selectively with cysteine residues, we performed the same washout assay in the presence of the highly reactive iodoacetamide (IA). IA alkylates the sulfhydryl groups of cysteine residues, making them unavailable for covalent interactions. Thus, before pre-incubation with **7** or **14**, U2OS-CCR2 membranes were pretreated with IA for 30 min in the dark. In presence of IA, binding of [<sup>3</sup>H]-CCR2-RA-[R] was fully recovered to ~100% for both compounds: 93 ± 5% for compound **14** and 104 ± 5% for compound **7** (Figure 2c). Notably, a comparable effect was observed by pretreating the membranes with 1mM *N*-ethylmaleimide, another common cysteine modifier<sup>23</sup> (data not shown). This loss of wash-resistant capacity of compound **14** in membranes pretreated with IA indicated that cysteine residues were indeed responsible for the irreversible binding of **14** with CCR2.

## Characterization of **14** as covalent probe using functional assays

### *Characterization of **14** using a [<sup>35</sup>S]GTPγS binding assay*

After demonstrating that interaction of compound **14** with CCR2 was wash-resistant, we investigated whether this compound was able to inhibit the receptor in a functional assay. First we characterized compounds **7** and **14** in a [<sup>35</sup>S]GTPγS binding assay. In this assay, both compounds behaved as negative allosteric modulators (NAMs) as they were able to inhibit [<sup>35</sup>S]GTPγS binding induced by a submaximal concentration of CCL2 (20 nM) in a concentration-dependent manner. The non-covalent control **7** inhibited [<sup>35</sup>S]GTPγS binding with a pIC<sub>50</sub> of 7.0 ± 0.02, while compound **14** showed a higher pIC<sub>50</sub> of 7.5 ± 0.04 (Figure 3a and Table 3). Of note, both compounds decreased the basal activity of CCR2 at the highest concentrations (Figure 3a). To evaluate the functional effect of irreversible binding of **14** with CCR2, we set up a [<sup>35</sup>S]GTPγS washout experiment similar to the previous [<sup>3</sup>H]-CCR2-RA-[R] washout assay. In this set up, a [<sup>35</sup>S]GTPγS binding assay was performed after four washing and centrifugation cycles with membranes pretreated with a single concentration

of **7** or **14**. Without the washing steps, both compounds were able to inhibit > 70% of the binding of [<sup>35</sup>S]GTPγS induced by 20 nM CCL2; in presence of compound **7** [<sup>35</sup>S]GTPγS binding was reduced to 34 ± 2%, while in presence of compound **14**, [<sup>35</sup>S]GTPγS binding was fully inhibited to -5 ± 6% (Figure 3b). However, after the four cycles of washing and centrifugation with compound **7**, [<sup>35</sup>S]GTPγS binding levels recovered to 98 ± 14%, which was comparable to CCL2 alone and significantly different from the “unwashed” situation (*p* < 0.05, Figure 3b), indicating that this compound was effectively washed away in this assay. In contrast, compound **14** remained fully functional after washout, displaying a complete inhibition of [<sup>35</sup>S]GTPγS binding (-24 ± 30%), which was comparable to the “unwashed” situation (Figure 3b). This confirms that the binding of this compound with CCR2 is wash-resistant, leading to persistent inhibition of the receptor.

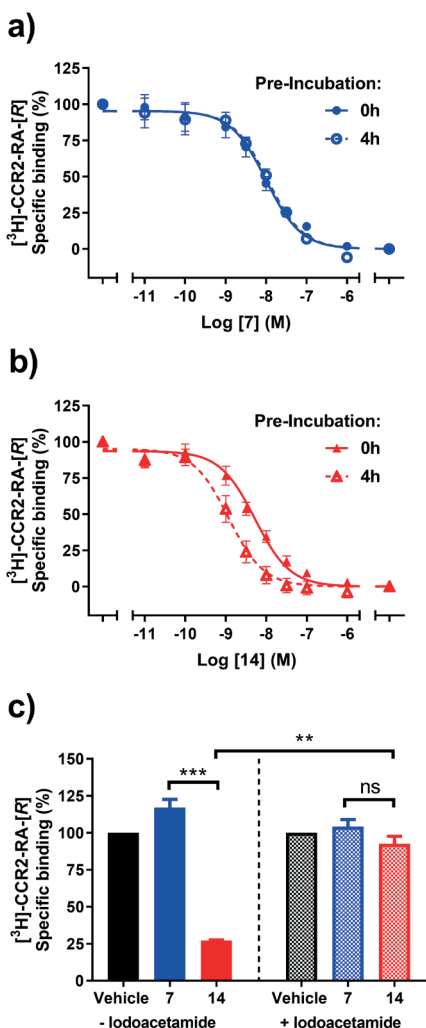


**Figure 2. Radioligand binding assays point to a covalent interaction.** (a, b) Time-dependent characterization of affinity of **7** (a) and **14** (b). Characterization of affinity in U2OS-CCR2 after i) 20 min co-incubation of unlabeled ligands with [<sup>3</sup>H]-CCR2-RA-[R] (0h Pre-incubation), and ii) 4h pre-incubation with unlabeled ligands followed by 20 min co-incubation with radioligand. *p*<sub>K<sub>i</sub></sub> values obtained from these graphs are described in Table 2. (c) Wash-out-radioligand experiments in absence or presence of lodoacetamide, followed by pre-incubation with 10X IC<sub>50</sub> concentration of **7** and **14**. Radioligand binding is recovered when **14** is pre-incubated in U2OS-CCR2 + lodoacetamide, indicating an interaction with cysteine residues. Data represent the mean ± SEM of at least three independent experiments performed in duplicate.

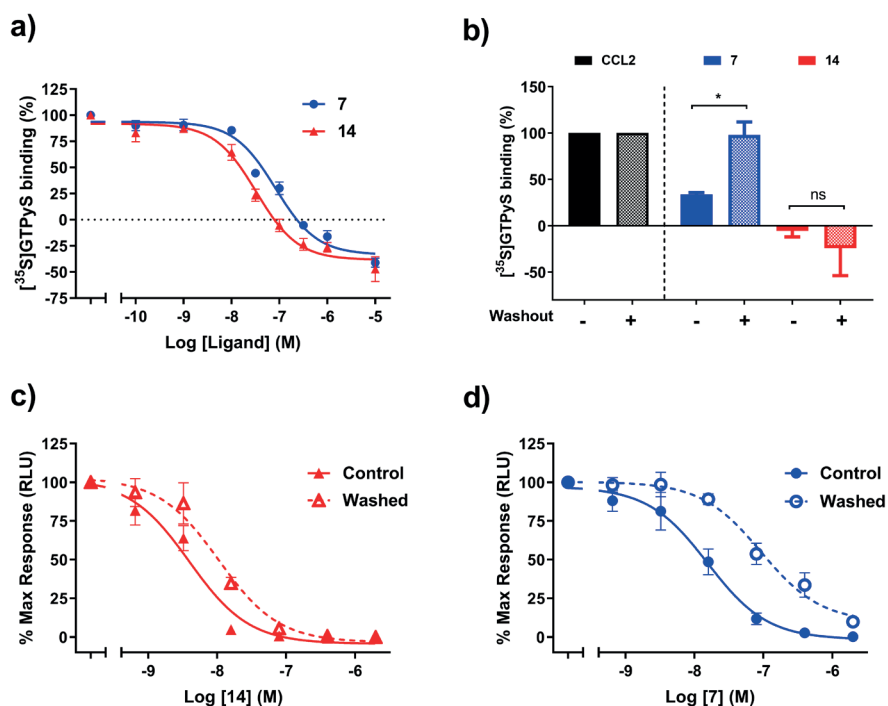


**Figure 3. Functional assays point to a covalent interaction.** (a) Inhibition of CCL2-stimulated  $[^{35}\text{S}]\text{GTPyS}$  binding by increasing concentration of **7** and **14**. (b) After washout, **7** is not able to inhibit  $[^{35}\text{S}]\text{GTPyS}$  binding anymore, while **14** remains capable of completely inhibiting  $[^{35}\text{S}]\text{GTPyS}$  binding after CCL2 stimulation. (c, d) Inhibition of CCL2-stimulated  $\beta$ -arrestin recruitment by increasing concentrations of **14** (c) and **7** (d) with or without two washing steps before addition of CCL2. Data represent the mean  $\pm$  SEM of at least three independent experiments performed in duplicate.  $\text{pIC}_{50}$  values obtained from these graphs are described in Table 3.

**Table 3. Functional characterization of compounds 7 and 14 in hCCR2, obtained in  $[^{35}\text{S}]\text{GTPyS}$  and  $\beta$ -arrestin recruitment assays.**

Compound	$\text{pIC}_{50} \pm \text{SEM} (\text{IC}_{50}, \text{nM})$		
	$[^{35}\text{S}]\text{GTPyS}$ binding <sup>a</sup>	$\beta$ -arrestin <sup>b</sup>	$\beta$ -arrestin_washed <sup>c</sup>
<b>7</b>	$7.1 \pm 0.05$ (82)	$7.8 \pm 0.15$ (16)	$7.0 \pm 0.09$ (103)**
<b>14</b>	$7.5 \pm 0.05$ (33)	$8.4 \pm 0.12$ (4)	$8.0 \pm 0.08$ (10)*

Data is presented as mean  $\pm$  S.E.M. of at least three individual experiments performed in duplicate. <sup>a</sup>Inhibition of  $[^{35}\text{S}]\text{GTPyS}$  binding in U2OS-CCR2 at 25  $^{\circ}\text{C}$ , after stimulation with 20 nM CCL2. <sup>b</sup>Inhibition of  $\beta$ -arrestin recruitment determined with a NanoBit CCR2 assay, after stimulation with 200 nM CCL2. <sup>c</sup>Inhibition of  $\beta$ -arrestin recruitment determined with a NanoBit CCR2 assay, after two washing steps followed by stimulation with 200 nM CCL2. Differences in  $\text{pIC}_{50}$  values between unwashed and washed samples were analyzed using a paired, two-tailed, Student's t-test, with differences as: \* $p < 0.05$  and \*\* $p < 0.01$ .

### ***Characterization of 14 using a $\beta$ -arrestin recruitment assay***

Using a NanoBit  $\beta$ -arrestin recruitment assay, we then explored the effect of irreversible binding in a whole-cell functional assay. In this assay, increasing concentrations of **7** or **14** were pre-incubated with HEK293t cells transiently transfected with hCCR2 for 20 min, followed by two washing steps and addition of new medium before incubation with a fixed concentration of CCL2 (200 nM) for another 10 min. In addition, a control experiment was performed using unwashed cells pretreated with **7** or **14**. In the unwashed control situation, **7** and **14** inhibited CCL2-induced  $\beta$ -arrestin recruitment with 5-fold and 8-fold higher potencies, respectively, than those measured in the [ $^{35}$ S]GTP $\gamma$ S binding assay (Table 3). After two washing steps, compound **7** displayed a  $\text{pIC}_{50}$  of  $7.0 \pm 0.09$ , corresponding to a 6-fold reduction in potency compared to the unwashed control ( $\text{pIC}_{50}$  of  $7.8 \pm 0.15$ ) (Table 3 and Figure 3d). For compound **14**, we observed a smaller shift in potency after the washing steps: from a  $\text{pIC}_{50}$  of  $8.4 \pm 0.12$  in unwashed cells to a  $\text{pIC}_{50}$  of  $8.0 \pm 0.08$  after washing, corresponding to a 2.5-fold reduction in potency (Table 3 and Figure 3c).

## **Cysteine C75 as possible anchor point for covalent interaction**

### ***Docking of compound 14 into the crystal structure of hCCR2b***

The results from the washout experiment in presence of IA prompted us to investigate the cysteine residue responsible for the irreversible binding of compound **14** with CCR2; thus, we investigated which cysteine residues are in close proximity to the intracellular binding pocket of CCR2. In the crystal structure of hCCR2b-T4L in complex with an orthosteric and an intracellular antagonist (PDB 5T1A, **Chapter 3**<sup>19</sup>), there are two cysteine residues in proximity of the crystallized intracellular ligand CCR2-RA-[R], where these compounds also bind: Cys75<sup>2x37</sup>, within 4Å, and Cys70<sup>1x60</sup>, at 6.4Å. Additionally, following the removal of T4L and re-building of the native ICL3, we discovered that it contains Cys232<sup>5x68</sup>, at 14Å from the intracellular binding pocket. Although this distance (14Å) is too large to be spanned by the ethylacetamide linker, we realized that the flexible nature of ICL3 and the resulting protein motions can bring Cys232<sup>5x68</sup> closer to the pocket. Next, we sought to illustrate that covalent binding of **14** in the allosteric binding pocket is sterically feasible, using molecular docking. A docking model was prepared from the crystal structure of hCCR2b-T4L described in **Chapter 3** and the binding pose of **14** was predicted via covalent docking, assuming that the closest of the three cysteines, Cys75<sup>2x37</sup>, is the covalent attachment point. The docking study supported a potential covalent interaction of compound **14** with Cys75<sup>2x37</sup>, as the predicted pose was (i) consistent with the predicted poses of non-covalent analogs from the same series, and (ii) compatible with the linker attachment to Cys75<sup>2x37</sup>. However, because



Cys70<sup>1x60</sup> and Cys232<sup>5x68</sup> are also in proximity to this binding site, and they could be brought even closer via unaccounted-for protein motions, they were included together with Cys75<sup>2x37</sup> in the subsequent mutagenesis study (Figure 4a).

### Site-directed mutagenesis study

To assess which of the three cysteines suggested by docking was responsible for the covalent binding of **14**, single-point mutations to serine were made: C70S<sup>1x60</sup>, C75S<sup>2x37</sup> and C232S<sup>5x68</sup>. These CCR2 mutants, together with a CCR2 wild-type (WT) as control, were transiently transfected into CHO cells. After transfection and membrane preparation, we first determined if these mutations affected the binding of [<sup>3</sup>H]-CCR2-RA-[R]. For this, we performed [<sup>3</sup>H]-CCR2-RA-[R] displacement assays, in order to determine the affinity of CCR2-RA-[R] for the mutant and WT receptors (Table 4). Compared to the WT (pIC<sub>50</sub> of 7.9 ± 0.06), the affinity of CCR2-RA-[R] was not affected in any of the mutants (Table 4), confirming the integrity of the intracellular pocket in all mutants. In contrast, the affinity of **14** was significantly decreased in both C70S and C75S mutants compared to the WT (pIC<sub>50</sub> of 8.8 ± 0.10). In the case of the non-covalent control **7**, opposite effects were observed in C70S and C75S: **7**'s affinity was significantly decreased in C70S and increased in C75S in comparison to the WT (pIC<sub>50</sub> of 7.9 ± 0.02). The affinity of both **7** and **14** was not affected in C232S, indicative that this residue is not involved in these compounds' binding (Table 4).

**Table 4. Binding affinities (pIC<sub>50</sub>) of **7** and **14** in the different CCR2 constructs, obtained from [<sup>3</sup>H]CCR2-RA-[R] displacement assays.**

Construct	pIC <sub>50</sub> ± SEM (IC <sub>50</sub> , nM)		
	<b>7</b>	<b>14</b>	CCR2-RA-[R]
WT	7.9 ± 0.02 (12)	8.8 ± 0.10 (2)	7.9 ± 0.06 (12)
C70S	7.7 ± 0.09 (22)*	8.4 ± 0.04 (4)*	7.9 ± 0.02 (13)
C75S	8.2 ± 0.05 (6)**	8.4 ± 0.10 (5)*	8.0 ± 0.05 (11)
C232S	7.9 ± 0.005 (12)	8.8 ± 0.06 (1)	8.0 ± 0.09 (9)

Data is presented as mean ± S.E.M. of at least three individual experiments performed in duplicate. Differences in pIC<sub>50</sub> values compared to WT were analyzed using a One-way ANOVA with Dunnett's posthoc test: \*p<0.05 and \*\*p<0.01.

Next, a [<sup>3</sup>H]-CCR2-RA-[R] washout assay was repeated using membrane preparations from mutant and WT CCR2 (Figure 4b). Similarly as in the washout assays in U2OS-CCR2 membranes, compound **7** was completely washed away from the WT receptor, leading to a full recovery of [<sup>3</sup>H]-CCR2-RA-[R] binding (~100%), while compound **14** only led to 9%

binding of [<sup>3</sup>H]-CCR2-RA-[R], in agreement with its irreversible nature (Figure 4b). For compound **7**, full recovery of radioligand binding was observed in the three mutants. In the case of compound **14**, mutants C70S and C232S showed similar [<sup>3</sup>H]-CCR2-RA-[R] binding levels as the WT receptor, indicating that **14** still binds covalently despite these mutations. However, [<sup>3</sup>H]-CCR2-RA-[R] binding was significantly increased to 30% in the C75S mutant ( $p < 0.0001$ ), indicating a loss of covalent binding in this mutant. This data indicates that Cys75<sup>2x37</sup> is responsible for the irreversible nature of compound **14**; yet, the recovery of [<sup>3</sup>H]-CCR2-RA-[R] binding was not complete, i.e. to similar levels as **7**, indicating that other residues might also be involved in the formation of a covalent bond with **14**, or become involved when Cys75<sup>2x37</sup> is not available. Of note, serine also contains a nucleophilic hydroxyl group, which might possibly interact with the thiocyanate warhead. Hence, we also mutated Cys75<sup>2x37</sup> to alanine; however, alanine mutation of this residue (C75A) did not improve the recovery of [<sup>3</sup>H]-CCR2-RA-[R] binding in comparison with C75S (data not shown), further supporting an interaction with multiple residues.

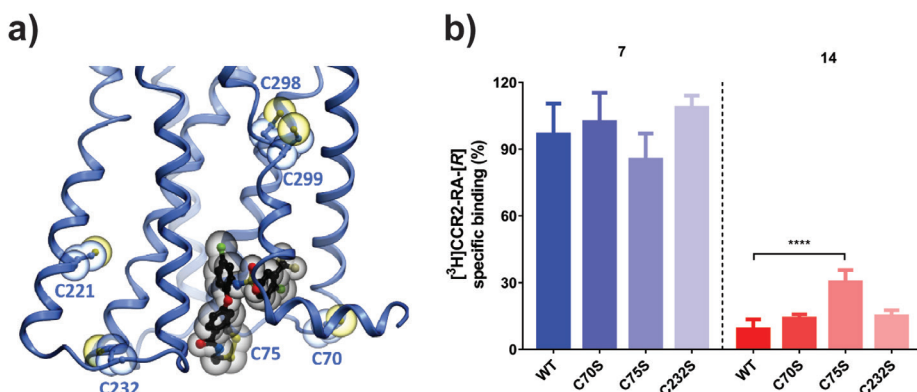


**Figure 4. Cysteine 75 seems to be involved in a covalent bond with compound 14.** (a) Docking of **14** in the crystal structure of CCR2 (PDB 5T1A, Chapter 3), showing the cysteine residues with potential to interact with this ligand: Cys75<sup>2x37</sup>, within 4Å; Cys70<sup>1x60</sup>, at 6.4Å; and Cys232<sup>5x68</sup>, at 14Å. (b) Washout-radioligand experiments performed after pre-incubation of 60 nM **14** or 200 nM **7** in membranes from CHO cells transiently transfected with CCR2 mutants. Data represent the mean  $\pm$  SEM of at least three independent experiments performed in duplicate.

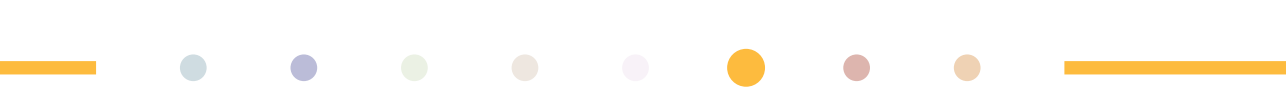
## DISCUSSION

Covalent ligands represent useful tool compounds to study the structure and function of GPCRs;<sup>9, 12</sup> furthermore, due to their ‘infinite residence time’, covalent inhibitors may lead to enhanced *in vivo* efficacy as a result of their extended duration of action and insurmountability.<sup>13-15</sup> Several orthosteric and allosteric antagonists have been previously

described for CCR2,<sup>24</sup> but no covalent binders have been described so far. Some of these CCR2 antagonists bind to an allosteric binding site located in the intracellular region of the receptor, from where they can inhibit the receptor in a noncompetitive and insurmountable manner.<sup>19, 25, 26</sup> In an attempt to combine the advantages provided by covalent inhibition and those of intracellular ligands, we aimed to design, synthesize and characterize a novel covalent intracellular ligand for CCR2.

Previous research in our group identified sulfonamide derivatives, similar to compound **7** in our study, as intracellular antagonists for CCR2<sup>21, 26</sup> (Figure 1). However, Wang *et al.* showed that these sulfonamide derivatives displayed a considerable loss of activity in whole blood assays due to high plasma protein binding.<sup>22</sup> Thus, with the aim of developing covalent probes that might be used in both *in vitro* and *in vivo* assays, we replaced the 3,4-dichlorophenyl sulfonamide scaffold of **7** with the 4-chloro-3-(trifluoromethyl)phenyl sulfonamide scaffold (Figure 1), which had shown improved activity in whole blood functional assays.<sup>22</sup> Building on this scaffold, we finally introduced several electrophilic warheads connected by a previously described ethylacetamide linker<sup>22</sup> (Figure 1). The choice of the electrophilic warhead is based on the desired reactivity towards a target amino acid, as well as the synthetic feasibility to attach it to the scaffold or 'pharmacophore'.<sup>12</sup> Based on the presence of lysine and cysteine residues in the intracellular region of CCR2, we chose four different electrophilic warheads: isothiocyanate, which targets both cysteine and lysine residues;<sup>27, 28</sup> acryloyl, a Michael acceptor that preferentially targets cysteine over lysine residues;<sup>29</sup> a non-selective fluorosulfonyl warhead, with reactivity towards serine, threonine, lysine, tyrosine, lysine, cysteine and histidine residues;<sup>30</sup> and a thiocyanate functionality, which selectively reacts with cysteine residues.<sup>12, 31</sup> As expected, all putative covalent ligands were able to fully displace [<sup>3</sup>H]-CCR2-RA, indicating that they bind to the same intracellular binding site with high to moderate affinities (Table 1). High affinity is key when designing covalent ligands, as it leads to lower non-specific binding to other nucleophilic residues or off-targets.<sup>12</sup> As only compound **14** with a thiocyanate warhead displayed comparable affinity to the non-covalent control **7** (Table 1), we decided to continue with this compound for further characterization.

It is important to note that equilibrium parameters ( $K_i/IC_{50}$  values) are poor indicators of the 'true' binding affinity or potency of covalent ligands, due to their two-step mechanism of inhibition which results in a time-dependent shift in affinity.<sup>32</sup> Taking advantage of this notion, we observed a significant increase in the affinity of compound **14** after a 4 hour pre-incubation step in radioligand displacement assays, in comparison with only co-incubation (Figure 2A,B and Table 2). Such increase in binding affinity might be related to an increase in receptor occupancy over time, and thus, to an increase in covalent binding. Similar results have been obtained with covalent ligands targeting other GPCRs.<sup>33-35</sup> However, a shift in affinity over time can also be obtained with slowly-dissociating ligands, i.e. long



residence-time ligands, as observed with long residence-time antagonists for CCR5 and CB<sub>1</sub> receptors.<sup>36,37</sup> Thus, we performed ‘wash-out’ assays, which are commonly used to assess the irreversibility of the interaction with the receptor.<sup>38</sup> These assays rely on extensive washing to ensure the removal of unbound ligand, and they have been previously used to validate the irreversible nature of covalent ligands for other GPCRs.<sup>33-35, 39, 40</sup> After four washing steps, [<sup>3</sup>H]-CCR2-RA-[R] binding was completely recovered in membranes pretreated with the non-covalent control **7**, while less than 30% [<sup>3</sup>H]-CCR2-RA-[R] binding was measured in membranes pretreated with compound **14**, indicative of an irreversible interaction with CCR2 (Figure 2C). The fact that radioligand binding was not completely abolished with compound **14** might be related to the assay conditions used in this study, such as ligand concentration, number of washing steps, and incubation times.

To further provide evidence for the covalent nature of compound **14**, we performed functional ‘wash-out’ experiments using two different functional assays: a membrane based [<sup>35</sup>S]GTPγS assay and a whole cell based β-arrestin recruitment assay (NanoBit assay). These assays showed that, both compounds are able to fully inhibit CCL2-induced G protein-activation and β-arrestin recruitment in CCR2 with high to moderate potencies (Figure 3 and Table 3), confirming their functional profile as negative allosteric modulators (NAMs), similarly as the previously characterized sulfonamide derivative SD-24.<sup>26</sup> After extensive washing, CCL2-induced [<sup>35</sup>S]GTPγS binding was fully restored in membranes pretreated with **7**; however, CCL2 failed to induce [<sup>35</sup>S]GTPγS binding in membranes pretreated with **14**, indicative again of an insurmountable and irreversible interaction with the receptor (Figure 3B). Of note, both compounds displayed an inverse agonistic behaviour in this assay, also observed with other intracellular ligands (Chapter 4).<sup>41</sup> In addition, the potencies of **7** and **14** to inhibit CCL2-induced β-arrestin recruitment were compared in ‘unwashed’ versus ‘washed’ samples. In this assay both compounds displayed a decrease in potency after the washing steps; however a bigger shift was observed for **7** than for **14** (Figures 3C,D and Table 3). In this regard, the shorter preincubation time in the NanoBit assay—20 min versus 2 hour preincubation time in radioligand binding and [<sup>35</sup>S]GTPγS assays—might not have been sufficient to allow compound **14** to fully bind CCR2 in an irreversible manner, resulting in the slight reduction of potency. Furthermore, the highly reducing nature of the intracellular environment, i.e. still intact in whole cell experiments, might limit the formation of the disulfide bond between the cysteine residue and the warhead.<sup>42</sup>

Finally, we sought to determine the target amino acid of the thiocyanate warhead. The radioligand washout assays in the presence of IA indicates that cysteine residues are critical for the irreversible interaction between compound **14** and CCR2, as the irreversible nature of **14** was lost in membranes treated with IA (Figure 2C). Docking of compound **14** into an *in silico* model of CCR2 supports a potential interaction between compound **14** and

Cys75<sup>2x37</sup>, resulting in a disulfide bond formation; however, the two other residues could not be completely ruled out due to their proximity to the binding site: Cys70<sup>1x60</sup> and Cys232<sup>5x68</sup> (Figure 4A). Notably, Cys75<sup>2x37</sup> is unique to CCR2, as most chemokine receptors possess a serine residue in this position. Therefore, the three cysteine residues were mutated to serine (C70S<sup>1x60</sup>, C75S<sup>2x37</sup> and C232S<sup>5x68</sup>) in order to reduce their nucleophilic nature and prevent the formation of a covalent bond. Radioligand washout assays showed that the irreversibility of compound **14** is only affected in the CCR2-C75S mutant (Figure 4B). However, this mutation did not lead to a full recovery of [<sup>3</sup>H]-CCR2-RA-[R] binding, as observed with compound **7**, suggesting that compound **14** interacts with multiple nucleophilic residues, not unlike other GPCRs.<sup>33, 43, 44</sup> In light of these results, further mutational studies are necessary to fully delineate the binding mode and amino acid contacts of **14** within CCR2.

To conclude, we report the design, synthesis and pharmacological characterization of compound **14**, the first intracellular covalent NAM for CCR2. A combination of radioligand binding and functional assays was used to provide evidence of an irreversible interaction between compound **14** and CCR2, which leads to a long-lasting functional effect. Moreover, *in silico* structure-based docking and receptor mutagenesis studies suggest that **14** forms a disulfide covalent bond primarily with Cys75<sup>2x37</sup>, located in the intracellular binding site of CCR2, although other (secondary) interaction sites are possible. Overall, this compound may represent a useful tool to further study CCR2 structure and function in a variety of *in vitro* and *in vivo* studies, which might ultimately enable a better translation of preclinical findings into successful clinical studies.

# MATERIALS AND METHODS

## Chemistry

### General Methods

All solvents and reagents were purchased from commercial sources and were used without further purification.  $^1\text{H}$  spectra were recorded on a Bruker AV 400 MHz liquid spectrometer at room temperature (rt) using  $\text{CDCl}_3$ , MeOD or DMSO as a solvent. Chemical shifts are reported in ppm relative to internal standard tetramethylsilane (TMS) or solvent resonance. Purity of the compounds was determined by HPLC with a C18 column (50 × 4.6 mm, 3  $\mu\text{m}$ ), flow rate 1.3 mL/min, using gradient 10-90% MeCN/ $\text{H}_2\text{O}$  (0.1% TFA) and measuring UV absorbance at 254 nm. Reactions were monitored by TLC using Merck TLC Silica gel 60 F<sub>254</sub> aluminum sheets. Compounds were visualized by UV irradiation or by staining with  $\text{KMnO}_4$  solution in  $\text{H}_2\text{O}$ . Biotage Initiator microwave synthesizer was used for the reactions performed in a microwave reactor. For the flash chromatography, Davisil silica gel (40-63  $\mu\text{m}$ ) was used. The automatic flash chromatography was performed on an Isolera One Automatic Flash Chromatography System by Biotage with pre-packed flash cartridges (ISCO RediSep or Biotage ZIP Sphere). Mass spectra were measured using a Shimadzu Prominence LCMS-2020 system and a Gemini C18 Phenomenex column (50 × 3 mm, 3  $\mu\text{m}$ ).

### Synthetic procedure for compound 7

Commercially available methyl 4-hydroxybenzoate (1 eq) and 5-chloro-2-fluoronitrobenzene (1 eq) were dissolved in dimethylformamide (DMF, 1 mL/mmol) together with potassium carbonate (2 eq) in a round-bottom flask. The mixture was stirred at 70°C under nitrogen atmosphere for 3.5 hours. After the solvent was evaporated, the residue was dissolved in EtOAc and washed with water. The organic layer was dried over  $\text{MgSO}_4$  and concentrated in vacuum to afford methyl 4-(4-chloro-2-nitrophenoxy)benzoate **1** (13.9 g, 45.1 mmol, 90%).  $^1\text{H}$  NMR (400 MHz, DMSO)  $\delta$  8.29 (d,  $J = 2.6$  Hz, 1H), 8.03 – 7.96 (m, 2H), 7.86 (dd,  $J = 8.9, 2.6$  Hz, 1H), 7.42 (d,  $J = 8.9$  Hz, 1H), 7.20 – 7.13 (m, 2H), 3.84 (s, 3H).

The product was dissolved in EtOAc (0.05 M) before addition of  $\text{SnCl}_2 \cdot 2\text{H}_2\text{O}$  (5 eq.). The reaction was stirred overnight at rt under nitrogen atmosphere. Upon completion, the reaction was quenched with 1M NaOH and extracted with EtOAc. The organic layer was then washed with  $\text{H}_2\text{O}$  and dried over  $\text{MgSO}_4$  to yield methyl 4-(2-amino-4-chlorophenoxy)benzoate **2** (4.13 g, 14.9 mmol, 75%).  $^1\text{H}$  NMR (400 MHz, DMSO)  $\delta$  7.98 – 7.88 (m, 2H), 7.01

– 6.93 (m, 2H), 6.89 (d,  $J = 8.5$  Hz, 1H), 6.85 (d,  $J = 2.5$  Hz, 1H), 6.57 (dd,  $J = 8.5, 2.6$  Hz, 1H), 5.36 (s, 2H).

Next,  $\text{CH}_3\text{CN}$  was used to dissolve the intermediate before addition of indium (0.1 eq) and commercially available 3,4-dichloro-benzenesulfonylchloride **3** (1 eq). The mixture was stirred overnight at rt, after purging the system with nitrogen. The solvents were then evaporated, the residue extracted with EtOAc and washed successively with  $\text{H}_2\text{O}$  and brine. The organic layer was dried over  $\text{MgSO}_4$ , filtered and evaporated, after which the product was purified by flash column chromatography ( $\text{CHCl}_3$ :petroleum ether 3:1) in order to obtain pure methyl 4-(4-chloro-2-((3,4-dichlorophenyl)sulfonamido)phenoxy)benzoate **5** (3.61 g, 7.41 mmol, 50%).  $^1\text{H}$  NMR (400 MHz, DMSO)  $\delta$  10.60 (s, 1H), 7.79 (d,  $J = 8.8$  Hz, 2H), 7.76 (d,  $J = 1.9$  Hz, 1H), 7.59 (d,  $J = 8.4$  Hz, 1H), 7.54 (dd,  $J = 11.1, 2.2$  Hz, 2H), 7.33 (dd,  $J = 8.8, 2.5$  Hz, 1H), 7.07 (d,  $J = 8.8$  Hz, 1H), 6.64 (d,  $J = 8.8$  Hz, 2H), 3.83 (s, 3H).

Finally, a mix of 2M NaOH (10 mL) dioxane (10 mL) was added to the intermediate and the mixture was stirred at rt for 2h. Solvents were evaporated and the residue was extracted with DCM. The organic layer was extracted with  $\text{H}_2\text{O}$ . The aqueous layers were pooled and acidified with 6M HCl. Filtration of the precipitate gave 1.47 g of 4-(4-chloro-2-((3,4-dichlorophenyl)sulfonamido)phenoxy)benzoic acid **7** (37 mg, 8%).  $^1\text{H}$  NMR (400 MHz, DMSO)  $\delta$  12.81 (s, 1H), 10.60 (s, 1H), 7.81 (s, 1H), 7.81 – 7.75 (m, 2H), 7.63 (d,  $J = 8.4$  Hz, 1H), 7.57 (dd,  $J = 8.4, 2.0$  Hz, 1H), 7.51 (d,  $J = 2.4$  Hz, 1H), 7.33 (dd,  $J = 8.4, 2.4$  Hz, 1H), 7.04 (d,  $J = 9.6$  Hz, 1H), 6.63 (d,  $J = 8.8$  Hz, 2H); MS: ESI [ $\text{M} - \text{H}$ ]: 469.8; HPLC: 10.2 min.

## Synthetic procedure of compound 11

Previously described **2** (1 eq) and commercially available 4-chloro-3-(trifluoro-methyl) benzenesulfonyl chloride **4** (1.1 eq.) were dissolved in pyridine (0.4 M) and *N,N*-dimethylaminopyridine (0.1eq) was added. The mixture was stirred at 95 °C for 3h under microwave irradiation. The mixture was extracted with DCM and the organic layer was washed with aqueous HCl, water and brine. The organic phase was dried over  $\text{MgSO}_4$  and evaporated, after which precipitation with DCM and PE gave methyl 4-(4-chloro-2-((4-chloro-3-(trifluoromethyl)phenyl)sulfonamido)phenoxy)benzoate **6** (1.15 g, 63%).  $^1\text{H}$  NMR (400 MHz,  $\text{CDCl}_3$ )  $\delta$  8.03 (d,  $J = 2.1$  Hz, 1H), 7.93 (d,  $J = 8.8$  Hz, 2H), 7.79 (dd,  $J = 8.4, 2.1$  Hz, 1H), 7.73 (d,  $J = 2.4$  Hz, 1H), 7.51 (d,  $J = 8.4$  Hz, 1H), 7.12 (dd,  $J = 8.8, 2.5$  Hz, 1H), 7.00 (s, 1H), 6.77 (d,  $J = 8.8$  Hz, 1H), 6.65-6.60 (m, 2H), 3.92 (s, 3H).

A mix of 2M NaOH (6 mL) and dioxane (30 mL) was added to the intermediate and the mixture was stirred for 2.5h at 60°C. Upon completion, the reaction was diluted with  $\text{H}_2\text{O}$  and acidified with aqueous HCl. The product was then extracted with EtOAc (2 × 150 ml),

dried over  $\text{MgSO}_4$  and evaporated to yield 4-(4-chloro-2-((4-chloro-3-(trifluoromethyl)phenyl)sulfonamido)phenoxy)benzoic acid **8** (1.64 g, 85%).  $^1\text{H}$  NMR (400 MHz,  $\text{CDCl}_3$ )  $\delta$  8.03 (d,  $J = 1.8$  Hz, 1H), 7.99 (d,  $J = 8.6$  Hz, 2H), 7.80 (dd,  $J = 8.3, 2.0$  Hz, 1H), 7.76 (d,  $J = 2.5$  Hz, 1H), 7.52 (d,  $J = 8.4$  Hz, 1H), 7.13 (dd,  $J = 8.8, 2.5$  Hz, 1H), 6.98 (s, 1H), 6.80 (d,  $J = 8.7$  Hz, 1H), 6.68 – 6.63 (m, 2H).

A mixture of the carboxylic acid **8** (1 eq), *N*-Boc-ethylenediamine (1 eq.), 1-ethyl-3-(3-dimethylaminopropyl)carbodiimide (EDC, 2 eq), and hydroxybenzotriazole (HOBt, 0.1 eq) was dissolved in dioxane (0.015M) and stirred at rt for at least 20 h until completion. The reaction mixture was diluted with EtOAc and the organic phase was washed with water and brine, dried over  $\text{MgSO}_4$  and concentrated. The crude product was purified on a silica gel column chromatography with DCM/MeOH to give tert-butyl(2-(4-(4-chloro-2-((4-chloro-3-(trifluoro-methyl)phenyl)sulfonamido)phenoxy)benzamido)ethyl)carbamate (581 mg, 61%).  $^1\text{H}$  NMR (400 MHz,  $\text{CDCl}_3$ )  $\delta$  8.10 (d,  $J = 1.5$  Hz, 1H), 7.83 (dd,  $J = 8.4, 1.8$  Hz, 1H), 7.75 – 7.68 (m, 3H), 7.54 (d,  $J = 8.4$  Hz, 1H), 7.46 (s, 1H), 7.33 (s, 1H), 7.08 (dd,  $J = 8.8, 2.5$  Hz, 1H), 6.70 (d,  $J = 8.8$  Hz, 1H), 6.64 (d,  $J = 8.7$  Hz, 2H), 5.07 (s, 1H), 3.56 - 3.53 (m, 2H), 3.40 (d,  $J = 4.6$  Hz, 2H), 1.43 (s, 9H).

The Boc-protected compound was dissolved in DCM (0.1 M), and trifluoroacetic acid (TFA, 4 ml/mmol) was added dropwise. The mixture was stirred at rt for 3 h. After completion, the solvents were evaporated and the residue was dissolved in  $\text{H}_2\text{O}$  and alkalinized with 2M NaOH. The aqueous phase was then extracted with EtOAc and washed successively with water and brine. After drying over  $\text{MgSO}_4$  and concentration, the residue was taken up in EtOAc and 1M HCl (1ml/mmol) was added. Evaporation gave *N*-(2-aminoethyl)-4-(4-chloro-2-((4-chloro-3-(trifluoromethyl)phenyl)sulfonamido)phenoxy)benzamide hydrochloride **9** (358 mg, 92%).  $^1\text{H}$  NMR (400 MHz, MeOD)  $\delta$  8.66 (t, 1H), 8.03 (d,  $J = 2.1$  Hz, 1H), 7.84 (dd,  $J = 8.3, 2.1$  Hz, 1H), 7.75 (d,  $J = 8.8$  Hz, 2H), 7.63 (d,  $J = 2.5$  Hz, 1H), 7.59 (d,  $J = 8.4$  Hz, 1H), 7.21 (dd,  $J = 8.8, 2.6$  Hz, 1H), 6.82 (d,  $J = 8.8$  Hz, 1H), 6.63 (d,  $J = 8.8$  Hz, 2H), 3.64 (q,  $J = 5.9$  Hz, 2H), 3.14 (t,  $J = 5.9$  Hz, 2H).

This intermediate (1 eq) was dissolved in THF (0.02M) and triethylamine (6 eq) was added. The mixture was cooled to 0 °C before adding carbon disulphide (4 eq) and the reaction mixture was stirred for approximately 2 h at 0 °C until complete conversion to an intermediate. Tosyl chloride (3.5 eq) was added and the mixture was stirred for an additional 19h. The reaction was quenched with a phosphate buffer and the products were extracted into DCM. The organic phase was washed with brine, dried over  $\text{MgSO}_4$  and concentrated. The crude compound was purified with flash column chromatography using DCM/MeOH as eluents to yield final compound 4-(4-Chloro-2-((4-chloro-3-(trifluoromethyl)phenyl)sulfonamido)phenoxy)-*N*-(2-isothiocyanatoethyl)benzamide **11** (6 mg, 6%).  $^1\text{H}$  NMR (400 MHz,  $\text{CDCl}_3$ )  $\delta$  8.07 (d,  $J = 2.1$  Hz, 1H), 7.83 (dd,  $J = 8.4, 2.2$  Hz, 1H), 7.72 (d,  $J = 2.5$  Hz, 1H), 7.71 – 7.67 (m,



2H), 7.54 (d,  $J = 8.4$  Hz, 1H), 7.32 (s, 1H), 7.11 (dd,  $J = 8.8, 2.5$  Hz, 1H), 6.75 (d,  $J = 8.8$  Hz, 1H), 6.69 – 6.62 (m, 2H), 6.54 (t,  $J = 5.9$  Hz, 1H), 3.83 – 3.76 (m, 2H), 3.76 – 3.69 (m, 2H); MS: ESI [M - H]<sup>-</sup>: 587.9; HPLC: 13.0 min.

## Synthetic procedure of compound 12

Previously described **9** (1 eq) was dissolved in acetonitrile (5 mL) and cooled to  $-78^{\circ}\text{C}$  in an acetone/dry ice bath. Triethylamine (3.5 eq) and acryloyl chloride (1.1 eq) were added. The reaction mixture was then allowed to warm to room temperature and stirred for 2 hours. The mixture was poured into water, acidified with aqueous HCl and the aqueous layer was extracted with ethyl acetate twice. The organic layers were washed with water, dried over  $\text{MgSO}_4$  and concentrated. Purification by preparative TLC with EtOAc/acetone 100:1 as an eluent gave final compound N-(2-acrylamidoethyl)-4-(4-chloro-2-((4-chloro-3-(trifluoromethyl)phenyl)sulfonamido)phenoxy)benzamide **12** (10 mg, 20%).  $^1\text{H}$  NMR (400 MHz,  $\text{CDCl}_3$ )  $\delta$  8.09 (d,  $J = 2.1$  Hz, 1H), 7.82 (dd,  $J = 8.4, 2.2$  Hz, 1H), 7.71 (d,  $J = 2.1$  Hz, 1H), 7.70 – 7.68 (m, 2H), 7.53 (d,  $J = 8.4$  Hz, 1H), 7.44 (s, 1H), 7.43 (s, 1H), 7.09 (dd,  $J = 8.8, 2.5$  Hz, 1H), 6.73 (d,  $J = 8.8$  Hz, 1H), 6.64 (d,  $J = 8.8$  Hz, 2H), 6.51 (s, 1H), 6.30 (dd,  $J = 17.0, 1.3$  Hz, 1H), 6.14 (dd,  $J = 17.0, 10.2$  Hz, 1H), 5.69 (dd,  $J = 10.2, 1.3$  Hz, 1H), 3.60 (s, 4H); MS: ESI [M - H]<sup>-</sup>: 600.0; HPLC: 11.7 min.

## Synthetic procedure of compound 13

A mixture of previously described **9** (1 eq), commercially available 4-fluorosulfonylbenzoic acid (1 eq.), EDC (2 eq), and HOBt (0.1 eq) was dissolved in dioxane (0.015M) and stirred at rt for at least 20 h until completion. The reaction mixture was diluted with EtOAc and the organic phase was washed with water and brine, dried over  $\text{MgSO}_4$  and concentrated. The crude product was purified on a silica gel column chromatography with DCM/MeOH to give 4-((2-(4-(4-Chloro-2-((4-chloro-3-(trifluoromethyl)phenyl)sulfonamido)phenoxy)benzamido)ethyl) carbamoyl)benzenesulfonyl fluoride **13** (8 mg, 31%).  $^1\text{H}$  NMR (400 MHz,  $\text{CDCl}_3$ )  $\delta$  8.07 (s, 4H), 8.06 (d,  $J = 2.1$  Hz, 1H), 7.89 (t,  $J = 4.4$  Hz, 1H), 7.82 (dd,  $J = 8.4, 2.1$  Hz, 1H), 7.71 (d,  $J = 2.5$  Hz, 1H), 7.67 (d,  $J = 8.8$  Hz, 2H), 7.52 (d,  $J = 8.4$  Hz, 1H), 7.30 (s, 1H), 7.10 (dd,  $J = 8.8, 2.5$  Hz, 1H), 6.93 (t,  $J = 5.2$  Hz, 1H), 6.74 (d,  $J = 8.8$  Hz, 1H), 6.65 (d,  $J = 8.8$  Hz, 2H), 3.81 – 3.69 (m, 4H); MS: ESI [M - H]<sup>-</sup>: 732.0; HPLC: 12.8 min.

## Synthetic procedure of compound 14

A mixture of the carboxylic acid **8** (1 eq), 2-bromoethylamine (1 eq.), EDC (2 eq), and HOBT (0.1 eq) was dissolved in dioxane (0.015M) and stirred at rt for at least 20 h until completion. The reaction mixture was diluted with EtOAc and the organic phase was washed with water and brine, dried over MgSO<sub>4</sub> and concentrated. The crude product was purified on a silica gel column chromatography with EtOAc/petroleum ether to yield N-(2-bromoethyl)-4-(4-chloro-2-((4-chloro-3-(trifluoromethyl)phenyl)sulfonamido)phenoxy)benzamide **10** (62 mg, 51%). <sup>1</sup>H NMR (400 MHz, CDCl<sub>3</sub>) δ 8.06 (s, 1H), 7.85 – 7.77 (m, 3H), 7.73 – 7.69 (m, 1H), 7.51 (d, *J* = 8.4 Hz, 1H), 7.09 (dd, *J* = 8.7, 2.5 Hz, 1H), 6.73 (d, *J* = 8.8 Hz, 1H), 6.60 (d, *J* = 8.8 Hz, 2H), 4.44 (t, *J* = 9.5 Hz, 2H), 4.05 (t, *J* = 9.5 Hz, 2H).

Finally, a mixture of KSCN (6 eq.) and the intermediate (1 eq) was dissolved in EtOH (0.025M) and the mixture was refluxed for 3 days. After completion of the reaction the solvent was evaporated and the residue was dissolved in EtOAc, washed with water and brine, dried over MgSO<sub>4</sub> and concentrated. Preparative TLC with DCM/MeOH 25:1 as an eluent gave final compound 4-(4-Chloro-2-((4-chloro-3-(trifluoromethyl)phenyl)sulfonamido)phenoxy)-N-(2-thiocyanatoethyl)benzamide **14** (4 mg, 21%). <sup>1</sup>H NMR (400 MHz, CDCl<sub>3</sub>) δ 8.05 (d, *J* = 2.1 Hz, 1H), 7.82 (dd, *J* = 8.4, 2.1 Hz, 1H), 7.73 (d, *J* = 2.5 Hz, 1H), 7.73 – 7.68 (m, 2H), 7.54 (d, *J* = 8.4 Hz, 1H), 7.19 (s, 1H), 7.11 (dd, *J* = 8.7, 2.5 Hz, 2H), 6.75 (d, *J* = 8.8 Hz, 1H), 6.68 – 6.63 (m, 2H), 6.62 (t, *J* = 5.8 Hz, 1H), 3.88 (q, *J* = 6.0 Hz, 2H), 3.26 (t, *J* = 6.0 Hz, 2H); MS: ESI [M - H]<sup>-</sup>: 587.9; HPLC: 12.5 min.

## Biology

### Chemicals and Reagents

[<sup>3</sup>H]-CCR2-RA-[R] (specific activity 59.6 Ci mmol<sup>-1</sup>) was custom-labelled by Vitrox (Placentia, CA) and [<sup>35</sup>S]GTPγS (specific activity 1250 Ci mmol<sup>-1</sup>) was purchased from PerkinElmer (Groningen, The Netherlands). The CCR2 ligands CCR2-RA-[R] and JNJ-27141491 were synthesized as previously described.<sup>45,46</sup> Human CCL2 was purchased from PeproTech (Rocky Hill, NJ). Bovine serum albumin (BSA, fraction V), guanosine 5'-diphosphate (GDP), and iodoacetamide (IA) were from Sigma Aldrich (St. Louis, MO, USA). Pierce™ Bicinchoninic acid (BCA) protein assay kit and Coelenterazine (CTZ-n) were obtained from Thermo Fisher Scientific (Rockford, IL). Polyethyleneimine (PEI) was purchased from Polysciences Inc. (Warrington, Pennsylvania). Tango CCR2-*bla* osteosarcoma cells stably expressing human CCR2b (U2OS-CCR2) were obtained from Invitrogen (Carlsbad, CA). Chinese hamster ovary (CHO) cells were kindly provided by Hans den Dulk (Leiden University, the Netherlands) and

originally obtained from ATCC. All other chemicals were from standard commercial sources.

## Plasmids used in the study

pCDNA3.1+ plasmids contacting the FLAG-tagged wild-type human CCR2 and the human CCR2 mutants C70S<sup>1x60</sup>, C75S<sup>2x37</sup> and C232S<sup>5x68</sup> were cloned in-house. The plasmids CCR2b-SmBit and LgBit- $\beta$ -arrestin1-EE were generous gifts from Asuka Inoue (Graduate School of Pharmaceutical Sciences, Tohoku University, Sendai, Japan). CCR2b-SmBit was obtained by fusing a small C-terminal fragment (residues 185-VTGYRLFEEIL-195) of engineered *Oplophorus gracilirostris* luciferase known as NanoLuc,<sup>47</sup> with a flexible 15-AA linker (GGSGGGGSGSSSSGG) preceding it, to the C-terminus of human CCR2b in pCDNA3.1+. LgBit- $\beta$ -arrestin1-EE was obtained by fusing the remaining larger fragment of NanoLuc (27-VFTLEDFVGD WEQTAAYNLD QVLEQGGVSS LLQNLAVSVT PIQRIVRSGE NALKIDIHVIIPYEGLSADQ MAQIEEVFKV VYPVDDHHFK VILPYGTLVI DGVTPNMLNY FGRPYEGIAVFDGKKITVTG TLWNGNKIID ERLITPDGSM LFRVTINS-184) to the N-terminus of clathrin-binding-deficient variant of human  $\beta$ -arrestin1 incorporated in pCAGGS vector, with a flexible 16AA linker GGSGGGGSGSSSSGGT between the two. The EE variant contains two mutations (R392E, R394E) in the clathrin/AP-2-binding motif of  $\beta$ -arrestin1, which leads to better retention at the cell plasma membrane and hence an increased receptor recruitment signal.<sup>48</sup> All plasmids were propagated in E coli using ampicillin (100  $\mu$ g/mL) as a bacterial selection marker.

## Cell culture

U2OS-CCR2 and CHO cells were grown as a monolayer in 10-cm  $\emptyset$  or 15-cm  $\emptyset$  culture plates at 37 °C and 5% CO<sub>2</sub>. U2OS-CCR2 were cultured in McCoy's 5A medium containing 10% fetal calf serum (FCS), 2 mM glutamine, 0.1 mM non-essential amino acids, 25 mM HEPES, 1 mM sodium pyruvate, 200 IU/mL penicillin, 200  $\mu$ g/mL streptomycin, 100  $\mu$ g/mL G418, 40-50  $\mu$ g/mL Hygromycin and 125  $\mu$ g/mL Zeocin. Empty CHO cells were cultured in DMEM/F12 medium supplemented with 10% (v/v) newborn calf serum, 200 IU/mL penicillin, 200  $\mu$ g/mL streptomycin and 2 mM glutamine. HEK293t cells were cultured in DMEM medium supplemented with 10% FCS. All cells were subcultured twice a week, by trypsinization, at a ratio of 1:3 to 1:8 or 1:30 to 1:50 in the case of CHO cells. Dialyzed fetal calf serum was used before membrane preparation of U2OS-CCR2 cells.

## Transfections

Transfections of CHO cells with FLAG-tagged WT or mutant CCR2 were performed using a previously described PEI method.<sup>26</sup> Briefly, empty CHO cells were grown to ~50% confluence in 15-cm  $\emptyset$  culture plates and transfected with a DNA/PEI mixture in 150 mM NaCl solution containing 10  $\mu$ g plasmid mixed with PEI (1 mg/ml) at a mass ratio of 1:6. Before transfection, the DNA/PEI mixture was incubated for 20 min and the culture medium of the cells was refreshed. After 24 hours, sodium butyrate (final concentration of 3 mM) was added to the plates to increase receptor expression.<sup>49</sup> Finally, cells were incubated for another 24 hours at 37 °C and 5% CO<sub>2</sub>. HEK293t cells were transiently transfected with CCR2b-SmBit and LgBit- $\beta$ -arrestin1-EE plasmids using TransIT<sup>®</sup>-LT1 transfection reagent (Mirus Bio, Madison, WI, USA). Empty cells were grown in 6-cm  $\emptyset$  culture plates to 60 – 80% confluence before transfection with DNA/reagent mixture, containing 6  $\mu$ g plasmid mixed with TransIT<sup>®</sup>-LT1 reagent at a 1:3 ratio. The DNA/reagent mixture was first incubated for 30 min at room temperature and the culture medium of the cells was refreshed before addition. The transfected cells were incubated for another 24 hours at 37 °C and 5% CO<sub>2</sub> before performing the NanoBit assays.

## Membrane preparation

Membranes from U2OS-CCR2 or CHO cells transiently transfected with wild-type (WT) human CCR2 or human CCR2 mutants were prepared as previously described, using several centrifugation and homogenization steps.<sup>25</sup> Final membrane pellets were resuspended in ice-cold Tris buffer (50 mM Tris-HCl pH 7.4, 5 mM MgCl<sub>2</sub>), homogenized with an Ultra Turrax homogenizer (IKA-Werke GmbH & Co. KG, Staufen, Germany) and stored in aliquots of 100 or 250  $\mu$ l at -80 °C. A standard BCA protein determination assay was used to measure the membrane protein concentrations (Pierce™ BCA protein assay kit).<sup>50</sup>

## Radioligand binding assays

### *[<sup>3</sup>H]-CCR2-RA and [<sup>3</sup>H]-CCR2-RA-[R] binding assays*

For all radioligand binding assays, membranes from U2OS-CCR2 cells or CHO cells transiently transfected with WT or mutant CCR2 were first thawed and homogenized using an Ultra Turrax homogenizer (IKA-Werke GmbH & Co. KG, Staufen, Germany). Membranes were then diluted in assay buffer (50 mM Tris-HCl pH 7.4, 5 mM MgCl<sub>2</sub>, 0.1% CHAPS) to a final concentration of 5 - 30  $\mu$ g membrane protein in a total volume of 100  $\mu$ l. For displacement assays, membranes were coincubated for 2 hours at 25 °C with multiple concentrations of

competing ligand, ranging from 0.01 nM to 10  $\mu$ M, and a fixed concentration of radioligand ( $\sim$ 6 nM [ $^3$ H]-CCR2-RA or [ $^3$ H]-CCR2-RA-[R]). At this concentration we ensured that total radioligand binding did not exceed 10% of the total radioactivity added, in order to prevent radioligand depletion. In all cases, nonspecific binding was determined using 10  $\mu$ M JNJ-27141491. In the case of preincubation experiments, membranes were preincubated for 4 hours with increasing concentrations of competing ligand, before addition of  $\sim$ 6 nM [ $^3$ H]-CCR2-RA-[R] and further coincubation of 20 minutes. In all assays, incubations were terminated by rapid vacuum filtration through pre-wetted GF/B filterplates using a PerkinElmer FilterMate harvester (Perkin Elmer, Groningen, the Netherlands). Filters were subsequently washed 10 times with ice-cold washbuffer (50 mM Tris-HCl pH 7.4, 5 mM MgCl<sub>2</sub>, 0.01% CHAPS) and dried at 55 °C for at least 30 minutes. Finally, filter-bound radioactivity was measured in a P-E 2450 Microbeta<sup>2</sup> counter (Perkin Elmer) after addition of 25  $\mu$ l Microscint scintillation cocktail (Perkin Elmer).

### ***Wash-out assays with [ $^3$ H]-CCR2-RA-[R]***

For wash-out assays, membrane homogenates (80 – 100  $\mu$ g) were preincubated in 1.5-ml Eppendorf tubes with a single concentration of compounds **7** and **14**, in a final volume of 300  $\mu$ l assay buffer (50 mM Tris-HCl pH 7.4, 5 mM MgCl<sub>2</sub>, 0.1% CHAPS). In the case of wash-out assays in U2OS-CCR2 membranes, a  $10 \times IC_{50}$  concentration was chosen for **7** (90 nM) and **14** (12 nM). In the case of wash-out assays in CHO-CCR2 mutant receptor membranes, a concentration of 200 nM **7** and 60 nM **14** was used to ensure a saturating concentration in all mutants despite changes in affinity. In the case of wash-out assays with IA, U2OS-CCR2 membranes were pretreated with 2 mg/ml IA for 30 minutes at room temperature and protected from light, prior to incubation with ligands. After incubation for 2 hours at 25 °C, while shaking at approximately 800 rpm, the mixture was centrifuged at 13,000 rpm for 5 min at 4 °C and the supernatant containing unbound ligand was removed. The remaining pellet was resuspended in 1 ml assay buffer (50 mM Tris-HCl pH 7.4, 5 mM MgCl<sub>2</sub>, 0.1% CHAPS) and incubated for an extra 20 minutes before another cycle of centrifugation and washing. After four cycles, the final membrane pellet was resuspended in 300  $\mu$ l assay buffer, transferred to test tubes and incubated with 100  $\mu$ l of  $\sim$ 6 nM [ $^3$ H]-CCR2-RA-[R] for 2 hours at 25 °C while shaking. Incubations were terminated by rapid filtration through a pre-wetted Whatman GF/B filter using a Brandel harvester 24 (Brandel, Gaithersburg, MD, USA). Filters were washed three times with 2 ml ice-cold wash buffer (50 mM Tris-HCl pH 7.4, 5 mM MgCl<sub>2</sub>, 0.01% CHAPS) and transferred to polyethylene Pony vials (Perkin Elmer) before measurement of filter-bound radioactivity in a Tri-Carb 2810TR Liquid scintillation analyzer (Perkin Elmer).

### ***[<sup>35</sup>S]GTPγS binding assays***

[<sup>35</sup>S]GTPγS binding assays were performed as previously described.<sup>41</sup> Briefly, U2OS-CCR2 membrane homogenates (10 μg) were diluted in assay buffer (50 mM Tris-HCl pH 7.4, 5 mM MgCl<sub>2</sub>, 100 mM NaCl, 1mM EDTA and 0.05% BSA) supplemented with saponin (0.5 mg/ml) and 10 μM GDP to a total volume of 100 μl. To determine the (p)IC<sub>50</sub> values of **7** and **14**, membranes were preincubated for 30 minutes at 25 °C with increasing concentrations of ligand in the presence of an EC<sub>80</sub> concentration of CCL2 (20 nM), as previously determined.<sup>41</sup> Basal activity was determined in the absence of any ligand or CCL2; maximal activity in the presence of 20 nM CCL2. After addition of 20 μl [<sup>35</sup>S]GTPγS (0.3 nM), the mixture was incubated for 90 more minutes at 25 °C before stopping the reaction with ice-cold wash-buffer (50 mM Tris-HCl pH 7.4, 5 mM MgCl<sub>2</sub>). Filtration and radioactivity measurement was performed as described under “[<sup>3</sup>H]-CCR2-RA and [<sup>3</sup>H]-CCR2-RA-[R] binding assays”.

### ***Wash-out assays with [<sup>35</sup>S]GTPγS***

Wash-out assays with [<sup>35</sup>S]GTPγS were performed as described under “Wash-out assays with [<sup>3</sup>H]-CCR2-RA-[R]”. Briefly, U2OS-CCR2 membrane homogenates (40 μg) were pre-incubated in the absence or presence of a single concentration of **7** (600 nM) and **14** (250 nM), in a final volume of 400 μl buffer containing 50 mM Tris-HCl (pH 7.4) and 5 mM MgCl<sub>2</sub>. After four cycles of centrifugation and washing, the remaining pellets were transferred to test tubes in a final volume of 320 μl containing [<sup>35</sup>S]GTPγS assay buffer (50 mM Tris-HCl pH 7.4, 5 mM MgCl<sub>2</sub>, 100 mM NaCl, 1 mM EDTA and 0.05% BSA), saponin (0.5 mg/ml), GDP (10 μM) and an EC<sub>80</sub> concentration of CCL2 (20 nM). For unwashed samples, only the last centrifugation step was performed in order to resuspend the sample in the same volume of 320 μl. All samples were then preincubated for 30 min at 25 °C before addition of 80 μl [<sup>35</sup>S]GTPγS (0.3 nM). Reaction was stopped after 90 minutes at 25 °C by rapid filtration as described under “Wash-out assays with [<sup>3</sup>H]-CCR2-RA-[R]”, but using [<sup>35</sup>S]GTPγS wash-buffer (50 mM Tris-HCl pH 7.4, 5 mM MgCl<sub>2</sub>).

## **NanoBit CCR2 assays**

24 hours post-transfection of HEK293t cells with CCR2b-SmBit and LgBit-β-arrestin1-EE plasmids, the cells were detached with PBS/EDTA (0.2 mM), centrifuged and resuspended in assay buffer (1× HBSS, 5 mM HEPES pH 7.2, 0.05% BSA) to a concentration of 1.3×10<sup>6</sup> cells/ml. The cells were seeded in a round-bottom 96-wells plate (Greiner Bio-One, NC, USA) at 120,000 cells per well in 90 μL assay buffer. Serial dilutions of test compounds in assay buffer, at 10 × final concentrations, were prepared from 10 mM DMSO stocks. Then, 10 μL of assay buffer (unwashed wells) or diluted test compounds (wash-out wells) were added to the

plate. After incubating the plate at room temperature for at least 20 min, cells were washed twice by spinning the plate at  $400 \times g$  for 5 min and discarding the supernatant. Afterwards, cells were resuspended in 80  $\mu\text{L}$  assay buffer and transferred to a Falcon™ 96-well black/clear bottom plate (Corning, NY, USA). 10  $\mu\text{L}$  of assay buffer or 10  $\mu\text{L}$  of test compound were added to wash-out and unwashed wells, respectively. 10  $\mu\text{L}$  of coelenterazine (CTZ-n, Fisher Scientific, Waltham, MA, USA), diluted in assay buffer from a 5mM stock in ethanol, was added to the plate to achieve a final concentration of 10  $\mu\text{M}$  and 100  $\mu\text{L}$  final volume in each well. The plate was then incubated at room temperature for approximately 90 min, protected from light. Basal luminescence was read for each well using a PerkinElmer Victor X Light 2030 apparatus (1 sec, no filter). Next, 10  $\mu\text{L}$  of 2  $\mu\text{M}$  CCL2 in assay buffer was added to each well and the cells were further incubated at room temperature for 10 min, protected from light, after which the plate was read again for endpoint luminescence generated by structural complementation.

## Molecular modeling and ligand docking

### *Generation of a model of WT CCR2*

The crystal structure of engineered human CCR2 in complex with an orthosteric and an allosteric antagonists (PDB 5T1A,<sup>19</sup> **Chapter 3**) was used as a template for the generation of the CCR2:14 complex model. All modeling and docking was performed in ICM v3.8-7a (Molsoft LLC, San Diego, CA<sup>51</sup>). The T4 lysozyme (T4L) fusion protein present in the structure was removed, the mutated residues in the intracellular part of TM6 reverted to WT, and the intracellular loop 3 (ICL3) rebuilt. For rebuilding the ICL3, a peptide containing residues 223:243 of CCR2 was built *ab-initio*, the backbones of residues 223:231,236:243 and the side chains of residues 223:226,241:243 tethered to their respective positions in the crystal structure, the receptor represented as a set of three dimensional (3D) grid maps representing van der Waals, electrostatic, hydrogen bonding, and surface energy potentials, and the peptide conformation was optimized using the biased probability Monte Carlo (BPMC) sampling in internal coordinates as implemented in ICM.<sup>51</sup> The simulation simultaneously optimized the intramolecular energy of the peptide and its interaction with the context potential grid maps. The best scoring conformation of the peptide was merged with the rest of the receptor coordinates, and the system was minimized in its full-atom representation, with harmonic restraints of gradually decreasing strength imposed between the model and either the X-ray coordinates or the best prediction conformations of the *ab initio* modeled ICL3. Towards the end of the optimization, the restraints were released entirely. The simulations were performed in the presence of crystallographic ligands.

### ***Generation of a model of CCR2:14 complex***

Alternative conformers of the allosteric pocket in CCR2 were generated by systematic sampling of aliphatic side-chain rotamers and translations of the intracellular ends of TM helices 6 and 7. The conformer that best predicted the binding poses of the sulfonamide series of allosteric CCR2 antagonists (analogous to **14**) was chosen. The binding pose of **14** was predicted by covalent docking in ICM under the assumption that the covalent attachment residue is C75 due to its proximity. For docking, the receptor atoms in the 4Å vicinity of the allosteric pocket were represented as 3D grid potential maps as above, with the exception of C75 for which the explicit representation was used. The covalent bond between **14** and C75 was imposed and the system was sampled as described above to generate a ranked list of alternative conformations for the ligand. Top 10 conformations were merged with the full-atom model of the receptor and re-scored using the ICM ligand scoring function previously optimized for ligand geometry prediction on a diverse benchmark of crystallographic protein-ligand complexes.<sup>52</sup> The top-scoring pose was selected.

### **Data analysis**

Data analyses were performed using Prism 7.00 (GraphPad software, San Diego, CA, USA). (p)IC<sub>50</sub> values from radioligand displacement assays, [<sup>35</sup>S]GTPγS binding assays and NanoBit assays were obtained by non-linear regression curve fitting into a sigmoidal concentration-response curve using the equation:  $Y = \text{Bottom} + (\text{Top} - \text{Bottom}) / (1 + 10^{-(X - \text{LogIC}_{50})})$ . pK<sub>i</sub> values were obtained from pIC<sub>50</sub> values using the ChengPrusoff equation.<sup>53</sup> Data are shown as mean ± SEM of at least three individual experiments performed in duplicate. Statistical analyses were performed as indicated. If p-values were below 0.05, observed differences were considered statistically significant.



## REFERENCES

1. Bachelier, F.; Ben-Baruch, A.; Burkhardt, A. M.; Combadiere, C.; Farber, J. M.; Graham, G. J.; Horuk, R.; Sparre-Ulrich, A. H.; Locati, M.; Luster, A. D.; Mantovani, A.; Matsushima, K.; Murphy, P. M.; Nibbs, R.; Nomiya, H.; Power, C. A.; Proudfoot, A. E.; Rosenkilde, M. M.; Rot, A.; Sozzani, S.; Thelen, M.; Yoshie, O.; Zlotnik, A. International Union of Basic and Clinical Pharmacology. [corrected]. LXXXIX. Update on the extended family of chemokine receptors and introducing a new nomenclature for atypical chemokine receptors. *Pharmacol Rev* **2014**, *66*, 1-79.
2. Viola, A.; Luster, A. D. Chemokines and their receptors: drug targets in immunity and inflammation. *Annu Rev Pharmacol Toxicol* **2008**, *48*, 171-197.
3. O'Connor, T.; Borsig, L.; Heikenwalder, M. CCL2-CCR2 signaling in disease pathogenesis. *Endocr. Metab. Immune Disord. Drug Targets* **2015**, *15*, 105-118.
4. Bot, I.; Ortiz Zacarias, N. V.; de Witte, W. E.; de Vries, H.; van Santbrink, P. J.; van der Velden, D.; Kroner, M. J.; van der Berg, D. J.; Stamos, D.; de Lange, E. C.; Kuiper, J.; Ilzerman, A. P.; Heitman, L. H. A novel CCR2 antagonist inhibits atherogenesis in apoE deficient mice by achieving high receptor occupancy. *Sci Rep* **2017**, *7*, 52.
5. Kang, Y. S.; Lee, M. H.; Song, H. K.; Ko, G. J.; Kwon, O. S.; Lim, T. K.; Kim, S. H.; Han, S. Y.; Han, K. H.; Lee, J. E.; Han, J. Y.; Kim, H. K.; Cha, D. R. CCR2 antagonism improves insulin resistance, lipid metabolism, and diabetic nephropathy in type 2 diabetic mice. *Kidney Int.* **2010**, *78*, 883-894.
6. Piotrowska, A.; Kwiatkowski, K.; Rojewska, E.; Slusarczyk, J.; Makuch, W.; Basta-Kaim, A.; Przewlocka, B.; Mika, J. Direct and indirect pharmacological modulation of CCL2/CCR2 pathway results in attenuation of neuropathic pain - In vivo and in vitro evidence. *J. Neuroimmunol.* **2016**, *297*, 9-19.
7. Qian, B. Z.; Li, J.; Zhang, H.; Kitamura, T.; Zhang, J.; Campion, L. R.; Kaiser, E. A.; Snyder, L. A.; Pollard, J. W. CCL2 recruits inflammatory monocytes to facilitate breast-tumour metastasis. *Nature* **2011**, *475*, 222-225.
8. Horuk, R. Chemokine receptor antagonists: overcoming developmental hurdles. *Nat Rev Drug Discov* **2009**, *8*, 23-33.
9. Weichert, D.; Gmeiner, P. Covalent molecular probes for class A G protein-coupled receptors: advances and applications. *ACS Chem. Biol.* **2015**, *10*, 1376-1386.
10. Ghosh, A. K.; Samanta, I.; Mondal, A.; Liu, W. R. Covalent inhibition in drug discovery. *ChemMedChem* **2019**, *14*, 889-906.
11. Jones, L. H. Cell permeable affinity- and activity-based probes. *Future Med. Chem.* **2015**, *7*, 2131-2141.
12. Jörg, M.; Scammells, P. J. Guidelines for the synthesis of small-molecule irreversible probes targeting G protein-coupled receptors. *ChemMedChem* **2016**, *11*, 1488-1498.
13. Bauer, R. A. Covalent inhibitors in drug discovery: from accidental discoveries to avoided liabilities and designed therapies. *Drug Discov Today* **2015**, *20*, 1061-1073.
14. González-Bello, C. Designing irreversible inhibitors--worth the effort? *ChemMedChem* **2016**, *11*, 22-30.
15. Baillie, T. A. Targeted covalent inhibitors for drug design. *Angew. Chem. Int. Ed. Engl.* **2016**, *55*, 13408-13421.
16. Hua, T.; Vemuri, K.; Nikas, S. P.; Laprairie, R. B.; Wu, Y.; Qu, L.; Pu, M.; Korde, A.; Jiang, S.; Ho, J. H.; Han, G. W.; Ding, K.; Li, X.; Liu, H.; Hanson, M. A.; Zhao, S.; Bohn, L. M.; Makriyannis, A.; Stevens, R. C.; Liu, Z. J. Crystal structures of agonist-bound human cannabinoid receptor CB<sub>1</sub>. *Nature* **2017**, *547*, 468-471.
17. Glukhova, A.; Thal, D. M.; Nguyen, A. T.; Vecchio, E. A.; Jörg, M.; Scammells, P. J.; May, L. T.; Sexton, P. M.; Christopoulos, A. Structure of the adenosine A1 receptor reveals the basis for subtype selectivity. *Cell* **2017**, *168*, 867-877.
18. Apel, A. K.; Cheng, R. K. Y.; Tautermann, C. S.; Brauchle, M.; Huang, C. Y.; Pautsch, A.; Hennig, M.; Nar, H.; Schnapp, G. Crystal structure of CC chemokine receptor 2A in complex with an orthosteric antagonist provides insights for the design of selective antagonists. *Structure* **2019**, *27*, 427-438.

19. Zheng, Y.; Qin, L.; Ortiz Zacarías, N. V.; de Vries, H.; Han, G. W.; Gustavsson, M.; Dabros, M.; Zhao, C.; Cherney, R. J.; Carter, P.; Stamos, D.; Abagyan, R.; Cherezov, V.; Stevens, R. C.; Iljerman, A. P.; Heitman, L. H.; Tebben, A.; Kufareva, I.; Handel, T. M. Structure of CC chemokine receptor 2 with orthosteric and allosteric antagonists. *Nature* **2016**, *540*, 458-461.
20. Ortiz Zacarias, N. V.; Lenselink, E. B.; Iljerman, A. P.; Handel, T. M.; Heitman, L. H. Intracellular receptor modulation: novel approach to target GPCRs. *Trends Pharmacol Sci* **2018**, *39*, 547-559.
21. Peace, S.; Philp, J.; Brooks, C.; Piercy, V.; Moores, K.; Smethurst, C.; Watson, S.; Gaines, S.; Zippoli, M.; Mookherjee, C.; Ife, R. Identification of a sulfonamide series of CCR2 antagonists. *Bioorg. Med. Chem. Lett.* **2010**, *20*, 3961-3964.
22. Wang, G. Z.; Haile, P. A.; Daniel, T.; Belot, B.; Viet, A. Q.; Goodman, K. B.; Sha, D.; Dowdell, S. E.; Varga, N.; Hong, X.; Chakravorty, S.; Webb, C.; Cornejo, C.; Olzinski, A.; Bernard, R.; Evans, C.; Emmons, A.; Briand, J.; Chung, C. W.; Quek, R.; Lee, D.; Gough, P. J.; Sehon, C. A. CCR2 receptor antagonists: optimization of biaryl sulfonamides to increase activity in whole blood. *Bioorg. Med. Chem. Lett.* **2011**, *21*, 7291-7294.
23. Garritsen, A.; Iljerman, A. P.; Beukers, M. W.; Soudijn, W. Chemical modification of adenosine A1 receptors: implications for the interaction with R-PIA, DPCPX and amiloride. *Biochem. Pharmacol.* **1990**, *40*, 835-842.
24. Carter, P. H. Progress in the discovery of CC chemokine receptor 2 antagonists, 2009 – 2012. *Expert Opin. Ther. Pat.* **2013**, *23*, 549-568.
25. Zweemer, A. J.; Nederpelt, I.; Vrieling, H.; Hafith, S.; Doornbos, M. L.; de Vries, H.; Abt, J.; Gross, R.; Stamos, D.; Saunders, J.; Smit, M. J.; Iljerman, A. P.; Heitman, L. H. Multiple binding sites for small-molecule antagonists at the CC chemokine receptor 2. *Mol. Pharmacol.* **2013**, *84*, 551-561.
26. Zweemer, A. J.; Bunnik, J.; Veenhuizen, M.; Miraglia, F.; Lenselink, E. B.; Vilums, M.; de Vries, H.; Gibert, A.; Thiele, S.; Rosenkilde, M. M.; Iljerman, A. P.; Heitman, L. H. Discovery and mapping of an intracellular antagonist binding site at the chemokine receptor CCR2. *Mol. Pharmacol.* **2014**, *86*, 358-368.
27. Burke, T. R.; Bajwa, B. S.; Jacobson, A. E.; Rice, K. C.; Streaty, R. A.; Klee, W. A. Probes for narcotic receptor mediated phenomena. 7. Synthesis and pharmacological properties of irreversible ligands specific for  $\mu$  or  $\delta$  opiate receptors. *J. Med. Chem.* **1984**, *27*, 1570-1574.
28. Nakamura, T.; Kawai, Y.; Kitamoto, N.; Osawa, T.; Kato, Y. Covalent modification of lysine residues by allyl isothiocyanate in physiological conditions: plausible transformation of isothiocyanate from thiol to amine. *Chem. Res. Toxicol.* **2009**, *22*, 536-542.
29. Doorn, J. A.; Petersen, D. R. Covalent modification of amino acid nucleophiles by the lipid peroxidation products 4-hydroxy-2-nonenal and 4-oxo-2-nonenal. *Chem. Res. Toxicol.* **2002**, *15*, 1445-1450.
30. Narayanan, A.; Jones, L. H. Sulfonyl fluorides as privileged warheads in chemical biology. *Chem. Sci.* **2015**, *6*, 2650-2659.
31. Yan, F.; Bikbulatov, R. V.; Mocanu, V.; Dicheva, N.; Parker, C. E.; Wetsel, W. C.; Mosier, P. D.; Westkaemper, R. B.; Allen, J. A.; Zjawiony, J. K.; Roth, B. L. Structure-based design, synthesis, and biochemical and pharmacological characterization of novel salvinorin A analogues as active state probes of the kappa-opioid receptor. *Biochemistry* **2009**, *48*, 6898-6908.
32. Strelow, J. M. A perspective on the kinetics of covalent and irreversible inhibition. *SLAS Discov* **2017**, *22*, 3-20.
33. Yang, X.; Dong, G.; Michiels, T. J. M.; Lenselink, E. B.; Heitman, L.; Louvel, J.; Iljerman, A. P. A covalent antagonist for the human adenosine A<sub>2A</sub> receptor. *Purinergic Signal.* **2017**, *13*, 191-201.
34. Yang, X.; van Veldhoven, J. P. D.; Offringa, J.; Kuiper, B. J.; Lenselink, E. B.; Heitman, L. H.; van der Es, D.; Iljerman, A. P. Development of covalent ligands for G protein-coupled receptors: a case for the human adenosine A(3) receptor. *J. Med. Chem.* **2019**, *62*, 3539-3552.
35. Doornbos, M. L. J.; Wang, X.; Vermond, S. C.; Peeters, L.; Perez-Benito, L.; Trabanco, A. A.; Lavreysen, H.; Cid, J. M.; Heitman, L. H.; Tresadern, G.; Iljerman, A. P. Covalent allosteric probe for the metabotropic glutamate receptor 2: design, synthesis, and pharmacological characterization. *J. Med. Chem.* **2019**, *62*, 223-233.

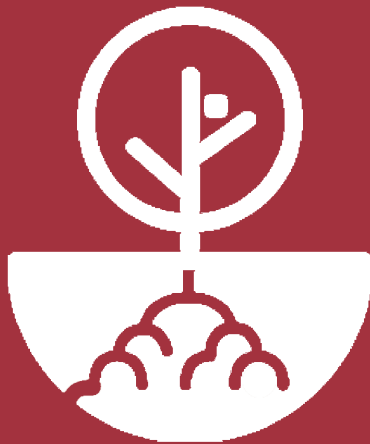
36. Xia, L.; de Vries, H.; Yang, X.; Lenselink, E. B.; Kyrizaki, A.; Barth, F.; Louvel, J.; Dreyer, M. K.; van der Es, D.; IJzerman, A. P.; Heitman, L. H. Kinetics of human cannabinoid 1 (CB1) receptor antagonists: structure-kinetics relationships (SKR) and implications for insurmountable antagonism. *Biochem. Pharmacol.* **2018**, *151*, 166-179.
37. Swinney, D. C.; Beavis, P.; Chuang, K. T.; Zheng, Y.; Lee, I.; Gee, P.; Deval, J.; Rotstein, D. M.; Dioszegi, M.; Ravendran, P. A study of the molecular mechanism of binding kinetics and long residence times of human CCR5 receptor small molecule allosteric ligands. *Br. J. Pharmacol.* **2014**, *171*, 3364-3375.
38. Mah, R.; Thomas, J. R.; Shafer, C. M. Drug discovery considerations in the development of covalent inhibitors. *Bioorg. Med. Chem. Lett.* **2014**, *24*, 33-39.
39. Moss, S. M.; Jayasekara, P. S.; Paoletta, S.; Gao, Z. G.; Jacobson, K. A. Structure-based design of reactive nucleosides for site-specific modification of the A2A adenosine receptor. *ACS Med Chem Lett* **2014**, *5*, 1043-1048.
40. Picone, R. P.; Khanolkar, A. D.; Xu, W.; Ayotte, L. A.; Thakur, G. A.; Hurst, D. P.; Abood, M. E.; Reggio, P. H.; Fournier, D. J.; Makriyannis, A. (-)-7'-Isothiocyanato-11-hydroxy-1',1'-dimethylheptylhexahydrocannabinol (AM841), a high-affinity electrophilic ligand, interacts covalently with a cysteine in helix six and activates the CB1 cannabinoid receptor. *Mol. Pharmacol.* **2005**, *68*, 1623-1635.
41. Ortiz Zacarías, N. V.; van Veldhoven, J. P. D.; Portner, L.; van Spronsen, E.; Ullo, S.; Veenhuizen, M.; van der Velden, W. J. C.; Zweemer, A. J. M.; Kreekel, R. M.; Oenema, K.; Lenselink, E. B.; Heitman, L. H.; IJzerman, A. P. Pyrrolone derivatives as intracellular allosteric modulators for chemokine receptors: selective and dual-targeting inhibitors of CC chemokine receptors 1 and 2. *J. Med. Chem.* **2018**, *61*, 9146-9161.
42. Rietsch, A.; Beckwith, J. The genetics of disulfide bond metabolism. *Annu. Rev. Genet.* **1998**, *32*, 163-184.
43. Mercier, R. W.; Pei, Y.; Pandarinathan, L.; Janero, D. R.; Zhang, J.; Makriyannis, A. hCB2 ligand-interaction landscape: cysteine residues critical to biarylpyrazole antagonist binding motif and receptor modulation. *Chem. Biol.* **2010**, *17*, 1132-1142.
44. Suga, H.; Sawyer, G. W.; Ehlerf, F. J. Mutagenesis of nucleophilic residues near the orthosteric binding pocket of M1 and M2 muscarinic receptors: effect on the binding of nitrogen mustard analogs of acetylcholine and McN-A-343. *Mol. Pharmacol.* **2010**, *78*, 745-755.
45. Doyon, J.; Coesemans, E.; Boeckx, S.; Buntinx, M.; Hermans, B.; Van Wauwe, J. P.; Gilissen, R. A.; De Groot, A. H.; Corens, D.; Van Lommen, G. Discovery of potent, orally bioavailable small-molecule inhibitors of the human CCR2 receptor. *ChemMedChem* **2008**, *3*, 660-669.
46. Zou, D.; Zhai, H.-X.; Eckman, J.; Higgins, P.; Gillard, M.; Knerr, L.; Carre, S.; Pasau, P.; Collart, P.; Grassi, J. Novel, acidic CCR2 receptor antagonists: from hit to lead. *Lett. Drug. Des. Discov.* **2007**, *4*, 185-191.
47. England, C. G.; Ehlerding, E. B.; Cai, W. NanoLuc: a small luciferase is brightening up the field of bioluminescence. *Bioconjug. Chem.* **2016**, *27*, 1175-1187.
48. Kim, Y.-M.; Benovic, J. L. Differential roles of arrestin-2 interaction with clathrin and adaptor protein 2 in G protein-coupled receptor trafficking. *J. Biol. Chem.* **2002**, *277*, 30760-30768.
49. Cuisset, L.; Tichonicky, L.; Jaffray, P.; Delpech, M. The effects of sodium butyrate on transcription are mediated through activation of a protein phosphatase. *J Biol Chem* **1997**, *272*, 24148-24153.
50. Smith, P. K.; Krohn, R. I.; Hermanson, G. T.; Mallia, A. K.; Gartner, F. H.; Provenzano, M. D.; Fujimoto, E. K.; Goeke, N. M.; Olson, B. J.; Klenk, D. C. Measurement of protein using bicinchoninic acid. *Anal. Biochem.* **1985**, *150*, 76-85.
51. Abagyan, R.; Totrov, M. Biased probability Monte Carlo conformational searches and electrostatic calculations for peptides and proteins. *J Mol Biol* **1994**, *235*, 983-1002.
52. Schapira, M.; Totrov, M.; Abagyan, R. Prediction of the binding energy for small molecules, peptides and proteins. *J Mol Recognit* **1999**, *12*, 177-190.
53. Cheng, Y.; Prusoff, W. H. Relationship between the inhibition constant (K<sub>1</sub>) and the concentration of inhibitor which causes 50 per cent inhibition (I<sub>50</sub>) of an enzymatic reaction. *Biochem. Pharmacol.* **1973**, *22*, 3099-3108.



## Chapter 7

---

# A novel CCR2 antagonist inhibits atherogenesis in apoE deficient mice by achieving high receptor occupancy



*Ilze Bot, Natalia V. Ortiz Zacarías, Wilhelmus E.A. de Witte, Henk de Vries, Peter J. van Santbrink, Daniël van der Velden, Mara J. Kröner, Dirk-Jan van der Berg, Dean Stamos, Elizabeth C.M. de Lange, Johan Kuiper, Adriaan P. IJzerman and Laura H. Heitman*

*Scientific Reports 2017, 7 (1): 52*



## ABSTRACT

CC Chemokine Receptor 2 (CCR2) and its endogenous ligand CCL2 are involved in a number of diseases, including atherosclerosis. Several CCR2 antagonists have been developed as potential therapeutic agents, however their *in vivo* clinical efficacy was limited. In this report, we aimed to determine whether **15a**, an antagonist with a long residence time on the human CCR2, is effective in inhibiting the development of atherosclerosis in a mouse disease model. First, radioligand binding assays were performed to determine affinity and binding kinetics of **15a** on murine CCR2. To assess the *in vivo* efficacy, western-type diet fed apoE<sup>-/-</sup> mice were treated daily with **15a** or vehicle as control. Treatment with **15a** reduced the amount of circulating CCR2<sup>+</sup> monocytes and the size of the atherosclerotic plaques in both the carotid artery and the aortic root. We then showed that the long pharmacokinetic half-life of **15a** combined with the high drug concentrations ensured prolonged CCR2 occupancy. These data render **15a** a promising compound for drug development and confirms high receptor occupancy as a key parameter when targeting chemokine receptors.

## INTRODUCTION

The chemokine system comprises more than 20 different chemokine receptors, which belong to the class A or rhodopsin-like family of G protein-coupled receptors (GPCRs). Almost 50 chemokine ligands play a critical role in the immune system, mediating the migration and differentiation of immune cells during homeostasis and inflammation.<sup>1</sup> Dysregulation of this system can lead to a variety of different pathologies, including inflammatory and autoimmune diseases.<sup>2, 3</sup> For instance, preclinical evidence suggests that CC Chemokine Receptor 2 (CCR2) and its high-affinity ligand CCL2 are involved in the pathogenesis of atherosclerosis,<sup>4,6</sup> neuropathic pain<sup>7</sup> and multiple sclerosis.<sup>8</sup> Genetic knockout of CCR2 (CCR2<sup>-/-</sup>) in the Apolipoprotein E-deficient (apoE<sup>-/-</sup>) mouse model of atherosclerosis resulted in a significant decrease in lesion size compared to apoE<sup>-/-</sup> controls, which was caused by a reduction in monocyte/macrophage recruitment to the atherosclerotic lesion.<sup>4,6</sup> Similar results have been reported in studies with genetic knockout of CCL2 in both the low density lipoprotein receptor-deficient (LDLR<sup>-/-</sup>) and the human Apolipoprotein B transgenic mouse models.<sup>9, 10</sup> These findings suggest that the CCR2/CCL2 axis is critically involved in the mobilization and recruitment of monocytes to the early atherosclerotic plaque.

The involvement of CCR2 in pathologies such as atherosclerosis has resulted in many efforts to develop biologic and small molecule antagonists targeting this receptor. However, despite inhibitory effects on for example monocyte recruitment,<sup>11</sup> a very limited number of compounds has shown *in vivo* efficacy in inhibiting atherosclerosis. In this regard, the characterization of the drug-target residence time (RT)—a measure of the ligand-receptor complex lifetime—has been proposed as a good predictor of *in vivo* efficacy and safety.<sup>12-15</sup> Although the link from *in vitro* kinetics to *in vivo* outcomes has only been studied in few drug targets, these studies confirm the importance of characterizing the RT of drug candidates.<sup>16-21</sup> Yet, the impact of RT to prolong the duration of effect can only be assessed when considering the whole target biology and pharmacokinetic properties of the drug of interest.<sup>22, 23</sup> Inclusion of RT in early hit-to-lead optimization has also been recently used for the development of high-affinity and long-RT CCR2 antagonists.<sup>24, 25</sup> The combination of structure-affinity and structure-kinetics optimization resulted in the discovery of compound **15a** (Figure 1), an orthosteric CCR2 small molecule antagonist with high affinity of 2.4 nM and a RT of 714 min for human CCR2 (hCCR2).<sup>24</sup> With such a prolonged CCR2 inhibition, **15a** emerges as a potential candidate to evaluate the *in vivo* effects of long RT.

In this study, we aimed to evaluate the binding kinetics and pharmacokinetics of **15a** for murine CCR2 (mCCR2) and determine whether this CCR2 antagonist is effective in an apoE<sup>-/-</sup> mouse model of atherosclerosis. Using a combination of *in vitro* radioligand binding assays and *in vivo* studies, we show that prolonged CCR2 antagonism with **15a**, due to high

target occupancy, is linked to a robust and significant inhibition of atherogenesis in mice. These results support the need of achieving more than 90% continuous inhibition when developing chemokine receptor antagonists.<sup>26</sup> This study also highlights the importance of *in vitro* characterization of drug candidates in all relevant species for *in vivo* pre-clinical studies, in order to improve the translational value of animal models, and thus to reduce the attrition in drug discovery programs.

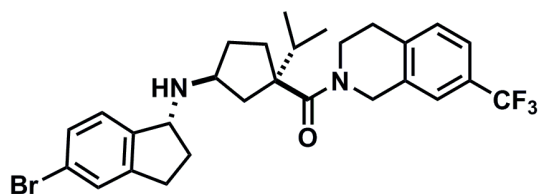


Figure 1. Chemical structure of CCR2 antagonist 15a.



## RESULTS

### Characterization of [<sup>3</sup>H]-INCB3344 and 15a in mouse CCR2 (mCCR2)

To determine the binding affinity and the kinetic profile of **15a** at mCCR2, the radioligand [<sup>3</sup>H]-INCB3344 was first characterized by performing association and dissociation binding assays in membranes of CHO cells transiently expressing mCCR2. At 25 °C, binding of [<sup>3</sup>H]-INCB3344 to mCCR2 reached equilibrium around 20 min and was best fit with a one-phase exponential model that yielded an association ( $k_{on}$ ) rate of 0.030 nM<sup>-1</sup> min<sup>-1</sup>. Dissociation of the radioligand from mCCR2 was also best fit with a one-phase model that yielded a dissociation rate ( $k_{off}$ ) of 0.227 min<sup>-1</sup> (Figure 2 and Table 1). These values resulted in a kinetic dissociation binding constant ( $K_D$ ) of 7.6 nM and a RT of 4.4 min for this receptor (Table 1).

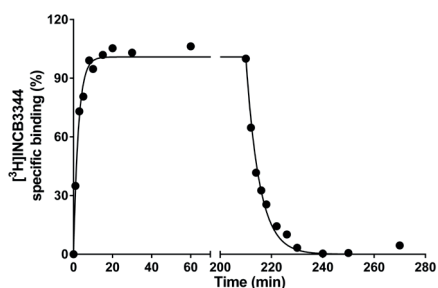


**Figure 2. Kinetic characterization of [<sup>3</sup>H]-INCB3344 in murine CCR2.** Association and dissociation kinetics of 5 nM [<sup>3</sup>H]-INCB3344 binding to membranes of CHO cell membranes transiently expressing murine CCR2 at 25 °C. Dissociation was initiated by the addition of 10 μM INCB3344. Association and dissociation data were fitted using a monophasic exponential association, or exponential decay model, respectively. Graphs shown are representative from one experiment performed in duplicate. Data for all association and dissociation experiments (n=3) are presented in Table 1.

After the characterization of [<sup>3</sup>H]-INCB3344, we performed displacement experiments at 25 °C with **15a** to determine its affinity for mCCR2. **15a** was able to displace [<sup>3</sup>H]-INCB3344 binding in a concentration-dependent way, with a  $K_i$  value of 10.6 nM (Figure 3a). In addition, a [<sup>3</sup>H]-INCB3344 competition association assay was performed in order to determine the kinetic profile of unlabeled **15a**. Figure 3b shows a representative competition association curve of [<sup>3</sup>H]-INCB3344 to mouse CCR2, in the absence or presence of 30 nM **15a** (approximately 3-fold its  $K_i$  value). We used 30 nM **15a** as this concentration provided a sufficient window for data analysis. Association curves of [<sup>3</sup>H]-INCB3344 in the presence of **15a** in mCCR2 resulted in the typical overshoot characteristic for long RT compounds (Figure 3b) and a  $KRI > 1.0$  ( $KRI = 1.6$ ). By fitting the curves to the competition association model of Motulsky and Mahan,<sup>27</sup> it was possible to determine the  $k_{on}$  and  $k_{off}$  values of **15a**:  $0.007 \pm 0.001$  nM<sup>-1</sup> min<sup>-1</sup> and  $0.051 \pm 0.008$  min<sup>-1</sup>, respectively. These results allowed the calculation of the kinetic  $K_D$  ( $7.4 \pm 1.5$  nM), which was comparable to the obtained  $K_i$  value, and confirmed a slower dissociation—and a longer RT of 20 min—compared to [<sup>3</sup>H]-INCB3344 (RT = 4.4 min, Table 1). For comparison the kinetic parameters of **15a** and [<sup>3</sup>H]-INCB3344 on human CCR2 (hCCR2) are also shown in Table 1, as previously published by Vilums *et al.*<sup>24, 25</sup>

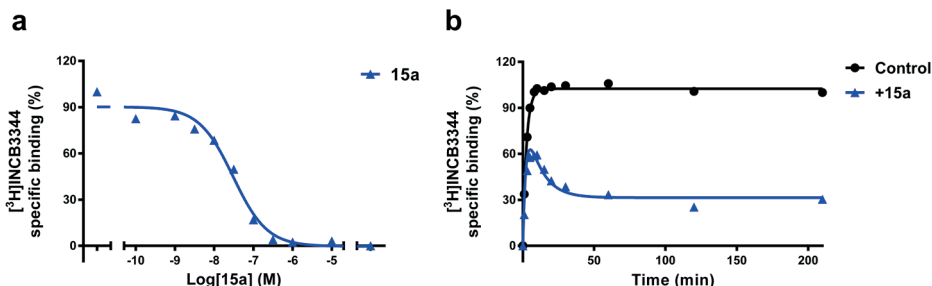


**Figure 3. Characterization of 15a in murine CCR2.** (a) Displacement of [<sup>3</sup>H]-INCB3344 binding from CHO cell membranes transiently expressing murine CCR2 at 25°C, upon addition of increasing concentrations of compound **15a**. (b) Competition association assay of [<sup>3</sup>H]-INCB3344 in the absence or presence of **15a**. Competition association of 5 nM [<sup>3</sup>H]-INCB3344 binding to membranes of CHO cells transiently expressing murine CCR2 at 25°C, in the absence or presence of 30 nM **15a**. Data were fitted to the competition association model of Motulsky and Mahan.<sup>27</sup> Graphs shown are representative from one experiment performed in duplicate. Data for kinetic experiments (n=3) are presented in Table 1.

**Table 1. Kinetic characterization of [<sup>3</sup>H]-INCB3344 and 15a in membranes of CHO cells transiently expressing murine CCR2 (mCCR2).**

	[ <sup>3</sup> H]-INCB3344 (hCCR2b*)	15a (hCCR2b*)
KRI <sup>†</sup>	1.0 (1.0)	1.6 (1.7)
k <sub>on</sub> (nM <sup>-1</sup> min <sup>-1</sup> )	0.030 ± 0.003 (0.054)	0.007 ± 0.001 (0.008)
k <sub>off</sub> (min <sup>-1</sup> )	0.227 ± 0.031 (0.013)	0.051 ± 0.008 (0.0014)
K <sub>D</sub> <sup>‡</sup> (nM)	7.6 ± 1.3 (0.23)	7.4 ± 1.5 (0.175)
RT <sup>  </sup> (min)	4.4 ± 0.6 (76)	19.7 ± 3.1 (714)

Values are means ± S.E.M of three separate experiments performed in duplicate

\*Values of [<sup>3</sup>H]-INCB3344 for hCCR2b were taken from Vilums et. al.<sup>21</sup>

†Values of 15a for hCCR2b were taken from Vilums et. al.<sup>20</sup>

‡Kinetic rate index (KRI) = B<sub>11</sub>/B<sub>12</sub> (see Materials and Methods).

<sup>§</sup>K<sub>D</sub> = k<sub>off</sub>/k<sub>on</sub>

<sup>||</sup>RT = 1/k<sub>off</sub>

## 15a reduces circulating CCR2<sup>+</sup> monocyte levels

In this study, apoE<sup>-/-</sup> mice were treated with the orthosteric antagonist **15a** or vehicle control for four weeks. During the study, body weight, body weight gain and plasma total cholesterol levels were not affected by administration of the CCR2 antagonist (Figure S1). Liver morphology was similar between the controls and the **15a**-treated mice, and **15a** did not affect liver mRNA expression of the toxicity markers ALT, apoH and GC. mRNA levels of AST were even somewhat decreased in the **15a**-treated group (P=0.02, Figure S2). Interestingly, treatment with **15a** resulted in increased plasma CCL2 levels, while plasma IL-6

levels remained unaffected (Figure S3). After two weeks of treatment, we determined CCR2<sup>+</sup> monocyte levels (defined as CD11b<sup>+</sup>Ly6G<sup>low</sup> cells) in blood of control and **15a**-treated mice at two hours after injection by means of flow cytometry. At that time point, we observed a significant reduction in the percentage of circulating CCR2<sup>+</sup> monocytes in the **15a**-treated mice (Figure 4a, controls: 8.7 ± 1.2%, **15a**: 1.8 ± 0.2%, P=0.0004).

At the time of sacrifice, the total number of monocytes was significantly reduced in the mice treated with **15a**, while total lymphocyte and neutrophil numbers remained unaffected (Figure S4). Flow cytometry analysis further confirmed that **15a** did not affect the number of neutrophils, CD19<sup>+</sup> B cells, CD4<sup>+</sup> or CD8<sup>+</sup> T cells in blood or spleen, nor did we detect any effects of the antagonist on splenic or circulating Tregs (data not shown). Of note, these analyses were performed at 18 hour after the last injection of the antagonists. At that time-point, we still observed that the number of circulating CCR2<sup>+</sup> monocytes was significantly reduced in the **15a**-treated mice compared to controls (Figure 4b, controls: 14.9 ± 3.2\*10<sup>3</sup> cells/mL versus **15a**: 4.5 ± 1.0\*10<sup>3</sup> cells/mL, P=0.01). The ratio of patrolling CD11b<sup>+</sup>Ly6C<sup>low</sup>CX3CR1<sup>+</sup> monocytes versus inflammatory CD11b<sup>+</sup>Ly6C<sup>high</sup>CCR2<sup>+</sup> in blood increased upon treatment with **15a** (Figure 4c), which was not only due to a reduction in the number of CCR2<sup>+</sup> monocytes, but also caused by a significant 1.5-fold increase in the amount of CD11b<sup>+</sup>Ly6C<sup>low</sup>CX3CR1<sup>+</sup> monocytes. We did not observe any change in the percentage of circulating CCR5<sup>+</sup> monocytes in both the treated and untreated mice, which suggests a selective interaction of **15a** with CCR2 (Figure S5).

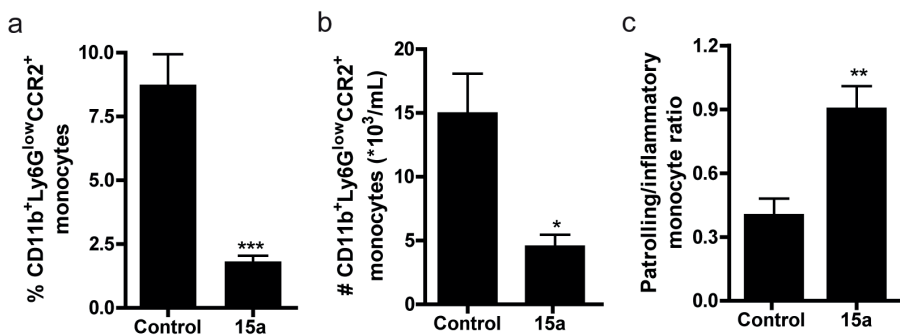


**Figure 4. Effect of 15a treatment on the amount of monocytes.** (a) At 2 hours after injection and two weeks of treatment, **15a** reduced the relative amount of circulating CCR2<sup>+</sup> monocytes (defined as CD11b<sup>+</sup>Ly6G<sup>low</sup> cells). (b) At 18 hours after the last injection (after 4 weeks of treatment), the number of circulating CD11b<sup>+</sup>Ly6G<sup>low</sup>CCR2<sup>+</sup> cells was significantly reduced by **15a** treatment. (c) The ratio of patrolling monocytes and pro-inflammatory monocytes was significantly increased upon treatment with **15a** (\*P<0.05, \*\*P<0.01, \*\*\*P<0.001). Graphs shown are representative from one experiment with n=5 per group in panel (a) and n=6 per group in panels (b) and (c).

## CCR2 antagonism inhibits atherosclerotic plaque development

Atherosclerotic plaque size in the carotid artery at the site of maximal stenosis was reduced from  $64.4 \pm 11.8 \times 10^3 \mu\text{m}^2$  in control mice to  $17.6 \pm 4.1 \times 10^3 \mu\text{m}^2$  in mice treated with **15a** (Figure 5a, -73%,  $P=0.002$ ). Furthermore, as depicted in Figure 5b and 5c, plaque volume throughout the carotid arteries was reduced from  $1.75 \pm 0.33 \times 10^7 \mu\text{m}^3$  in control mice to  $0.46 \pm 0.13 \times 10^7 \mu\text{m}^3$  in **15a**-treated mice ( $P=0.003$ ). In addition, relative necrotic area was reduced from  $35.3 \pm 8.2\%$  in controls to  $7.6 \pm 4.5\%$  in the **15a**-treated mice ( $P=0.01$ ).

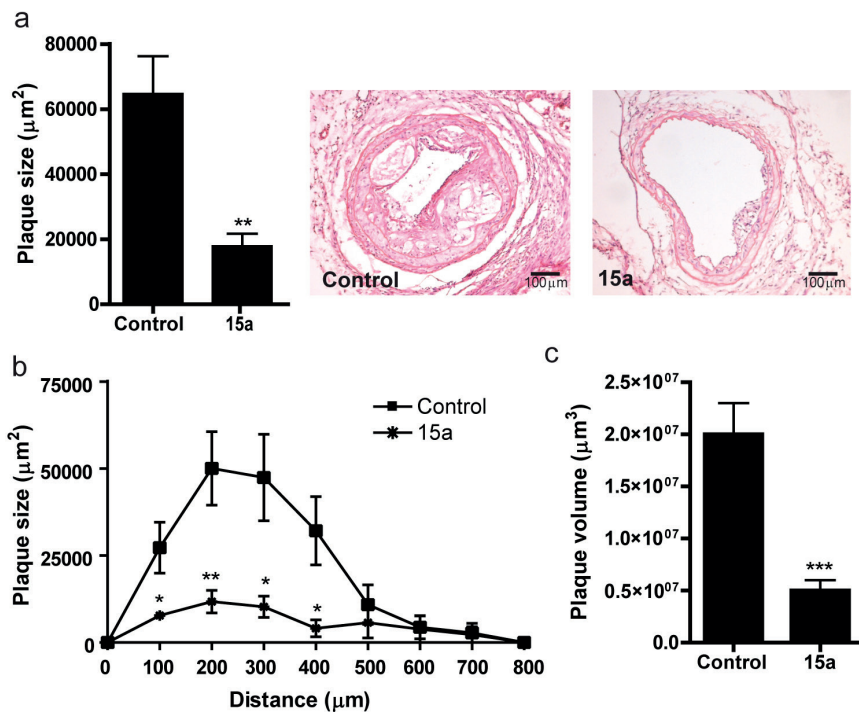


**Figure 5. Inhibition of lesion development in the carotid artery by 15a.** (a) The CCR2 antagonist **15a** significantly reduced atherosclerotic plaque size in the carotid artery at the site of maximal stenosis. (b) Similarly, plaque volume, given as plaque size at increasing distance from the collar and (c) as total volume in  $\mu\text{m}^3$  was significantly reduced by **15a**. Micrographs show representative images of the individual groups (100X magnification). \* $P<0.05$ , \*\* $P<0.01$ , \*\*\* $P<0.001$ . Graphs shown are representative from one experiment with  $n=10$  controls versus  $n=9$  **15a**-treated mice.

In the aortic root, average plaque size was significantly reduced by treatment with **15a** (Figure 6a, controls:  $215.9 \pm 24.6 \times 10^3 \mu\text{m}^2$ , **15a**:  $157.0 \pm 15.7 \times 10^3 \mu\text{m}^2$ ,  $P=0.005$ ) and also aortic root plaque volume was lower in the **15a**-treated mice (Figure 6b and 6c, controls:  $11.8 \pm 1.2 \times 10^7 \mu\text{m}^3$ , **15a**:  $7.4 \pm 0.7 \times 10^7 \mu\text{m}^3$ ,  $P=0.005$ ).

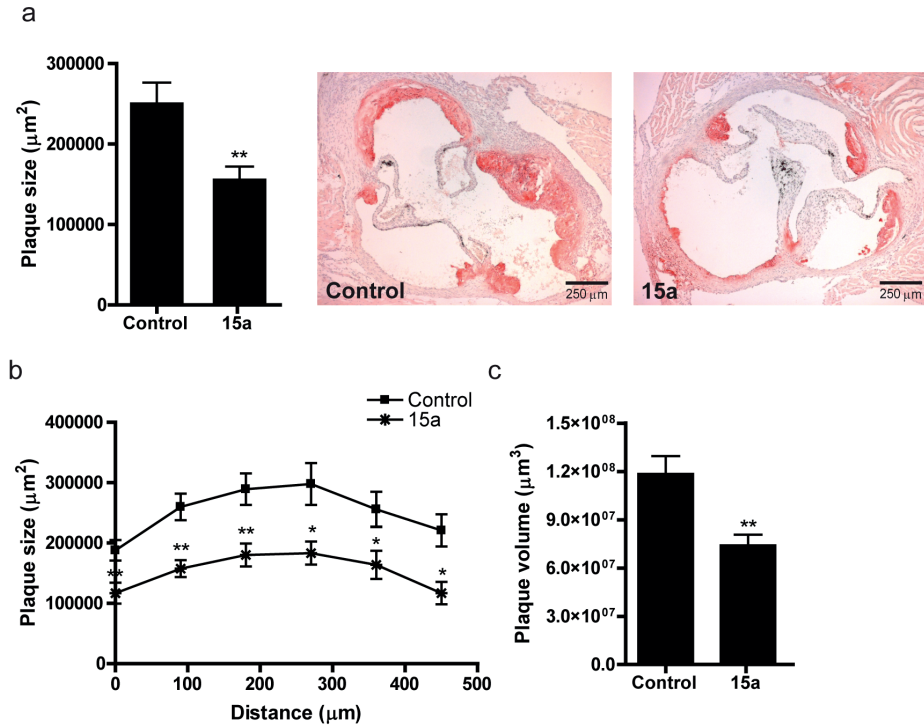


**Figure 6. Inhibition of lesion development in the aortic root by 15a.** (a) Also in the aortic root, **15a** inhibited atherosclerotic lesion development after 6 weeks of Western type diet. (b) Lesion area in the aortic roots presented for each group every 90 μm of the aortic root. (c) Plaque volume was also significantly reduced in the **15a**-treated group. \* $P < 0.05$ , \*\* $P < 0.01$ . Graphs shown are representative from one experiment with  $n = 10$  controls versus  $n = 9$  **15a**-treated mice.

The macrophage content as measured by MOMA2 staining revealed that the macrophage positive area of the carotid artery plaques was significantly reduced in the **15a**-treated mice (Figure 7a, left panel; controls:  $22.3 \pm 4.1 \times 10^3 \mu\text{m}^2$ , **15a**:  $6.2 \pm 2.5 \times 10^3 \mu\text{m}^2$ ,  $P = 0.005$ ). Similarly, relative macrophage content (corrected for lesion size) was reduced in the **15a**-treated group (Figure 7a, right panel; controls:  $46 \pm 4\%$ , **15a**:  $25 \pm 8\%$ ,  $P = 0.02$ ). In the aortic root, macrophage positive area was also significantly lower in the **15a**-treated mice (Figure 7b, controls:  $92.0 \pm 15.6 \times 10^3 \mu\text{m}^2$ , **15a**:  $37.2 \pm 8.7 \times 10^3 \mu\text{m}^2$ ,  $P = 0.008$ ).

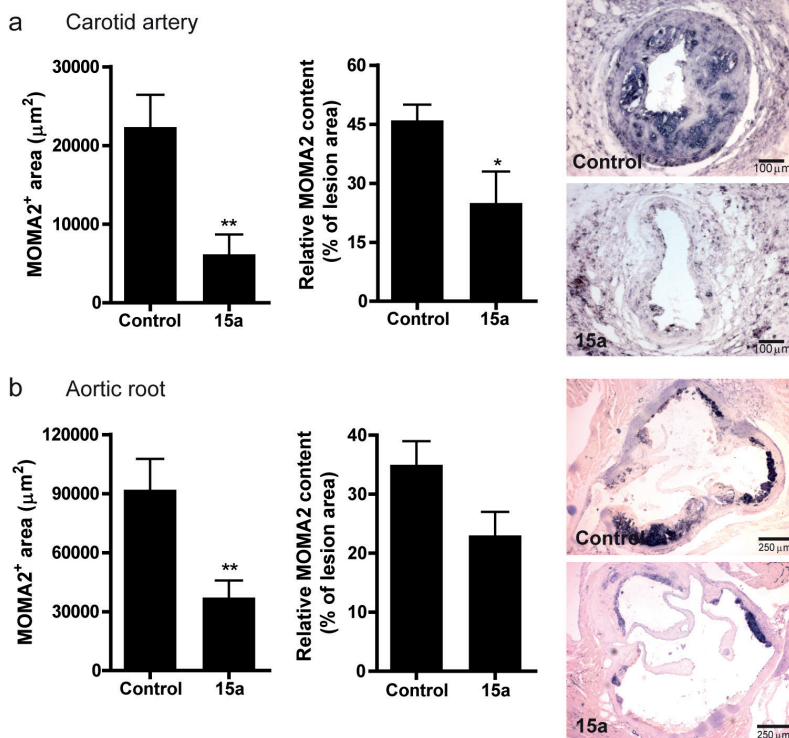


**Figure 7. Macrophage content in carotid artery and aortic root atherosclerotic lesions.** (a) Macrophage content in the carotid artery lesions as measured by MOMA2 staining was reduced upon treatment with **15a**, both in total macrophage positive area (left panel) and relatively as percentage of lesion size (right panel). Micrographs show representative images of the individual groups (100X magnification). (b) Also in the aortic root, **15a** significantly reduced the macrophage<sup>+</sup> area (left panel). Relative macrophage content did not significantly differ between the groups (right panel). Micrographs show representative images of the individual groups (40X magnification). \*P<0.05, \*\*P<0.01. Graphs shown are representative from one experiment with n=10 controls versus n=9 **15a**-treated mice.

## Pharmacokinetics-based prediction of target occupancy

To investigate the role of pharmacokinetics in the generation of the effective drug response of **15a**, we measured the plasma levels of **15a** over a 24 hours period using a LC-MS method. Following a single intraperitoneal dose of 5 mg/kg, plasma levels of **15a** varied from 12 to 1456 ng/mL 1 h after administration; 2 h after dosing, plasma levels were above 600 ng/mL in all individual mice (613 to 1048 ng/mL), which remained relatively constant at 6 h after administration (182 to 1024 ng/mL) and fell to 32 to 331 ng/mL at 24 h after administration (Figure 8a). Pharmacokinetic analysis at this dose revealed a relatively slow pharmacokinetic profile (Figure 8a, elimination half-life = 10.7 hours), with an elimination half-life that exceeds

by far the determined RT in mCCR2. Using these plasma concentrations, we predicted the target occupancy attained by **15a** using two different approaches: i) calculation of “equilibrium” target occupancy using equation (1) as shown in Materials and Methods, which accounts for both the pharmacokinetics and affinity of **15a**, and ii) simulation of target occupancy using equations (3) - (5), which account for the pharmacokinetics and binding kinetics of this compound. These calculations demonstrated that the combination of slow pharmacokinetics (Figure 8a) and high drug concentrations relative to affinity leads to a high target occupancy of >90% for 24 hours (Figure 8b, dots). This was confirmed by the simulations of receptor occupancy (Figure 8b, line), indicating that a simpler calculation method (equation (1)) is sufficient to predict receptor occupancy in this study. Comparing the long duration of target occupancy for equilibrium binding with the RT of **15a** (of 24 minutes) makes clear that RT is not a contributing factor in prolonging target occupancy under these conditions. In this regard, equation (2) allowed us to determine the maximal value of  $k_{off}$  that could contribute to a prolonged duration of target occupancy. As previously demonstrated, the level of target saturation can be used to compare the plasma elimination with the  $k_{off}$  by multiplying the pharmacokinetic elimination rate with a factor  $(1-BF)$ , where BF represents the percentage of target occupancy divided by 100.<sup>28</sup> This means that if the target occupancy needs to be above 90% for effective treatment, the  $k_{off}$  of the drug candidate needs to be ten times lower than the pharmacokinetic elimination rate.

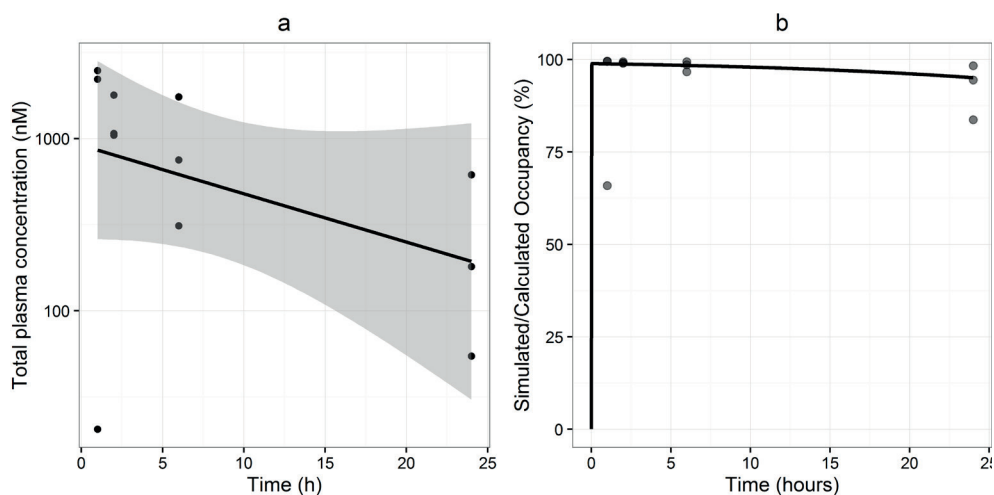


**Figure 8. Total plasma concentrations, calculated and simulated target occupancy.** (a) Observed plasma concentrations (dots), linear fit of the data (line) and 95% confidence interval of the linear regression (shaded area). (b) Equilibrium occupancy derived from the experimentally observed plasma concentrations (dots) and simulated occupancy on basis of the observed binding kinetics and plasma elimination rate (line). Graphs shown are representative from one experiment ( $n=3$  per time point).



## DISCUSSION AND CONCLUSIONS

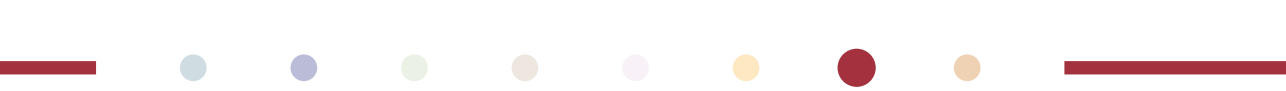
In this study, we investigated the efficacy of the novel CCR2 antagonist **15a**—designed to display a long residence time (RT) on human CCR2 (hCCR2)—in inhibiting the development of atherosclerosis in apoE<sup>-/-</sup> mice. Characterization of the drug-target complex lifetime or RT in early phases of the drug discovery and development process might help to improve the prediction of *in vivo* efficacy and safety.<sup>12-15</sup> Evidence from retrospective studies has shown that several marketed drugs exhibit a long RT on their target,<sup>13, 29</sup> prompting the prospective optimization of both affinity and kinetic properties of compounds for a variety of targets.<sup>17, 25, 30-32</sup> In this regard, **15a** was discovered by optimizing a reported lead in the development of MK-0812, a Merck CCR2 antagonist that has failed in clinical trials due to lack of efficacy.<sup>33</sup> Although the RT of MK-0812 in mCCR2 is not known, in hCCR2 it exhibited an almost 8-fold shorter RT than compound **15a** (92 min versus 714 min, respectively).<sup>24</sup> Thus, our selection of **15a** was based on the need of advancing drug candidates with high affinity and favorable binding kinetics. In this study, we first determined the kinetic profile of **15a** on mouse CCR2 (mCCR2), as the pharmacological properties of drug candidates, including the kinetic profile, can differ between species orthologues.<sup>34</sup> This renders it necessary to characterize the binding kinetics of lead compounds in all relevant species for preclinical testing.<sup>12</sup> Using [<sup>3</sup>H]-INCB3344 we were able to determine the binding affinity and the kinetic profile of **15a** in mCCR2. The determination of RT using the competition association model of Motulsky and Mahan<sup>27</sup> confirmed the longer RT of **15a** in comparison with the control [<sup>3</sup>H]-INCB3344, a CCR2 receptor antagonist with similar affinity for mCCR2. This is in line with previous studies in hCCR2, where **15a** showed a RT of 714 min compared with 76 min of [<sup>3</sup>H]-INCB3344 (Table 1).<sup>24</sup> However, a clear difference was found between species, as **15a** dissociates much faster from mCCR2 than from hCCR2: **15a** has a lifetime of less than 30 min on mCCR2, but more than 10 hours on hCCR2. This poor translation of kinetic parameters between species represents a clear limitation in understanding the effect of RT in *in vivo* efficacy, adding an extra level of complexity when selecting relevant animal models for preclinical studies.

Next we showed that **15a** significantly reduced the number of circulating inflammatory CCR2<sup>+</sup> monocytes and that **15a** was very effective in inhibiting atherosclerotic plaque development in both the carotid artery and the aortic root of apoE<sup>-/-</sup> mice. In addition, relative macrophage content in the lesion was reduced in the **15a** treated mice at both sites of lesion development. CCR2 was previously shown to be predominantly involved in lesion initiation,<sup>4, 6</sup> but seemed less effective in inhibiting lesion progression.<sup>30</sup> For therapeutic application, halting lesion progression would be favorable to prevent an existing plaque to progress to an advanced and unstable lesion. In this study, **15a** almost completely blocked lesion initiation in the carotid artery, as treatment was commenced immediately from time of collar placement and thus of lesion development at that site. In the aortic root, early



atherosclerosis had already developed before treatment was initiated, and treatment was also effective in inhibiting plaque progression in this location. Aiello *et al.* showed that treatment with the CCR2 antagonist INCB3344 failed to decrease the size of early and advanced atherosclerotic lesions in apoE<sup>-/-</sup> mice,<sup>11</sup> which may be related to both the shorter RT of this drug in mCCR2, and the use of an ineffective dose. Although the plasma levels of INCB3344 were not investigated in this study, previous data suggest that a single oral dose of 50 mg/kg leads to approximately 75% CCR2 inhibition in mice.<sup>35</sup> In the study by Aiello *et al.*, inflammatory monocyte levels were significantly reduced up to 6 hours after oral infusion, which was lost at 9 hours,<sup>11</sup> while we still observed a >60% reduction in circulating CCR2<sup>+</sup> monocyte numbers at 18 hours after treatment, suggestive of a longer therapeutic effect. Interestingly, we also observed an increase in the relative amount of Ly6C<sup>low</sup>CX3CR1<sup>+</sup> monocytes, which is indicative of a more patrolling response.<sup>36</sup> Similarly as in the study by Aiello *et al.*, we did not observe any effects on bone marrow monocyte subpopulations upon treatment (data not shown), suggesting that the reduction observed on circulating CCR2<sup>+</sup> monocytes is not due to changes in migration of these cells from the bone marrow. Further studies should shed more light on the exact mechanisms of depletion of this specific monocyte subset from the circulation, and how this affects the immune system, including effects on other chemokine receptors expressed by monocytes. In both studies however, plasma cholesterol studies were not affected, while an increase in plasma CCL2, one of the endogenous ligands for CCR2, was observed, which may be explained by the fact that clearance of CCL2 is mediated by CCR2.<sup>37</sup> Noteworthy, treatment with **15a** resulted in more than 70% reduction in carotid artery lesion size, which even exceeds the effects of the CCR2/CCR5/CXCR3 triple antagonist TAK-779 in inhibiting atherogenesis,<sup>38</sup> suggesting that inhibition of a single receptor, CCR2, might be sufficient for the therapeutic effect in atherosclerosis.

Finally we also investigated the pharmacokinetics of **15a** in apoE<sup>-/-</sup> mice, which allowed us to determine drug exposure and predict the target occupancy achieved by **15a** after a single dose. For a drug to exert its pharmacological effect, it must be bound to its target, making target occupancy a requisite for any *in vivo* effect. Previous analysis of clinical trials with CCR1 antagonists led to the conclusion that a receptor occupancy of > 90% is required for an effective anti-inflammatory response.<sup>26,39</sup> Calculation of CCR2 occupancy levels in our study revealed that, after a single dose, **15a** was able to block more than 90% of the receptors for over 24 hours. Such high level of target engagement can be achieved by slow drug-target dissociation or by target-saturating drug concentrations. In our case, the calculated high receptor occupancy is the result of saturating concentrations and slow plasma elimination of **15a**. For RT to play a key role in increasing the target occupancy, the  $k_{off}$  of the drug candidate must at least surpass its pharmacokinetic elimination rate.<sup>22, 23</sup> However, the direct comparison of the pharmacokinetic elimination rate and the  $k_{off}$  is only informative



when the target occupancy is low, since it assumes that the declines of the target occupancy and the unbound drug concentration are parallel lines on a semi-logarithmic scale. For high levels of target occupancy (i.e. high target saturation), a steep decline of unbound drug concentrations is not directly reflected in a steep decline of target occupancy,<sup>28</sup> as we have predicted. This reasoning was used to determine the  $k_{\text{off}}$  value required to prolong target occupancy even further: at least a ten-fold difference between the dissociation rate and the plasma elimination rate is required. Although the contribution of target saturation is not always recognized in literature,<sup>19</sup> we provide evidence that the use of saturating concentrations can result in the required occupancy levels for an anti-inflammatory effect. However, caution must be taken in order to avoid safety risks and toxicity with high doses. These results highlight the need of obtaining pharmacokinetic data and using experimental or mathematical approaches to determine receptor occupancy in early preclinical studies. In this regard, we have established that a simple “equilibrium” occupancy calculation can be sufficient to explain the *in vivo* efficacy in this study, providing a simple method that can be readily used in a range of *in vitro* and *in vivo* preclinical studies. This calculation method allows for further optimization towards a clinical candidate, for example by developing an oral dosing regimen to improve patient compliance.

Although the role of the CCR2-CCL2 axis in the development of atherosclerosis has been recognized in literature, previous studies with CCR2 small-molecule antagonists failed to successfully inhibit atherosclerosis.<sup>11, 40</sup> We are the first to prove that CCR2 antagonism with a selective small molecule antagonist can result in effective atherogenesis inhibition. The results of our *in vivo* study provide direct evidence that high receptor occupancy might be one of the key factors to improve the translation from *in vitro* findings into *in vivo* efficacy in inflammatory diseases. In addition, our findings in the *in vitro* study support the need of characterizing the affinity and kinetic profile of drug candidates in multiple species, as a way to improve preclinical and clinical translation of efficacy and safety findings.<sup>12, 41</sup> To conclude, the CCR2 antagonist **15a** emerges as a potential candidate for further drug development to inhibit atherosclerotic lesion development and progression, and may also be of therapeutic value for other diseases involving CCR2.

## MATERIALS AND METHODS

### Chemicals and reagents

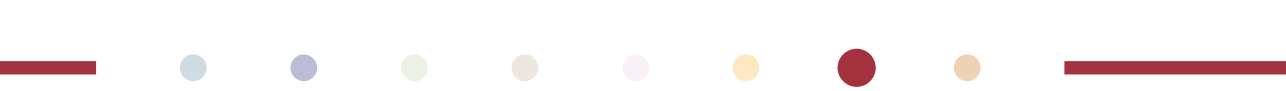
CCR2 antagonists INCB3344, **15a** ((1*S*,3*R*)-3-(((*R*)-5-bromo-2,3-dihydro-1*H*-inden-1-yl)amino)-1-isopropylcyclopentyl)(7-(trifluoromethyl)-3,4-dihydroisoquinolin-2(1*H*)-yl) methanone) and the internal standard 15b ((1*S*,3*R*)-3-(((*S*)-5-bromo-2,3-dihydro-1*H*-inden-1-yl)amino)-1-isopropylcyclopentyl)(7-(trifluoromethyl)-3,4-dihydroisoquinolin-2(1*H*)-yl) methanone) were synthesized in-house as described previously.<sup>24, 42, 43</sup> [<sup>3</sup>H]-INCB3344 (specific activity 32 Ci mmol<sup>-1</sup>) was custom-labeled by Vitrox (Placentia, CA) as a racemic mixture of the two isomers *N*-(2-(((3*S*,4*S*)-1-((1*r*,4*S*)-4-(benzo[d][1,3]dioxol-5-yl)-4-hydroxy cyclohexyl)-4-ethoxy pyrrolidin-3-yl)amino)-2-oxoethyl)-3-(trifluoromethyl)benzamide and *N*-(2-(((3*R*,4*R*)-1-((1*r*,4*R*)-4-(benzo[d][1,3]dioxol-5-yl)-4-hydroxycyclohexyl)-4-ethoxy pyrrolidin-3-yl)amino)-2-oxoethyl)-3-(trifluoromethyl)benzamide. Bovine serum albumin (BSA, fraction V) was purchased from Sigma (St. Louis, MO, USA). Bicinchoninic acid (BCA) and BCA protein assay reagent were obtained from Pierce Chemical Company (Rockford, IL, USA). Acetonitrile (LC-MS grade), trifluoroacetic acid (TFA) and ULC-MS water were from Biosolve (Valkenswaard, the Netherlands); and ethyl acetate from Baker (Deventer, The Netherlands). pcDNA3.1+ plasmid containing the murine CCR2 (mCCR2) with an hemagglutinin (HA) epitope tag at the N-terminus was cloned in-house. All other chemicals were obtained from standard commercial sources.

### Cell culture

Chinese hamster ovary (CHO) cells were cultured at 37°C and 5% CO<sub>2</sub> in Dulbecco's Modified Eagle Medium: Nutrient Mixture F-12 (DMEM/F-12) supplemented with 10% (v/v) newborn calf serum, 50 IU/mL penicillin and 50 µg/mL streptomycin. Cells were subcultured twice a week on 10-cm ø plates, at a ratio of 1:20 to 1:40 using trypsinization.

### Transfections

Transient transfection of CHO cells with HA-tagged mouse CCR2 (mCCR2) was performed using a polyethyleneimine (PEI) method, as described previously.<sup>44</sup> Briefly, CHO cells were seeded at 50-60% confluence on 15-cm ø plates, transfected with 10 µg of plasmid DNA per plate, and incubated for 48 hrs at 37°C and 5% CO<sub>2</sub>. Before transfection, the plasmid DNA was diluted in sterile 150 mM NaCl solution and mixed with PEI solution (1 mg/mL) to obtain



a DNA:PEI mass ratio of 1:6. Finally, the culture medium of the cells was refreshed and 1 mL of DNA/PEI mixture was added to the cells, after incubation of the mixture for 20 min at room temperature.

## Cell membrane preparation

Membranes were prepared as described before.<sup>44</sup> Briefly, cells were detached from 15-cm  $\varnothing$  plates by scraping them with 5 ml phosphate-buffered saline (PBS), and the membranes were separated from the cytosolic fractions by several centrifugation and homogenization steps. The remaining membrane pellet was resuspended in ice-cold Tris buffer (50mM Tris-HCl, pH 7.4) containing 5 mM MgCl<sub>2</sub>. Membrane protein concentrations were measured using a bicinchoninic acid (BCA) protein determination with bovine serum albumin (BSA) as a standard.<sup>45</sup>

## [<sup>3</sup>H]-INCB3344 Binding assays

Radioligand binding assays were performed in a 100  $\mu$ L reaction volume containing 50 mM Tris-HCl buffer (pH 7.4), 5 mM MgCl<sub>2</sub>, 0.1% 3-[(3-cholamidopropyl)-dimethylammonio]-1-propanesulfonic acid (CHAPS), 5 nM [<sup>3</sup>H]-INCB3344 and 50 to 60  $\mu$ g of membrane protein at 25 °C. Non-specific binding was determined with 10  $\mu$ M of the cold ligand INCB3344. Displacement assays were carried out using 9 concentrations of competing ligand, ranging from 0.1 nM to 100  $\mu$ M, for 120 min of incubation. The kinetic parameters of **15a** were also determined at 25°C using a competition association assay as previously described.<sup>25, 27</sup> For association and competition association experiments, CHO-mCCR2 membranes were added to the reaction volume at different time points, in the absence or presence of 30 nM of competing ligand. For dissociation experiments, CHO-mCCR2 membranes were first incubated with 5 nM [<sup>3</sup>H]-INCB3344 for 60 min. Dissociation was initiated by addition of 10  $\mu$ M of INCB3344 at different time points. For all experiments, incubation was terminated by dilution with ice-cold 50 mM Tris-HCl buffer supplemented with 5 mM MgCl<sub>2</sub> and 0.05% CHAPS. Separation of bound from free radioligand was performed by rapid filtration over a 96-well GF/B filter plate using a Perkin Elmer Filtermate-harvester (Perkin Elmer, Groningen, the Netherlands) in the case of displacement assays; or over GF/B filters using a Brandel harvester 24 (Brandel, Gaithersburg, MD, USA) for kinetic assays. Filter-bound radioactivity was determined by scintillation spectrometry after addition of Microscint scintillation cocktail (Perkin-Elmer, Groningen, the Netherlands). The P-E 2450 Microbeta<sup>2</sup> plate counter (Perkin Elmer, Groningen, The Netherlands) was used for displacement assays, and the TRI Carb 2900 TR counter (Perkin Elmer, Groningen, The Netherlands) for kinetic assays. In all

cases, total radioligand binding did not exceed 10% of the amount of radioligand added to prevent ligand depletion.

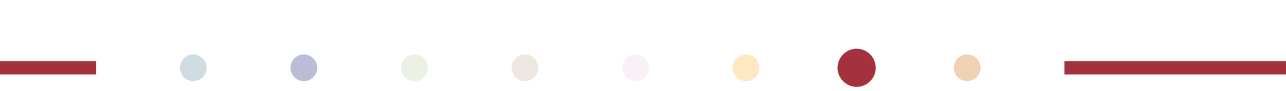
## Animals

This study was performed in compliance with Dutch government guidelines and the Directive 2010/63/EU of the European Parliament. All animal experiments were approved by the animal welfare committee of Leiden University (approval reference number 13213).

Male apoE<sup>-/-</sup> mice (10-12 weeks old), obtained from the local animal breeding facility (Gorlaeus Laboratories, Leiden, The Netherlands), were fed a Western type diet, containing 0.25% cholesterol and 15% cocoabutter (SDS, Sussex, UK).

To measure plasma concentrations of **15a** over time, Western type diet fed mice were injected with 5 mg/kg **15a**, after which blood samples were taken at fixed time points (1, 2, 6 and 24 hours after injection). Blood samples were processed as described below under “Measurement of **15a** plasma levels”. The final dose of 5 mg/kg/day was based on a pilot study in which two different doses (1.5 and 5 mg/kg/day) were tested using leucocyte migration towards the peritoneal cavity as a read-out. Results from this pilot study showed that 1.5 mg/kg per day was not effective in inhibiting migration, while 5 mg/kg per day was (data not shown). In addition, the dose of 5 mg/kg was also based on a previous study with TAK-779,<sup>38</sup> in which a dose of 5 mg/kg was used.

To determine the effect of the CCR2 antagonist on atherosclerotic lesion development, mice were fed a Western type diet, containing 0.25% cholesterol and 15% cocoabutter (SDS, Sussex, UK) throughout the experiment starting two week before surgery. Carotid artery plaque formation was induced by perivascular collar placement as described previously<sup>46</sup> and from the time of surgery, the mice received daily intraperitoneal injections containing **15a** (5 mg/kg/day) or vehicle control (n=9-10 per group). During the experiment, total body weight and weight gain were measured. Serum total cholesterol levels were determined using an enzymatic colorimetric assay according to manufacturer’s protocol (Roche Diagnostics). Precipath (standardized serum; Boehringer Mannheim, Germany) was used as an internal standard. Plasma cytokine levels were measured by ELISA according to manufacturer’s protocol (BD Biosciences). Blood was collected weekly via tail cut. Total cell count and cellular differentiation patterns in blood were analyzed using an automated XT-2000iV veterinary hematology analyzer (Sysmex Europe GMBH, Norderstedt, Germany). After erythrocyte lysis, blood leukocyte suspensions were stained for surface markers, after which their expression was determined by FACS analysis (FACS Canto, BD Biosciences). After 4 weeks of lesion development, the animals were anaesthetized and blood was collected.



After *in situ* perfusion through the left cardiac chamber, the carotid arteries and hearts were harvested.

## Measurement of 15a plasma levels

Blood plasma from mice was analyzed by LC-MS to determine **15a** plasma levels. 20  $\mu\text{L}$  of internal standard (compound 15b, a diastereomer of **15a**<sup>24</sup>) and 20  $\mu\text{L}$  of solvent C (20% (v/v) Acetonitrile and 0.1% (v/v) TFA in LC-MS water) were first mixed with 20  $\mu\text{L}$  of plasma. A calibration curve from 2 to 200 ng/ml of **15a** was prepared using solvent C. Calibration samples were prepared as normal samples using blanc plasma and calibration solution instead of solvent C. Aliquots of 40  $\mu\text{L}$  of 1% TFA were added to the samples and mixed well. After addition of 900  $\mu\text{L}$  of ethyl acetate, mixing was performed for 5 minutes at a titramax plate shaker (Heidolph, Swabach, Germany). Samples were then centrifuged at 15,000  $\times g$  during 10 minutes and 800  $\mu\text{L}$  of the supernatant was evaporated in a vacuum centrifuge (Labconco, Kansas City, Missouri). The sample was reconstituted by mixing with 10  $\mu\text{L}$  of acetonitrile, followed by addition of 40  $\mu\text{L}$  solvent C. After a second centrifugation at 15,000  $\times g$  for 10 minutes, 35  $\mu\text{L}$  of supernatant were transferred to LC vials and inserted into the LC-MS system consisting of a Nexera X2 UHPLC system with two UHPLC pumps (Shimadzu, 's Hertogenbosch, The Netherlands) connected to a TSQ Quantum Ultra (Thermo Fisher Scientific, Breda, The Netherlands). Separation of **15a** was accomplished in a Gemini 3  $\mu\text{m}$  C18 reversed phase HPLC column (50  $\times$  4.6 mm) (Phenomenex, Amstelveen, The Netherlands) using an injection volume of 10  $\mu\text{L}$  and a flow rate of 0.6 ml/min at 40°C. After elution of **15a** with a 9:11 (v/v) ratio of acetonitrile in water with 0.1 % TFA, the column was flushed with a gradient up to 90% acetonitrile with 0.1% TFA. The column was re-equilibrated with a 9:11 (v/v) ratio of acetonitrile in water with 0.1% TFA before the next injection. Samples were analyzed by mass spectrometry using Electro Spray Ionization at a voltage of 3000 V. **15a** and the internal standard 15b showed the same fragmentation pattern and were quantified by monitoring the transition of 549.17 to 202.08 ( $m/z$ ). The collision energy used was 26 V at a skimmer offset of 16 V, the scan peak width was 0.5  $m/z$ , while the scan time was 0.3 seconds. Sheath gas and auxiliary gas pressure (Nitrogen) were set to 60 and 5 respectively (arbitrary units), and the collision gas Argon was set at 1.0 atm.

## Histology and morphometry

Carotid artery cryosections of 5  $\mu\text{m}$  thick were prepared, which were stained with hematoxylin-eosin to determine plaque size and necrotic core size. Morphometric analysis was performed on sections throughout the atherosclerotic lesion (100  $\mu\text{m}$  apart) and at the

site of maximal stenosis using Leica Qwin image analysis software. The relative necrotic area was defined as the a-cellular, debris-rich plaque area as percentage of total plaque area, and also quantified using Leica QWin software.

The hearts were dissected just below the atria and sectioned perpendicular to the axis of the aorta, starting within the heart and working in the direction of the aortic arch. Once the aortic root was identified by the appearance of aortic valve leaflets, 10  $\mu\text{m}$  sections were collected. Mean lesion area (in  $\mu\text{m}^2$ ) of the aortic root was calculated from six Oil-Red-O stained sections in distal direction starting at the point where all three aortic valve leaflets first appeared.

Macrophage content of the lesions in carotid arteries and aortic roots was stained using a rat monoclonal MOMA2 antibody (1:1000, Serotec, Kidlington, Oxford, UK). Macrophage positive areas were analyzed using computer-assisted colour-gated analysis, and related to the total intimal surface area (Leica QWin). Liver cryosections of 10  $\mu\text{m}$  thick were prepared and subsequently stained with hematoxylin-eosin to analyze liver morphology, which was assessed using a Leica DMRE microscope (Leica Ltd., Cambridge, England).

## RNA isolation and gene expression analysis

Total RNA was extracted from homogenized liver tissue with the guanidium thiocyanate-phenol-bromochloropropane extraction method.<sup>38</sup> RNA concentration, purity and integrity were examined by nanodrop (Nanodrop® Technologies). RNA was reverse transcribed by M-MuLV reverse transcriptase (RevertAid, MBI Fermentas, Landsmeer, The Netherlands) and used for quantitative analysis of the mouse genes ALT, AST, apoH and GC with an ABI PRISM 7700 Taqman apparatus (Applied Biosystems). For qPCR primer pairs refer to Table S1.

## Data analysis

All radioligand binding assays were analyzed using Prism 6.0 (GraphPad software, San Diego, CA, USA). All data shown represent means  $\pm$  SEM of at least three independent experiments performed in duplicate.  $K_i$  values were calculated from  $\text{IC}_{50}$  values obtained by non-linear regression analysis of the displacement assays and by using the Cheng-Prusoff equation.<sup>47</sup> Dissociation rate constants  $k_{\text{off}}$  were determined by fitting the dissociation data using an exponential decay model. Association rate constants  $k_{\text{on}}$  were obtained by converting the apparent association rate constants  $k_{\text{obs}}$  according to the equation  $k_{\text{on}} = (k_{\text{obs}} - k_{\text{off}})/[L]$ , in which L is the radioligand concentration used for the experiments,  $k_{\text{obs}}$  is the constant rate determined using exponential association analysis and  $k_{\text{off}}$  represents the mean  $k_{\text{off}}$  value

obtained independently in the dissociation experiments. The kinetic profile of compound **15a** was determined by calculation of its kinetic rate index (KRI) value.<sup>48</sup> The KRI values were calculated according to the equation  $KRI = B_{t_1} / B_{t_2}$ , in which  $B_t$  represents the specific radioligand binding measured at  $t_1 = 15$  min and  $t_2 = 210$  min. In addition, the association and dissociation rates of **15a** were obtained by nonlinear regression analysis of the competition association data using the equations described by Motulsky and Mahan.<sup>27</sup> The association and dissociation rates obtained with this model were used to calculate the kinetic  $K_D$ , according to the equation  $K_D = k_{off}/k_{on}$ . In addition, the RT was calculated by obtaining the reciprocal of the  $k_{off}$ . Data obtained from *in vivo* experiments are expressed as mean  $\pm$  SEM. An unpaired two-tailed Student's t-test was used to compare individual groups. Non-Gaussian distributed data were analyzed using a two-tailed Mann-Whitney U test. A level of  $P < 0.05$  was considered significant.

## Pharmacokinetics-based prediction of target occupancy

The equilibrium target occupancy was calculated by assuming that binding was fast and the drug-target residence time did not prolong the target occupancy. The target occupancy was calculated for each measurement of the drug concentration, according to equation (1), in which  $[C]$  is the concentration of the drug in the blood and  $K_D$  is the drug target affinity.

$$\text{Target Occupancy (\%)} = \frac{[C]}{[C] + K_D} \times 100\% \quad (1)$$

In addition, a simple mathematical model was used to simulate target occupancy for the observed *in vivo* pharmacokinetics and *in vitro* binding kinetics according to the equations in the next section (equations (3) to (5)).

To determine the maximal value of  $k_{off}$  that would prolong the receptor occupancy even further, we used equation (2),<sup>28</sup> in which BF represents the percentage of target occupancy divided by 100 and  $t_{1/2el}$  represents the plasma elimination half-life ( $0.693/k_{el}$ ). In this case we set BF to 0.90, as 90% represents the minimum value of target occupancy to achieve efficacy. To obtain the elimination rate constant of compound **15a**, a linear regression analysis of the natural logarithm of the concentrations versus time was performed, and the slope coefficient was used as the elimination rate constant  $k_{el}$ .

$$k_{off} < 0.693 \cdot (1 - BF) / t_{1/2el} \quad (2)$$



## Differential equations for the simulations of target occupancy

The concentrations of unbound drug in the blood  $[C]$  and target-bound drug  $[LR]$  were modeled according to equations (3) to (5). In these equations,  $k_{el}$  is the first-order elimination rate constant,  $k_{on}$  is the second-order association rate constant,  $k_{off}$  is the first-order dissociation rate constant,  $[R_{free}]$  is the concentration of unbound receptor and  $[R_{tot}]$  is the concentration of bound plus unbound receptor, which is assumed to be constant.

$$\frac{d[C]}{dt} = -k_{el} \cdot [C] - k_{on} \cdot [C] \cdot [R_{free}] + k_{off} \cdot [LR] \quad (3)$$

$$[R_{free}] = [R_{tot}] - [LR] \quad (4)$$

The concentration of the target-bound drug is calculated according to equation (5):

$$\frac{d[LR]}{dt} = k_{on} \cdot [C] \cdot [R_{free}] - k_{off} \cdot [LR] \quad (5)$$

Parameter values: for the simulations in Figure 8b,  $k_{el}$  was set to  $0.0647 \text{ hr}^{-1}$ , based on the slope of the linear regression of the pharmacokinetic data (Figure 8a). On basis of in-house measurements,  $k_{off}$  was set to  $3.06 \text{ hr}^{-1}$  (corresponding to  $0.051 \text{ min}^{-1}$ , as shown in Table 1) and the  $K_D$  was set to  $10 \text{ nM}$ , which corresponds to the  $K_i$  value of **15a** determined in  $[^3\text{H}]$ -INC3344 displacement assays. The  $K_i$  value was used instead of the  $K_D$  (from Table 1) as this represents a more conservative choice with regard to target saturation. The receptor concentration was set to an arbitrarily low number of  $1 \text{ pM}$ .

## REFERENCES

1. Griffith, J. W.; Sokol, C. L.; Luster, A. D. Chemokines and chemokine receptors: positioning cells for host defense and immunity. *Annu. Rev. Immunol.* **2014**, *32*, 659-702.
2. Viola, A.; Luster, A. D. Chemokines and their receptors: drug targets in immunity and inflammation. *Annu Rev Pharmacol Toxicol.* **2008**, *48*, 171-197.
3. White, G. E.; Iqbal, A. J.; Greaves, D. R. CC chemokine receptors and chronic inflammation—therapeutic opportunities and pharmacological challenges. *Pharmacol Rev* **2013**, *65*, 47-89.
4. Boring, L.; Gosling, J.; Cleary, M.; Charo, I. F. Decreased lesion formation in CCR2<sup>-/-</sup> mice reveals a role for chemokines in the initiation of atherosclerosis. *Nature* **1998**, *394*, 894-897.
5. Dawson, T. C.; Kuziel, W. A.; Osahar, T. A.; Maeda, N. Absence of CC chemokine receptor-2 reduces atherosclerosis in apolipoprotein E-deficient mice. *Atherosclerosis* **1999**, *143*, 205-211.
6. Guo, J.; Van Eck, M.; Twisk, J.; Maeda, N.; Benson, G. M.; Groot, P. H.; Van Berkel, T. J. Transplantation of monocyte CC-chemokine receptor 2-deficient bone marrow into ApoE3-Leiden mice inhibits atherogenesis. *Arterioscler Thromb Vasc Biol* **2003**, *23*, 447-453.
7. Abbadie, C.; Lindia, J. A.; Cumiskey, A. M.; Peterson, L. B.; Mudgett, J. S.; Bayne, E. K.; DeMartino, J. A.; MacIntyre, D. E.; Forrest, M. J. Impaired neuropathic pain responses in mice lacking the chemokine receptor CCR2. *Proc. Natl. Acad. Sci. U. S. A.* **2003**, *100*, 7947-7952.
8. Fife, B. T.; Huffnagle, G. B.; Kuziel, W. A.; Karpus, W. J. CC chemokine receptor 2 is critical for induction of experimental autoimmune encephalomyelitis. *J Exp Med* **2000**, *192*.
9. Gosling, J.; Slaymaker, S.; Gu, L.; Tseng, S.; Zlot, C. H.; Young, S. G.; Rollins, B. J.; Charo, I. F. MCP-1 deficiency reduces susceptibility to atherosclerosis in mice that overexpress human apolipoprotein B. *J Clin Invest* **1999**, *103*, 773-778.
10. Gu, L.; Okada, Y.; Clinton, S. K.; Gerard, C.; Sukhova, G. K.; Libby, P.; Rollins, B. J. Absence of monocyte chemoattractant protein-1 reduces atherosclerosis in low density lipoprotein receptor-deficient mice. *Mol Cell* **1998**, *2*, 275-281.
11. Aiello, R. J.; Perry, B. D.; Bourassa, P. A.; Robertson, A.; Weng, W.; Knight, D. R.; Smith, A. H.; Frederick, K. S.; Kalgutkar, A.; Gladue, R. P. CCR2 receptor blockade alters blood monocyte subpopulations but does not affect atherosclerotic lesions in apoE<sup>(-/-)</sup> mice. *Atherosclerosis* **2010**, *208*, 370-375.
12. Guo, D.; Heitman, L. H.; IJzerman, A. P. The role of target binding kinetics in drug discovery. *ChemMedChem* **2015**, *10*, 1793-1796.
13. Copeland, R. A. The dynamics of drug-target interactions: drug-target residence time and its impact on efficacy and safety. *Expert Opin Drug Discov* **2010**, *5*, 305-310.
14. Zhang, R.; Monsma, F. Binding kinetics and mechanism of action: toward the discovery and development of better and best in class drugs. *Expert Opin Drug Discov* **2010**, *5*, 1023-1029.
15. Tummino, P. J.; Copeland, R. A. Residence time of receptor-ligand complexes and its effect on biological function. *Biochemistry* **2008**, *47*, 5481-5492.
16. Ramsey, S. J.; Atkins, N. J.; Fish, R.; van der Graaf, P. H. Quantitative pharmacological analysis of antagonist binding kinetics at CRF1 receptors in vitro and in vivo. *Br. J. Pharmacol.* **2011**, *164*, 992-1007.
17. Fleck, B. A.; Hoare, S. R.; Pick, R. R.; Bradbury, M. J.; Grigoriadis, D. E. Binding kinetics redefine the antagonist pharmacology of the corticotropin-releasing factor type 1 receptor. *J. Pharmacol. Exp. Ther.* **2012**, *341*, 518-531.
18. Lu, H.; England, K.; am Ende, C.; Truglio, J. J.; Luckner, S.; Reddy, B. G.; Marlenee, N. L.; Knudson, S. E.; Knudson, D. L.; Bowen, R. A. Slow-onset inhibition of the FabI enoyl reductase from *Francisella tularensis*: residence time and in vivo activity. *ACS Chem Biol* **2009**, *4*, 221-231.
19. Lindström, E.; von Mentzer, B.; Pählman, I.; Ahlstedt, I.; Uvebrant, A.; Kristensson, E.; Martinsson, R.; Novén, A.; de Verdier, J.; Vauquelin, G. Neurokinin 1 receptor antagonists: correlation between in vitro receptor interaction and in vivo efficacy. *J. Pharmacol. Exp. Ther.* **2007**, *322*, 1286-1293.

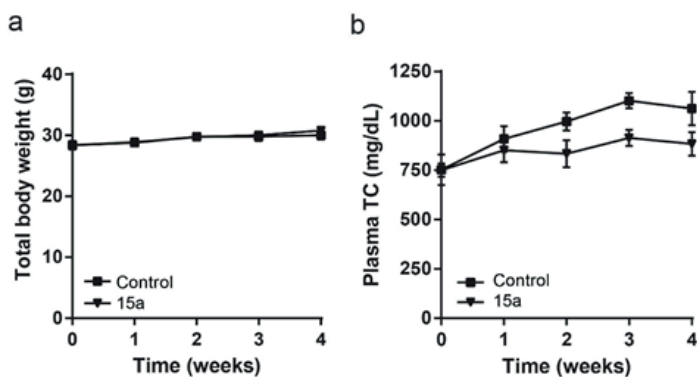
20. Seow, V.; Lim, J.; Cotterell, A. J.; Yau, M. K.; Xu, W.; Lohman, R. J.; Kok, W. M.; Stoermer, M. J.; Sweet, M. J.; Reid, R. C.; Suen, J. Y.; Fairlie, D. P. Receptor residence time trumps drug-likeness and oral bioavailability in determining efficacy of complement C5a antagonists. *Sci Rep* **2016**, *6*, 24575.
21. Calbet, M.; Andres, M.; Armengol, C.; Bravo, M.; Eichhorn, P.; Lopez, R.; Garcia-Gonzalez, V.; Roberts, R.; Miralpeix, M. Pharmacological characterization of CRTh2 antagonist LAS191859: long receptor residence time translates into long-lasting in vivo efficacy. *Pharmacol Res* **2016**, *111*, 208-216.
22. Dahl, G.; Akerud, T. Pharmacokinetics and the drug-target residence time concept. *Drug Discov Today* **2013**, *18*, 697-707.
23. Vauquelin, G.; Van Liefde, I. Slow antagonist dissociation and long-lasting in vivo receptor protection. *Trends Pharmacol Sci* **2006**, *27*, 356-359.
24. Vilums, M.; Zweemer, A. J.; Barmare, F.; van der Gracht, A. M.; Bleeker, D. C.; Yu, Z.; de Vries, H.; Gross, R.; Clemens, J.; Krenitsky, P.; Brussee, J.; Stamos, D.; Saunders, J.; Heitman, L. H.; IJzerman, A. P. When structure-affinity relationships meet structure-kinetics relationships: 3-((1-Inden-1-yl)amino)-1-isopropyl-cyclopentane-1-carboxamides as CCR2 antagonists. *Eur. J. Med. Chem.* **2015**, *93*, 121-134.
25. Vilums, M.; Zweemer, A. J.; Yu, Z.; de Vries, H.; Hillger, J. M.; Wapenaar, H.; Bollen, I. A.; Barmare, F.; Gross, R.; Clemens, J.; Krenitsky, P.; Brussee, J.; Stamos, D.; Saunders, J.; Heitman, L. H.; IJzerman, A. P. Structure-kinetic relationships—an overlooked parameter in hit-to-lead optimization: a case of cyclopentylamines as chemokine receptor 2 antagonists. *J. Med. Chem.* **2013**, *56*, 7706-7714.
26. Schall, T. J.; Proudfoot, A. E. Overcoming hurdles in developing successful drugs targeting chemokine receptors. *Nat Rev Immunol* **2011**, *11*, 355-363.
27. Motulsky, H. J.; Mahan, L. C. The kinetics of competitive radioligand binding predicted by the law of mass action. *Mol. Pharmacol.* **1984**, *25*, 1-9.
28. de Witte, W. E.; Danhof, M.; van der Graaf, P. H.; de Lange, E. C. In vivo target residence time and kinetic selectivity: the association rate constant as determinant. *Trends Pharmacol Sci* **2016**, *37*, 831-842.
29. Guo, D.; Hillger, J. M.; IJzerman, A. P.; Heitman, L. H. Drug-target residence time—a case for G protein-coupled receptors. *Med Res Rev* **2014**, *34*, 856-892.
30. Yu, Z.; van Veldhoven, J. P.; Louvel, J.; t Hart, I. M.; Rook, M. B.; van der Heyden, M. A.; Heitman, L. H.; IJzerman, A. Structure-affinity relationships (SARs) and structure-kinetics relationships (SKRs) of Kv11.1 blockers. *J. Med. Chem.* **2015**, *58*, 5916-5929.
31. Louvel, J.; Guo, D.; Agliardi, M.; Mocking, T. A.; Kars, R.; Pham, T. P. t.; Xia, L.; de Vries, H.; Brussee, J.; Heitman, L. H.; IJzerman, A. P. Agonists for the adenosine A1 receptor with tunable residence time. A case for nonribose 4-amino-6-aryl-5-cyano-2-thiopyrimidines. *J. Med. Chem.* **2014**, *57*, 3213-3222.
32. Andrés, M.; Buil, M. A.; Calbet, M.; Casado, O.; Castro, J.; Eastwood, P. R.; Eichhorn, P.; Ferrer, M.; Forns, P.; Moreno, I. Structure-activity relationships (SAR) and structure-kinetic relationships (SKR) of pyrroliperidinone acetic acids as CRTh2 antagonists. *Bioorg Med Chem Lett* **2014**, *24*, 5111-5117.
33. Struthers, M.; Pasternak, A. CCR2 antagonists. *Curr Top Med Chem* **2010**, *10*, 1278-1298.
34. Kohout, T. A.; Xie, Q.; Reijmers, S.; Finn, K. J.; Guo, Z.; Zhu, Y. F.; Struthers, R. S. Trapping of a nonpeptide ligand by the extracellular domains of the gonadotropin-releasing hormone receptor results in insurmountable antagonism. *Mol. Pharmacol.* **2007**, *72*, 238-247.
35. Brodmerkel, C. M.; Huber, R.; Covington, M.; Diamond, S.; Hall, L.; Collins, R.; Leffet, L.; Gallagher, K.; Feldman, P.; Collier, P.; Stow, M.; Gu, X.; Baribaud, F.; Shin, N.; Thomas, B.; Burn, T.; Hollis, G.; Yeleswaram, S.; Solomon, K.; Friedman, S.; Wang, A.; Xue, C. B.; Newton, R. C.; Scherle, P.; Vaddi, K. Discovery and pharmacological characterization of a novel rodent-active CCR2 antagonist, INCB3344. *J Immunol* **2005**, *175*, 5370-5378.
36. Auffray, C.; Fogg, D.; Garfa, M.; Elain, G.; Join-Lambert, O.; Kayal, S.; Sarnacki, S.; Cumano, A.; Lauvau, G.; Geissmann, F. Monitoring of blood vessels and tissues by a population of monocytes with patrolling behavior. *Science* **2007**, *317*, 666-670.

37. Tylaska, L. A.; Boring, L.; Weng, W.; Aiello, R.; Charo, I. F.; Rollins, B. J.; Gladue, R. P. CCR2 regulates the level of MCP-1/CCL2 in vitro and at inflammatory sites and controls T cell activation in response to alloantigen. *Cytokine* **2002**, *18*, 184-190.
38. van Wanrooij, E. J.; Happe, H.; Hauer, A. D.; de Vos, P.; Imanishi, T.; Fujiwara, H.; van Berkel, T. J.; Kuiper, J. HIV entry inhibitor TAK-779 attenuates atherogenesis in low-density lipoprotein receptor-deficient mice. *Arterioscler Thromb Vasc Biol* **2005**, *25*, 2642-2647.
39. Dairaghi, D. J.; Zhang, P.; Wang, Y.; Seitz, L. C.; Johnson, D. A.; Miao, S.; Ertl, L. S.; Zeng, Y.; Powers, J. P.; Pennell, A. M.; Bekker, P.; Schall, T. J.; Jaen, J. C. Pharmacokinetic and pharmacodynamic evaluation of the novel CCR1 antagonist CCX354 in healthy human subjects: implications for selection of clinical dose. *Clin. Pharmacol. Ther.* **2011**, *89*, 726-734.
40. Olzinski, A. R.; Turner, G. H.; Bernard, R. E.; Karr, H.; Cornejo, C. A.; Aravindhan, K.; Hoang, B.; Ringenberg, M. A.; Qin, P.; Goodman, K. B.; Willette, R. N.; Macphee, C. H.; Jucker, B. M.; Sehon, C. A.; Gough, P. J. Pharmacological inhibition of C-C chemokine receptor 2 decreases macrophage infiltration in the aortic root of the human C-C chemokine receptor 2/apolipoprotein E<sup>-/-</sup> mouse: magnetic resonance imaging assessment. *Arterioscler Thromb Vasc Biol* **2010**, *30*, 253-259.
41. Cusack, K. P.; Wang, Y.; Hoemann, M. Z.; Marjanovic, J.; Heym, R. G.; Vasudevan, A. Design strategies to address kinetics of drug binding and residence time. *Bioorg Med Chem Lett* **2015**, *25*, 2019-2027.
42. Xue, C. B.; Metcalf, B.; Feng, H.; Cao, G.; Huang, T.; Zheng, C.; Robinson, D. J.; Han, A. Q. 3-aminopyrrolidine derivatives as modulators of chemokine receptors. Patent WO2004/050024 (A2). **2004**.
43. Xue, C. B.; Wang, A.; Meloni, D.; Zhang, K.; Kong, L.; Feng, H.; Glenn, J.; Huang, T.; Zhang, Y.; Cao, G.; Anand, R.; Zheng, C.; Xia, M.; Han, Q.; Robinson, D. J.; Storace, L.; Shao, L.; Li, M.; Brodmerkel, C. M.; Covington, M.; Scherle, P.; Diamond, S.; Yeleswaram, S.; Vaddi, K.; Newton, R.; Hollis, G.; Friedman, S.; Metcalf, B. Discovery of INCB3344, a potent, selective and orally bioavailable antagonist of human and murine CCR2. *Bioorg Med Chem Lett* **2010**, *20*, 7473-7478.
44. Zweemer, A. J.; Nederpelt, I.; Vrieling, H.; Hafith, S.; Doornbos, M. L.; de Vries, H.; Abt, J.; Gross, R.; Stamos, D.; Saunders, J.; Smit, M. J.; IJzerman, A. P.; Heitman, L. H. Multiple binding sites for small-molecule antagonists at the CC chemokine receptor 2. *Mol. Pharmacol.* **2013**, *84*, 551-561.
45. Smith, P. K.; Krohn, R. I.; Hermanson, G. T.; Mallia, A. K.; Gartner, F. H.; Provenzano, M. D.; Fujimoto, E. K.; Goeke, N. M.; Olson, B. J.; Klenk, D. C. Measurement of protein using bicinchoninic acid. *Anal. Biochem.* **1985**, *150*, 76-85.
46. von der Thusen, J. H.; van Berkel, T. J.; Biessen, E. A. Induction of rapid atherogenesis by perivascular carotid collar placement in apolipoprotein E-deficient and low-density lipoprotein receptor-deficient mice. *Circulation* **2001**, *103*, 1164-1170.
47. Cheng, Y.; Prusoff, W. H. Relationship between the inhibition constant (K<sub>1</sub>) and the concentration of inhibitor which causes 50 per cent inhibition (I<sub>50</sub>) of an enzymatic reaction. *Biochem. Pharmacol.* **1973**, *22*, 3099-3108.
48. Guo, D.; van Dorp, E. J.; Mulder-Krieger, T.; van Veldhoven, J. P.; Brussee, J.; IJzerman, A. P.; Heitman, L. H. Dual-point competition association assay: a fast and high-throughput kinetic screening method for assessing ligand-receptor binding kinetics. *J Biomol Screen* **2013**, *18*, 309-320.

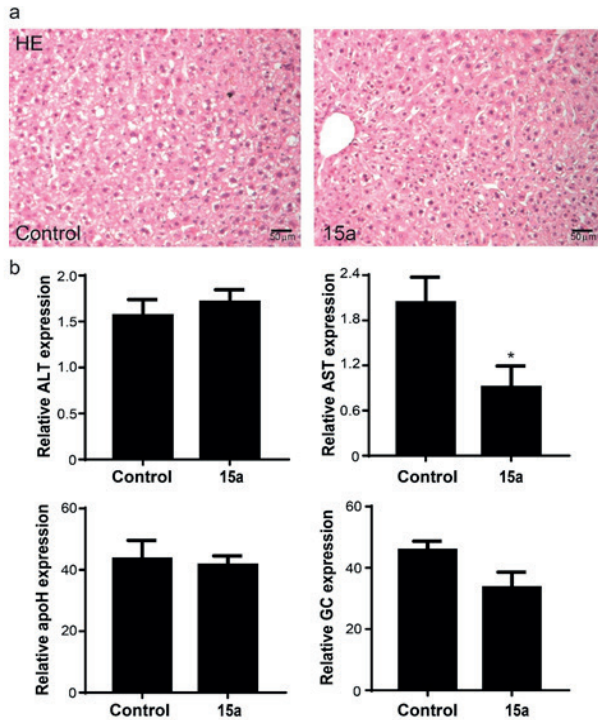
## SUPPORTING INFORMATION

Gene	Forward primer (5'-3')	Reverse primer (3'-5')
ALT	CCCTGACATGTTCTTCTGTCTGTGCC	CCTCAGTTTCTCCAGCAGCACCC
AST	TGACCGGATTCTGACCATGAGATCCG	GGTCAAGCCGCACATGTTGATCCG
apoH	CATGAGACATACAAGCTGGACGGCC	TACAGCACGGTGGCTTTCTTAACGG
GC	GCAGAACGGCTAAGGACAAAA	AGTCCGAGTGTTCCTCCACCAT
Rpl27	CGCCAAGCGATCCAAGATCAAGTCC	AGCTGGGTCCCTGAACACATCCTTG
$\beta$ -actin	AACCGTGAAAAGATGACCCAGAT	CACAGCCTGGATGGCTACGTA
TAF7	AGTCTGGGCATGTCAACCTGAA	CGTAACACAAGGCAAATCGACCA

**Table S1. qPCR gene primer sequences.** All gene expression analysis was performed using three housekeeping genes (Rpl27,  $\beta$ -actin and TAF7). Abbreviations: ALT: alanine aminotransferase; AST: aspartate aminotransferase; apoH: apolipoprotein H; GC: group specific component; Rpl27: 60s ribosomal protein ligand 27; TAF7: TATA-box-binding protein.

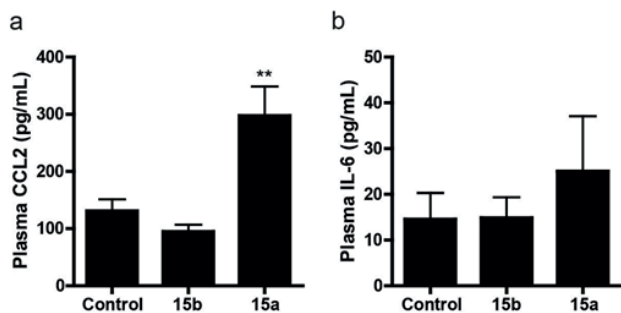


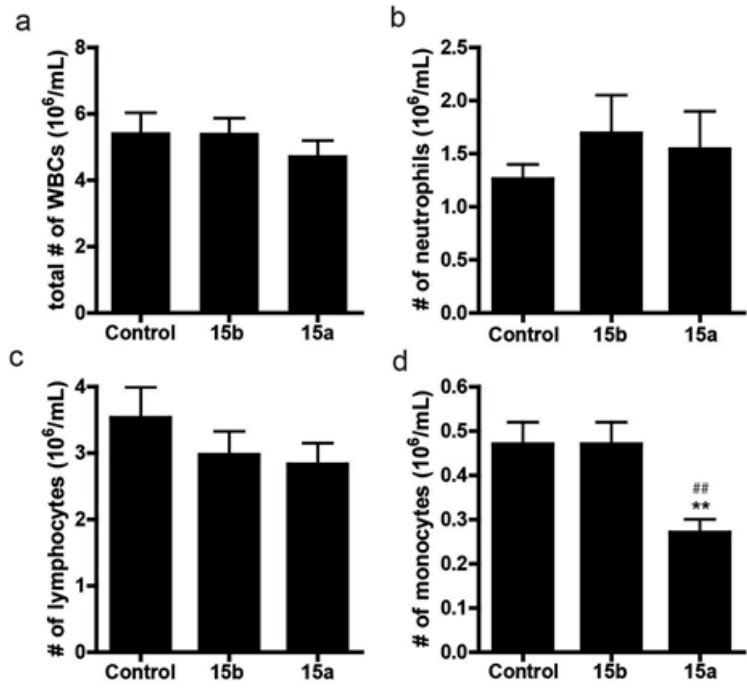
**Supplementary Figure S1. Effect of 15a on body weight and cholesterol levels.** Total body weight (**a**) and plasma total cholesterol (TC) levels (**b**) were not significantly affected by treatment with 15a. Graphs shown are representative from one experiment with n=10 controls versus n=9 15a-treated mice.



**Supplementary Figure S2. 15a does not affect liver function.** (a) Histological analysis of the liver did not reveal any adverse effects of the 15a treatment as shown by an HE staining. (b) Also, gene expression analysis did not show any differences in mRNA expression of liver toxicity markers ALT, apoH and GC, while liver AST expression levels were even somewhat decreased (\* $P=0.02$ ). Graphs shown are representative from one experiment with  $n=6$  per group.

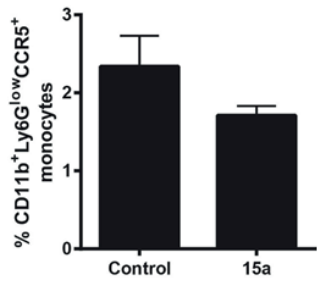
**Supplementary Figure S3. Effect of 15a on CCL2 and IL-6 plasma levels.** Plasma CCL2 levels were increased upon treatment with 15a (a), while IL-6 levels remained unaffected by treatment with 15a (b). \*\* $P<0.01$ . Graphs shown are representative from one experiment with  $n=10$  controls versus  $n=9$  15a-treated mice.





**Supplementary Figure S4. Effect of 15a on white blood cells.** No differences were found in circulating total white blood cell (WBCs) (a), neutrophil (b) or lymphocyte (c) counts between the groups, but 15a significantly reduced the number of circulating monocytes (d).  $**P < 0.01$ . Graphs shown are representative from one experiment with  $n=10$  controls versus  $n=9$  15a-treated mice.

**Supplementary Figure S5. Effect of 15a on CCR5<sup>+</sup> monocytes.** Treatment with 15a did not affect the circulating % of CD11b<sup>+</sup>Ly6G<sup>low</sup>CCR5<sup>+</sup> monocytes. Graphs shown are representative from one experiment with  $n=6$  per group.







## Chapter 8

---

# Conclusions and Future Perspectives



## CONCLUSIONS

### Crystal structures to advance drug discovery

The first X-ray crystal structure of CC chemokine receptor 2 isoform b (CCR2) in complex with two antagonists, crystallized at 2.8 Å resolution, is described in **Chapter 3**. Engineering of CCR2 resulted in the more stable crystallization construct CCR2-T4L, in which the flexible intracellular loop 3 (ICL3) was replaced by the T4 lysozyme (T4L) fusion protein, among other modifications. However, sufficient stabilization and subsequent crystallization was only achieved after the simultaneous addition of two antagonists: the orthosteric BMS-681 and the allosteric CCR2-RA-[R]. The obtained crystal structure (PDB 5T1A, **Chapter 3**) provided insight on the binding mode and mechanism of inhibition of the two antagonists. The structure shows that BMS-681 binds in the minor subpocket of the canonical orthosteric binding site of CCR2, while CCR2-RA-[R] binds in a previously suggested intracellular binding site,<sup>1, 2</sup> located ~30 Å away from the chemokine binding site. By binding at this intracellular site, CCR2-RA-[R] inhibits the receptor in a noncompetitive manner with regard to chemokine binding, which results in its previously observed insurmountable behavior: CCR2-RA-[R] decreased the maximum receptor response even at the highest agonist concentration tested.<sup>2</sup> This is particularly relevant due to the high local concentration of chemokine ligands, such as CCL2, during inflammatory conditions.<sup>3-5</sup>

In addition, the structure suggests a cooperative mechanism of inhibition between the two antagonists: BMS-681 directly interferes with chemokine binding through competition in the orthosteric binding site, but is not associated with G protein coupling, while CCR2-RA-[R] directly disrupts G protein binding and allosterically intervenes with chemokine binding. Hence, both BMS and CCR2-RA-[R] help to stabilize the receptor in an inactive conformation (Figure 1). This cooperative binding between these antagonists was further supported by data from the stability and radioligand binding assays. For instance, the binding capacity of CCR2-RA-[R] was increased by the presence of BMS-681 in both equilibrium and kinetic radioligand binding assays, indicative of allosteric enhancement. Finally, this crystal structure may facilitate the rational design of novel antagonists for CCR2.

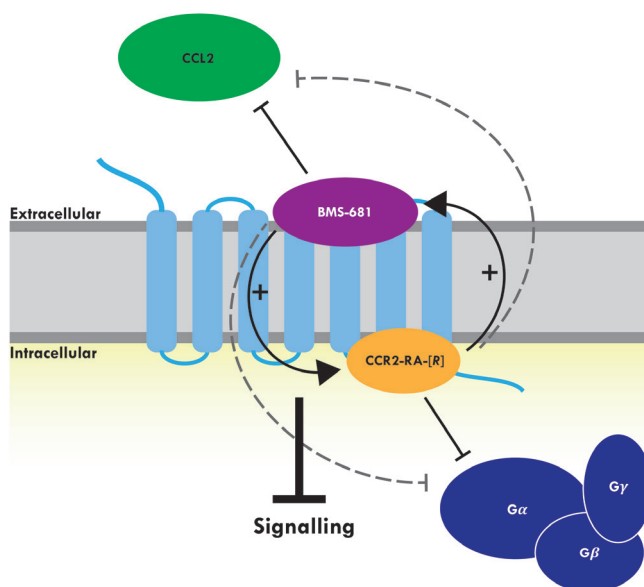
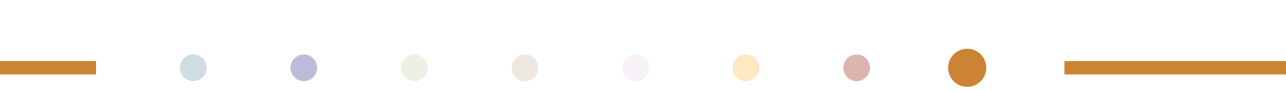


**Figure 1. Binding and mechanism of inhibition of BMS-681 and CCR2-RA-[R] based on the crystal structure of CCR2.** BMS-681 binds at the orthosteric binding site, where it directly interferes with CCL2 binding, and promotes an inactive, G protein-uncoupled CCR2 conformation. CCR2-RA-[R] binds in an allosteric binding site located at the intracellular region of the receptor, where it directly interferes with G protein-coupling and allosterically inhibits CCL2 binding. As a consequence, when the two inhibitors bind simultaneously, they act in a cooperative manner as shown by an enhancement of each other's binding, resulting in a highly inactive conformation of CCR2.

## Intracellular ligands to better target CCR1, CCR2 and CCR5

As reviewed in **Chapter 2**, targeting the intracellular binding site of GPCRs offers several advantages over targeting the orthosteric binding site: allosteric modulation of the affinity/efficacy of orthosteric ligands, insurmountable mode of inhibition, possibility to design multitarget ligands and potential biased signaling (**Chapter 2**). Thus, throughout **Chapters 4** and **5**, we explored the possibility of targeting other chemokine receptors with intracellular allosteric modulators. For this, we focused on the highly homologous CC chemokine receptors 1 (CCR1) and 5 (CCR5), where intracellular pockets for small-molecules have been previously suggested.<sup>6-9</sup> The radiolabeled version of the co-crystallized intracellular ligand CCR2-RA-[R] in **Chapter 3**, [<sup>3</sup>H]-CCR2-RA-[R], was first characterized in both CCR2 and CCR1 (**Chapter 4**). In addition to its high affinity in CCR2, [<sup>3</sup>H]-CCR2-RA-[R] also displayed high affinity for CCR1, rendering it a suitable tool for studying CCR1. Moreover, in [<sup>3</sup>H]-CCR2-RA-[R] displacement assays, the CCR1 orthosteric antagonist BX471 was not able to displace the radioligand, further supporting that CCR1 also possesses an intracellular binding pocket, which may be used for the design of both selective and 'multitarget' inhibitors. The fact



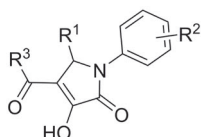
that the CCR1, CCR2 and CCR5 are involved in the pathogenesis of many inflammatory diseases, such as rheumatoid arthritis (RA) and multiple sclerosis (MS), makes a strong case for the development of multitarget ligands, i.e. dual/triple antagonists, as a promising therapeutic approach.<sup>10,11</sup> Several dual antagonists have already been reported for CCR2/CCR5;<sup>12</sup> however, we are the first to undertake the design of CCR1/CCR2 dual antagonists (**Chapter 4**). Based on the pyrrolone scaffold of CCR2-RA-[R], ~50 pyrrolone derivatives were synthesized and evaluated in both CCR1 and CCR2 (Figure 2). This medicinal chemistry approach allowed us to find several compounds with improved selectivity towards CCR1, as well as potential dual CCR1/CCR2 antagonists. Functional characterization of selected compounds revealed that these intracellular ligands behave as inverse agonists in CCR1, which has previously been characterized as a constitutively active receptor.<sup>13</sup> To the best of our knowledge, these ligands represent the first intracellular inverse agonists for CCR1, providing a new pharmacological approach to modulate this receptor.

All previously reported CCR2/CCR5 dual antagonists<sup>12</sup> bind to the orthosteric binding site of the receptors, which results in a competitive and surmountable mode of inhibition. Thus, in **Chapter 5** we explored the potential of developing intracellular CCR2/CCR5 antagonists by synthesizing and evaluating the activity of a series of triazolo-pyrimidinone derivatives (Figure 2), which also bind to the intracellular binding site as confirmed in CCR2 radioligand binding assays. However, CCR2-RA-[R] binds with much lower affinity to CCR5 (~100 nM) compared with CCR2 and CCR1, preventing us from using this radioligand to determine the affinity of triazolo-pyrimidinone derivatives in CCR5. Thus, we relied on functional  $\beta$ -arrestin recruitment assays to evaluate the activity of the derivatives in CCR5. In contrast to **Chapter 4**, where we found several pyrrolone derivatives with high-affinity towards CCR1, most triazolo-pyrimidinone derivatives remained selective towards CCR2; however, few derivatives were able to inhibit CCR5 signaling with approximately 100 nM potency, indicating that the design of intracellular multitarget ligands is quite feasible for these receptors as well. Moreover, evaluation of two compounds in [<sup>35</sup>S]GTP $\gamma$ S binding assays confirmed that these compounds behave as insurmountable antagonists in both CCR2 and CCR5, which might translate into higher *in vivo* efficacy in inflammatory diseases where these receptors are involved.

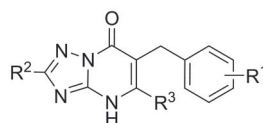
Development of covalent ligands, either as tool compounds or pharmaceutical products, has gained increased interest due to their many potential applications and therapeutic advantages.<sup>14, 15</sup> Thus, while **Chapters 4** and **5** focused on the design of reversible intracellular ligands, **Chapter 6** describes the design, synthesis and characterization of the first irreversible intracellular ligand for CCR2. Using a variety of assays, including time-dependent affinity determination, radioligand wash-out assays, and functional (wash-out) assays, we validated compound **14** as a covalent negative allosteric modulator (NAM) for

CCR2 (Figure 2). The binding mode of compound **14** was studied using computational modeling followed by site-directed mutagenesis of CCR2. These studies identified Cys75<sup>2x37</sup>, at the intracellular binding pocket, as the primary residue for covalent interaction, although secondary interaction sites remain possible. Altogether, compound **14** represents a potential tool compound to further study CCR2 pharmacology.

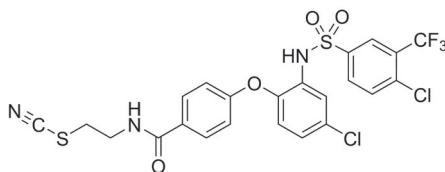
**Scaffolds for potential intracellular multitarget ligands:**



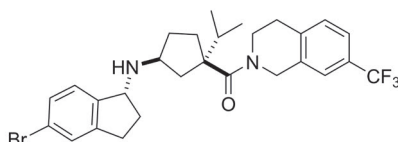
**Pyrrolidinone scaffold**  
Intracellular CCR1/CCR2 ligands



**Triazolo-pyrimidinone scaffold**  
Intracellular CCR2/CCR5 ligands



**Compound 14**  
Intracellular covalent CCR2 negative allosteric modulator



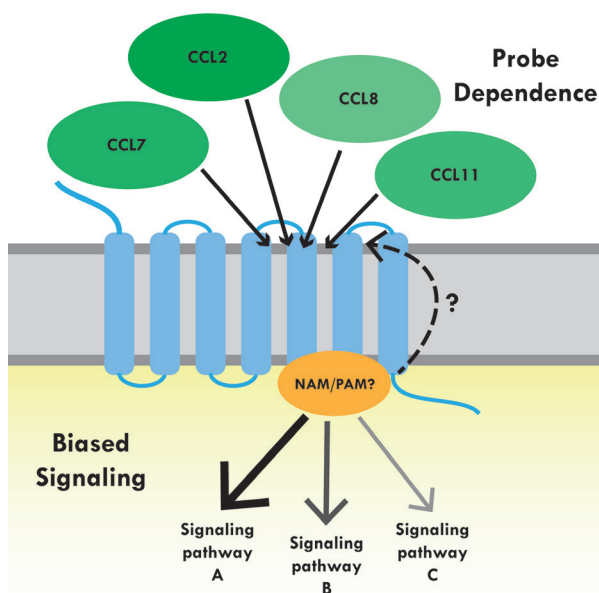
**Compound 15a**  
CCR2 orthosteric antagonist  
Residence Time (RT) = 714 min on hCCR2, 20 min on mCCR2

Figure 2. Scaffolds and chemical structures of compounds discussed in this thesis.

## CCR2 antagonists for the treatment of atherosclerosis

CCR2 and its endogenous ligand CCL2 have been found to play a key role in the recruitment of monocytes to atherosclerotic lesions, representing potential targets for the treatment of atherosclerosis. Previous research in our group led to the discovery of the CCR2 orthosteric antagonist **15a** (Figure 2), which displays a prolonged residence time (RT) on its target (RT of 714 min).<sup>16</sup> Long RT antagonists can also inhibit the receptor in an insurmountable manner,<sup>17</sup> and they have been proposed to lead to enhanced *in vivo* efficacy.<sup>18</sup> Thus, we aimed to determine whether **15a** is effective in inhibiting atherogenesis in the apolipoprotein

E-deficient (apoE<sup>-/-</sup>) mouse model of atherosclerosis. Compared to vehicle control, treatment of apoE<sup>-/-</sup> mice with **15a** resulted in significant inhibition of CCR2<sup>+</sup> monocytes recruitment to the atherosclerotic plaques, as well as significant reduction of the plaques size at both the carotid artery and the aortic root. Assessment of **15a** binding kinetics in mouse CCR2 (mCCR2) revealed a poor translation of kinetic parameters between the human and mouse orthologues: **15a** displays a RT of less than 30 min in mCCR2 compared with 714 min in human CCR2 (Figure 2), while its affinity was comparable in both receptors. These findings emphasize the need to characterize equilibrium and kinetic parameters of drug candidates in all relevant species for preclinical studies, especially among chemokine receptors, where high species variation has been found.<sup>19</sup> Pharmacokinetic analysis and calculation of CCR2 occupancy levels indicated that a single dose of **15a** led to >90% CCR2 occupancy levels for over 24 hours. Such prolonged target occupancy resulted from the long elimination half-life of **15a** combined with the use of target-saturating concentrations. Overall, these data support high receptor occupancy as a key parameter for an effective anti-inflammatory response, and suggests **15a** as a promising candidate for further drug development studies.

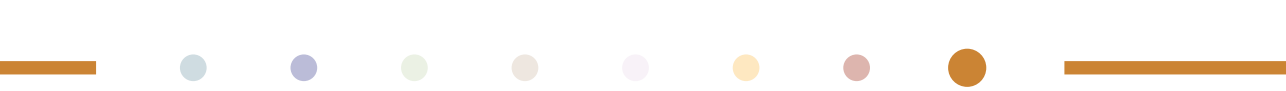


**Figure 3. Intracellular modulation of G protein-coupled receptors (GPCRs).** Targeting the intracellular binding site of GPCRs provides several opportunities and challenges. For example, this binding site can be used for the development of both negative allosteric modulators (NAM), which inhibit the receptor, and positive allosteric modulators (PAM), which activate or enhance the receptor activity. These intracellular ligands also have the potential to promote biased signaling, by preferentially activating or inhibiting one pathway over another. Finally, it is important to investigate a potential probe dependent behavior of intracellular ligands, as their effect might differ depending on the agonist bound. The latter is particularly important for chemokine receptors, where multiple chemokines can activate one receptor.

## FUTURE PERSPECTIVES

### Intracellular modulation of GPCRs

Although this thesis is mostly focused on intracellular modulation of CCR1, CCR2 and CCR5, this strategy should not be limited to chemokine receptors (**Chapter 2**). In fact, small-molecule ligands have been reported to bind to the intracellular region of  $\beta_2$  adrenergic receptor ( $\beta_2$ AR),<sup>20, 21</sup> proteinase activated receptor 1 (PAR1)<sup>22</sup> and dopamine D1 receptor (D1R),<sup>23</sup> suggesting the presence of intracellular binding pockets among class A GPCRs in general. For instance, the crystal structure of  $\beta_2$ AR in complex with the negative allosteric modulator (NAM) 15PA (PDB 5X7D),<sup>20</sup> demonstrates that 15PA binds to a similar intracellular pocket compared to that of CCR2-RA-[R] in CCR2 (**Chapter 3**) and vercirnon in CCR9.<sup>24</sup> In addition, another crystal structure of  $\beta_2$ AR (PDB 6N48)<sup>21</sup> shows that the  $\beta_2$ AR positive allosteric modulator (PAM) 6FA also binds to the intracellular region, but at the interface between the cytoplasm and the lipid membrane, suggesting an additional intracellular pocket to modulate GPCR signaling.<sup>21</sup> In combination with screening campaigns, the increasing number of crystal structures with intracellular ligands can be used for *in silico* drug discovery studies, such as virtual screening, in order to identify novel intracellular ligands for chemokine receptors and GPCRs in general. The potential to activate the receptor via the intracellular site has also been demonstrated by the recently described intracellular PAMs for  $\beta_2$ AR<sup>21</sup> and dopamine D1 receptor (D1R).<sup>23</sup> Although no intracellular small-molecule PAMs have been reported for chemokine receptors, intracellular pepducins, i.e. lipidated peptides derived from the ICLs, with agonistic activity have been developed for CXCR4, such as ATI-2341.<sup>25</sup> Moreover, ATI-2341 displayed biased signaling towards  $G\alpha_i$ -coupling over  $G\alpha_{13}$ -coupling or  $\beta$ -arrestin recruitment,<sup>25</sup> suggesting that functional bias can also be achieved by targeting this intracellular pocket. In line with this, the suggested intracellular modulator AZD8797, targeting the CX<sub>3</sub>CR1 receptor, has been found to act as a NAM of G protein-activation, and as a PAM for  $\beta$ -arrestin recruitment.<sup>26</sup> Indications of functional bias have also been found with CCR2 intracellular NAMs; for instance, the CCR2 intracellular ligand JNJ-27141491 displayed a higher potency in inhibiting G protein activation than  $\beta$ -arrestin recruitment,<sup>2</sup> while compounds **7** and **14** described in **Chapter 6** of this thesis appeared more potent in the  $\beta$ -arrestin recruitment assay than in the [<sup>35</sup>S]GTP $\gamma$ S binding assay. Biased ligands for chemokine receptors have been found to differentially control physiological responses, such as leukocyte recruitment and inflammation,<sup>27</sup> as well as receptor endocytosis and the development of tolerance,<sup>28</sup> which highlights their potential therapeutic benefit. Thus, further studies are warranted to investigate the functional profile of intracellular allosteric modulators in multiple signaling pathways, in order to identify functional bias (Figure 3). Finally, evaluation of their functional effects in the presence of different chemokines, i.e. probe-dependence, is particularly relevant for the development



of intracellular ligands for chemokine receptors, as many chemokines are known to activate a single receptor (Figure 3).<sup>29</sup>

## Multitarget ligands for GPCRs

The development of multitarget drugs, which act on multiple receptors or enzymes, has been proposed as a more effective approach to treat complex, multifactorial diseases such as multiple sclerosis (MS), rheumatoid arthritis (RA) and cancer.<sup>10, 11, 30, 31</sup> Thus, in **Chapters 4** and **5** from this thesis, we explored the possibility to design multitarget intracellular ligands for CCR1, CCR2 and CCR5, which resulted in the identification of potential CCR1/CCR2 (**Chapter 4**) and CCR2/CCR5 (**Chapter 5**) multitarget ligands. Multitarget ligands have been reported for many chemokine receptor pairs, including CCR1/CCR3,<sup>32</sup> CCR2/CCR5,<sup>12</sup> CCR2/CXCR2,<sup>33</sup> CCR5/CXCR4,<sup>34</sup> CXCR1/CXCR2,<sup>35</sup> and CXCR3/CXCR4.<sup>36</sup> Multitarget ligands can also be developed to target different receptor classes, such as CCR3 and histamine receptor H<sub>1</sub> (H<sub>1</sub>R), which are both involved in the pathogenesis of asthma and atopic dermatitis.<sup>37</sup> Although CCR3 and H<sub>1</sub>R have limited homology, high-affinity dual-target antagonists have been developed for this pair,<sup>37</sup> opening up the possibility to design multitarget ligands against highly dissimilar proteins. Although there is ample evidence on the beneficial effects of CCR2/CCR5 combined inhibition in several (pre)clinical studies,<sup>38-44</sup> more studies are still needed to investigate whether combined inhibition of other receptor pairs is in fact more efficacious than selective inhibition. However, one of the main challenges in the development of multitarget drugs is choosing the right targets. For instance, several chemokine receptors seem to play a role in RA, including CCR1, CCR2, CCR5, CXCR2 and CXCR3,<sup>45</sup> which complicates the selection of relevant combinations of drug targets. In this regard, the generation of *in silico* biological network models may be used in combination with *in vitro/in vivo* studies to identify successful combinations of drug targets to achieve the highest efficacy.<sup>46</sup> These biological network models have also shown that inhibition of several network components, even if partially, is more effective than inhibition of a single component in modulating complex and robust disease models.<sup>46</sup> This implies that the use of low-affinity ligands might be sufficient to achieve the desired effect; thus, selection of multitarget ligands should not be based purely on affinity but on the desired activity profile.<sup>47</sup> Finally, optimization of selectivity for the desired targets remains a challenge in the rational design of multitarget ligands, warranting more structure-affinity/activity relationships studies as well as target structure-based studies.<sup>47</sup> Overall, the described multitarget inhibitors represent potential tool compounds to study the *in vitro* and *in vivo* effects of combined inhibition.



## Covalent ligands as tools for GPCRs

Covalent probes are increasingly being developed for GPCRs as they can be used to further elucidate receptor function in both *in vitro* and *in vivo* systems, as well as to facilitate target crystallization.<sup>14, 48</sup> Such covalent probes have been reported for several class A GPCRs,<sup>14, 49</sup> however, no covalent probes have been reported for chemokine receptors, with the exception of the covalent reversible boronic acid-based probes for CXCR3, which were used to study CXCR3 allosteric modulation.<sup>50</sup> Thus, compound **14** described in **Chapter 6** of this thesis represents the first irreversible covalent ligand for chemokine receptors, in this case CCR2. Using a similar approach, allosteric or orthosteric covalent ligands can be designed for other chemokine receptors, including the constitutively active CCR1. These covalent ligands can be particularly useful in receptor stabilization for X-ray structure determination, as demonstrated by the crystal structures of  $\beta_2$ AR,<sup>51</sup> cannabinoid receptor CB<sub>1</sub>,<sup>52</sup> and adenosine A<sub>1</sub> receptor,<sup>53</sup> all co-crystallized with covalent ligands. A covalent inverse agonist targeting CCR1 could represent an important step to stabilize the receptor, achieve crystallization and thus provide insight on the binding mode and mechanism of inhibition of CCR1 intracellular modulators. In addition, covalent ligands can be further functionalized as affinity-based probes by addition of a ligation or click handle (alkyne or azide group) to their chemical structure, which allows the introduction through “click chemistry” of a fluorophore or a biotin tag after covalently binding to a protein.<sup>54</sup> Although this is a relatively new field for membrane proteins, (photo)affinity-based protein profiling has been used in GPCRs to study target expression profiles and drug-target engagement, identification of off-targets, and target visualization in biological systems.<sup>55-58</sup> Thus, the development of affinity-based probes represents a novel and promising approach to advance drug discovery in the field of chemokine receptors (Figure 4).

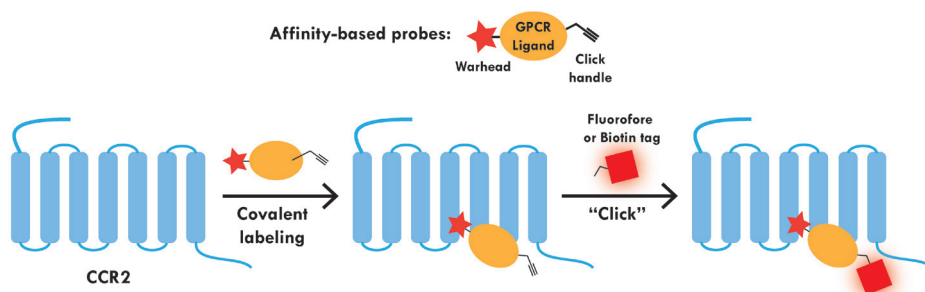


**Figure 4. Covalent ligands as affinity-based probes.** Covalent ligands such as compound **14** described in this thesis (**Chapter 6**), can be further functionalized as affinity-based probes by adding a ligation or “click” handle to the molecule, such as an alkyne group. In this way, a fluorophore or a biotin tag can be introduced to the receptor via “click-chemistry”, allowing GPCR visualization or isolation from a complex cellular mixture.

## Intracellular ligands as PROTACs

In addition to GPCR modulation by small-molecule inhibitors, other strategies are now emerging to inhibit receptor function, including pepducins and nanobodies described in **Chapter 2**. Induced protein degradation has recently emerged as a novel strategy to inhibit protein function by using, for instance, proteolysis-targeting chimeras (PROTACs) that exploit the ubiquitin-proteasome system (UPS).<sup>59</sup> PROTACs are bifunctional molecules composed of a ligand that targets the protein of interest connected via a linker group to another ligand that recruits an E3 ubiquitin ligase. By forming a ternary complex with both the E3 ligase and the protein of interest, PROTACs induce poly-ubiquitination of the protein target and subsequent degradation of the protein of interest by the 26S proteasome (Figure 5).<sup>60, 61</sup> Recent advances in this technology have led to the development of the first PROTAC clinical candidate, which targets the nuclear androgen receptor for the treatment of prostate cancer.<sup>62</sup> Due to their mechanism of action, PROTACs need to engage their targets within the intracellular space, and thus, they have been mostly developed for cytosolic targets such as enzymes, nuclear receptors, transcription factors and kinases, among others.<sup>61</sup> Intracellular ligands for GPCRs, such as those described in **Chapters 2, 3, 4** and **5**, represent valuable starting points for PROTACs design, as they engage their target from the intracellular site. By linking these intracellular ligands to E3 ligase ligands, we can investigate whether the ubiquitination machinery can be hijacked to induce GPCR degradation (Figure 5).<sup>63</sup> In this regard, poly-ubiquitination of GPCRs has been found to play an important role not only on lysosomal or proteasomal degradation, but also on receptor signaling. For example, the E3 ligase VHL has been found to ubiquitinate the  $\beta_2$ -adrenergic receptor ( $\beta_2$ AR) to promote proteasomal degradation via 26S,<sup>64</sup> indicating that this strategy might be feasible for some, if not all, GPCRs. Moreover, Burslem *et al.* recently developed PROTACs for three different transmembrane receptor tyrosine kinases (RTK), suggesting that targeting transmembrane proteins is indeed possible.<sup>65</sup> Of note, lysosome targeting chimeras (LYTACs)<sup>66</sup> and endosome targeting chimeras (ENDTACs)<sup>67</sup> have been recently developed to induce lysosomal degradation of extracellular targets; providing another strategy to induce degradation of GPCRs. Due to their catalytic mode of action—in contrast to the occupancy-based mode of action of small-molecule inhibitors—PROTACs may offer several advantages for GPCRs, including potent target degradation at low concentrations, enhanced target selectivity, and prolonged inhibition of receptor signaling.<sup>68, 69</sup> Thus, the development of novel small-molecule intracellular ligands for GPCRs may facilitate the design of GPCR-targeting PROTACs as a novel strategy to modulate receptor pharmacology (Figure 5).

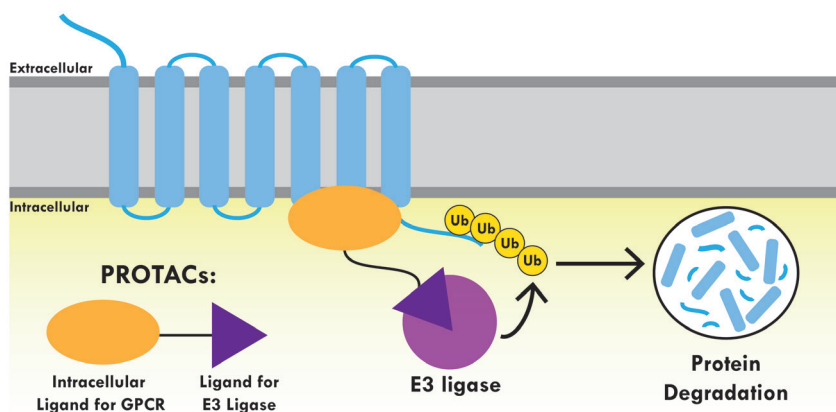


**Figure 5. Intracellular ligands as PROTACs.** Induced-protein degradation represents an alternative to inhibit protein function. Proteolysis-targeting chimeras (PROTACs) for GPCRs can be designed by linking an intracellular binding GPCR ligand to an E3 ligase ligand. By binding to both the GPCR of interest and the E3 ligase, PROTACs induce poly-ubiquitination (Ub) and subsequent degradation of the protein of interest.

## Final notes

All in all, in this thesis we have explored different mechanisms to achieve insurmountable inhibition for chemokine receptors, including intracellular allosteric inhibition, covalent inhibition and long RT inhibitors, as this may lead to improved *in vivo* efficacy of chemokine receptors' inhibitors. In addition, with the crystallization of CCR2 and the identification of several intracellular ligands for CCR1, CCR2 and CCR5—including selective, multitarget and covalent ligands—we are expanding the toolbox to further study and modulate chemokine receptors. Finally, we hope that the data presented in this thesis contributes to advance drug discovery in the field of chemokine receptors and GPCRs in general.

## REFERENCES

1. Zweemer, A. J.; Bunnik, J.; Veenhuizen, M.; Miraglia, F.; Lenselink, E. B.; Vilums, M.; de Vries, H.; Gibert, A.; Thiele, S.; Rosenkilde, M. M.; IJzerman, A. P.; Heitman, L. H. Discovery and mapping of an intracellular antagonist binding site at the chemokine receptor CCR2. *Mol. Pharmacol.* **2014**, *86*, 358-368.
2. Zweemer, A. J.; Nederpelt, I.; Vrieling, H.; Hafith, S.; Doornbos, M. L.; de Vries, H.; Abt, J.; Gross, R.; Stamos, D.; Saunders, J.; Smit, M. J.; IJzerman, A. P.; Heitman, L. H. Multiple binding sites for small-molecule antagonists at the CC chemokine receptor 2. *Mol. Pharmacol.* **2013**, *84*, 551-561.
3. Turner, M. D.; Nedjai, B.; Hurst, T.; Pennington, D. J. Cytokines and chemokines: at the crossroads of cell signalling and inflammatory disease. *Biochim Biophys Acta* **2014**, *1843*, 2563-2582.
4. Haukeland, J. W.; Damås, J. K.; Konopski, Z.; Løberg, E. M.; Haaland, T.; Goverud, I.; Torjesen, P. A.; Birkeland, K.; Bjørø, K.; Aukrust, P. Systemic inflammation in nonalcoholic fatty liver disease is characterized by elevated levels of CCL2. *J. Hepatol.* **2006**, *44*, 1167-1174.
5. Raghu, H.; Lopus, C. M.; Wang, Q.; Wong, H. H.; Lingampalli, N.; Oliviero, F.; Punzi, L.; Giori, N. J.; Goodman, S. B.; Chu, C. R.; Sokolove, J. B.; Robinson, W. H. CCL2/CCR2, but not CCL5/CCR5, mediates monocyte recruitment, inflammation and cartilage destruction in osteoarthritis. *Ann Rheum Dis* **2017**, *76*, 914-922.
6. Andrews, G.; Jones, C.; Wreggett, K. A. An intracellular allosteric site for a specific class of antagonists of the CC chemokine G protein-coupled receptors CCR4 and CCR5. *Mol. Pharmacol.* **2008**, *73*, 855-867.
7. Dasse, O.; Evans, J.; Zhai, H.-X.; Zou, D.; Kintigh, J.; Chan, F.; Hamilton, K.; Hill, E.; Eckman, J.; Higgins, P. Novel, acidic CCR2 receptor antagonists: lead optimization. *Lett. Drug. Des. Discov.* **2007**, *4*, 263-271.
8. Peace, S.; Philp, J.; Brooks, C.; Piercy, V.; Moores, K.; Smethurst, C.; Watson, S.; Gaines, S.; Zippoli, M.; Mookherjee, C.; Ife, R. Identification of a sulfonamide series of CCR2 antagonists. *Bioorg Med Chem Lett* **2010**, *20*, 3961-3964.
9. Buntinx, M.; Hermans, B.; Goossens, J.; Moechars, D.; Gilissen, R. A.; Doyon, J.; Boeckx, S.; Coesemans, E.; Van Lommen, G.; Van Wauwe, J. P. Pharmacological profile of JNJ-27141491 [(S)-3-[3, 4-difluorophenyl]-propyl]-5-isoxazol-5-yl-2-thioxo-2, 3-dihydro-1H-imidazole-4-carboxyl acid methyl ester], as a noncompetitive and orally active antagonist of the human chemokine receptor CCR2. *J. Pharmacol. Exp. Ther.* **2008**, *327*, 1-9.
10. Horuk, R. Chemokine receptor antagonists: overcoming developmental hurdles. *Nat Rev Drug Discov* **2009**, *8*, 23-33.
11. Horuk, R. Promiscuous drugs as therapeutics for chemokine receptors. *Expert Rev. Mol. Med.* **2009**, *11*, e1.
12. Junker, A.; Kokornaczyk, A. K.; Strunz, A. K.; Wunsch, B. Selective and dual targeting of CCR2 and CCR5 receptors: a current overview. In *Chemokines: Chemokines and Their Receptors in Drug Discovery*, Tschammer, N., Ed. Springer International Publishing: Cham, 2015; pp 187-241.
13. Gilliland, C. T.; Salanga, C. L.; Kawamura, T.; Trejo, J.; Handel, T. M. The chemokine receptor CCR1 is constitutively active, which leads to G protein-independent, b-arrestin-mediated internalization. *J. Biol. Chem.* **2013**, *288*, 32194-32210.
14. Weichert, D.; Gmeiner, P. Covalent molecular probes for class A G protein-coupled receptors: advances and applications. *ACS Chem Biol* **2015**, *10*, 1376-1386.
15. Ghosh, A. K.; Samanta, I.; Mondal, A.; Liu, W. R. Covalent inhibition in drug discovery. *ChemMedChem* **2019**, *14*, 889-906.
16. Vilums, M.; Zweemer, A. J.; Barmare, F.; van der Gracht, A. M.; Bleeker, D. C.; Yu, Z.; de Vries, H.; Gross, R.; Clemens, J.; Krenitsky, P.; Brussee, J.; Stamos, D.; Saunders, J.; Heitman, L. H.; IJzerman, A. P. When structure-affinity relationships meet structure-kinetics relationships: 3-((Inden-1-yl)amino)-1-isopropyl-cyclopentane-1-carboxamides as CCR2 antagonists. *Eur. J. Med. Chem.* **2015**, *93*, 121-134.
17. Vauquelin, G.; Szczuka, A. Kinetic versus allosteric mechanisms to explain insurmountable antagonism and delayed ligand dissociation. *Neurochem. Int.* **2007**, *51*, 254-260.
18. Copeland, R. A. The dynamics of drug-target interactions: drug-target residence time and its impact on efficacy and safety. *Expert Opin Drug Discov* **2010**, *5*, 305-310.

19. Zlotnik, A.; Yoshie, O. The chemokine superfamily revisited. *Immunity* **2012**, *36*, 705-716.
20. Liu, X.; Ahn, S.; Kahsai, A. W.; Meng, K.-C.; Latorraca, N. R.; Pani, B.; Venkatakrishnan, A.; Masoudi, A.; Weis, W. I.; Dror, R. O.; Chen, X.; Lefkowitz, R. J.; Kobilka, B. K. Mechanism of intracellular allosteric  $\beta_2$ AR antagonist revealed by X-ray crystal structure. *Nature* **2017**, *548*, 480-484.
21. Liu, X.; Masoudi, A.; Kahsai, A. W.; Huang, L. Y.; Pani, B.; Staus, D. P.; Shim, P. J.; Hirata, K.; Simhal, R. K.; Schwab, A. M.; Rambarat, P. K.; Ahn, S.; Lefkowitz, R. J.; Kobilka, B. Mechanism of  $\beta_2$ AR regulation by an intracellular positive allosteric modulator. *Science* **2019**, *364*, 1283-1287.
22. Dowal, L.; Sim, D. S.; Dilks, J. R.; Blair, P.; Beaudry, S.; Denker, B. M.; Koukos, G.; Kuliopulos, A.; Flaumenhaft, R. Identification of an antithrombotic allosteric modulator that acts through helix 8 of PAR1. *Proc. Natl. Acad. Sci. U. S. A.* **2011**, *108*, 2951-2956.
23. Wang, X.; Heinz, B. A.; Qian, Y.-W.; Carter, J. H.; Gadski, R. A.; Beavers, L. S.; Little, S. P.; Yang, C. R.; Beck, J. P.; Hao, J.; Schaus, J. M.; Svensson, K. A.; Bruns, R. F. Intracellular binding site for a positive allosteric modulator of the dopamine D1 receptor. *Mol. Pharmacol.* **2018**, *94*, 1232-1245.
24. Oswald, C.; Rappas, M.; Kean, J.; Dore, A. S.; Errey, J. C.; Bennett, K.; Deflorian, F.; Christopher, J. A.; Jazayeri, A.; Mason, J. S.; Congreve, M.; Cooke, R. M.; Marshall, F. H. Intracellular allosteric antagonism of the CCR9 receptor. *Nature* **2016**, *540*, 462-465.
25. Quoyer, J.; Janz, J. M.; Luo, J.; Ren, Y.; Armando, S.; Lukashova, V.; Benovic, J. L.; Carlson, K. E.; Hunt, S. W., 3rd; Bouvier, M. Pepducin targeting the C-X-C chemokine receptor type 4 acts as a biased agonist favoring activation of the inhibitory G protein. *Proc. Natl. Acad. Sci. U. S. A.* **2013**, *110*, E5088-5097.
26. Cederblad, L.; Rosengren, B.; Ryberg, E.; Hermansson, N. O. AZD8797 is an allosteric non-competitive modulator of the human CX3CR1 receptor. *Biochem J.* **2016**, *473*, 641-649.
27. Smith, J. S.; Nicholson, L. T.; Suwanpradid, J.; Glenn, R. A.; Knape, N. M.; Alagesan, P.; Gundry, J. N.; Wehrman, T. S.; Atwater, A. R.; Gunn, M. D.; MacLeod, A. S.; Rajagopal, S. Biased agonists of the chemokine receptor CXCR3 differentially control chemotaxis and inflammation. *Sci Signal.* **2018**, *11*, eaaq1075.
28. Hitchinson, B.; Eby, J. M.; Gao, X.; Guite-Vinet, F.; Ziarek, J. J.; Abdelkarim, H.; Lee, Y.; Okamoto, Y.; Shikano, S.; Majetschak, M.; Heveker, N.; Volkman, B. F.; Tarasova, N. I.; Gaponenko, V. Biased antagonism of CXCR4 avoids antagonist tolerance. *Sci Signal.* **2018**, *11*, eaat2214.
29. Zweemer, A. J.; Toraskar, J.; Heitman, L. H.; IJzerman, A. P. Bias in chemokine receptor signalling. *Trends Immunol.* **2014**, *35*, 243-252.
30. Hornberg, J. J. Simple drugs do not cure complex diseases: The need for multi-targeted drugs. In *Designing Multi-Target Drugs*, Morphy, J. R.; Harris, C. J., Eds. Royal Society of Chemistry: 2012; pp 1-13.
31. Ramsay, R. R.; Popovic-Nikolic, M. R.; Nikolic, K.; Uliassi, E.; Bolognesi, M. L. A perspective on multi-target drug discovery and design for complex diseases. *Clin Transl Med* **2018**, *7*, 3.
32. Sabroe, I.; Peck, M. J.; Van Keulen, B. J.; Jorritsma, A.; Simmons, G.; Clapham, P. R.; Williams, T. J.; Pease, J. E. A small molecule antagonist of chemokine receptors CCR1 and CCR3. Potent inhibition of eosinophil function and CCR3-mediated HIV-1 entry. *J. Biol. Chem.* **2000**, *275*, 25985-25992.
33. Walters, I.; Austin, C.; Austin, R.; Bonnert, R.; Cage, P.; Christie, M.; Ebden, M.; Gardiner, S.; Grahames, C.; Hill, S.; Hunt, F.; Jewell, R.; Lewis, S.; Martin, I.; Nicholls, D.; Robinson, D. Evaluation of a series of bicyclic CXCR2 antagonists. *Bioorg Med Chem Lett* **2008**, *18*, 798-803.
34. Cox, B. D.; Prosser, A. R.; Sun, Y.; Li, Z.; Lee, S.; Huang, M. B.; Bond, V. C.; Snyder, J. P.; Krystal, M.; Wilson, L. J.; Liotta, D. C. Pyrazolo-piperidines exhibit dual inhibition of CCR5/CXCR4 HIV entry and reverse transcriptase. *ACS Med. Chem. Lett.* **2015**, *6*, 753-757.
35. Moriconi, A.; Cesta, M. C.; Cervellera, M. N.; Aramini, A.; Coniglio, S.; Colagioia, S.; Beccari, A. R.; Bizzarri, C.; Cavicchia, M. R.; Locati, M. Design of noncompetitive interleukin-8 inhibitors acting on CXCR1 and CXCR2. *J. Med. Chem.* **2007**, *50*, 3984-4002.
36. Schmidt, D.; Bernat, V.; Brox, R.; Tschammer, N.; Kolb, P. Identifying modulators of CXC receptors 3 and 4 with tailored selectivity using multi-target docking. *ACS Chem Biol* **2015**, *10*, 715-724.
37. Suzuki, K.; Morokata, T.; Morihira, K.; Sato, I.; Takizawa, S.; Kaneko, M.; Takahashi, K.; Shimizu, Y. A dual antagonist for chemokine CCR3 receptor and histamine H1 receptor. *Eur. J. Pharmacol.* **2007**, *563*, 224-232.

38. Yang, Y. F.; Mukai, T.; Gao, P.; Yamaguchi, N.; Ono, S.; Iwaki, H.; Obika, S.; Imanishi, T.; Tsujimura, T.; Hamaoka, T.; Fujiwara, H. A non-peptide CCR5 antagonist inhibits collagen-induced arthritis by modulating T cell migration without affecting anti-collagen T cell responses. *Eur. J. Immunol.* **2002**, *32*, 2124-2132.
39. van Wanrooij, E. J.; Happe, H.; Hauer, A. D.; de Vos, P.; Imanishi, T.; Fujiwara, H.; van Berkel, T. J.; Kuiper, J. HIV entry inhibitor TAK-779 attenuates atherogenesis in low-density lipoprotein receptor-deficient mice. *Arterioscler Thromb Vasc Biol* **2005**, *25*, 2642-2647.
40. Ni, J.; Zhu, Y. N.; Zhong, X. G.; Ding, Y.; Hou, L. F.; Tong, X. K.; Tang, W.; Ono, S.; Yang, Y. F.; Zuo, J. P. The chemokine receptor antagonist, TAK-779, decreased experimental autoimmune encephalomyelitis by reducing inflammatory cell migration into the central nervous system, without affecting T cell function. *Br J Pharmacol* **2009**, *158*, 2046-2056.
41. Huh, J. H.; Kim, H. M.; Lee, E. S.; Kwon, M. H.; Lee, B. R.; Ko, H. J.; Chung, C. H. Dual CCR2/5 antagonist attenuates obesity-induced insulin resistance by regulating macrophage recruitment and M1/M2 status. *Obesity (Silver Spring)* **2018**, *26*, 378-386.
42. Friedman, S. L.; Ratzl, V.; Harrison, S. A.; Abdelmalek, M. F.; Aithal, G. P.; Caballeria, J.; Francque, S.; Farrell, G.; Kowdley, K. V.; Craxi, A. A randomized, placebo-controlled trial of cenicriviroc for treatment of nonalcoholic steatohepatitis with fibrosis. *Hepatology* **2018**, *67*, 1754-1767.
43. Lefebvre, E.; Gottwald, M.; Lasseter, K.; Chang, W.; Willett, M.; Smith, P.; Somasunderam, A.; Utay, N. Pharmacokinetics, safety, and CCR2/CCR5 antagonist activity of cenicriviroc in participants with mild or moderate hepatic impairment. *Clin. Transl. Sci.* **2016**, *9*, 139-148.
44. Thompson, M.; Saag, M.; DeJesus, E.; Gathe, J.; Lalezari, J.; Landay, A. L.; Cade, J.; Enejosa, J.; Lefebvre, E.; Feinberg, J. A 48-week randomized phase 2b study evaluating cenicriviroc versus efavirenz in treatment-naive HIV-infected adults with C-C chemokine receptor type 5-tropic virus. *AIDS* **2016**, *30*, 869-878.
45. Szekanecz, Z.; Vegvari, A.; Szabo, Z.; Koch, A. E. Chemokines and chemokine receptors in arthritis. *Front Biosci (Schol Ed)* **2010**, *2*, 153-167.
46. Csermely, P.; Ágoston, V.; Pongor, S. The efficiency of multi-target drugs: the network approach might help drug design. *Trends Pharmacol. Sci.* **2005**, *26*, 178-182.
47. Richard Morphy, J. The Challenges of Multi-Target Lead Optimization. In *Designing Multi-Target Drugs*, Morphy, J. R.; Harris, C. J., Eds. The Royal Society of Chemistry: 2012; pp 141-154.
48. Jörg, M.; Scammells, P. J. Guidelines for the synthesis of small-molecule irreversible probes targeting G protein-coupled receptors. *ChemMedChem* **2016**, *11*, 1488-1498.
49. Cooper, A.; Singh, S.; Hook, S.; Tyndall, J. D. A.; Vernall, A. J. Chemical tools for studying lipid-binding class A G protein-coupled receptors. *Pharmacol Rev* **2017**, *69*, 316-353.
50. Bernat, V.; Admas, T. H.; Brox, R.; Heinemann, F. W.; Tschammer, N. Boronic acids as probes for investigation of allosteric modulation of the chemokine receptor CXCR3. *ACS Chem Biol* **2014**, *9*, 2664-2677.
51. Weichert, D.; Kruse, A. C.; Manglik, A.; Hiller, C.; Zhang, C.; Hübner, H.; Kobilka, B. K.; Gmeiner, P. Covalent agonists for studying G protein-coupled receptor activation. *Proc. Natl. Acad. Sci. U. S. A.* **2014**, *111*, 10744-10748.
52. Hua, T.; Vemuri, K.; Nikas, S. P.; Laprairie, R. B.; Wu, Y.; Qu, L.; Pu, M.; Korde, A.; Jiang, S.; Ho, J. H.; Han, G. W.; Ding, K.; Li, X.; Liu, H.; Hanson, M. A.; Zhao, S.; Bohn, L. M.; Makriyannis, A.; Stevens, R. C.; Liu, Z. J. Crystal structures of agonist-bound human cannabinoid receptor CB<sub>1</sub>. *Nature* **2017**, *547*, 468-471.
53. Glukhova, A.; Thal, D. M.; Nguyen, A. T.; Vecchio, E. A.; Jörg, M.; Scammells, P. J.; May, L. T.; Sexton, P. M.; Christopoulos, A. Structure of the adenosine A1 receptor reveals the basis for subtype selectivity. *Cell* **2017**, *168*, 867-877.
54. Yang, P.; Liu, K. Activity-based protein profiling: recent advances in probe development and applications. *ChemBioChem* **2015**, *16*, 712-724.
55. Yang, X.; Michiels, T. J. M.; de Jong, C.; Soethoudt, M.; Dekker, N.; Gordon, E.; van der Stelt, M.; Heitman, L. H.; van der Es, D.; IJzerman, A. P. An affinity-based probe for the human adenosine A2A receptor. *J. Med. Chem.* **2018**, *61*, 7892-7901.

56. Soethoudt, M.; Stolze, S. C.; Westphal, M. V.; van Stralen, L.; Martella, A.; van Rooden, E. J.; Guba, W.; Varga, Z. V.; Deng, H.; van Kasteren, S. I.; Grether, U.; IJzerman, A. P.; Pacher, P.; Carreira, E. M.; Overkleeft, H. S.; Ioan-Facsinay, A.; Heitman, L. H.; van der Stelt, M. Selective photoaffinity probe that enables assessment of cannabinoid CB2 receptor expression and ligand engagement in human cells. *J. Am. Chem. Soc.* **2018**, *140*, 6067-6075.
57. Gamo, A. M.; González-Vera, J. A.; Rueda-Zubiaurre, A.; Alonso, D.; Vázquez-Villa, H.; Martín-Couce, L.; Palomares, Ó.; López, J. A.; Martín-Fontecha, M.; Benhamú, B.; López-Rodríguez, M. L.; Ortega-Gutiérrez, S. Chemoproteomic approach to explore the target profile of GPCR ligands: application to 5-HT1A and 5-HT6 receptors. *Chemistry* **2016**, *22*, 1313-1321.
58. Müskens, F. M.; Ward, R. J.; Herkt, D.; van de Langemheen, H.; Tobin, A. B.; Liskamp, R. M. J.; Milligan, G. Design, synthesis, and evaluation of a diazirine photoaffinity probe for ligand-based receptor capture targeting G protein-coupled receptors. *Mol. Pharmacol.* **2019**, *95*, 196-209.
59. Lai, A. C.; Crews, C. M. Induced protein degradation: an emerging drug discovery paradigm. *Nat Rev Drug Discov* **2016**, *16*, 101-114.
60. Neklesa, T. K.; Winkler, J. D.; Crews, C. M. Targeted protein degradation by PROTACs. *Pharmacol Ther.* **2017**, *174*, 138-144.
61. Pettersson, M.; Crews, C. M. PROteolysis TARgeting Chimeras (PROTACs) — Past, present and future. *Drug Discov Today Technol* **2019**, *31*, 15-27.
62. Mullard, A. First targeted protein degrader hits the clinic. *Nat Rev Drug Discov* **2019**, *18*, 237-239.
63. Toure, M.; Crews, C. M. Small-molecule PROTACs: new approaches to protein degradation. *Angew Chem Int Ed Engl* **2016**, *55*, 1966-1973.
64. Xie, L.; Xiao, K.; Whalen, E. J.; Forrester, M. T.; Freeman, R. S.; Fong, G.; Gygi, S. P.; Lefkowitz, R. J.; Stamler, J. S. Oxygen-regulated  $\beta_2$ -adrenergic receptor hydroxylation by EGLN3 and ubiquitylation by pVHL. *Sci Signal.* **2009**, *2*, ra33.
65. Burslem, G. M.; Smith, B. E.; Lai, A. C.; Jaime-Figueroa, S.; McQuaid, D. C.; Bondeson, D. P.; Toure, M.; Dong, H.; Qian, Y.; Wang, J.; Crew, A. P.; Hines, J.; Crews, C. M. The advantages of targeted protein degradation over inhibition: an RTK case study. *Cell Chem Biol* **2018**, *25*, 67-77.
66. Steven, B.; Kayvon, P.; Simon, W.; Nicholas, R.; Carolyn, B. Lysosome targeting chimeras (LYTACs) for the degradation of secreted and membrane proteins. *ChemRxiv* **2019**.
67. Nalawansa, D. A.; Paiva, S.-L.; Rafizadeh, D. N.; Pettersson, M.; Qin, L.; Crews, C. M. Targeted protein internalization and degradation by ENDosome TARgeting Chimeras (ENDTACs). *ACS Cent Sci* **2019**, *5*, 1079-1084.
68. Churcher, I. Protac-induced protein degradation in drug discovery: breaking the rules or just making new ones? *J. Med. Chem.* **2018**, *61*, 444-452.
69. An, S.; Fu, L. Small-molecule PROTACs: an emerging and promising approach for the development of targeted therapy drugs. *EBioMedicine* **2018**, *36*, 553-562.



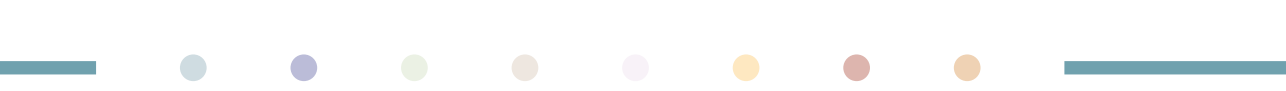


# SUMMARY

Chemokine receptors, including CCR1, CCR2 and CCR5, have been implicated in many inflammatory and immune diseases, such as atherosclerosis, rheumatoid arthritis and cancer. Thus, numerous drug discovery efforts have been made to develop drugs for these receptors. Yet, only one—maraviroc, targeting CCR5—has reached the market, while all other drug candidates have failed in clinical trials mostly due to lack of efficacy. Therefore, it is crucial to develop novel tools and concepts that allow us to better study and target these receptors in early phases of drug discovery, in order to develop safer and more efficacious drug candidates. **Chapter 1** introduces chemokine receptors, and the chemokine system in general, as potential drug targets, as well as the difficulties encountered when targeting such a complex system. In addition, this chapter introduces the main concepts studied throughout this thesis, including allosteric modulation, insurmountability, target residence time, multitarget and covalent inhibition.

While orthosteric ligands bind to the same binding site as the endogenous ligands, allosteric ligands bind to a nonoverlapping, spatially distinct site. All allosteric ligands described in this thesis bind to a highly conserved intracellular pocket, which (partially) overlaps with the binding site of intracellular signaling effectors, such as G proteins or  $\beta$ -arrestins. Thus, **Chapter 2** reviews the evidence for such an intracellular pocket among chemokine receptors and other class A G protein-coupled receptors (GPCRs). In addition, the structural features of this binding site, the different strategies to target it, and the potential advantages of intracellular ligands are discussed. One of the first crystal structures to provide direct evidence of an intracellular binding site is that of CCR2, described in **Chapter 3**. We solved the X-ray crystal structure of CCR2 in complex with two antagonists, BMS-681 and CCR2-RA-[R]. The structure showed that BMS-681 binds at the so-called orthosteric binding site, where the endogenous chemokines also bind. In this way, BMS-681 appears to inhibit chemokine binding by directly competing for the same binding site. In contrast, CCR2-RA-[R] binds to an intracellular pocket located more than 30 Å away from the orthosteric site. Thus, CCR2-RA-[R] inhibits chemokine binding in a noncompetitive, insurmountable manner, while it directly interferes with the binding of signaling effectors. Simultaneous binding of both ligands was not only crucial to achieve crystallization of CCR2, but it resulted in a highly inactive conformation of this receptor. Overall, this structure provides novel insights on how to better target CCR2, and chemokine receptors in general.

As this intracellular binding site is highly conserved among chemokine receptors, it was used for the design and development of ‘multitarget’ ligands, i.e. ligands that inhibit multiple



receptors. Thus, in **Chapter 4** we aimed to determine if CCR1 could also be targeted with intracellular antagonists. Using [ $^3\text{H}$ ]-CCR2-RA-[R] as intracellular tool, we found that this compound also binds to CCR1 with high affinity. We synthesized around 40 different CCR2-RA-[R] analogues, which were further characterized in both CCR1 and CCR2 in order to perform a structure-activity relationships (SAR) analysis for both receptors. This strategy allowed us to identify ligands with higher selectivity towards CCR1 or CCR2, but also ligands with potential multitarget activity. Moreover, these intracellular ligands behaved as inverse agonists in CCR1, as they were able to decrease the basal activity of this receptor. Due to the high constitutive activity of CCR1, the development of inverse agonists for CCR1 is highly relevant. In addition to CCR1/CCR2 ligands, in **Chapter 5** we focused on the development of intracellular CCR2/CCR5 ligands. For this, we focused on a triazolo-pyrimidinone scaffold, which displayed the best activity in both receptors in comparison with other intracellular ligands. Next, we performed an SAR study in both receptors by synthesizing and characterizing a series of triazolo-pyrimidinone derivatives. Although most derivatives displayed much higher selectivity towards CCR2, we also found some compounds with improved activity towards CCR5, and thus, improved dual activity. Their mechanism of inhibition was also investigated, providing evidence that these ligands display insurmountable antagonism, as they led to a significant decrease in receptor activity even at the highest concentration of agonist tested.

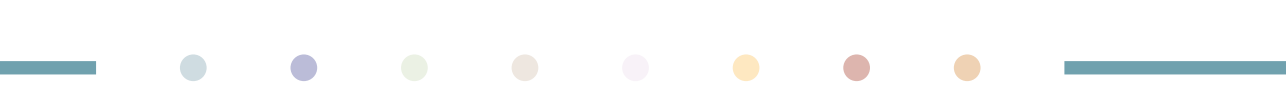
**Chapter 6** focuses on the design and pharmacological characterization of the first intracellular covalent ligand for CCR2. Based on the structure of a known intracellular ligand for CCR2, we designed a potential covalent ligand containing a reactive thiocyanate group. To validate its covalent binding mode, we used a variety of radioligand binding and functional assays, which showed that, even after extensive washing, this ligand remains bound and functional in CCR2. Furthermore, we used computational modelling followed by a mutagenesis study in order to identify the amino acids responsible for such covalent interaction. The results from this study point to one cysteine residue as the main interaction point, although other potential secondary interaction sites are also suggested.

In **Chapter 7** we investigated whether a previously characterized ‘long residence-time’ orthosteric CCR2 antagonist was efficacious in atherosclerosis. For this, the affinity and binding kinetics of this antagonist were characterized in murine CCR2, while its efficacy was determined in an apolipoprotein E-deficient mouse model of atherosclerosis. Treatment with the antagonist resulted in a significant reduction of monocytes recruitment and plaque size at both the carotid artery and the aortic root. Furthermore, pharmacokinetic data and calculation of occupancy levels showed that this compound achieved full receptor occupancy for a prolonged time. Lastly, **Chapter 8** summarizes the main conclusions and future perspectives that have been derived from the research presented in this thesis.

# SAMENVATTING

Chemokine receptoren, waaronder CCR1, CCR2 en CCR5, zijn betrokken bij diverse ontstekings- en immuunziekten, zoals atherosclerose, reumatoïde artritis en kanker. Daarom zijn er talrijke pogingen gedaan om nieuwe geneesmiddelen voor deze receptoren te ontwikkelen. Toch heeft slechts één—maraviroc, gericht tegen CCR5—de markt bereikt, terwijl alle andere kandidaat-geneesmiddelen niet succesvol bleken in klinische onderzoeken, voornamelijk wegens een gebrek aan werkzaamheid. Het is van cruciaal belang om nieuwe hulpmiddelen en concepten te ontwikkelen waarmee we deze receptoren in de vroege ontwikkelingsfase van geneesmiddelen beter kunnen bestuderen en aangrijpen, om veiligere en effectievere geneesmiddelen te ontwikkelen. **Hoofdstuk 1** introduceert chemokine receptoren, en het chemokine systeem in het algemeen, als potentiële aangrijpingspunten voor geneesmiddelen, evenals de moeilijkheden die zich voordoen bij het onderzoeken van een dergelijk complex systeem. Daarnaast introduceert dit hoofdstuk de belangrijkste concepten die in dit proefschrift zijn bestudeerd, waaronder allosterische modulatie, 'insurmountability', verblijfstijd op de receptor, polyfarmacologie en covalente remming.

Terwijl orthostere liganden binden op dezelfde bindingsplaats als de endogene liganden, binden allosterische liganden op een niet-overlappende, in de ruimte verschillende plaats. Alle allosterische liganden die in dit proefschrift worden beschreven, binden aan een zeer geconserveerde intracellulaire pocket, die (gedeeltelijk) overlapt met de bindingsplaats van intracellulaire signalerende effectoren, zoals G-eiwitten of  $\beta$ -arrestines. Dus wordt in **Hoofdstuk 2** het bewijs voor een dergelijke intracellulaire pocket onder chemokine receptoren en andere klasse A van G-eiwit gekoppelde receptoren (GPCRs) beoordeeld. Bovendien worden de structurele kenmerken van deze bindingsplaats, de verschillende strategieën deze aan te grijpen en de potentiële voordelen van intracellulaire liganden besproken. Een van de eerste kristalstructuren die direct bewijs levert van een intracellulaire bindingsplaats is die van CCR2, beschreven in **Hoofdstuk 3**. We hebben de kristalstructuur van CCR2 opgelost in complex met twee antagonist, BMS-681 en CCR2-RA-[R]. De structuur toonde aan dat BMS-681 bindt op de orthostere bindingsplaats, waar de endogene chemokines ook binden. Op deze manier inhibeert BMS-681 chemokine binding door rechtstreeks te concurreren om dezelfde bindingsplaats. CCR2-RA-[R] bindt zich aan een intracellulaire pocket die meer dan 30 Å verwijderd is van de orthostere plaats. Dus inhibeert CCR2-RA-[R] chemokine binding op een niet-competitieve, onoverkomelijke (*insurmountable*) manier, terwijl het direct de binding van signalerende effectoren verstoort. Gelijktijdige binding van beide liganden was niet alleen cruciaal om kristallisatie van CCR2 te bereiken, maar het resulteerde ook in een



zeer inactieve conformatie van deze receptor. Deze structuur biedt nieuwe inzichten over hoe CCR2 en chemokine receptoren in het algemeen beter kunnen worden aangegrepen.

Omdat deze intracellulaire bindingsplaats zeer geconserveerd is bij chemokine receptoren, werd deze gebruikt voor het ontwerp en de ontwikkeling van 'poly-farmacologische' liganden, d.w.z. liganden die meerdere receptoren remmen. Daarom wilden we in **Hoofdstuk 4** bepalen of CCR1 ook kan worden aangegrepen met intracellulaire antagonisten. Met behulp van [<sup>3</sup>H]-CCR2-RA-[R] als intracellulair hulpmiddel, vonden we dat dit ligand ook met hoge affiniteit bindt aan CCR1. We synthetiseerden ongeveer 40 verschillende CCR2-RA-[R] analogen, die verder werden gekarakteriseerd in zowel CCR1 als CCR2 om een structuur-activiteit relatie (SAR) analyse voor beide receptoren uit te voeren. Met deze strategie konden we liganden identificeren met een hogere selectiviteit voor CCR1 of CCR2, maar ook liganden met potentiële poly-farmacologische activiteit. Bovendien gedroegen deze intracellulaire liganden zich als inverse agonisten in CCR1, omdat ze de basale activiteit van deze receptor konden verminderen. Vanwege de hoge constitutieve activiteit van CCR1 is de ontwikkeling van inverse agonisten voor CCR1 zeer relevant. Naast CCR1/CCR2 liganden hebben we ons in **Hoofdstuk 5** gericht op de ontwikkeling van intracellulaire CCR2/CCR5 liganden. Hiervoor hebben we ons gericht op een triazolo-pyrimidinone structuur, die de beste activiteit in beide receptoren vertoonde in vergelijking met andere intracellulaire liganden. Vervolgens hebben we een SAR-studie uitgevoerd in beide receptoren door een reeks triazolo-pyrimidinone analogen te synthetiseren en te karakteriseren. Hoewel de meeste derivaten een veel hogere selectiviteit voor CCR2 vertoonden, vonden we ook enkele verbindingen met verbeterde activiteit voor CCR5 en dus verbeterde dubbele activiteit. Hun remmingsmechanisme werd ook onderzocht, wat het bewijs levert dat deze liganden onoverkomelijk antagonisme vertonen, omdat ze zelfs bij de hoogste concentratie van geteste agonisten tot een significante afname van receptoractiviteit leidden.

**Hoofdstuk 6** richt zich op het ontwerp en de farmacologische karakterisering van het eerste intracellulaire covalente ligand voor CCR2. Op basis van de structuur van een bekend intracellulair ligand voor CCR2 hebben we een potentieel covalent ligand ontworpen met een reactieve thiocynaat groep. Om de covalente bindingsmodus te valideren, gebruikten we verscheidene radioligand-binding en functionele studies, die aantoonde dat, zelfs na uitgebreid wassen, dit ligand gebonden en functioneel blijft in CCR2. Verder hebben we *in silico* modellering uitgevoerd gevolgd door een mutagenesestudie om de aminozuren te identificeren die verantwoordelijk zijn voor een dergelijke covalente interactie. De resultaten van dit onderzoek wijzen op één cysteïne residu als het belangrijkste interactiepunt, hoewel ook andere mogelijke secundaire interactiesites worden voorgesteld.

In **Hoofdstuk 7** hebben we onderzocht of een eerder gekarakteriseerde 'lange verblijftijd' orthostere CCR2 antagonist werkzaam was tegen atherosclerose. Hiervoor werden de

affiniteit en bindingskinetiek van deze antagonist gekarakteriseerd voor de muis-CCR2, terwijl de werkzaamheid ervan werd bepaald in een apolipoproteïne E-deficiënt muismodel van atherosclerose. Behandeling met de antagonist resulteerde in een significante vermindering van de rekrutering van monocytën en plaquegrootte bij zowel de halsslagader als de aortawortel. Bovendien toonden farmacokinetische gegevens en berekening van bezettingsgraden dat deze verbinding gedurende langere tijd volledige receptorbezetting bereikte. Ten slotte vat **Hoofdstuk 8** de belangrijkste conclusies en toekomstperspectieven samen die zijn afgeleid uit het onderzoek in dit proefschrift.



# CURRICULUM VITAE

Natalia Veneranda Ortiz Zacarías was born in Monterrey, Nuevo León, Mexico on the 13th of February 1987. After graduating from high school at the *Research and Development Center for Bilingual Education (CIDEB)*, she studied Pharmaceutical Chemistry and Biology at the Faculty of Chemical Sciences of the *Autonomous University of Nuevo León (UANL)*. In 2009, she graduated with honors after pursuing a specialization in Pharmacy. She also received the first academic place award of her study generation 2005-2009.

Before continuing with a master degree, she worked for two years as Hospital Pharmacist in the San José Tec de Monterrey Hospital. In 2012, she obtained a scholarship from Mexican *National Council of Science and Technology (CONACYT)* and a Leiden University Excellence Scholarship (LExS) to study at Leiden University, in The Netherlands. Thus, she moved to Leiden to follow the master's program in Bio-Pharmaceutical Sciences, where she specialized in Medicinal Chemistry. During her master studies, she performed a 9-month research internship in the Division of Medicinal Chemistry, at the Leiden Academic Centre for Drug Research (LACDR), under the supervision of Dr. Arnault Massink, Dr. Laura Heitman and Prof. Dr. Ad IJzerman. The project focused on exploring the role of the sodium ion binding pocket in an adenosine receptor, and it resulted in a publication. After her first internship, she wrote a literature review under the supervision of Dr. Ron de Kloet, which was published later as a book chapter. In 2014, she performed a second 6-month research internship at the Centre for Human Drug Research (CHDR) under the supervision of Dr. Ingrid de Visser and Dr. Jasper Stevens. There, she worked on two projects focused on the revival of 'old' antibiotics for the treatment of multidrug-resistant bacteria. These projects led to the publication of two reviews and one research article. In 2014 she obtained her MSc. Degree *cum laude*, and was awarded the KNMP student prize 2014 for her academic achievements.

In November 2014, she started as PhD candidate at the Division of Drug Discovery and Safety, LACDR (former Division of Medicinal Chemistry), with Dr. Laura Heitman and Prof. Dr. Ad IJzerman as promotors. She also collaborated with Dr. Ilze Bot and Prof. Dr. Johan Kuiper, from the Division of BioTherapeutics at the LACDR, and with Dr. Irina Kufareva and Prof. Dr. Tracy Handel, from the University of California, San Diego. Throughout her PhD, she presented her research in posters and oral communications at several national and international conferences, including the FIGON Dutch Medicine Days (2015-2018), Keystone Symposia (2018) and the EFMC-ISMIC (2018). In 2017, she was awarded the 1<sup>st</sup> prize at the LACDR Spring Symposium and the 1<sup>st</sup> prize of the national PhD Student Competition at the FIGON Dutch Medicine Days 2017 for her oral presentation entitled "Killing one bird

with two stones: Insights from the CCR2 Crystal Structure”. In 2018, she obtained a FIGON travel award to present part of her research at the Keystone Symposia “GPCR Structure and Function: Taking GPCR Drug Development and Discovery to the Next Level” in Santa Fe, New Mexico, USA. Currently, she works at the same division as a postdoctoral research scientist under the umbrella of the Dutch Onco Institute.

## LIST OF PUBLICATIONS

Ortiz Zacarías NV, Louvel J, Šimková T, Chahal K, Zheng Y, Theunissen E, Mallee L, van der Es D, Handel TM, Kufareva I, IJzerman AP, Heitman LH. *Design and characterization of an intracellular covalent ligand for CC Chemokine Receptor 2 (CCR2)*. Manuscript in preparation.

Ortiz Zacarías NV, van Veldhoven JPD, den Hollander L, Dogan B, Openy J, Hsiao Y, Lenselink EB, Heitman LH, IJzerman AP. *Synthesis and pharmacological evaluation of triazolo-pyrimidinone derivatives as noncompetitive, intracellular antagonists for CC chemokine receptors 2 and 5*. Manuscript submitted.

Ortiz Zacarías NV, van Veldhoven JPD, Portner L, van Spronsen E, Ullo S, Veenhuizen M, van der Velden WJC, Zweemer AJM, Kreekel RM, Oenema K, Lenselink EB, Heitman LH, IJzerman AP. *Pyrralone derivatives as intracellular allosteric modulators for chemokine receptors: selective and dual-targeting inhibitors of CC chemokine receptors 1 and 2*. *J Med Chem* **2018**, 61, 9146-9161.

Ortiz Zacarías NV, Lenselink EB, IJzerman AP, Handel TM, Heitman LH. *Intracellular receptor modulation: novel approach to target GPCRs*. *Trends Pharmacol Sci* **2018**, 39, 547-559.

Bot I,\* Ortiz Zacarias NV,\* de Witte WE, de Vries H, van Santbrink PJ, van der Velden D, Kroner MJ, van der Berg DJ, Stamos D, de Lange EC, Kuiper J, IJzerman AP, Heitman LH. *A novel CCR2 antagonist inhibits atherogenesis in apoE deficient mice by achieving high receptor occupancy*. *Sci Rep* **2017**, 7, 52.

\*these authors contributed equally.

Zheng Y, Qin L, [Ortiz Zacarías NV](#), de Vries H, Han GW, Gustavsson M, Dabros M, Zhao C, Cherney RJ, Carter P, Stamos D, Abagyan R, Cherezov V, Stevens RC, IJzerman AP, Heitman LH, Tebben A, Kufareva I, Handel TM. *Structure of CC chemokine receptor 2 with orthosteric and allosteric antagonists*. Nature **2016**, 540, 458-461.

[Ortiz Zacarías NV](#), Dijkmans AC, Burggraaf J, Mouton JW, Wilms EB, van Nieuwkoop C, Touw DJ, Kamerling IMC, Stevens J. *Fosfomycin as a potential therapy for the treatment of systemic infections: a population pharmacokinetic model to simulate multiple dosing regimens*. Pharmacol Res Perspect **2018**, 6, e00378.

de Kloet ER, [Ortiz Zacarias NV](#), Meijer OC. *Chapter 37 - Manipulating the Brain Corticosteroid Receptor Balance: Focus on Ligands and Modulators*. In: Stress: Neuroendocrinology and Neurobiology. Fink, George (Ed), Academic Press: San Diego, **2017**; pp 367-383.

Dijkmans AC, [Ortiz Zacarías NV](#), Burggraaf J, Mouton JW, Wilms EB, van Nieuwkoop C, Touw DJ, Stevens J, Kamerling IMC. *Fosfomycin: Pharmacological, Clinical and Future Perspectives*. Antibiotics **2017**, 6, 24.

Thum S, Kokornaczyk AK, Seki T, De Maria M, [Ortiz Zacarias NV](#), de Vries H, Weiss C, Koch M, Schepmann D, Kitamura M, Tschammer N, Heitman LH, Junker A, Wunsch B. *Synthesis and biological evaluation of chemokine receptor ligands with 2-benzazepine scaffold*. Eur J Med Chem **2017**, 135, 401-413.

Dijkmans AC, Wilms EB, Kamerling IMC, Birkhoff W, [Ortiz Zacarias NV](#), van Nieuwkoop C, Verbrugh HA, Touw DJ. *Colistin: Revival of an Old Polymyxin Antibiotic*. Ther Drug Monit **2015**, 37, 419-427.

Massink A, Gutierrez-de-Teran H, Lenselink EB, [Ortiz Zacarias NV](#), Xia L, Heitman LH, Katritch V, Stevens RC, IJzerman AP. *Sodium ion binding pocket mutations and adenosine A2A receptor function*. Mol Pharmacol **2015**, 87, 305-313.



# ACKNOWLEDGEMENTS

This thesis represents the work of the past four years and it would not have been possible without the contributions and support of many people, to whom I'm deeply grateful. To my promoters Ad and Laura: thank you for the innumerable lessons, for the trust you placed in me, and for your constant guidance during every stage of this journey. It has been truly a great pleasure working with you.

I'm also filled with gratitude for the opportunity to meet and collaborate with many people, including Ilze Bot, Wilbert de Witte, and Liesbeth de Lange from the LACDR, as well as Irina Kufareva and Tracy Handel from UCSD. Thank you for the fruitful collaborations over the years; your input and expertise were key to complete this thesis in its current form.

Special thanks to all my colleagues in the division, with whom I shared many conferences, lab outings, dinners, parties, beers and coffee... It was great working with all of you! In particular to Jaco and Julien, for the constant supply of compounds. To Bart, for the crucial computational work. To Henk and Thea, for the tips, tricks, and all the help in the lab. And to the many office mates over the years: thank you for the countless and valuable advice, continuous support, and all the fun times. I am especially grateful to all the students who did their research internships with me, in particular to my master students Laura, Wijnand, Burak, Lisa, Emy, and Arwin. You helped me become a better supervisor; and without your contributions and motivation, this thesis would not be complete.

Thank you to all my friends in Mexico, in the Netherlands, and all over the world: your friendship and support kept me and still keeps me going! To my paranymphs: thank you for being by my side during such a special day. To my beloved mom and dad, Maria de Jesus Zacarías and Rogelio Ortiz: thank you for always encouraging me to follow my dreams and for your unwavering support along the way. To my sisters, Magda, Dany and Diana: thank you for always believing in me, for inspiring me, and for always being there for me no matter the distance between us.

I end with you, Oscar: Your love has been my rock during these years and I simply cannot thank you enough.

